NASA Technical Paper 1667

Analysis of the Space Shuttle Orbiter Entry Dynamics From Mach 10 to Mach 2.5 With the November 1976 Flight Control System

Richard W. Powell and Howard W. Stone

AUGUST 1980

NASA

NASA Technical Paper 1667

Analysis of the Space Shuttle Orbiter Entry Dynamics From Mach 10 to Mach 2.5 With the November 1976 Flight Control System

Richard W. Powell and Howard W. Stone
Langley Research Center
Hampton, Virginia

NASA
National Aeronautics
and Space Administration

**Scientific and Technical
Information Branch**

1980

SUMMARY

A six-degree-of-freedom simulation analysis has been performed for the Space Shuttle Orbiter entry from Mach 10 to Mach 2.5 with realistic off-nominal conditions using the flight control system referred to as the November 1976 Integrated Digital Autopilot. The off-nominal conditions included: (1) aerodynamic uncertainties in extrapolating from wind-tunnel to flight characteristics, (2) error in deriving angle of attack from onboard instrumentation, (3) failure of two of the four reaction control-system thrusters on each side (design specification), and (4) lateral center-of-gravity offset.

The control system displayed three main weaknesses. First, there was an extreme sensitivity to error in derived angle of attack. Second, some off-nominal aerodynamic combinations caused the aileron, which provides the directional trim control for much of the entry, to actually deflect the wrong way. Third, off-nominal aerodynamics which produced an increased rudder effectiveness could result in an overgained control circuit. These weaknesses could lead to a loss of the orbiter. Modifications to the control system and pilot intervention techniques were designed to allow the orbiter to fly safely under all the assumed off-nominal conditions.

INTRODUCTION

A reusable Earth-to-orbit transportation system known as the Space Shuttle is being developed by the National Aeronautics and Space Administration (NASA). The Space Shuttle is designed to insert payloads of up to 29 500 kg into a near-Earth orbit, retrieve payloads already in orbit, and land with a payload of up to 14 500 kg. The Space Shuttle consists of an orbiter, an external fuel tank, and two solid rocket boosters (SRB). The SRB's will be recovered after each launch for reuse. The external tank is designed for one use and is not recovered.

The orbiter will have the capability to enter the Earth's atmosphere, fly up to 2040-km cross range, and land horizontally. A closed-loop entry guidance system is being developed to provide the necessary commands for either the automatic flight control system or a pilot-operated, augmented flight control system. A general description of the Space Shuttle configuration and mission is given in reference 1, and the orbiter avionics are described in reference 2.

The first orbital flights of the Space Shuttle are designed to verify the vehicle flight worthiness. The first flight is designed to demonstrate safe ascent and return of the orbiter and crew for the most conservative flight conditions. The flight will be launched from the NASA Kennedy Space Center into a 220-km circular orbit inclined 38°. After approximately 20 orbits, a deorbit maneuver will occur, followed by the entry and landing at the NASA Dryden Flight Research Center. A further description of this flight is presented in reference 3. The NASA Langley Research Center has been performing evaluations of the guidance and flight control system as it evolves for the first mission. This analysis is concerned with the control system that is usually referred to as the November 1976 Integrated Digital Autopilot. This control system has been developed under the guidance of the NASA Johnson Space Center and has evolved from the one that was analyzed in references 4 and 5. With the aid of a six-degree-of-freedom simulation with man-in-the-loop capability, the flight regime was studied from a Mach number of approximately 10 and an altitude of 50 km down to the initiation of the terminal-area-energy-management (TAEM) guidance phase, which occurs at an altitude of approximately 26 km at a Mach number of 2.5. This 360-second segment of the entry represents the period where the orbiter performs its most extreme maneuvers, where the aerodynamic parameters are undergoing significant changes as the vehicle decelerates from hypersonic to low-supersonic velocities, and where the angle of attack is lowered from 36° to 10°. These simulation studies considered the center of gravity to be located at 66.25 percent of the body reference length with a lateral center-of-gravity offset of 0.0381 m towards the right wing (maximum amount allowed by shuttle design specifications). In addition, two of the four yaw thrusters on each side were assumed to be inoperable (off). The design specification calls for the Space Shuttle Orbiter to be able to fly safely with this condition. To these were added the aerodynamic uncertainties (ref. 6) that are intended to encompass any differences that might occur between wind-tunnel and actual flight values. These uncertainties are based on the scatter in the wind-tunnel data and historical comparisons of flight and wind-tunnel data for various aircraft and lifting-body configurations. In addition to uncertainties, projected errors in deriving angle of attack from onboard instrumentation were included in the simulations. Since the orbiter has no method of directly measuring angle of attack until velocity has been reduced to Mach 2.5, this error was assumed to be as much as $\pm 4^{\circ}$. Without the aerodynamic uncertainties and the sensed angle-of-attack error, the flight control system is able to fly the entry mission safely. This paper will describe the effects of these aerodynamic uncertainties and angle-of-attack error and will suggest control-system modifications to handle the problems that are encountered.

SYMBOLS

All coefficients and vehicle rates are in the body axis system except where otherwise noted.

b	reference wing span, m
$\bar{c}$	mean aerodynamic chord, m
C_ℓ	rolling-moment coefficient, Rolling moment/$q_\infty Sb$
C_{ℓ_β}	effective-dihedral parameter, $C_\ell/\partial\beta$, deg^{-1}
$C_{\ell_{\delta_a}}$	rolling-moment coefficient due to aileron deflection, $C_\ell/\partial\delta_a$, deg^{-1}
$C_{\ell_{\delta_r}}$	rolling-moment coefficient due to rudder deflection, $C_\ell/\partial\delta_r$, deg^{-1}
C_m	pitching-moment coefficient, Pitching moment/$q_\infty S\bar{c}$
C_n	yawing-moment coefficient, Yawing moment/$q_\infty Sb$
C_{n_β}	directional-stability parameter, $\partial C_n/\partial\beta$, deg^{-1}
$\left(C_{n_\beta}\right)_{dyn}$	dynamic-stability parameter, $C_{n_\beta}\cos\alpha - \left(I_Z/I_X\right)C_{\ell_\beta}\sin\alpha$, deg^{-1}
$C_{n_{\delta_a}}$	yawing-moment coefficient due to aileron deflection, $C_n/\partial\delta_a$, deg^{-1}
$C_{n_{\delta_r}}$	yawing-moment coefficient due to rudder deflection, $C_n/\partial\delta_r$, deg^{-1}
C_Y	side-force coefficient, Side force/$q_\infty S$
$C_{Y_{\delta_r}}$	side-force coefficient due to rudder deflection, $C_Y/\partial\delta_r$, deg^{-1}
g	acceleration due to gravity (1g = 9.8 m/sec^2)

I_X	moment of inertia about body roll axis, kg-m^2
I_Y	moment of inertia about body pitch axis, kg-m^2
I_Z	moment of inertia about body yaw axis, kg-m^2
I_{XY}	product of inertia in body XY-plane, kg-m^2
I_{XZ}	product of inertia in body XZ-plane, kg-m^2
I_{YZ}	product of inertia in body YZ-plane, kg-m^2
M	Mach number
N_Y	side acceleration, g units
p	roll rate, deg/sec
P	period of oscillation, sec
q_∞	free-stream dynamic pressure, Pa
r	yaw rate, deg/sec
r_{stab}	yaw rate about stability axis, deg
r'	$= r - (180g \sin \phi \cos \theta)/\pi V_R$
RCS	reaction control system
S	reference area, m^2
$t_{1/2}$	time to half-amplitude, sec
V_R	Earth relative velocity, m/sec
Yawjets	number of yaw RCS thrusters firing (positive right side thrusters)

α	angle of attack, deg
α_c	commanded angle of attack, deg
β	sideslip angle, deg
δ_a	aileron-deflection angle, (Left elevon - Right elevon)/2, deg
$(\delta_a)_{trim}$	aileron deflection calculated by control system required for directional trim, deg
δ_{BF}	body-flap-deflection angle (positive down), deg
δ_e	elevator-deflection angle (positive down), (Left elevon + Right elevon)/2, deg
δ_r	rudder-deflection angle (positive trailing edge left), deg
δ_{SB}	speed-brake-deflection angle, deg
θ	pitch angle about body axis, deg
ϕ	roll angle about body axis, deg
ϕ_c	commanded roll angle, deg
σ	standard deviation

A dot over a symbol denotes differentiation with respect to time.

DESCRIPTION OF SPACE SHUTTLE ORBITER

The physical characteristics of the orbiter are summarized in table I. The longitudinal center of gravity is located at 66.25 percent of the body reference length measured from the nose. A sketch of the orbiter and its control effectors (control surfaces and RCS thrusters) is shown in figure 1. The first entry is depicted on a world map in figure 2, and figure 3 shows the time history of selected nominal trajectory parameters.

Guidance System

The guidance system has separate algorithms for the three different guidance regimes: entry, terminal area energy management, and autoland. The entry guidance is designed to take the orbiter from the atmospheric interface, 120 km, down to the initiation of the terminal-area-energy-management (TAEM) phase at approximately 26 km at Mach 2.5. At an altitude of approximately 3 km, the autoland guidance is engaged and directs the orbiter until touchdown. Since the current study was concerned with flight from $M \approx 10$ to 2.5, only the entry algorithm was needed. During entry, the angle of attack follows a preselected schedule, whereas roll angle is modulated to control both down range and cross range. Additional information on the guidance algorithms can be obtained in reference 7.

Flight Control System

The flight control system, usually referred to as the November 1976 Integrated Digital Autopilot (DAP), converts either guidance-system commands or pilot-control commands into aerodynamic control-surface deflections and reaction-control-system (RCS) thruster firings. It also takes rate gyro and accelerometer feedbacks and provides stability, damping, and turn coordination outputs to these effectors. The aerodynamic control surfaces depicted in figure 1 include elevons which are used as ailerons and elevators, rudder with speed-brake capability, and body flap for longitudinal trim. RCS thrusters are used to supplement control about the roll, pitch, and yaw axes. The roll and pitch thrusters are used only during the early portion of the entry at low dynamic pressures. The yaw RCS thrusters are used down to an altitude of 15 km. In order to approximate the effect of thrust buildup with time and the effect of thrust loss due to back-pressure increases with decreasing altitude, an average thrust level of 3870 n and a specific impulse of 289 sec was used for the study. (The following discussion, except where noted, assumes the orbiter is configured for automatic control, i.e., no pilot inputs.) During entry, the control system nulls the angle-of-attack error signal by using the pitch thrusters (dynamic pressures less than 960 Pa) and the elevons.

Control about the lateral-directional axes for dynamic pressure less than 96 Pa is achieved with roll and yaw RCS thrusters only. As the dynamic pressure increases, the ailerons are added for control. At a dynamic pressure of 480 Pa the roll thrusters are turned off. Down to about Mach 1.5, the control system operates in a "spacecraft mode," where the roll-rate command is directed to the yaw RCS channel to produce a yawing rate and a small sideslip angle β. This β generates a rolling moment because of the effective dihedral of the orbiter. In this mode, the ailerons are used for turn coordination and directional trim. The spacecraft mode was chosen for two reasons. First, the aerodynamics for this flight regime of the orbiter are such that the vehicle exhibits roll reversal

characteristics; that is, if the ailerons are used to roll the vehicle with no yaw input from any other surface or RCS, the vehicle will start to roll in the desired direction and then roll in the opposite direction. The rudder is ineffective at these angles of attack and speeds; and, thus, the RCS system would be required to coordinate the maneuver. Second, to roll about the velocity vector at high values of α requires a large yawing moment about the body axis. After Mach 1.5, the control system switches to a more conventional aircraft mode where ailerons are used for roll control and the rudder is used for turn coordination.

The body flap is a trim device used to maintain the average elevon deflection (elevator) near a preselected profile. The elevons are also used as ailerons, the characteristics of which are a function of the elevator deflection. Thus, this preselected profile is used to help insure the proper aileron characteristics.

The commanded speed-brake deflection follows a schedule down to Mach 0.9 to help maintain longitudinal trim by providing a pitch-up moment. Figure 3(b) shows the control surfaces history during a nominal first entry. More detailed information on the control system is in the appendix.

SIMULATION DESCRIPTION

The reentry flight dynamics simulator (RFDS) used for this study is a nonlinear, six-degree-of-freedom, interactive, digital computer program, with man-in-the-loop capability, developed by the NASA Langley Research Center. The cockpit is not a replica of the Space Shuttle Orbiter cockpit, but it does have the instrumentation and controls necessary for engineering investigations. The vehicle response was recorded on time-history strip charts. A more complete simulation description is available in reference 7.

TEST CONDITIONS

The off-nominal conditions considered in this evaluation involved aerodynamics, sensed angle-of-attack errors, yaw RCS thruster failures and lateral center-of-gravity offset. The Space Shuttle design specification requires that the orbiter be able to fly safely with two of the four yaw thrusters on each side inoperable (off). Because of this requirement, all runs for the study had such a failure.

The nominal and off-nominal aerodynamics used in this study were obtained from reference 6. The off-nominal values were estimated 3σ envelopes of possible variations between wind-tunnel-derived characteristics and expected full-scale flight characteristics. Because a normal distribution was assumed, the variations could be either added to or subtracted from the nominal aerodynamics. The aerodynamic data base consisted of the

six force and moment coefficients for the airframe with undeflected controls. These coefficients are functions of Mach number, angle of attack, and sideslip angle. To these are added the force and moment contribution of the control surfaces (functions of Mach number and angle of attack). The elevons (when used as an elevator), the body flap, and the speed brake are all considered to have nonlinear aerodynamic increments which are functions of Mach number, angle of attack, and surface position. The aileron and rudder both have linear aerodynamics that are a function of Mach number and angle of attack, with the aileron aerodynamics also being a function of the average elevon position. The off-nominal aerodynamics are functions of Mach number.

All possible lateral-directional combinations involving moments generated by the bare airframe and the aileron were considered in this study. Table II shows the nomenclature used in the discussion of the results to describe these 16 cases of off-nominal conditions. Examination of the aerodynamic data of reference 6 revealed that the rudder derivatives $C_{\ell_{\delta_r}}$, $C_{Y_{\delta_r}}$, and $C_{n_{\delta_r}}$ are approximately linearly dependent; therefore, they were varied together. In addition, none of the rudder derivatives were allowed to differ in sign from the nominal. All cases that have decreased rudder effectiveness are denoted by number only; if the rudder effectiveness is increased, the letter "A" is added to the case number shown in table II. Figure 4 shows the range of off-nominal lateral-directional stability and the aileron and rudder control effectiveness. The curves were generated by assuming that the angle of attack was exactly the value commanded by the guidance algorithm and that the elevator position was the desired position used by the body-flap-control logic. As shown in the appendix, the aileron is used for directional trim. This requirement places a great deal of dependence on $C_{n_{\delta_a}}$. However, figure 4(b) indicates that because of the uncertainty in the data, $C_{n_{\delta_a}}$ could switch signs below Mach 5.5 and the magnitude could vary greatly above Mach 5.5. Thus, the control system should show a high sensitivity to uncertainties in $C_{n_{\delta_a}}$. This sensitivity will be confirmed in the discussion of the results that follows.

Reference 6 also presents the longitudinal aerodynamic characteristics. However, longitudinal uncertainties were not, in general, included in the present study because reference 4 showed that variations in longitudinal aerodynamics do not impact the control of the orbiter unless: (1) the vehicle no longer can be trimmed or (2) the elevator must move to a position that adversely affects the aileron characteristics. This control system uses the body flap to maintain the proper elevator position; thus, no effects of pitching-moment variation would be expected until the body flap was forced to its limit and the elevator had to move from its desired position. In cases where this would happen, the effect of pitching-moment variation has been included.

Because angle of attack is not measured directly during the portion of the entry investigated in this study, it must be derived from onboard inertial platform data. When error sources such as platform drift and winds are considered, angle of attack can be in error by as much as $\pm 4^{\circ}$. Since the flight control system (see appendix) uses angle of attack extensively, the system should be sensitive to this error.

DISCUSSION OF RESULTS

In order to evaluate these off-nominal effects on the flying qualities of the Space Shuttle Orbiter, a test maneuver was devised to represent the maneuvering required during the entry phase. As noted earlier, the orbiter flies a preselected angle-of-attack schedule and modulates the commanded value of ϕ to control both down range and cross range. The test maneuver was to maintain the initial ϕ for a short period of time, roll 60° at maximum roll rate, and then roll back 55°. The commanded angle of attack was generated by the guidance algorithm. The test maneuver was initiated at Mach 10, Mach 7.5, Mach 5.0, and Mach 3.5 along the entry profile; and the orbiter's behavior was examined. Unless otherwise noted, all cases were flown with the automatic control system – that is, no pilot inputs.

Mach 10 Maneuver

Figure 5 shows the vehicle response with the test maneuver initiated at Mach 10 and with nominal aerodynamics, no error in sensed α, two yaw RCS thrusters on each side inoperable (off), and a lateral center-of-gravity offset of 0.0381 m. The α profile shows the orbiter transitioning from its initial α of 36° to lower values. The data indicate that the orbiter follows the prescribed α command closely with no lateral oscillation, with only minor overshoots in p and r', and with very little sideslip. The steps noted in the commanded angle-of-attack values occur because the guidance algorithm is interrogated every 1.92 sec; thus, the flight control sees the guidance commands as a series of step commands. At Mach 10, the yaw thrusters receive the roll-angle error signal and are fired to produce a body-axis yawing rate and small sideslip angle, thus allowing the effective dihedral to generate a rolling moment. The aileron is used to achieve proper coordination. The signal sent to the aileron is

$$r_{stab}(\sin \alpha)^{-1} = r' \cot \alpha - p$$

Thus, proper balance between the body-axis yawing rate and rolling rate is achieved, while r_{stab}, which is approximately $\dot{\beta}$, is minimized and, therefore, very small values of β occur in the presence of a substantial yawing rate. The yaw jets fire only to establish and stop the maneuver. The aileron deflections required to coordinate the maneuver were

approximately 0.05° and are difficult to see on figure 5. The apparent steady-state aileron deflection is the deflection required to trim the 0.0381-m lateral center-of-gravity offset.

The effects of off-nominal lateral-directional aerodynamics were investigated in combination with the failed RCS jets and the lateral center-of-gravity offset. The simulation shows that there was little effect of off-nominal aerodynamics at this Mach number (fig. 6) as the results were very similar to those with only the lateral offset and failed RCS.

Next, a sensed angle-of-attack error of -4° or $+4^{\circ}$ was added to the other off-nominal conditions. (See figs. 7 to 11.) The angle-of-attack error of -4°, which causes the vehicle to fly 4° higher than desired, results in the error signal to the aileron $r' \cot \alpha - p$ to be incorrect. The value of $\cot \alpha$ is too large by approximately 15 percent, resulting in a reduction in maximum roll rate by 15 percent. Note that this angle-of-attack error results in poorer control of β and increased yaw RCS activity. (Compare figs. 5 and 7.) Combining off-nominal aerodynamics with a sensed angle-of-attack error of -4° produced no significant difference from the case with the angle-of-attack error alone. Example cases are shown in figure 8.

The effects of a sensed angle-of-attack error of $+4^{\circ}$ (the vehicle is flying 4° lower than desired) are shown in figure 9. With this α error, $\cot \alpha$ is too small, resulting in larger than nominal roll rate. (Compare figs. 5 and 9.) In addition, there is a large roll-angle overshoot, poorer control of β, and increased yaw RCS activity. For this low α condition, off-nominal aerodynamics do influence the time histories. Cases 3, 9, 11, 12, and 15, shown in figure 10, all produce unsatisfactory responses. Case 11, figure 10(c), was the worst case observed following the Mach 10 maneuver. There was a large overshoot of the commanded roll angle; and, when the orbiter rolled back, the vehicle diverged in sideslip, rolling rate increased, and the orbiter was lost. This case was also flown manually by an astronaut with similar results. Table III shows the bare airframe characteristic modes (no stability augmentation) for both the case with nominal aerodynamics and with off-nominal aerodynamics (case 11) at the nominal angle of attack of 36° and at an angle of attack 4° lower. As indicated earlier, case 11 with no angle-of-attack error performed satisfactorily. A comparison with the bare airframe characteristics of case 11 reveals that lowering the angle of attack by 4° does not affect the characteristics significantly. Thus, the problem must be the coordination signal that is sent to the ailerons. As a result of this observation, the control system was desensitized to angle-of-attack error by multiplying the aileron turn coordination signal $r' \cot \alpha - p$ by 0.5 (approximately $\sin \alpha$ for these angles of attack) and adding a β feedback. The aileron error signal was cut in half and became $0.5(r' \cot \alpha - p) - \beta \sin \alpha$. Also, a β feedback was added to the yaw jets error signal as $\beta \cos \alpha$. Figure 11 shows the time

histories with these modifications for both the nominal aerodynamic case and case 11 with a sensed α error of $+4^{\circ}$. The response is satisfactory for both cases. However, β is, like α, derived from onboard inertial platform data and is subject to large errors. The turn coordination circuit can be modified to include sideforce (N_Y) feedback instead of β and should produce similar results. Sideforce N_Y is derived from accelerometer data and will be a more accurate signal.

In summary, with the test maneuver initiated at Mach 10, all cases with two yaw RCS thrusters on each side inoperable (off), a lateral center-of-gravity offset of 0.0381 m, and off-nominal aerodynamics with no sensed angle-of-attack error performed satisfactorily. When a sensed α error was introduced that caused the orbiter to fly at a higher-than-nominal α, the responses were still satisfactory. However, when the α error was introduced to make the orbiter fly at lower-than-nominal α, many combinations of off-nominal aerodynamics resulted in unsatisfactory characteristics and, in some cases, loss of vehicle. To correct this situation, the aileron turn coordination signal must be modified.

Mach 7.5 Maneuver

The vehicle-response results with the test maneuver initiated at Mach 7.5 are shown in figure 12. As with the nominal case at Mach 10 (fig. 5), the orbiter follows the α command closely and completes the required roll maneuver with no overshoot in p, r', or β. Cases involving the off-nominal aerodynamics (see table II) produced responses (not shown) that were similar to the nominal.

Figure 13 shows the effects of a sensed α error of -4°, which causes the orbiter to fly 4° higher than desired. Note that as with the Mach 10 cases (fig. 8), the error in cot α results in a lower maximum roll rate, poorer control of β, and increased yaw RCS activity. Again, no cases combining off-nominal aerodynamics with a sensed α error of -4° produced responses significantly different from the case with the α error alone.

Figure 14(a) shows the effects of a sensed α error of $+4^{\circ}$ (vehicle flying 4° lower than desired). This case results in loss of vehicle with nominal aerodynamics. The loss occurs for two reasons: first, the vehicle is at a lower angle of attack than at the Mach 10 maneuver so that the error in cot α produced by 4° is slightly more than the error seen at Mach 10; second, the dynamic pressure has increased from approximately 4700 to 5900 Pa so that the ailerons are more effective. Case 11, shown in figure 14(b), is again the worst case. Calculations of the characteristics of the bare airframe were made (table IV) and showed, as at $M = 10$, no significant change with decreased angle of attack. The same control-system modifications to the aileron and yaw RCS circuits that proved successful for the previous Mach 10 case were applied to this Mach 7.5 problem; and, as the results in figure 15 show, the vehicle performed satisfactorily.

In summary, when the maneuver is initiated at Mach 7.5, all cases with no error in sensed angle of attack, or an error requiring the orbiter to fly 4° higher than nominal, performed satisfactorily. However, as at Mach 10, there is an extreme sensitivity to sensed angle-of-attack errors that require the orbiter to fly 4° lower than the nominal. The modifications that produced satisfactory results at Mach 10 also produce satisfactory results at Mach 7.5.

Mach 5 Maneuver

At Mach 5, the rudder is activated and is used to augment the yaw RCS thrusters. Figure 16 shows the vehicle-response results with the maneuver initiated just before Mach 5. The control-system modifications discussed previously have been included. The orbiter performs the commanded maneuver, with only a small overshoot in roll rate and a small residual p oscillation after the maneuver.

The control system at this point is still using the ailerons for directional trim. If the static yawing and rolling moment equations are solved for trim ($\dot{p}$ and $\dot{r} = 0$) using δ_a and β as the independent variables, the determinant becomes $C_{\ell_\beta} C_{n_{\delta_a}} - C_{n_\beta} C_{\ell_{\delta_a}}$. (See ref. 7.) If the sign of this determinant changes, the direction that the aileron should move to trim the vehicle also changes. The control system has no way of determining if this sign change occurs; thus, it may move the aileron the wrong direction for trim. If this happens, the orbiter may be able to perform the maneuver, but it requires many positive yaw thruster firings to maintain the proper roll attitude following the maneuver. (See fig. 17.)

The parameter responsible for the switch in sign is $C_{n_{\delta_a}}$ which is nominally negative at these Mach numbers; however, off-nominal aerodynamics (fig. 4(b)) can make it positive. Table V shows the bare airframe characteristics along with values of the trim determinant for the nominal and some off-nominal conditions. Note that for the off-nominal aerodynamics (cases 6 and 7), the trim determinant switches signs for $\alpha = 17^{\circ}$ with $\delta_e = 0^{\circ}$. This condition occurs at approximately 40 sec in figure 17. The sign switch would occur sooner for the orbiter flying at a lower α than commanded. As seen for the cases discussed earlier, the bare airframe characteristics offer no clue as to the source of the controllability problem.

The cause of the control problem can be minimized by making $C_{n_{\delta_a}}$ more negative, which can be accomplished with a more positive elevator deflection. (See ref. 6.) Thus, to correct this trim problem, the body-flap circuit was modified to make the elevator more positive. As can be seen in the appendix, the desired elevator schedule that drives the body flap is for the elevator to ramp from 2.5° at Mach 5 to -3° at Mach 3. This modified

schedule maintains 2.5° until Mach 3.5 and then ramps to -3° at Mach 3. The effect of this elevator deflection is shown in table V where the trim determinant remains positive through $\alpha = 17^{\circ}$.

The speed-brake schedule was also modified so that the speed brake would close from 98.6° to 80°, instead of from 98.6° to 65°, between Mach 4.5 and Mach 4.0. This increased flare in the speed brake reduces the amount of pitch-down moment and, therefore, helps the body flap maintain the desired (more positive) elevator position. Figure 18(a) shows the results of off-nominal aerodynamics, case 7, with these modifications. Figure 18(b) shows the maneuver with these modifications and nominal aerodynamics and indicates that the modified schedules present no problem. All cases of the off-nominal aerodynamics with reduced rudder effectiveness had responses that were similar to those shown in figure 18.

The orbiter response with these modifications and off-nominal aerodynamics with increased rudder effectiveness was then examined. The worst case, case 5A in figure 19, resulted in an overgained rudder circuit as shown by the oscillation in p, β, α, and δ_r. Control was maintained, however, and the thruster firings were not excessive.

Figure 20 shows the effects of a sensed α error of -4° with these modifications. Again, when the orbiter flies at a higher α than desired, this α error results in a lower roll rate than nominal; but, otherwise, the vehicle response is similar to the nominal. Adding off-nominal aerodynamics with reduced rudder effectiveness produced responses similar to the case with no off-nominal aerodynamics. (Fig. 21 shows case 7 as an example.) Increased rudder effectiveness results in an overgained situation (shown in fig. 22 for case 5A) with oscillations in p, β, and δ_r, but control is maintained as it was for the case with no-sensed α error.

Figure 23 shows the effects of a sensed α error of $+4^{\circ}$ with the control modifications. As shown previously, this α error, which causes the vehicle to fly at an angle of attack 4° lower than desired, results in a higher roll rate than nominal; but, otherwise, the response was similar to the nominal case. The reduced α makes $C_{n_{\delta_a}}$ nominally less negative. (See ref. 6.) Thus, $C_{n_{\delta_a}}$ can become more positive with off-nominal aerodynamics and a sensed α error of $+4^{\circ}$ than at the nominal α. Case 7, shown in figure 24, results in increased yaw RCS thruster firings due to the more positive $C_{n_{\delta_a}}$ (compare with fig. 18(a)); and case 5A, shown in figure 25, again shows the overgained situation that can exist with a more effective rudder.

Because of the dependence of $C_{n_{\delta_a}}$ on elevon deflection, the negative pitching-moment uncertainty of reference 6 was added to the analysis. With a sensed α error

The control system displayed the following three main weaknesses:

(1) An extreme sensitivity to error was noted in derived angle of attack.

(2) Some off-nominal aerodynamic combinations caused the aileron, which provides the directional trim control for much of the entry, to actually deflect the wrong way.

(3) Off-nominal aerodynamics which produced an increased rudder effectiveness could result in an overgained control circuit.

Many of these weaknesses could lead to a loss of the orbiter. Modifications to the control system and pilot intervention techniques were designed that allowed the orbiter to fly safely under all the assumed off-nominal conditions.

Langley Research Center
National Aeronautics and Space Administration
Hampton, VA 23665
May 15, 1980

APPENDIX

DESCRIPTION OF THE NOVEMBER 1976 INTEGRATED DIGITAL AUTOPILOT FLIGHT CONTROL SYSTEM

The flight control system used in this simulation (known as the November 1976 Integrated Digital Autopilot) is designed to provide orbiter stability and control from after deorbit to touchdown. The system takes guidance system commands in the automatic mode and pilot commands in the manual mode and produces reaction-control-system (RCS) thruster commands and/or aerodynamic-control-surface deflection commands to the actuators. The pilot inputs include rotation-hand-controller deflections in pitch and roll, rudder-pedal command, speed-brake position command, body-flap rate command, panel-mounted rate trims (roll, pitch, and yaw), and system mode switches. Multiple RCS thrusters are located on pods at the base of the vertical tail (fig. 1) and provide roll, yaw, and pitching-moment capability. The aerodynamic surfaces include elevons, differentially deflected elevons (referred to as the aileron), rudder, speed brake, and body flap. This appendix describes the flight-control-system software in detail.

Notation

The flight control system was designed for measurements in the U.S. Customary Units. Therefore, units are given in both the SI and U.S. Customary Units.

ADI normal-acceleration error for flight director, g units

ADIF filtered normal-acceleration error for flight director, g units

AL approach and landing guidance

ALFERR angle-of-attack error, deg

ALFERRL limited angle-of-attack error, deg

ALPDG angle of attack, deg

ALPHACM entry-guidance angle-of-attack command, deg

ALPHCMS smoothed entry-guidance angle-of-attack command, deg

AUTO autopilot control mode

APPENDIX

BANKERR	roll-angle error, deg
BANKYAW	roll-rate command, deg/sec
BCSL	filtered pitch-rate error, deg/sec
BETAF	filtered angle of sideslip, deg
BETDG	angle of sideslip, deg
BFT	commanded body-flap-deflection rate, deg/sec
BFTI	body-flap-deflection command, deg
BINC	increment used in description of FADER
CM	guidance-system command used in description of SMOOTHER
CMS	smoothed command used in description of SMOOTHER
COSALP	cosine of angle of attack
COSPHIL	cosine of limited sensed roll angle
COSTHE	cosine of pitch angle
COTALP	cotangent of angle of attack
DAM	roll rotation-hand-controller (RHC) command, deg
DAMS	shaped roll-stick command, deg
DAMSF	filtered roll-stick command, deg
DAMTR	roll-panel-trim command
DAMTRS	roll-panel-trim rate, deg/sec
DAT	aileron-trim rate, deg/sec

APPENDIX

DATRIM aileron-trim command, deg

DAY lateral-acceleration error, g units

DAYF filtered lateral-acceleration error, g units

DBFDC body-flap-deflection-rate change

DBFPC body-flap-deflection command, deg

DBFRM manual body-flap command, deg/sec

DEC preliminary elevator-deflection command, deg

DECC preliminary elevator command, deg

DEL left-elevon-command rate, deg/sec

DELAC aileron-deflection command, deg

DELBF body-flap-position feedback, deg

DELBFRC commanded body-flap-deflection change, deg

DELEC elevator-deflection command, deg

DELEFB elevator-position feedback, deg

DELELC rate-limited left-elevon-deflection command, deg

DELELT left-elevon-deflection command, deg

DELERC rate-limited right-elevon-deflection command, deg

DELERT right-elevon-deflection command, deg

DELES preliminary pitch-trim command, deg

DELRC rate-limited rudder-deflection command, deg

DELRCP past value of rate-limited rudder-deflection command, deg

DELSBC rate-limited speed-brake-deflection command, deg

DELSBCP past value of rate-limited speed-brake-deflection command, deg

DELSBE speed-brake-increment cross feed, deg

DEM pitch-rotation-hand-controller command, deg

DEMS shaped-pitch-controller command, deg

DEMTR panel-pitch trim, deg/sec

DEMTRS trim rate due to panel-pitch trim, deg/sec

DER right-elevon-command rate, deg/sec

DETRIM pitch-trim command, deg

DNCAL turn-compensated pitch rate, deg/sec

DPJET pitch-rate error, deg/sec

DR coordinated rudder command, deg

DRC rudder-deflection command, deg

DRCRL rudder-deflection-command rate, deg/sec

DRF filtered rudder-deflection command, deg

DRFS rudder-trim rate, deg/sec

DRFSI rudder-trim command, deg

DRI rudder command, deg

DRINCLM rudder-command-rate limit, deg/sec

APPENDIX

DRJET yaw-rate error, deg/sec

DRM rudder-pedal command, deg

DRMS shaped-rudder-pedal command, deg

DRPC rudder command, deg

DRRC yaw-rate error, deg/sec

DRT filtered rudder-deflection command, deg

DSBC speed-brake command, deg

DSBCM guidance speed-brake command, deg

DSBCOM entry-guidance speed-brake command schedule, deg

DSBM manual speed-brake command, deg

DSBNLM negative speed-brake-rate limit, deg/sec

DSBPLM positive speed-brake-rate limit, deg/sec

DSBRL speed-brake-deflection-command rate, deg/sec

EARLY flight-control-system subphase

ENTRY entry guidance

ERRNZ pitch rate due to normal-acceleration error, deg/sec

ERRNZF filtered pitch rate due to normal-acceleration error, deg/sec

FADER signal fading logic

FADOFF FADER logic flag

FLATURN flat-turn regime

GBFT body-flap-positive-deflection-limit schedule, deg

GDAC gain to convert roll-rate error into aileron command, deg/(deg/sec)

GDAM gain to convert roll-stick command to rate command, (deg/sec)/deg

GDAY gain to convert lateral-acceleration error to yaw-rate command, (deg/sec)/g units

GDBF gain to scale body-flap-deflection rate, deg/sec

GDEM gain to convert pitch-controller command into pitch-rate command, (deg/sec)/deg

GDQ gain to convert pitch-rate error into elevator command, deg/(deg/sec)

GDRE gain to convert yaw-rate error into rudder command, deg/(deg/sec)

GDRF gain to convert rudder command to rudder-trim rate, deg/(deg/sec)

GGDRC gain to convert yaw-rate error to rudder command, deg/(deg/sec)

GLIN linear coefficient in roll-stick shaping, deg/deg

GNY gain to convert rudder-pedal command to lateral-acceleration command, g units per degree

GNZ airspeed-variable gain

GPDAC scale factor

GPE gain to convert compensated roll-rate error into aileron command, deg/(deg/sec)

GPIT variable used to calculate GDQ, $\frac{\text{deg } (\text{N/m}^2)^{1/2}}{\text{deg/sec}} \left(\frac{\text{deg } (\text{lb/ft}^2)^{1/2}}{\text{deg/sec}} \right)$

GPPHI gain to convert roll-angle error to roll-rate command, (deg/sec)/deg

GQAL	gain to convert angle-of-attack error into pitch-rate command, (deg/sec)/deg
GRJ	gain to scale RCS thruster pulses into trim rate, deg/sec
GRPF	gain to scale filtered yaw rate
GSBB	scaling gain to convert trim increment into trim rate, (deg/sec)/deg
GSBP	gain to convert speed-brake increment into pitch-trim increment
GTEMB	gain to scale coordinating rudder command
GTRE	gain to convert preliminary pitch-trim command into pitch-trim rate, (deg/sec)/deg
GUIDDT	guidance-system step size, sec
GUY	gain to convert pitch RCS thruster command into pitch-trim rate, deg/sec
GXALR	gain to convert aileron command to coordinating rudder command
HA	altitude, m (ft)
HS	SMOOTHER step size, sec
H1	flight-control fast-cycle time, sec
IMAJ	SMOOTHER control flag
KGDRE	variable used for computation of GDRE
LATE	flight-control-system subphase
MACH	Mach number
MANBF	pilot-commanded body-flap mode
MANP	pilot-commanded pitch mode

MANRY	pilot-commanded roll and yaw modes
MANSB	pilot-commanded speed-brake mode
NUM	number of FADER steps remaining
NY	lateral-acceleration feedback, g units
NZ	normal-acceleration feedback, g units
NZCM	TAEM/AL guidance normal-acceleration command, g units
NZCMS	smoothed guidance normal-acceleration command, g units
PAR	coefficient of squared term in roll-stick shaping, deg/deg^2
PC	roll-rate command, deg/sec
PCLIM	roll-rate limit, deg/sec
PCP	roll-stick-rate command, deg/sec
PDAC	scaled aileron command, deg
PDACF	filtered aileron command, deg
PDG	sensed roll rate, deg/sec
PE	roll-rate error, deg/sec
PES	compensated roll-rate error, deg/sec
PHICM	guidance roll-angle command, deg
PHICMS	smoothed guidance roll-angle command, deg
PHIDG	sensed roll angle, deg
PSTABDG	stability-axis roll rate, deg/sec

QB dynamic pressure, N/m^2 (lb/ft^2)

QC pitch-rate command, deg/sec

QCAL pitch-rate error, deg/sec

QDG sensed pitch rate, deg/sec

QTR pitch-trim rate, deg/sec

QTRU unlimited pitch-trim rate, deg/sec

RDG sensed yaw rate, deg/sec

RJPULSE net RCS thruster pulses

RLIMR rudder-deflection limit, deg

RNZ = (GNZ)(NZCMS)

RP = (RDG) - $\left[(RTDG)(SINPHI)(COSTHE)\right]/V$, deg/sec

RSTAB scaled stability-axis yaw rate, deg/sec

RSTABG gain to scale yaw rate

RTDG = 57.3 g, deg-m/sec^2 (deg-ft/sec^2)

RTPHI = (RDG)(TANPHI), deg/sec

SINALP sine of angle of attack

SINPHI sine of roll angle

SMERR command increment used in each SMOOTHER step

SMOOTHER guidance-command smoothing logic

TAEM terminal-area-energy-management guidance

TANPHI	tangent of roll angle
TEMA	lateral-acceleration command due to rudder pedals, g units
TEMB	preliminary aileron command, deg
TEMD	guidance yaw-rate command, deg/sec
TEME	coordinating rudder command, deg
TEMF	elevator trim-deflection error, deg
TEMI	scaled coordinating rudder command, deg
THEPHI	= -(COSTHE)/(COSPHIL)
TRBF	scheduled elevator trim deflection, deg
UIN	combination of roll and yaw RCS thrusters commanded to fire on current pass
UINP	past value of UIN
UXC	number of roll RCS thrusters commanded to fire
UYC	number of pitch RCS thrusters commanded to fire
UZC	number of yaw RCS thrusters commanded to fire
V	airspeed, m/sec (ft/sec)
X	past value of signal to be faded
XNEW	current value of signal to be faded
YALCM	guidance yaw-rate command, deg/sec
YAWJET	yaw-rate error, deg/sec
Z	Z-transform variable

APPENDIX

Description of Flight Control System

The block diagrams of the flight control system are presented in figures 35 to 44. The system was designed to minimize the time required to complete the flight-control calculations in the onboard digital computers. Thus, several computational frequencies exist among the various signal paths of the flight control system. The particular frequency for a path is indicated on the block diagram either in the figure legend or by the dashed boxes around the control-system signal paths.

Many of the guidance commands are computed at a significantly lower frequency than that used by the flight control system (PHICM in fig. 35(a)); thus, a smoothing function (SMOOTHER) is used to give the control system a more continuous command signal during that period when the RCS is active. The SMOOTHER logic is presented in sketch (a).

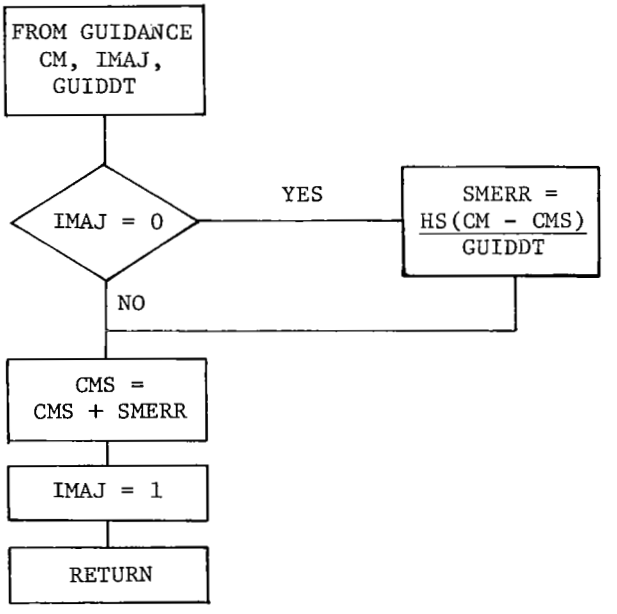

Sketch (a).

Each time the guidance algorithm is computed (low frequency), a new command (CM) is sent to the SMOOTHER and IMAJ is set to zero. Thus, SMERR is computed only when the guidance system is computed. Since HS is the flight-control-system sample time (higher frequency) for the SMOOTHER element and GUIDDT is the guidance-system sample time (lower frequency), SMERR is the fraction of the command change for each SMOOTHER step, which when added successively (i.e., CMS = CMS + SMERR for each flight-control-system step) will equal CM by the time the guidance system is computed again. Two observations should be noted: First, for the SMOOTHER to operate properly, the guidance-system sample time must be an integer multiple of the control-system

sample time; second, the value of CMS used in the calculation of SMERR is simply the output command of the SMOOTHER when the guidance command CM update occurs.

Since the vehicle angle of attack and the Mach number change considerably throughout the entry and, consequently, the aerodynamic characteristics change significantly, considerable control system modification is required. To attain proper stability augmentation and roll-angle control with the changing aerodynamics, the roll and yaw axes have two modes of operation. The first mode incurred during the entry; the EARLY, or spacecraft mode, uses the yaw thrusters to produce a yawing rate and a small sideslip angle which results in a rolling moment due to the effective dihedral of the orbiter. The yawing moment produced by the ailerons is used to provide turn coordination. Because the rudder is shielded from the free stream, it is not activated until the speed is reduced to Mach 5. At this point the rudder is used to augment the yaw RCS. Late in the entry after the orbiter pitches down to lower angles of attack and the rudder has become effective, the flight control system switches to the LATE or aircraft mode where the ailerons are used to produce a rolling rate and the rudder is deflected to coordinate the turn. This switch from EARLY to LATE nominally occurs at Mach 1.5, but the pilot can force this change anytime. In order to prevent undesirable switching transients from propagating through the system, signal fading logic (FADER) is used in both the aileron- and rudder-command channels. (See figs. 35(b) and 37(b).) This logic is illustrated in sketch (b).

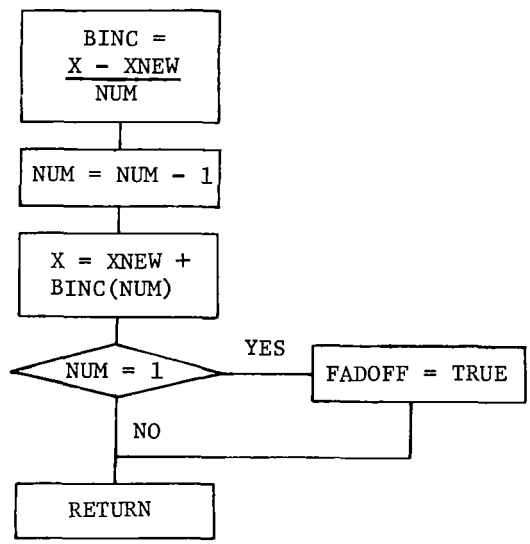

Sketch (b).

When a signal source is changed, the old signal must be faded out. FADOFF is set false in the main flight-control code which allows the FADER subroutine to be called. The parameter NUM is calculated on the first pass only by multiplying the flight-control-system

frequency by the fade time in seconds. In this system design, the fade time was 1 sec. The value of X used in the first pass to calculate the bias BINC is the value of the parameter being faded on the previous pass through the control system, and XNEW is the value of this parameter on the current pass. For recalculation of BINC, X is retained on each pass. Thus, the parameter being faded is successively changed from the initial value of X to XNEW as NUM approaches a value of 1. When NUM does reach 1, FADOFF is set TRUE and the FADER subroutine is bypassed.

Roll axis.- The aileron command and roll RCS command control laws are presented in figures 35 and 36. Figure 35(a) shows how either the roll-stick command (DAM) or the smoothed roll-angle-guidance command (PHICM → PHICMS), depending on pilot selection in the cockpit, is converted to roll-rate commands (PC). In the EARLY mode, either the signal PCP derived from the stick input or the difference between the guidance command PHICM and the actual roll angle PHIDG is sent to the yaw channel to execute the roll maneuver. In the LATE mode, the difference between the commanded roll rate PC and the actual stability-axis roll rate PSTABDG is calculated, converted to an aileron-deflection command, TEMB, and sent on to the aileron. Figure 35(b) shows that the aileron-deflection command in both the EARLY and LATE modes is scaled by a function of dynamic pressure GPDAC and then filtered by a second-order bending filter to prevent any of the bending modes from driving the aileron command PDACF. The aileron-trim calculation DATRIM is also a function of EARLY/LATE mode and Mach number switching. (See fig. 35(b).) For both of these switches in the trim network, the FADER is triggered to eliminate transients due to the switching. For Mach numbers greater than 3.5 and dynamic pressures QB greater than 96 Pa (2 lb/ft^2), the aileron trim is a function of RJPULSE, the output of a pulse counter diagramed in sketch (c).

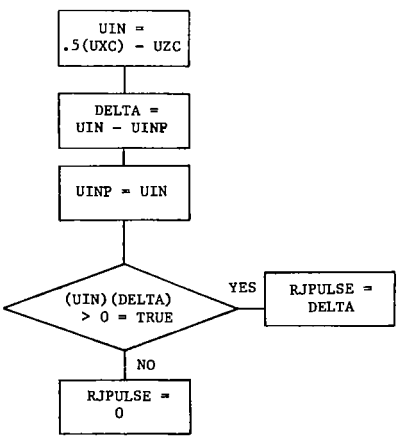

Sketch (c).

APPENDIX

The pulse counter takes the roll RCS (i.e., the UXC) and yaw RCS (i.e., the UZC) thruster commands and determines if the aileron-trim function should be changed. If the magnitude of the combination of roll and yaw RCS commands (UIN) increases from one step of the flight control system to the next and the sign doesn't change or if the signs of both UIN and DELTA change, the RJPULSE value will cause the integrated value DATRIM to change. When the control system switches to the LATE mode, the aileron-trim integrator is driven by the forward-loop signal PDACF and the panel trim DAMTR, as shown in figure 35(b).

The roll RCS command (UXC), shown in figure 36, is driven by the turn-coordination signal PE which passes through a hysteresis filter. The operation of these types of filters is described in appendix B of reference 8. The signal PE is also sent to the aileron in the EARLY mode and goes through a deadband to remove any low amplitude signal (sensor noise) in the channel. (See fig. 35(b).)

Yaw axis.- The rudder and yaw RCS command diagrams are presented in figures 37 and 38. Again, the EARLY and LATE modes determine the signal source. In the LATE mode (fig. 37(a)), a side-acceleration command (TEMA) from the rudder pedals (DRM) in the cockpit is compared to the side acceleration NY to generate a side-acceleration error which is filtered and converted to a yaw-rate command. This yaw-rate command is summed with the stability-axis yaw rate RSTAB and a guidance-system yaw-rate command YALCM when the approach and landing guidance AL is engaged. The resultant yaw-rate error DRRC is sent to both the rudder, figure 37(b), and the yaw thrusters, figure 38. Also in the LATE mode (fig. 37(b)), an aileron cross-feed term (TEMB) is sampled to provide a coordinated rudder command (DR). This signal is filtered and limited to form the rudder-deflection command DRC. In the EARLY mode, the roll-stick command (DAM to PCP) or the guidance-roll command (PHICM to BANKERR) is used to generate a yaw-rate error YAWJET (fig. 38) which is sent to the yaw thrusters DRJET and to the rudder, (DRPC) = (GDRE) (YAWJET), below Mach 5. The switching between EARLY and LATE triggers the FADER (fig. 37(b)) to eliminate switching transients. The yaw thrusters remain on until an altitude of 15 km (50 000 ft) is reached to provide sufficient control power in the yaw axis.

Pitch axis.- The elevator and pitch RCS command diagrams are presented in figures 39 and 40. Figure 39(a) shows that a pitch-rate command QC is generated either by converting a stick command DEM from the cockpit in the manual pitch mode, or by either an angle-of-attack error ALFERR or a normal-acceleration command NZCM, depending on the guidance phase. In the approach and landing guidance phase, the NZCM signal is not smoothed since the guidance and flight control systems are being sampled at the same frequency. Also, a filtered normal-acceleration error ADIF is sent to the attitude-director-indicator error needles. The pitch-rate command QC is compared to the actual

pitch rate QDG as shown in figure 39(b). This error signal QCAL is also compensated for the pitch rate due to yawing at large roll angles RTPHI in the TAEM and AL guidance phases. The pitch-rate error QCAL is filtered, scaled to an elevator deflection, compared to the trim elevator setting DETRIM, filtered by a second-order bending filter, and limited to form the elevator-deflection command DELEC.

For dynamic pressures less than 960 Pa (20 lb/ft^2), a forward loop trim integrator (fig. 39(c)) with compensation for pitch RCS thruster firings (UYC) is used to determine the elevator trim value DETRIM. For higher dynamic pressures, the actual elevator position DELEFB and speed-brake command increment DELSBE are cross fed to the elevator trim. DEMTR is the pitch panel trim from the cockpit.

The pitch RCS thrusters (fig. 40) are turned off when QB reaches 960 Pa (20 lb/ft^2). In the AUTO mode the angle-of-attack error signal derived from the guidance command, ALFERRL, is compared to the pitch rate QDG to form a pitch-rate error DPJET which is used to command the thruster firings. In the manual mode MANP, the pitch-rate command QC derived from the hand controller is used to form the pitch-rate error DPJET.

Body-flap command.- The body flap responds to either a manual pilot command DBFRM or, in the automatic mode, to the difference between the elevon pitch trim DETRIM and the scheduled value TRBF. (See fig. 41.) This body-flap mechanization is designed to keep the elevator at the deflection required to obtain the desired yaw due to aileron. The body-flap-rate command BFT is integrated, limited, and then compared to the actual body-flap position DELBF. The command signal DELBFRC to the actuator scaling software program is a rate command. When the orbiter reaches the first flare maneuver, just prior to touchdown, the AL guidance sends a body-flap-retract signal, and the body flap is driven to its undeflected position (DBFPC = 0°) for landing.

Speed-brake command.- The speed-brake command (fig. 42) is a function of the limited speed-brake deflection DSBM in the manual speed-brake mode. In the automatic mode, the command follows a schedule DSBCOM during the entry guidance phase and a guidance-system command during the TAEM and AL guidance phases. The command from the guidance system is $\delta_{SB} = 65^{\circ}$ until $M = 0.9$, where the speed brake becomes an active energy control device.

Control-surface rate limiting.- The elevator, aileron, rudder, and speed-brake commands (DELEC, DELAC, DRC, and DSBC, respectively) are subject to software rate-limiting logic which is diagramed in figures 43 and 44. This logic limits the step change in the aerodynamic-surface command to either the maximum surface rate or to a rate consistent with the hydraulic power available. The elevons which deflect due to elevator and aileron commands are rate limited only by the maximum actuator rate. The rudder and speed brake are limited, based on the elevon rates, the hydraulic fluid flow, and the

number of auxiliary power units operating. (DRINCLM, DSBNLM, and DSBPLM are functions of these conditions.) Also, the speed brake may be required to move, based on rudder demand.

REFERENCES

1. Space Shuttle. NASA SP-407, 1976.

2. Carrier, L. M.; and Minor, R. G.: Space Shuttle Orbiter Avionics. A Collection of Technical Papers – AIAA 2nd Digital Avionics Systems Conference, Nov. 1977, pp. 146-156. (Available as AIAA Paper 77-1501.)

3. Brand, Vance D.: Return to Earth in the Space Shuttle. 1977 Report to the Aerospace Profession, Tech. Rev., vol. 13, no. 4, Soc. Exp. Test Pilots, c.1978, pp. 223-231.

4. Stone, Howard W.; and Powell, Richard W.: Entry Dynamics of Space Shuttle Orbiter With Longitudinal Stability and Control Uncertainties at Supersonic and Hypersonic Speeds. NASA TP-1084, 1977.

5. Stone, Howard W.; and Powell, Richard W.: Entry Dynamics of Space Shuttle Orbiter With Lateral-Directional Stability and Control Uncertainties at Supersonic and Hypersonic Speeds. NASA TP-1011, 1977.

6. Aerodynamic Design Data Book. Volume I: Orbiter Vehicle. NASA CR-60386, 1978.

7. Rowell, Lawrence F.; Powell, Richard W.; and Stone, Howard W., Jr.: Development of the Reentry Flight Dynamics Simulator for Evaluation of Space Shuttle Orbiter Entry Systems. NASA TP-1700, 1980.

8. Kaylor, Jack T.; Rowell, Lawrence F.; and Powell, Richard W.: A Real-Time Digital Computer Program for the Simulation of Automatic Spacecraft Reentries. NASA TM X-3496, 1977.

TABLE I.- ENTRY PHYSICAL CHARACTERISTICS OF SPACE SHUTTLE ORBITER

Mass properties:	
Mass, kg	83 388
Moments of inertia:	
I_X, kg-m^2	1 169 236
I_Y, kg-m^2	8 729 397
I_Z, kg-m^2	8 991 771
I_{XY}, kg-m^2	3868
I_{XZ}, kg-m^2	-218 615
I_{YZ}, kg-m^2	3441
Wing:	
Reference area, m^2	249.91
Mean aerodynamic chord, m	12.06
Span, m	23.79
Elevon (per side):	
Reference area, m^2	19.51
Mean aerodynamic chord, m	2.30
Rudder (per side panel):	
Reference area, m^2	9.30
Mean aerodynamic chord, m	1.86
Body flap:	
Reference area, m^2	12.54
Mean aerodynamic chord, m	2.06

TABLE II.- OFF-NOMINAL AERODYNAMIC VARIATIONS[a]

Case (b)	C_{n_β}	C_{ℓ_β}	$C_{n_{\delta_a}}$	$C_{\ell_{\delta_a}}$	$C_{Y_{\delta_r}}$	$C_{n_{\delta_r}}$	$C_{\ell_{\delta_r}}$
1	-	-	-	-	-	+	-
2	+	-	-	-	-	+	-
3	-	+	-	-	-	+	-
4	+	+	-	-	-	+	-
5	-	-	+	-	-	+	-
6	+	-	+	-	-	+	-
7	-	+	+	-	-	+	-
8	+	+	+	-	-	+	-
9	-	-	-	+	-	+	-
10	+	-	-	+	-	+	-
11	-	+	-	+	-	+	-
12	+	+	-	+	-	+	-
13	-	-	+	+	-	+	-
14	+	-	+	+	-	+	-
15	-	+	+	+	-	+	-
16	+	+	+	+	-	+	-

[a]A plus sign indicates aerodynamic variation is added to nominal coefficient; a minus sign indicates aerodynamic variation is subtracted from nominal coefficient.

[b]An "A" after case number indicates that rudder coefficients $C_{Y_{\delta_r}}$, $C_{n_{\delta_r}}$, and $C_{\ell_{\delta_r}}$ change signs.

TABLE III.- LATERAL-DIRECTIONAL BARE-AIRFRAME CHARACTERISTICS AT MACH 10

Case	Angle of attack, deg	$(C_{n_\beta})_{dyn}$	Oscillatory modes	
			1	2
Nominal aerodynamics	36	0.0097	P = 4.2 sec $t_{1/2}$ = 53.7 sec	P = 1833 sec $t_{1/2}$ = 248 sec
11	36	.0075	P = 4.8 sec $t_{1/2}$ = 9.4 sec	P = 1306 sec $t_{1/2}$ = 317 sec
Nominal aerodynamics	32	.0076	P = 4.8 sec $t_{1/2}$ = 54 sec	P = 1634 sec $t_{1/2}$ = 240 sec
11	32	.0055	P = 5.6 sec $t_{1/2}$ = 9.4 sec	P = 1132 sec $t_{1/2}$ = 355 sec

TABLE IV.- LATERAL-DIRECTIONAL BARE-AIRFRAME CHARACTERISTICS AT MACH 7.5

Case	Angle of attack, deg	$(C_{n_\beta})_{dyn}$	Oscillatory modes	
			1	2
Nominal aerodynamics	30	0.0064	P = 4.7 sec $t_{1/2}$ = 30.8 sec	P = 878 sec $t_{1/2}$ = 159 sec
11	30	.0045	P = 5.7 sec $t_{1/2}$ = 5.5 sec	P = 629 sec $t_{1/2}$ = 323 sec
Nominal aerodynamics	26	.0056	P = 5.1 sec $t_{1/2}$ = 32.0 sec	P = 817 sec $t_{1/2}$ = 164 sec
11	26	.0036	P = 6.4 sec $t_{1/2}$ = 5.6 sec	P = 577 sec $t_{1/2}$ = 404 sec

TABLE V.- LATERAL-DIRECTIONAL BARE-AIRFRAME CHARACTERISTICS AT MACH 5

Case	α, deg	$(C_{n_\beta})_{dyn}$	Trim determinant function, $C_{\ell_\beta} C_{n_{\delta_a}} - C_{n_\beta} C_{\ell_{\delta_a}}$	Oscillatory modes		Aperiodic modes			
				1	2	1	2	3	4
$\delta_e = 0^o$									
Nominal aerodynamics	21	0.0026	1.529×10^{-6}	P = 6.4 $t_{1/2}$ = 20.9	P = 293 $t_{1/2}$ = 35.4				
5	21	.0032	8.004×10^{-7}	P = 5.9 $t_{1/2}$ = 2.68	P = 284 $t_{1/2}$ = 36.2				
6	21	.0041	3.320×10^{-7}			$t_{1/2}$ = 44.7	$t_{1/2}$ = 36.8	$t_{1/2}$ = 5.8	$t_{1/2}$ = 0.03
7	21	.0011	8.620×10^{-7}			$t_{1/2}$ = 3183	$t_{1/2}$ = 23.7	$t_{1/2}$ = 10.2	$t_{1/2}$ = 0.0004
Nominal aerodynamics	17	.0027	8.180×10^{-7}	P = 6.2 $t_{1/2}$ = 18.6	P = 333 $t_{1/2}$ = 39.6				
5	17	.0031	1.843×10^{-7}	P = 5.9 $t_{1/2}$ = 2.2	P = 292 $t_{1/2}$ = 43.5				
6	17	.0040	-1.371×10^{-7}			$t_{1/2}$ = 62	$t_{1/2}$ = 37.3	$t_{1/2}$ = 5.9	$t_{1/2}$ = 0.02
7	17	.0014	-8.225×10^{-6}			$t_{1/2}$ = 4082	$t_{1/2}$ = 29.3	$t_{1/2}$ = 9.1	$t_{1/2}$ = 0.0004
$\delta_e = 2.5^o$									
Nominal aerodynamics	21	0.0027	1.837×10^{-6}	P = 6.3 $t_{1/2}$ = 20.9	P = 297 $t_{1/2}$ = 35.3				
5	21	.0033	1.189×10^{-6}	P = 5.8 $t_{1/2}$ = 2.6	P = 287 $t_{1/2}$ = 36.1				
6	21	.0042	6.098×10^{-7}			$t_{1/2}$ = 44.7	$t_{1/2}$ = 36.6	$t_{1/2}$ = 5.8	$t_{1/2}$ = 0.03
7	21	.0011	1.182×10^{-6}			$t_{1/2}$ = 3126	$t_{1/2}$ = 23.7	$t_{1/2}$ = 10.2	$t_{1/2}$ = 0.0004
Nominal aerodynamics	17	.0028	1.024×10^{-6}	P = 6.1 $t_{1/2}$ = 18.6	P = 337 $t_{1/2}$ = 39.4				
5	17	.0031	4.595×10^{-6}	P = 5.9 $t_{1/2}$ = 2.2	P = 295 $t_{1/2}$ = 43.2				
6	17	.0041	4.057×10^{-8}			$t_{1/2}$ = 61.4	$t_{1/2}$ = 37.4	$t_{1/2}$ = 5.9	$t_{1/2}$ = 0.02
7	17	.0014	5.002×10^{-7}			$t_{1/2}$ = 4009	$t_{1/2}$ = 29.3	$t_{1/2}$ = 9.1	$t_{1/2}$ = 0.0004

TABLE VI.- LATERAL-DIRECTIONAL BARE-AIRFRAME CHARACTERISTICS AT MACH 3.5

Case	α, deg	$\left(C_{n_\beta}\right)_{dyn}$	Trim determinant function, $C_{\ell_\beta} C_{n_{\delta_a}} - C_{n_\beta} C_{\ell_{\delta_a}}$	Oscillatory modes		Aperiodic modes			
				1	2	1	2	3	4
Nominal aerodynamics	17	0.0021	1.012×10^{-6}	P = 6.7 $t_{1/2}$ = 8.4	P = 143 $t_{1/2}$ = 29.1				
5	17	.0027	3.169×10^{-7}	P = 6.5 $t_{1/2}$ = 1.1	P = 151 $t_{1/2}$ = 30.9				
7	17	.0007	4.652×10^{-7}			$t_{1/2}$ = 163	$t_{1/2}$ = 16.8	$t_{1/2}$ = 4.5	$t_{1/2}$ = 0.01
Nominal aerodynamics	13	.0024	2.699×10^{-7}	P = 6.2 $t_{1/2}$ = 10.1	P = 231 $t_{1/2}$ = 23.9				
5	13	.0028	-2.253×10^{-7}	P = 6.6 $t_{1/2}$ = 1.0	P = 195 $t_{1/2}$ = 28.8				
7	13	.0012	-3.742×10^{-8}			$t_{1/2}$ = 191	$t_{1/2}$ = 21.1	$t_{1/2}$ = 4.8	$t_{1/2}$ = 0.01

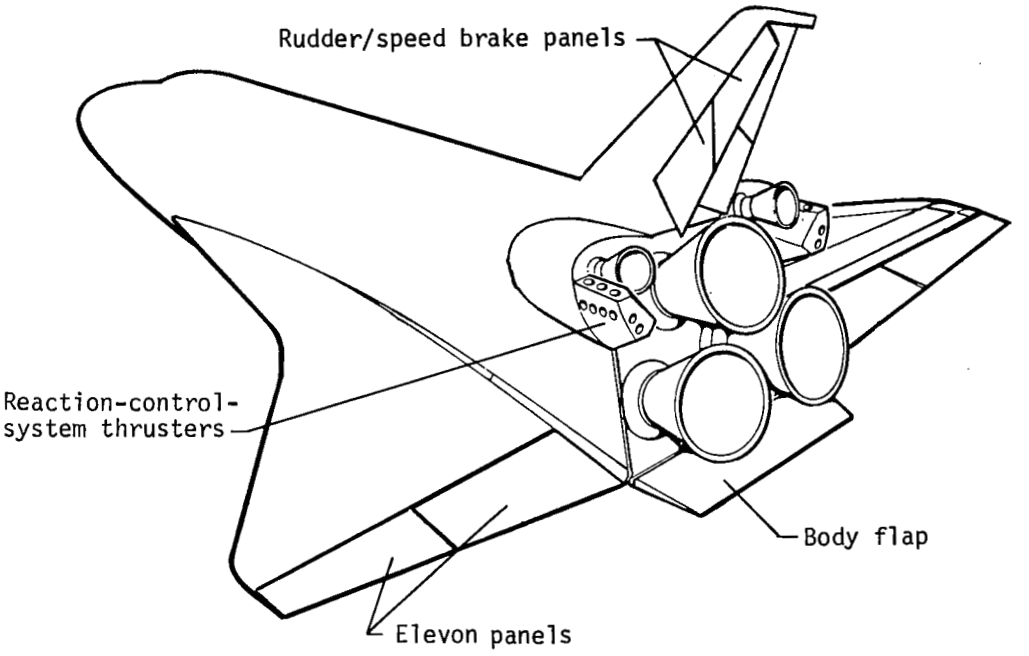

Figure 1.- Sketch of Space Shuttle Orbiter.

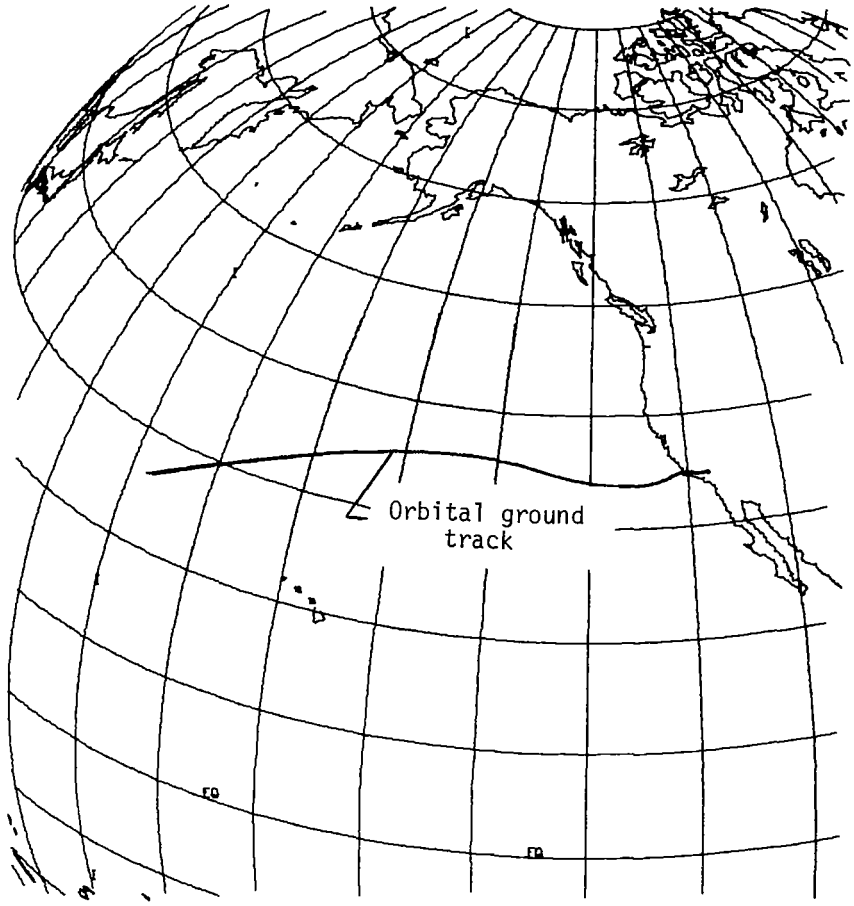

Figure 2.- First entry of Space Shuttle Orbiter.

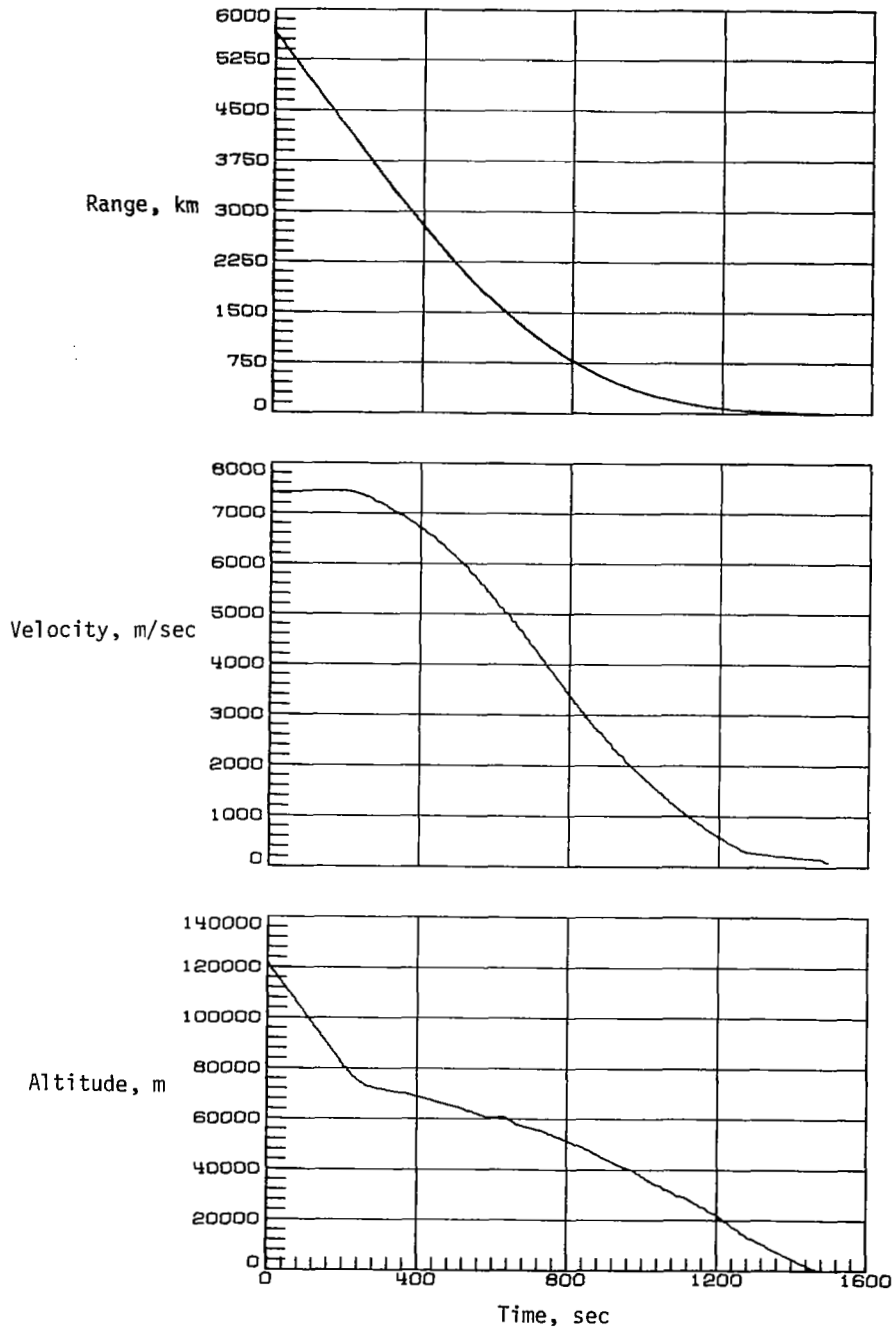

(a) State conditions.

Figure 3.- Trajectory parameters of Space Shuttle Orbiter for first entry.

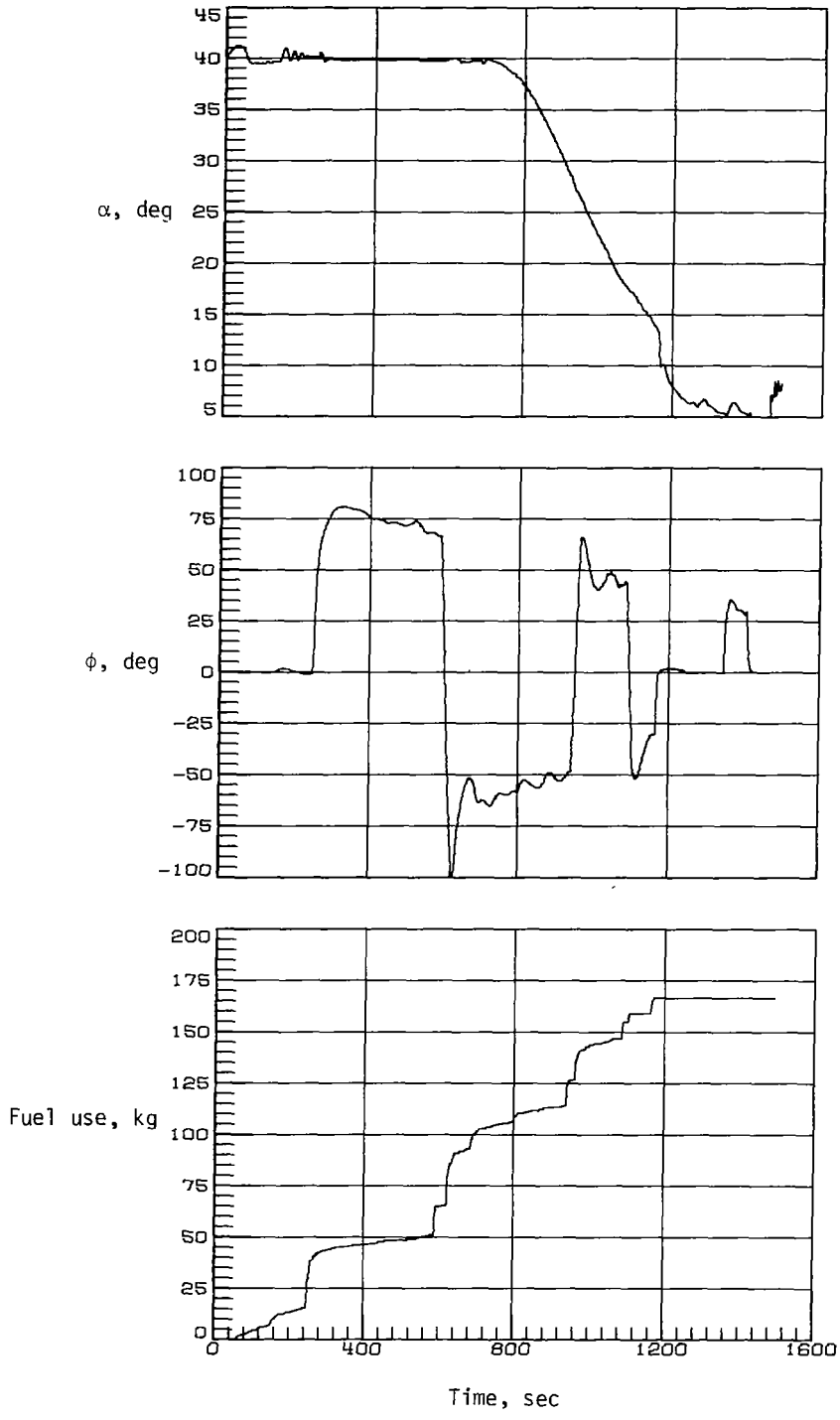

(a) Concluded.

Figure 3.- Continued.

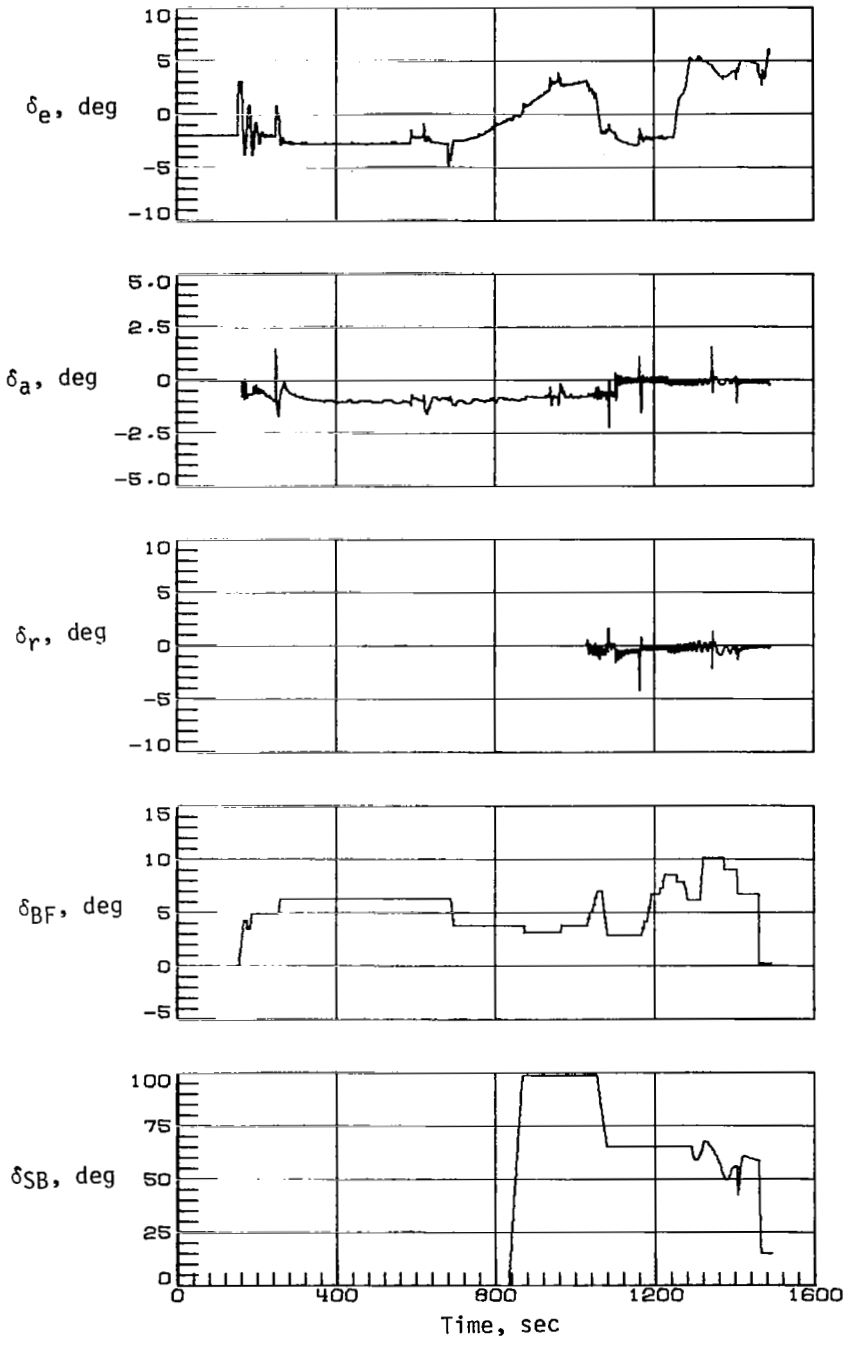

(b) Control history.

Figure 3.- Concluded.

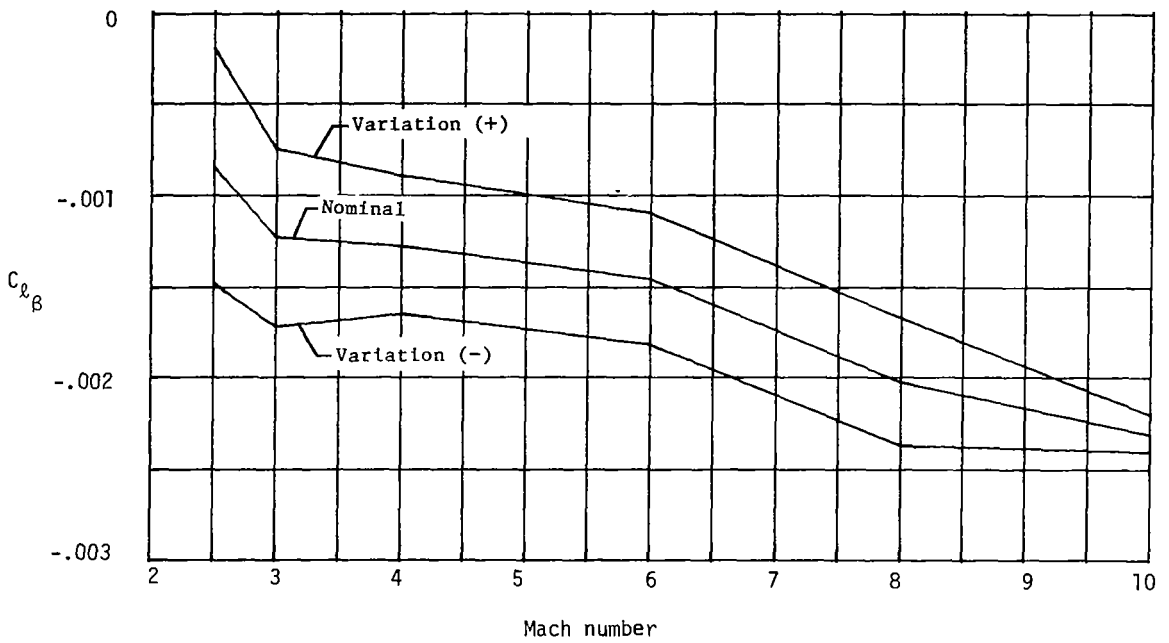

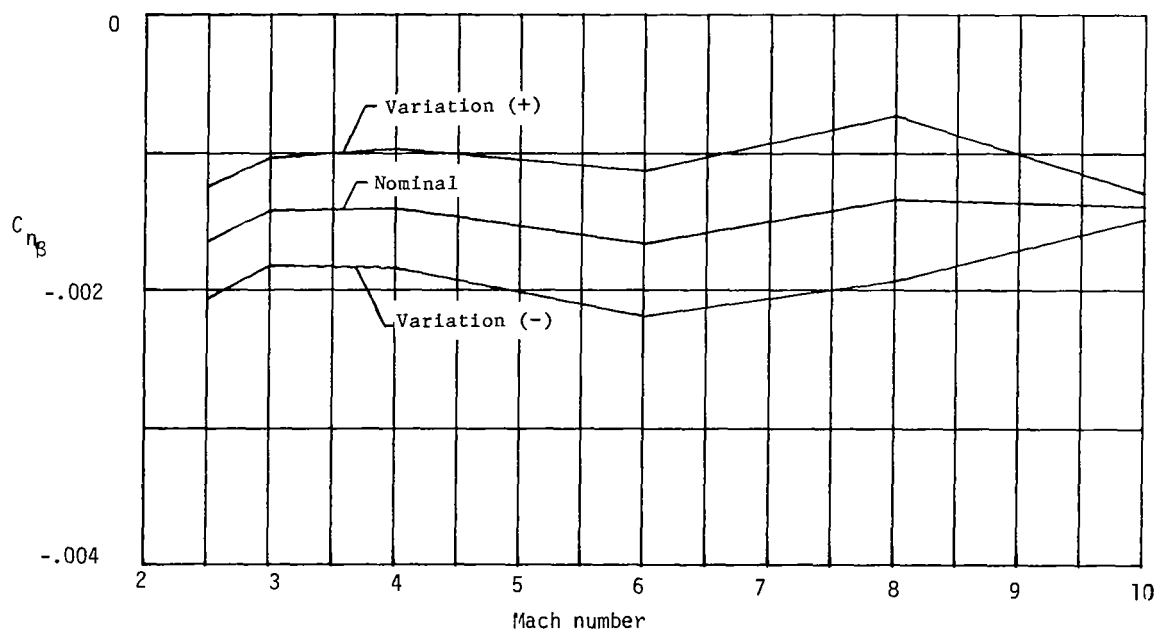

(a) Lateral-directional stability derivatives.

Figure 4.- Space Shuttle Orbiter aerodynamics, including uncertainties.

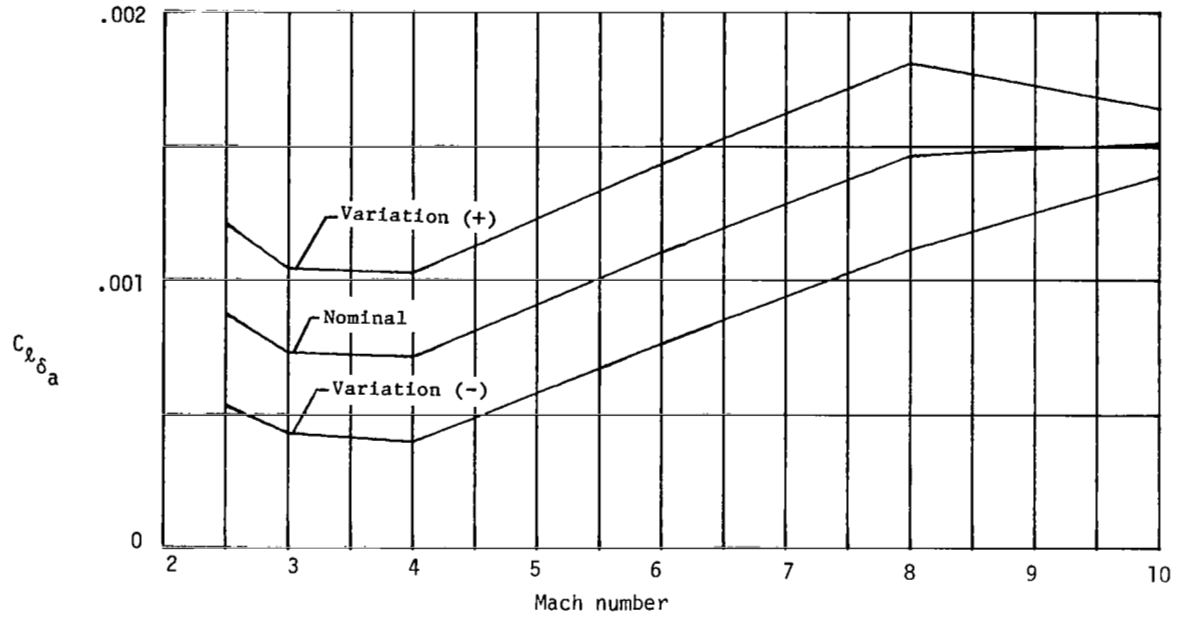

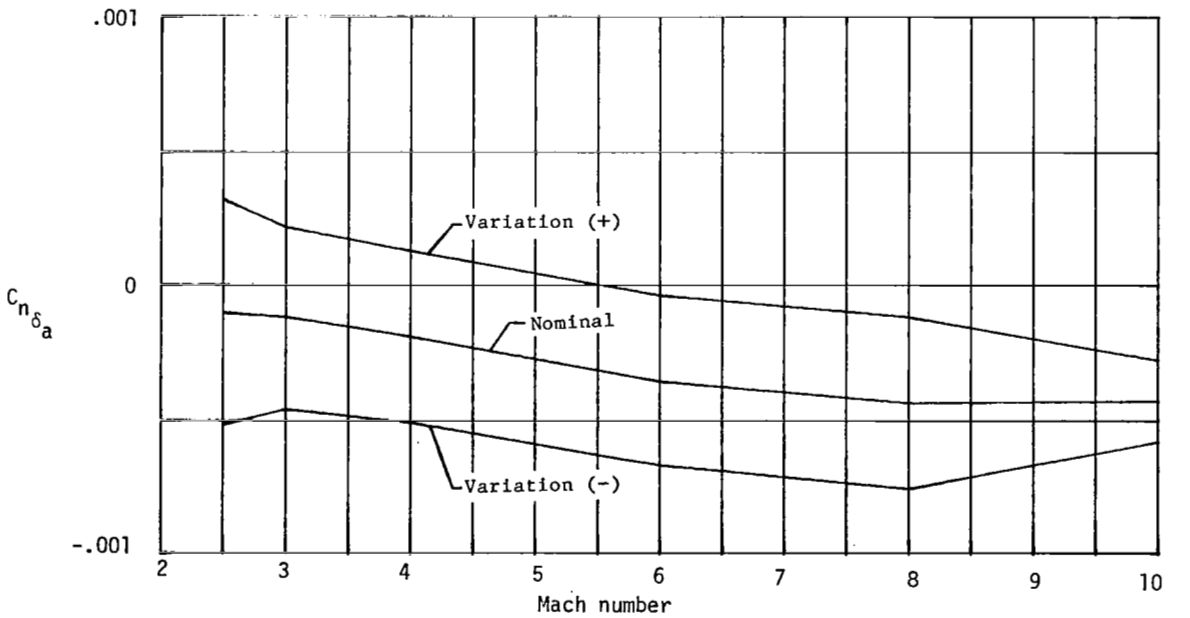

(b) Aileron derivatives.

Figure 4.- Continued.

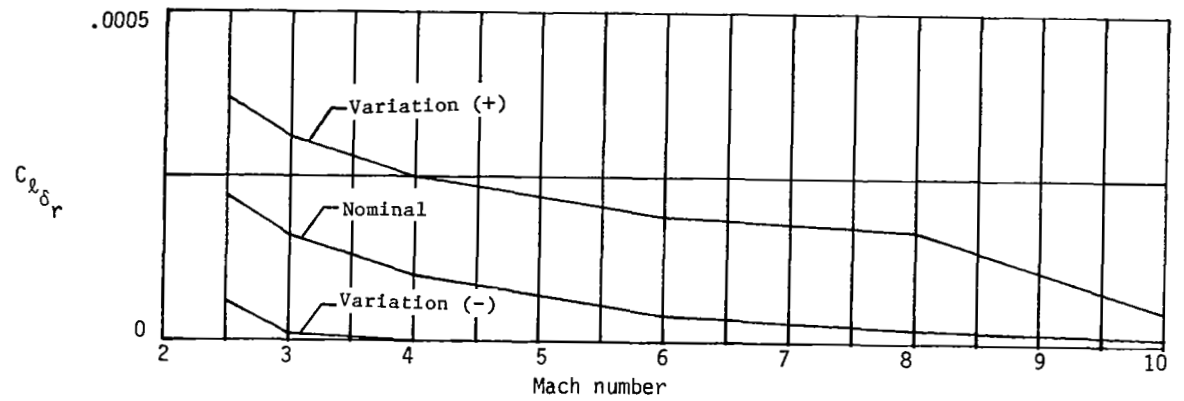

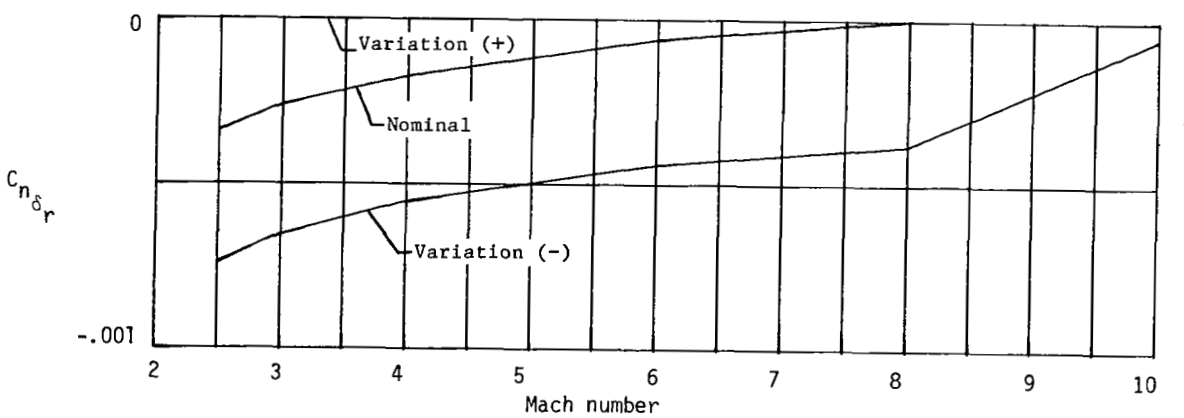

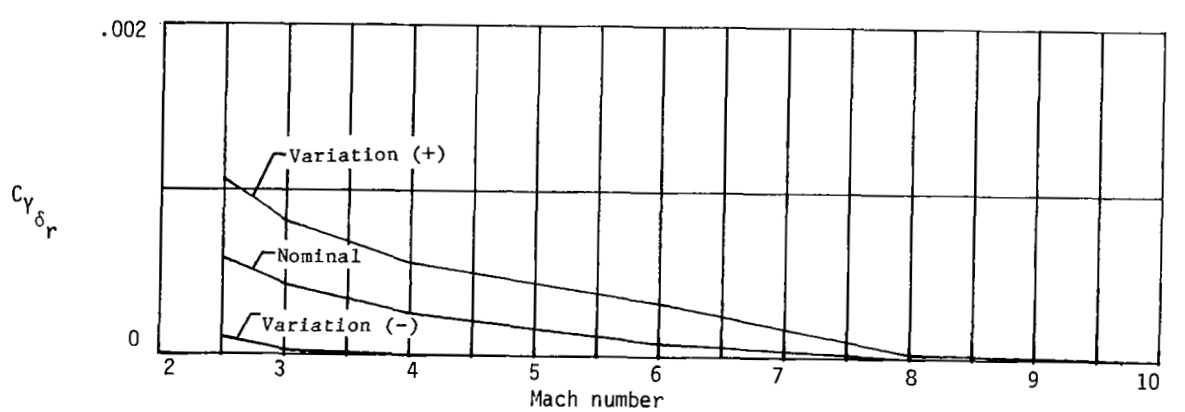

(c) Rudder derivatives.

Figure 4.- Concluded.

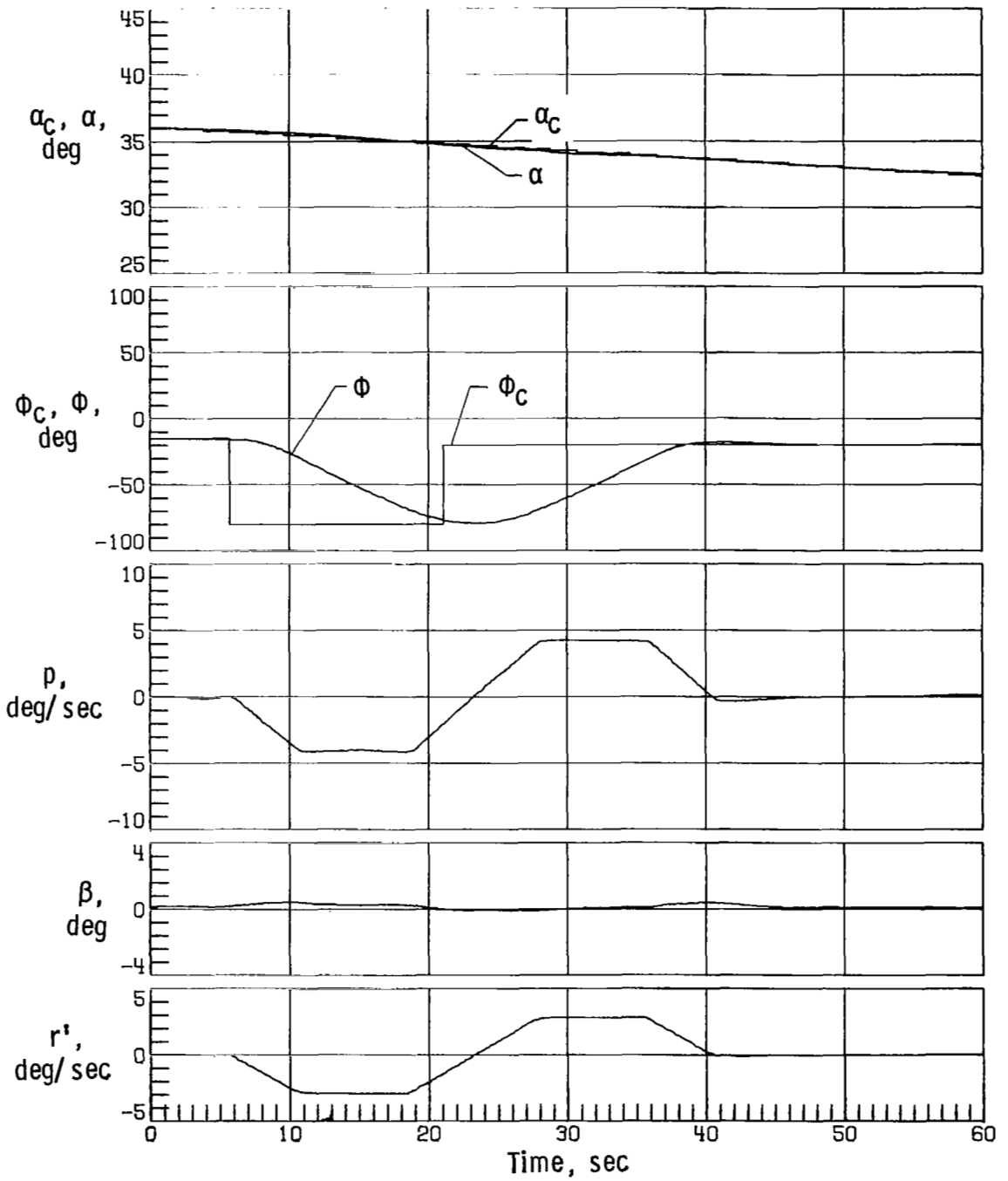

Figure 5.- Space Shuttle Orbiter response with simulation initiated at Mach 10 with nominal aerodynamics, no-sensed α error, two yaw RCS thrusters on each side inoperable, and 0.0381-m lateral center-of-gravity offset.

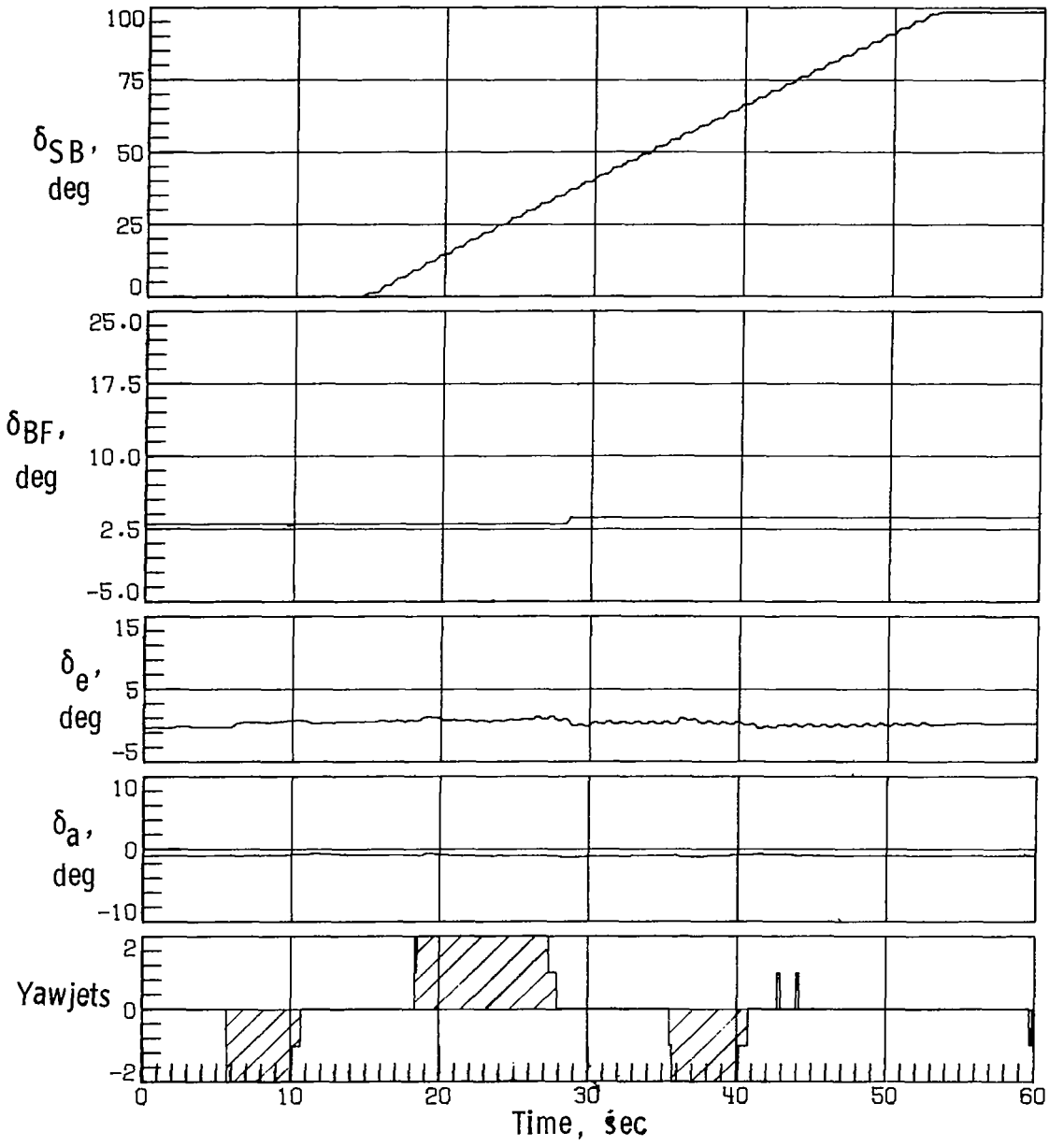

Figure 5.- Concluded.

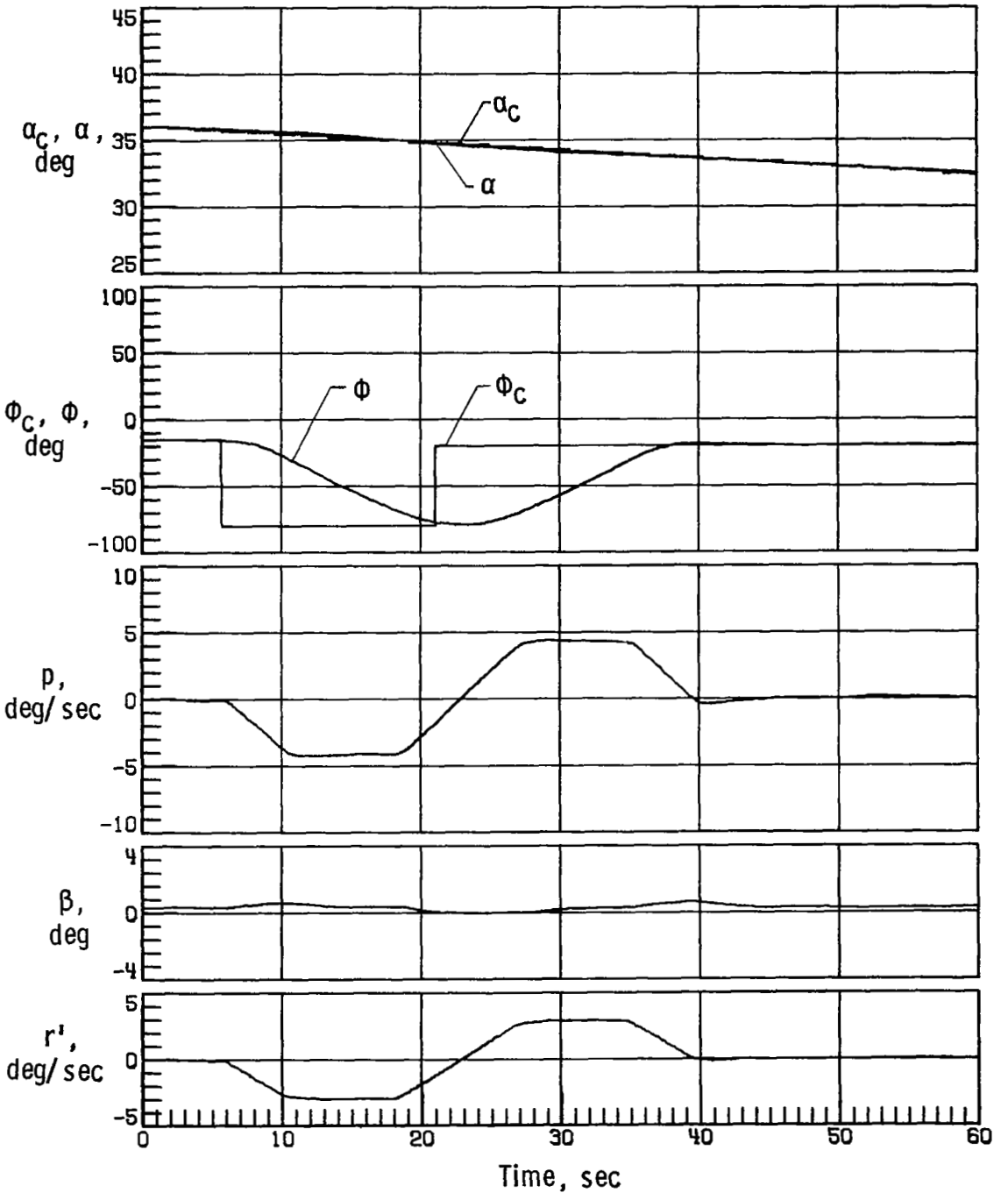

(a) Case 3.

Figure 6.- Space Shuttle Orbiter response with simulation initiated at Mach 10 with off-nominal aerodynamics, no-sensed α error, two yaw RCS thrusters on each side inoperable, and 0.0381-m lateral center-of-gravity offset.

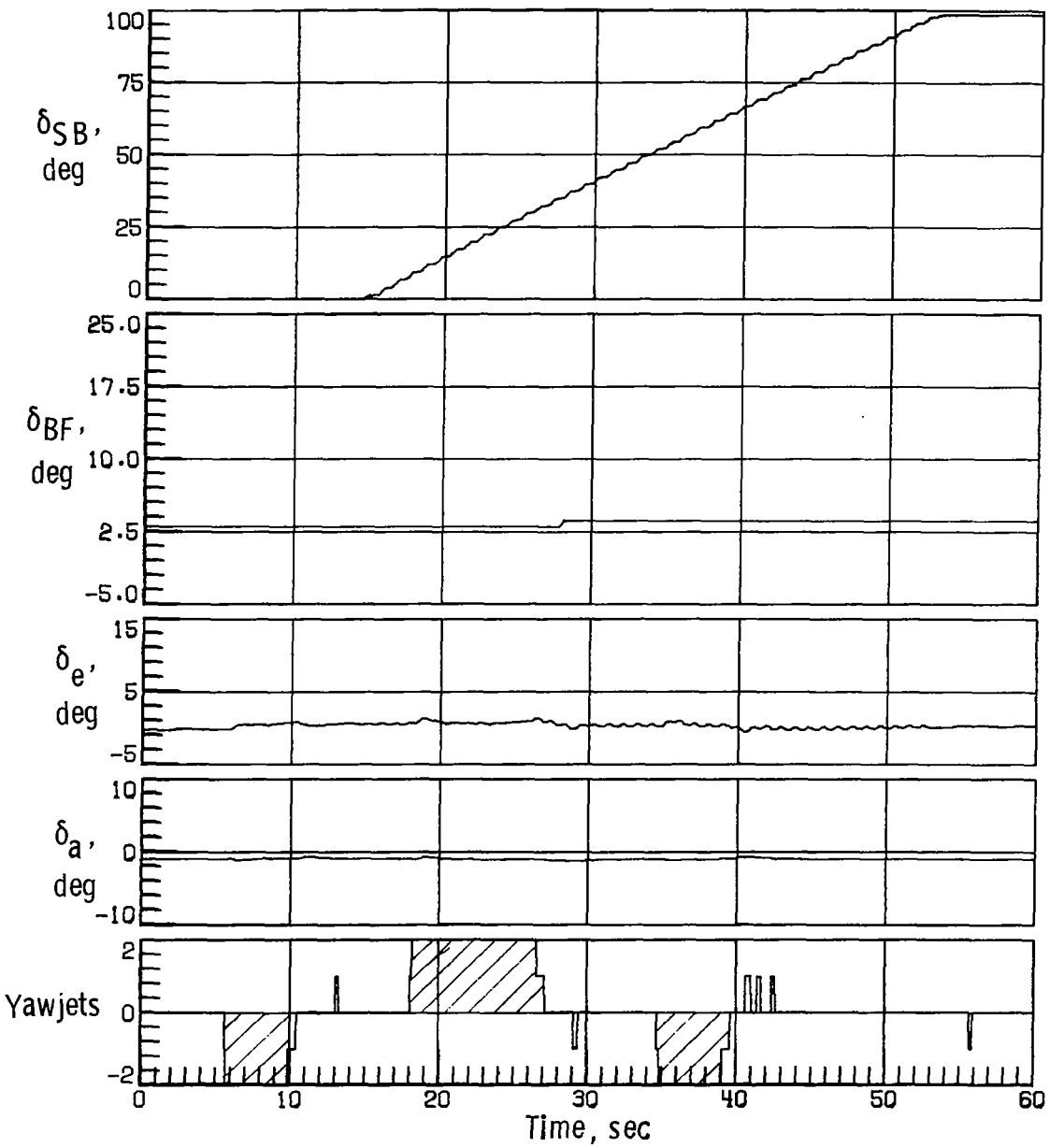

(a) Concluded.

Figure 6.- Continued.

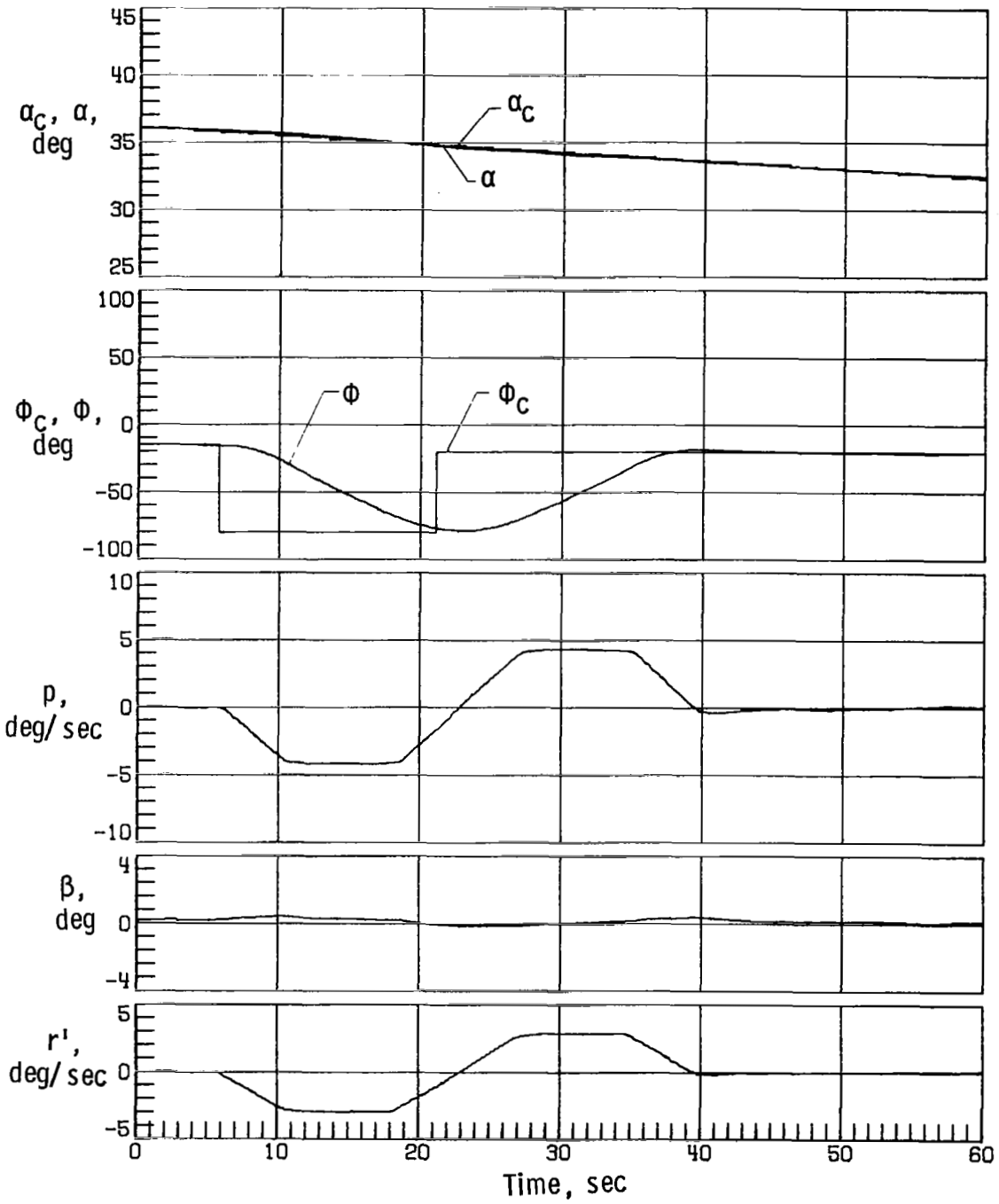

(b) Case 9.

Figure 6.- Continued.

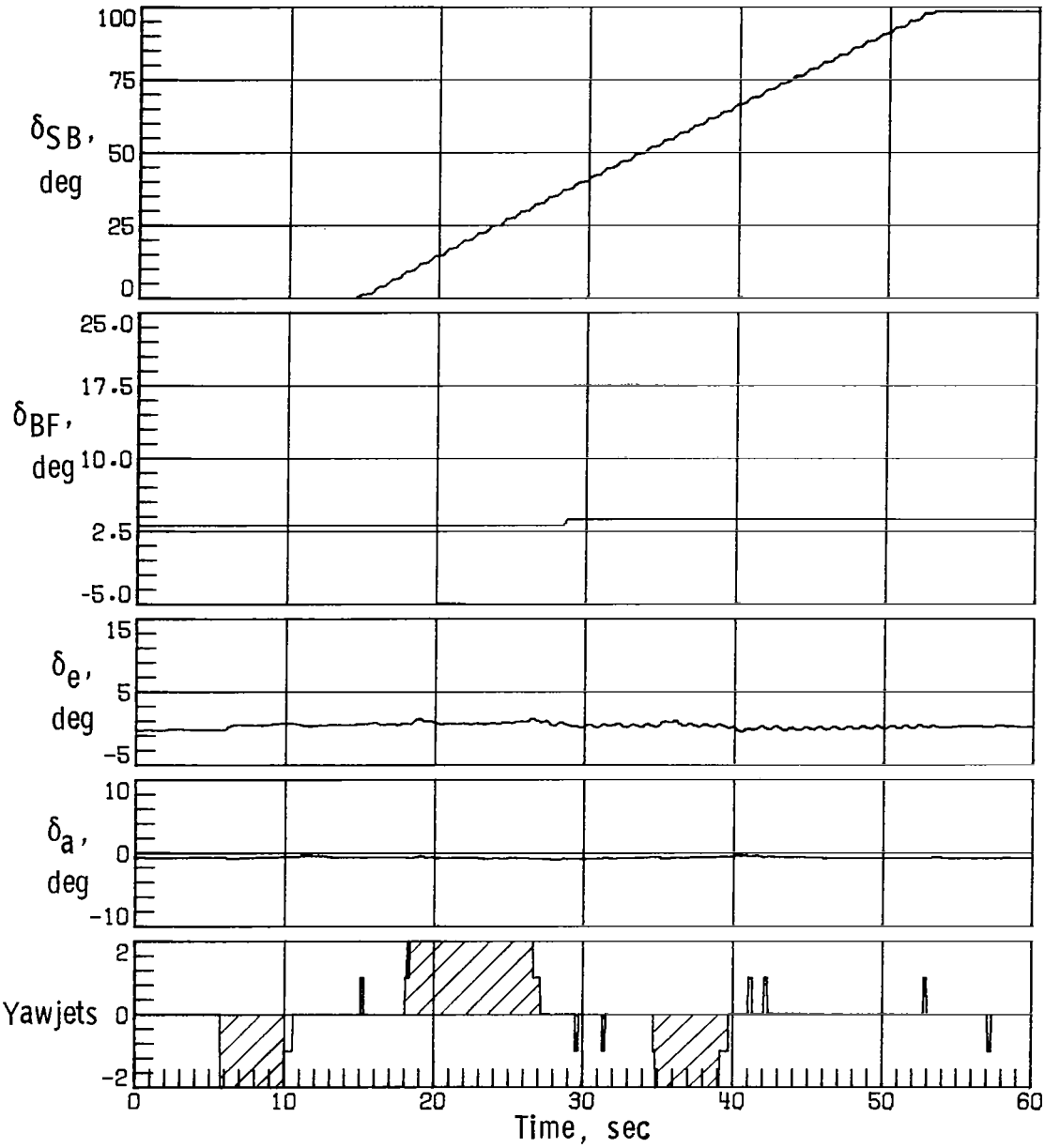

(b) Concluded.

Figure 6.- Continued.

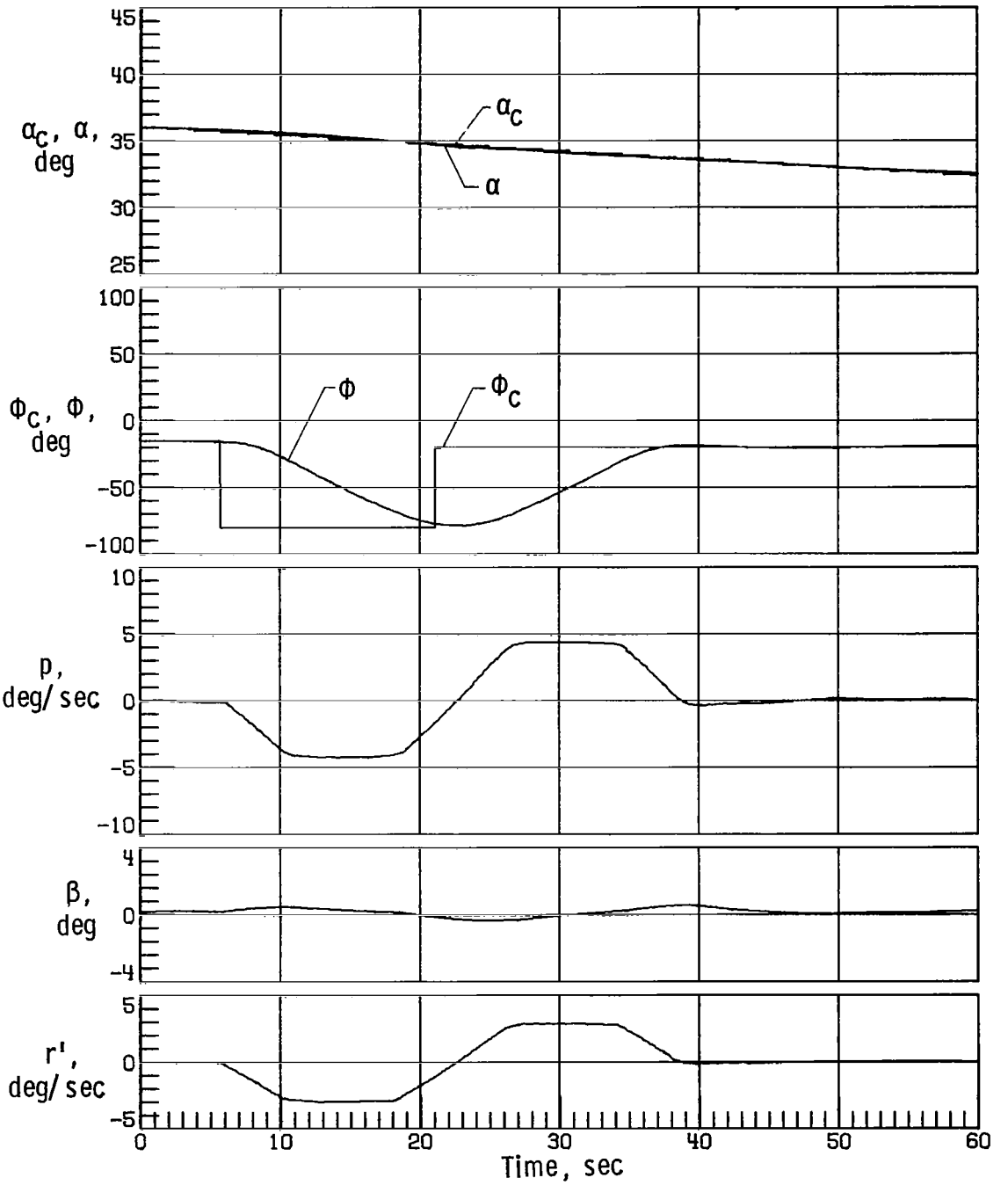

(c) Case 11.

Figure 6.- Continued.

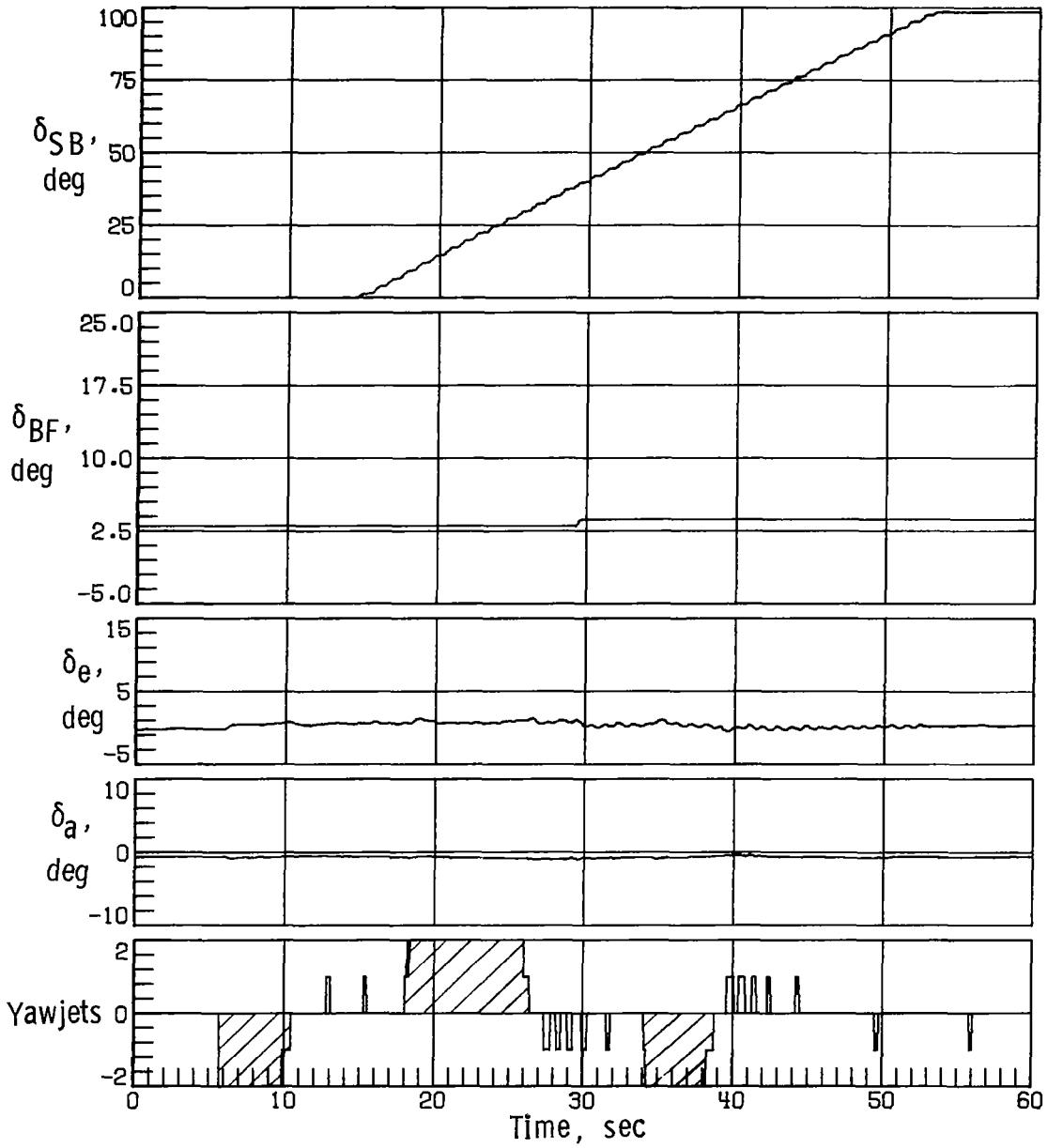

(c) Concluded.

Figure 6.- Continued.

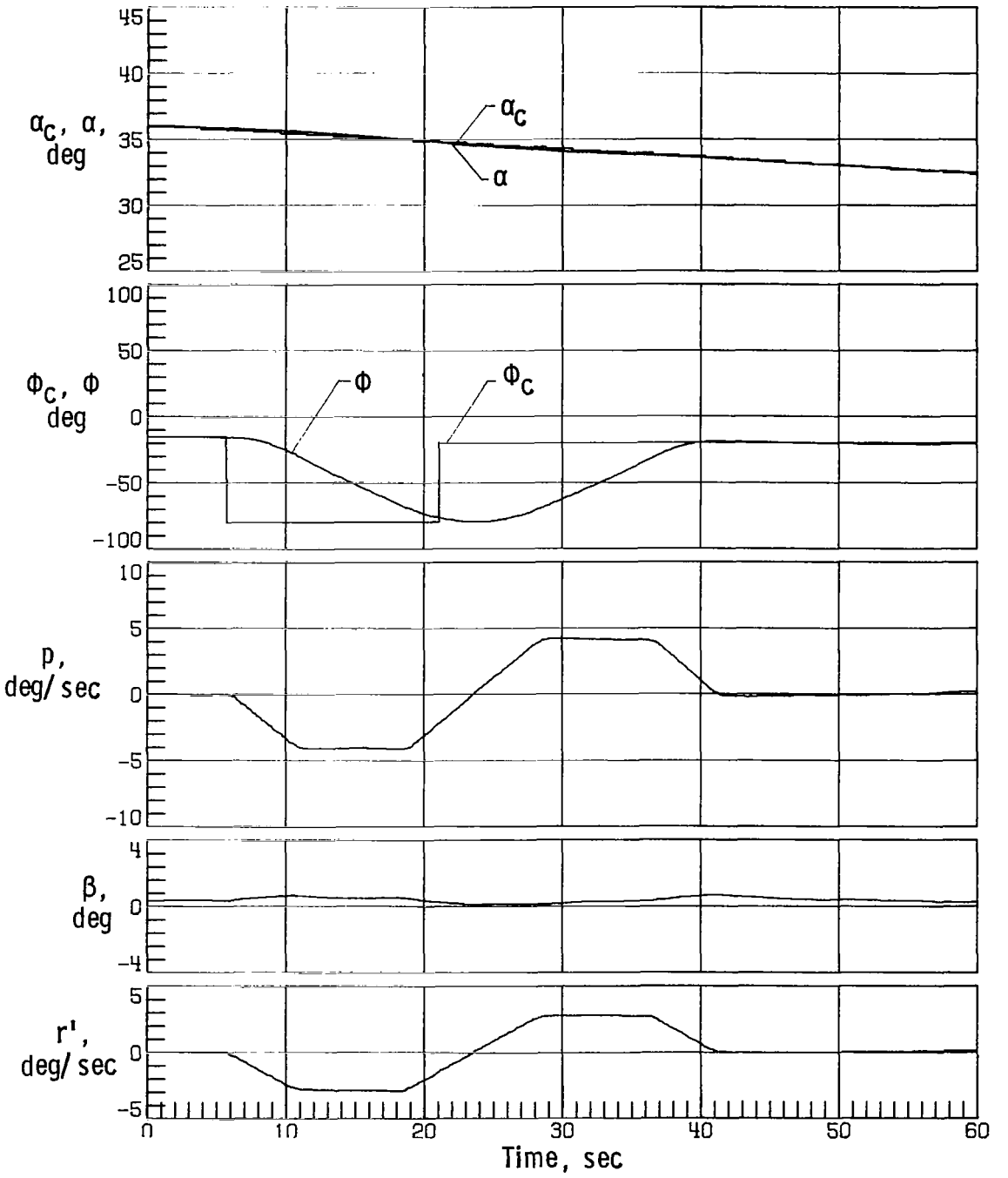

(d) Case 12.

Figure 6.- Continued.

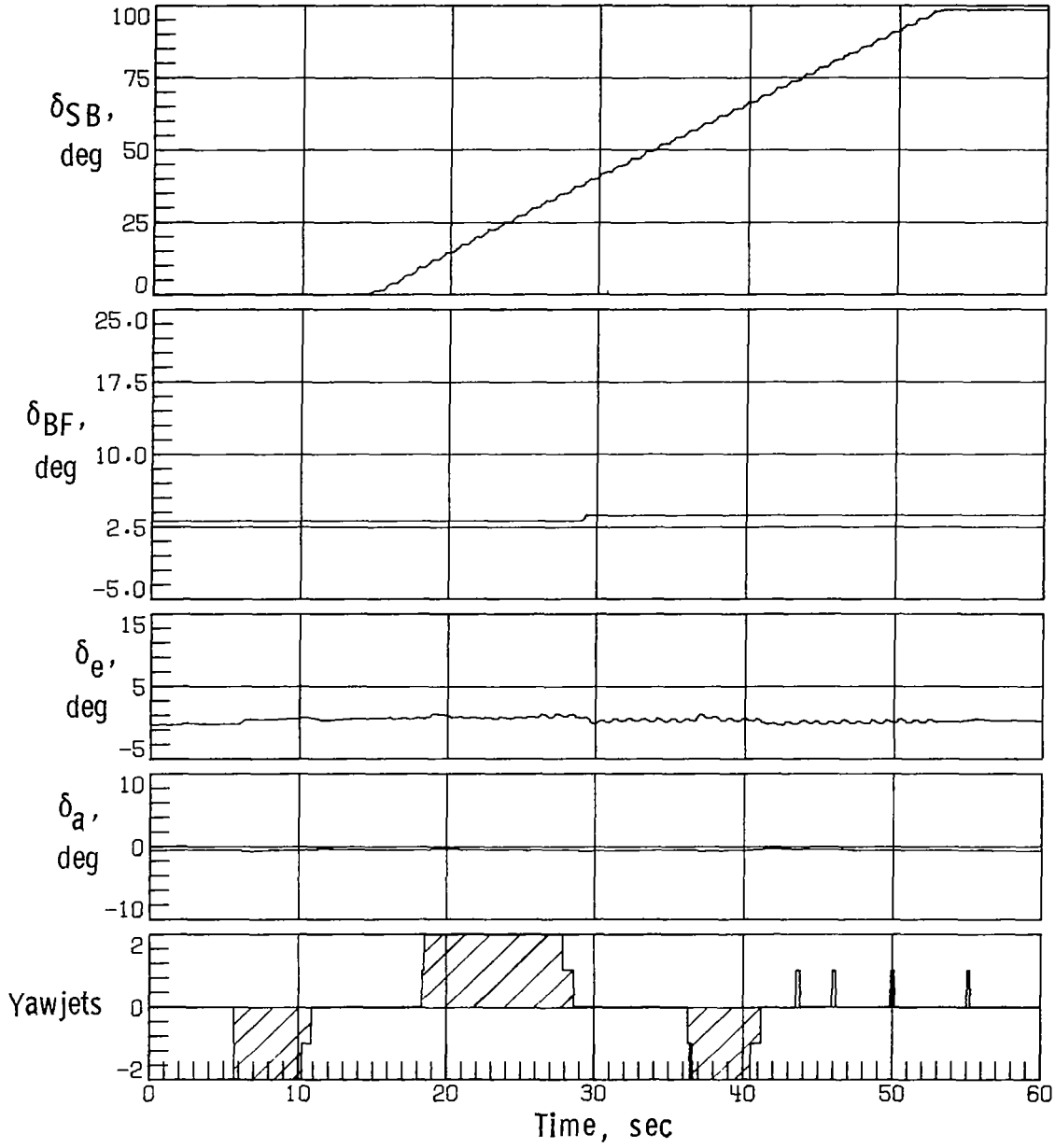

(d) Concluded.

Figure 6.- Continued.

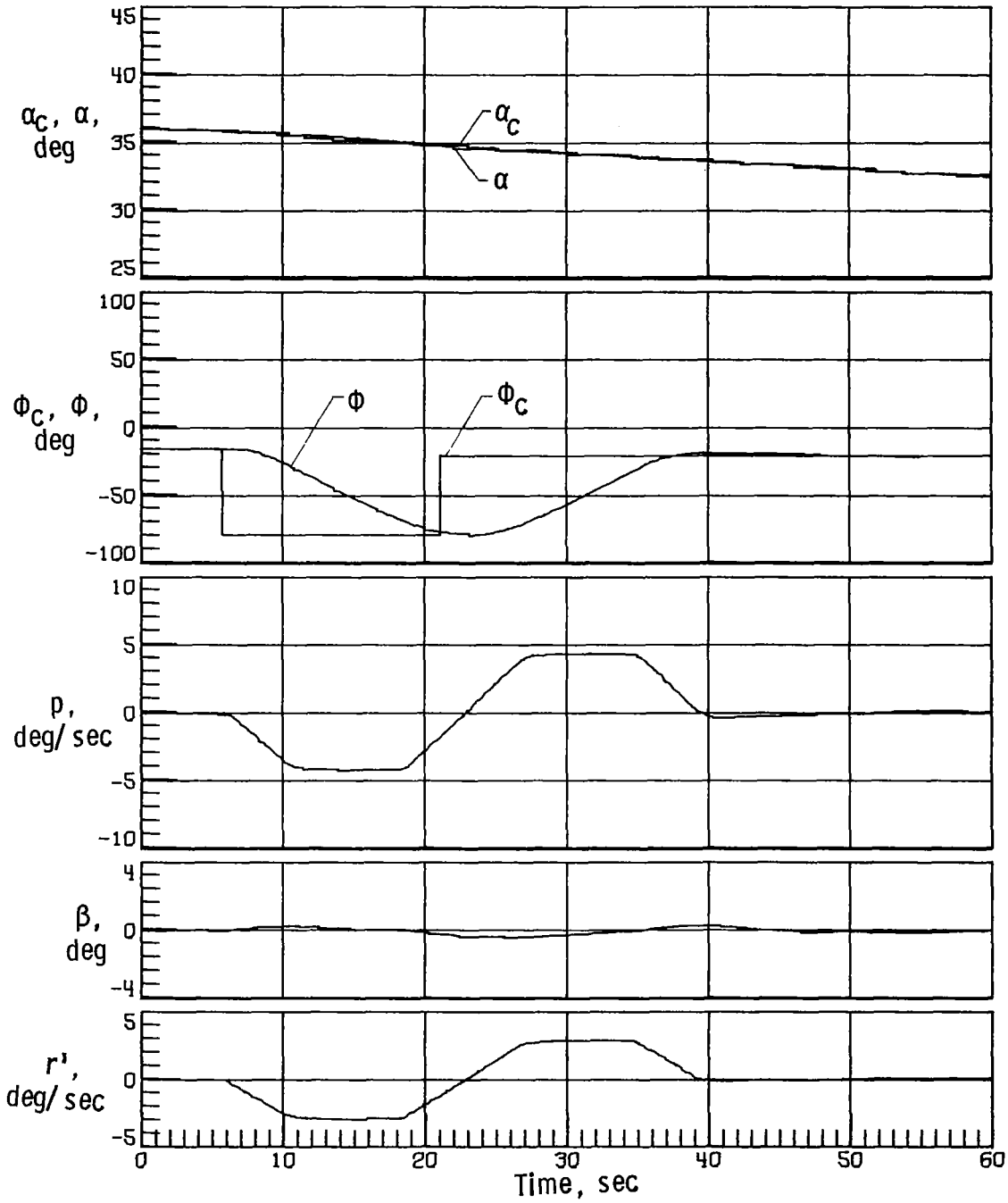

(e) Case 15.

Figure 6.- Continued.

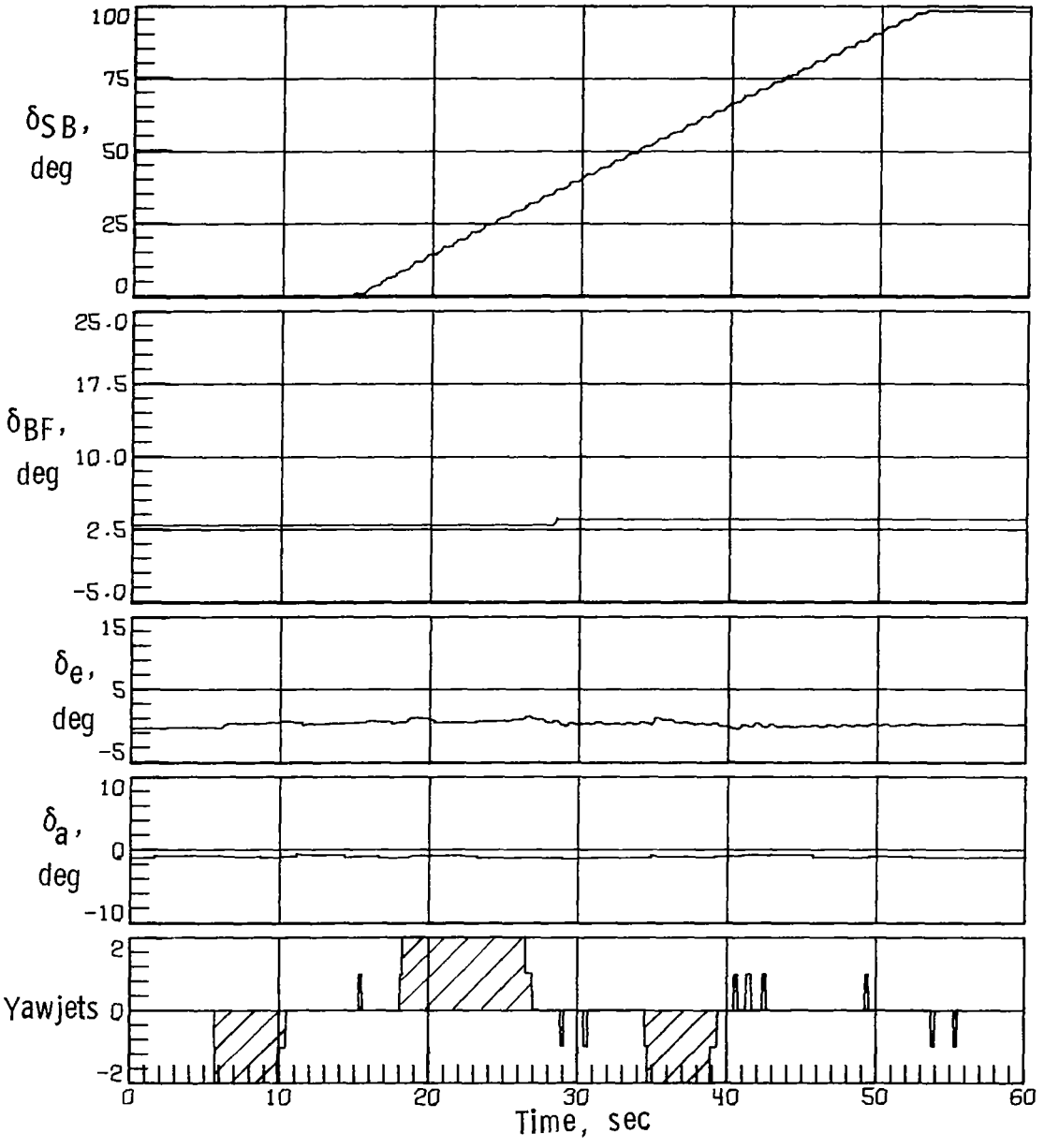

(e) Concluded.

Figure 6.- Concluded.

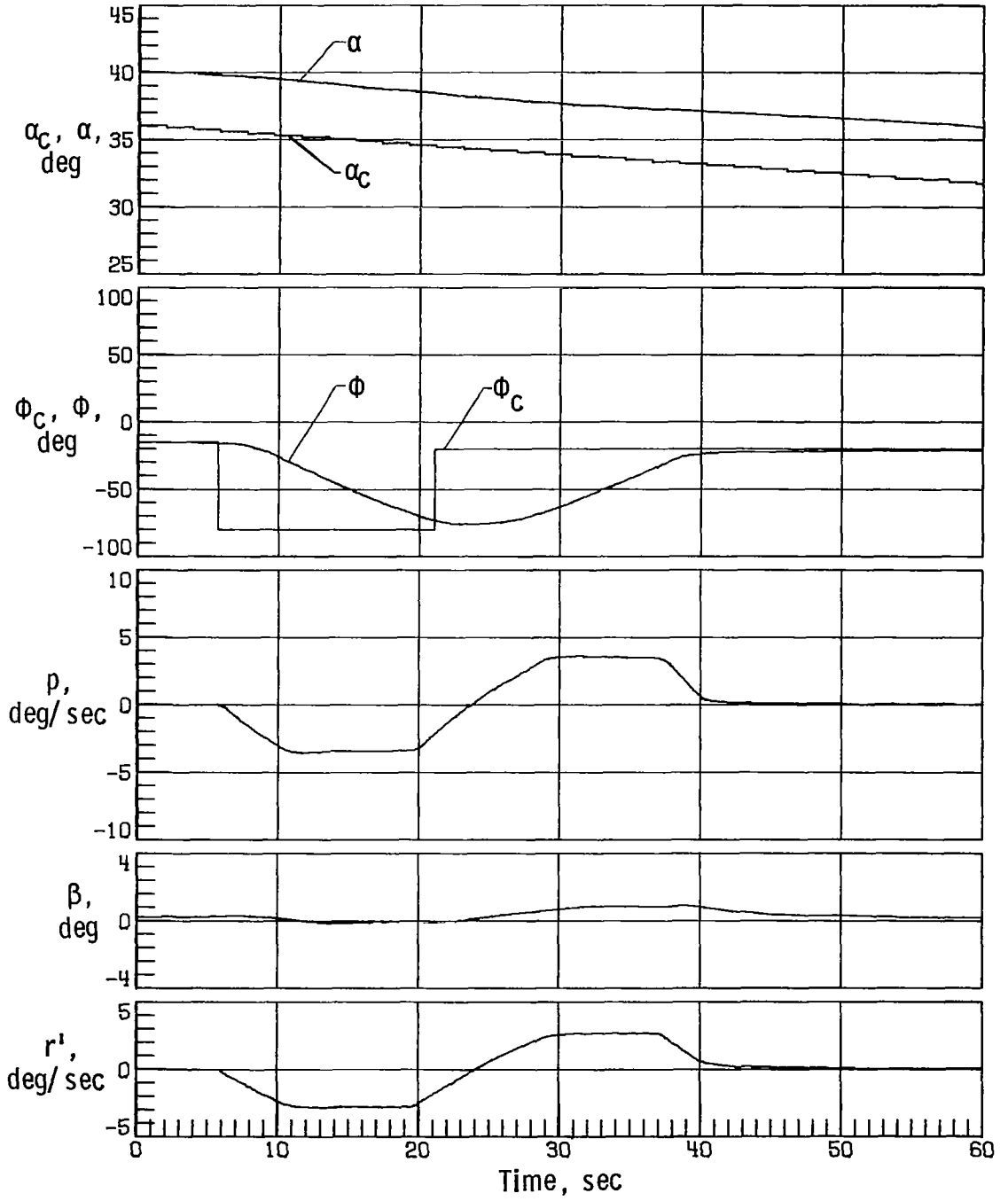

Figure 7.- Space Shuttle Orbiter response with simulation initiated at Mach 10 with nominal aerodynamics, sensed α error of -4°, two yaw RCS thrusters on each side inoperable, and 0.0381-m lateral center-of-gravity offset.

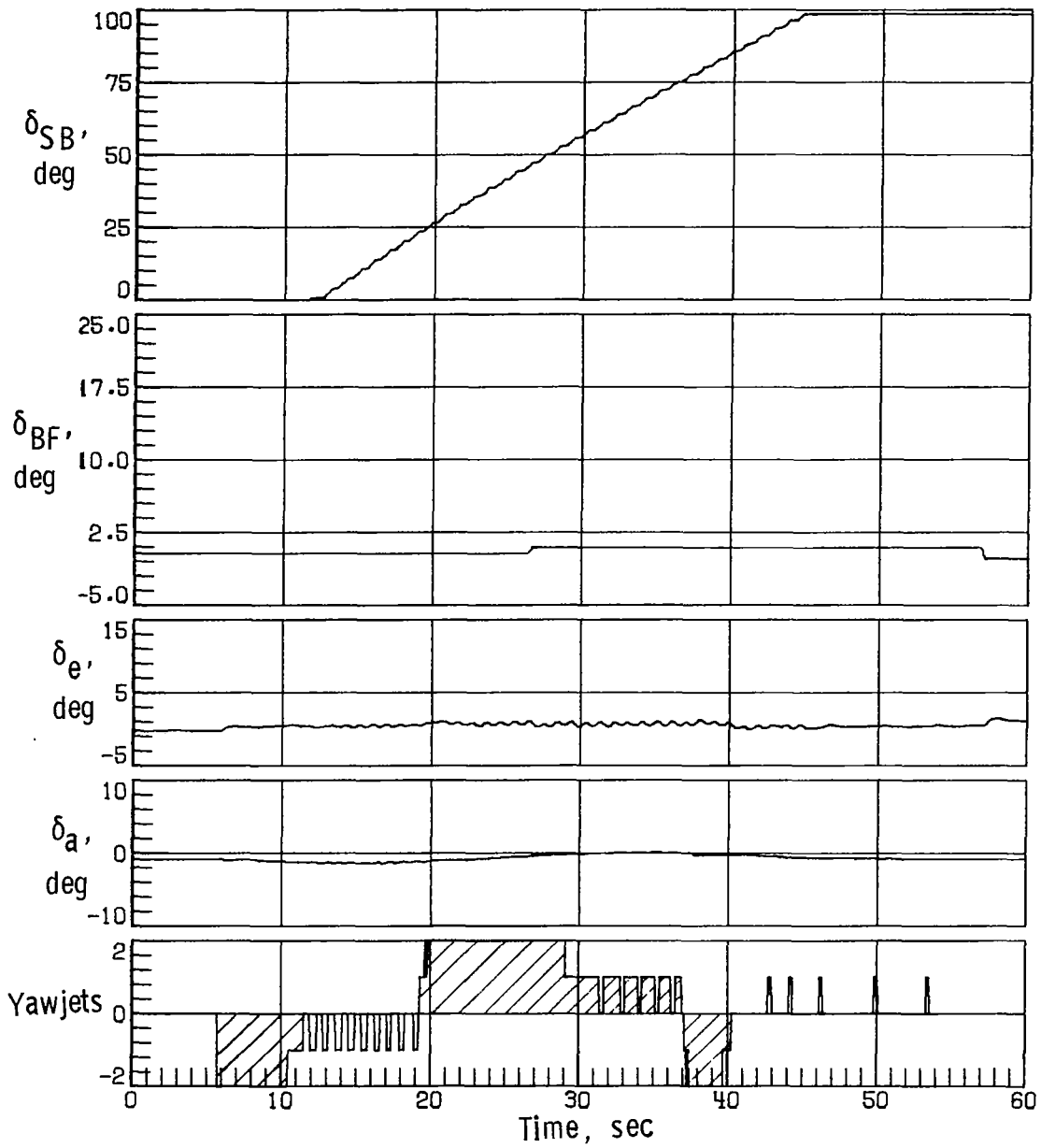

Figure 7.- Concluded.

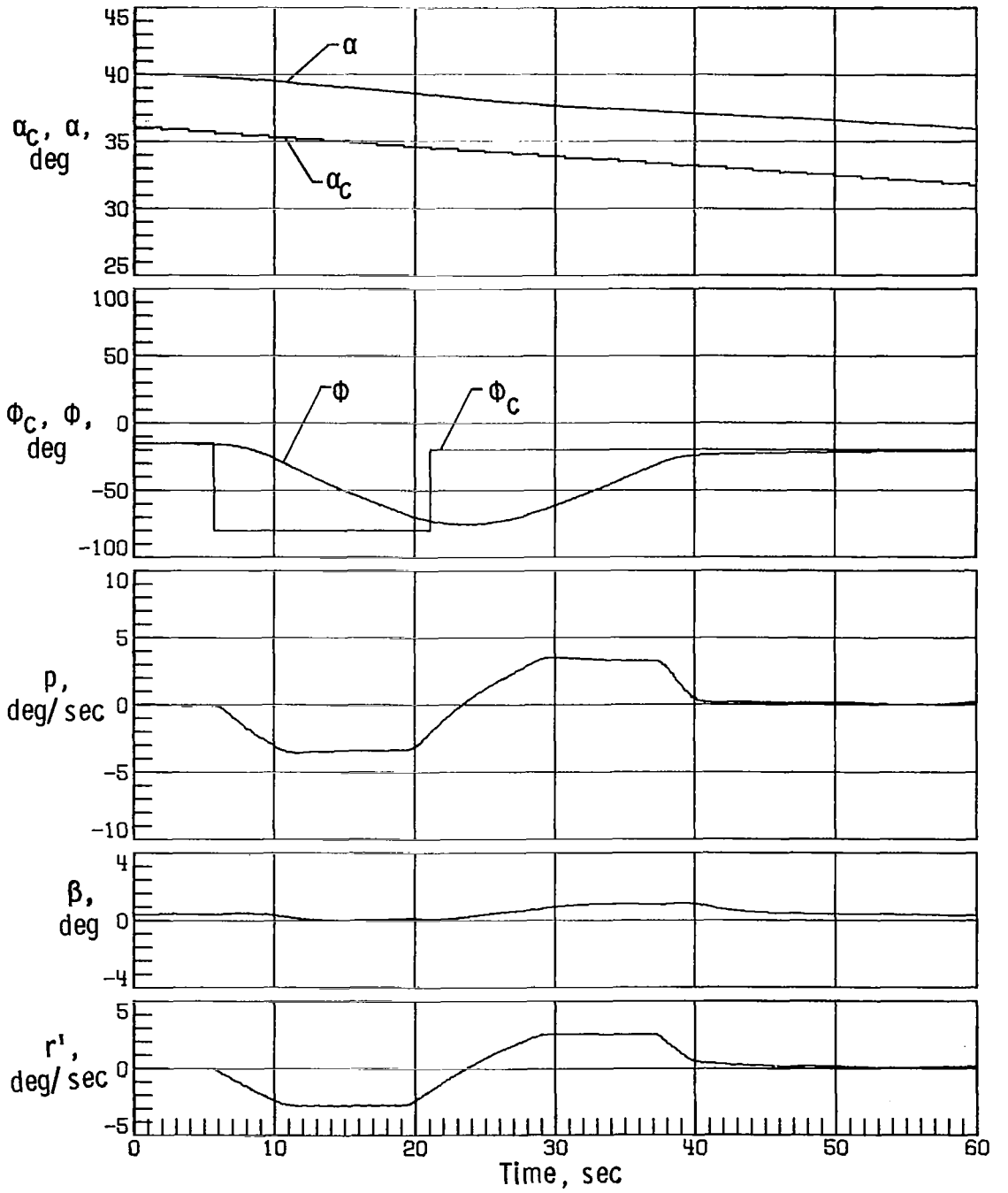

(a) Case 3.

Figure 8.- Space Shuttle Orbiter response with simulation initiated at Mach 10 with off-nominal aerodynamics, sensed α error of -4°, two yaw RCS thrusters on each side inoperable, and 0.0381-m lateral center-of-gravity offset.

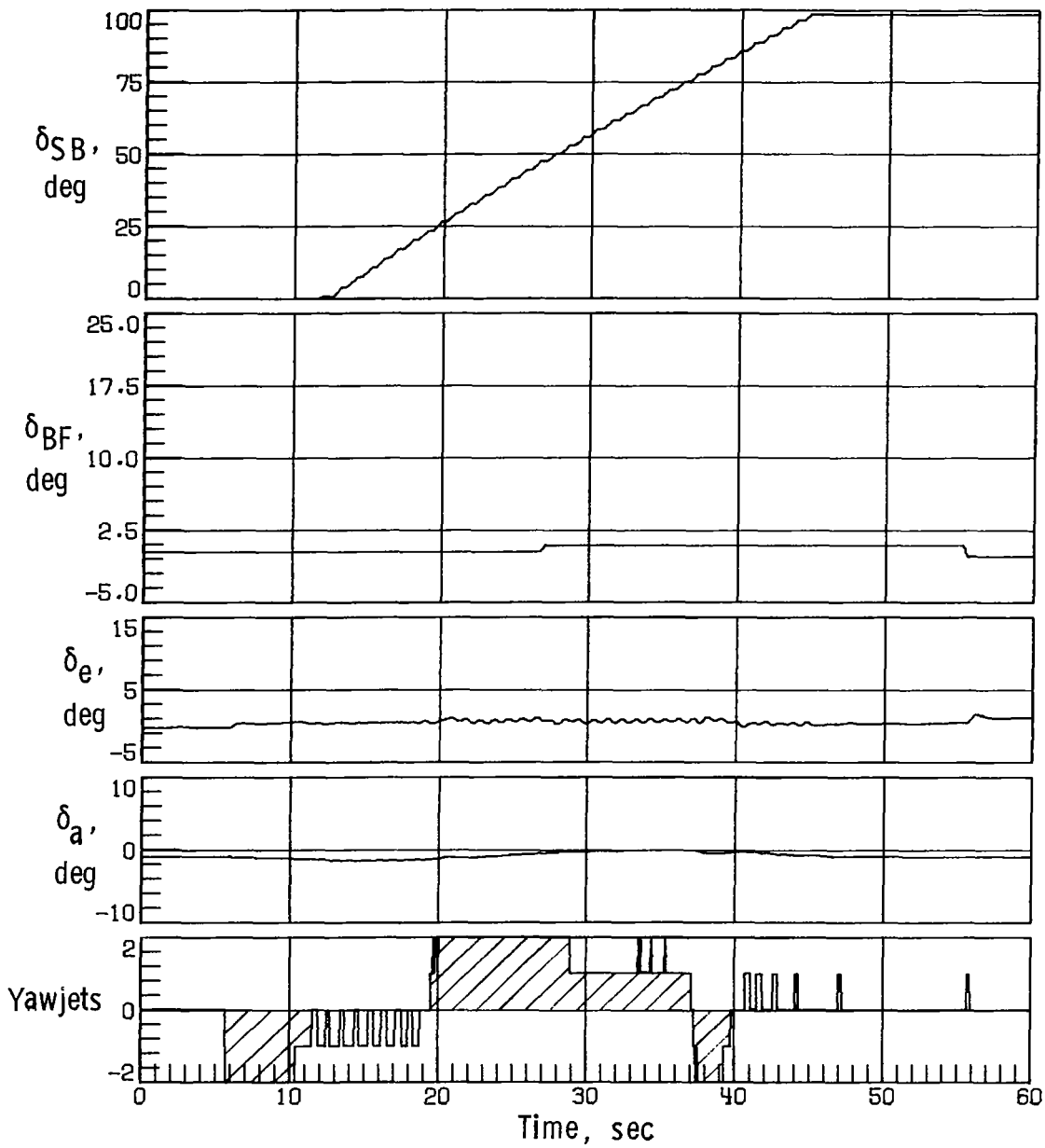

(a) Concluded.

Figure 8.- Continued.

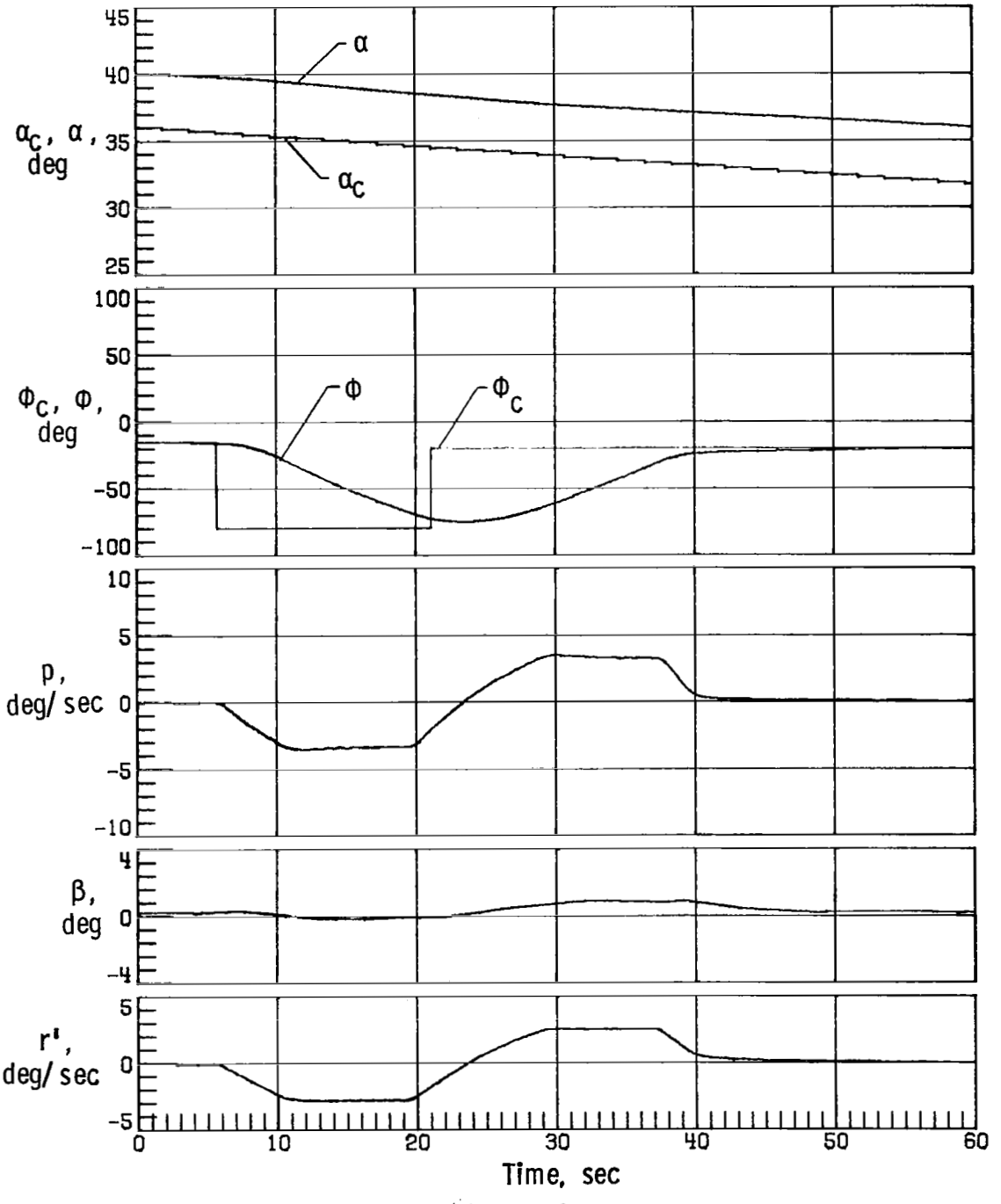

(b) Case 9.

Figure 8.- Continued.

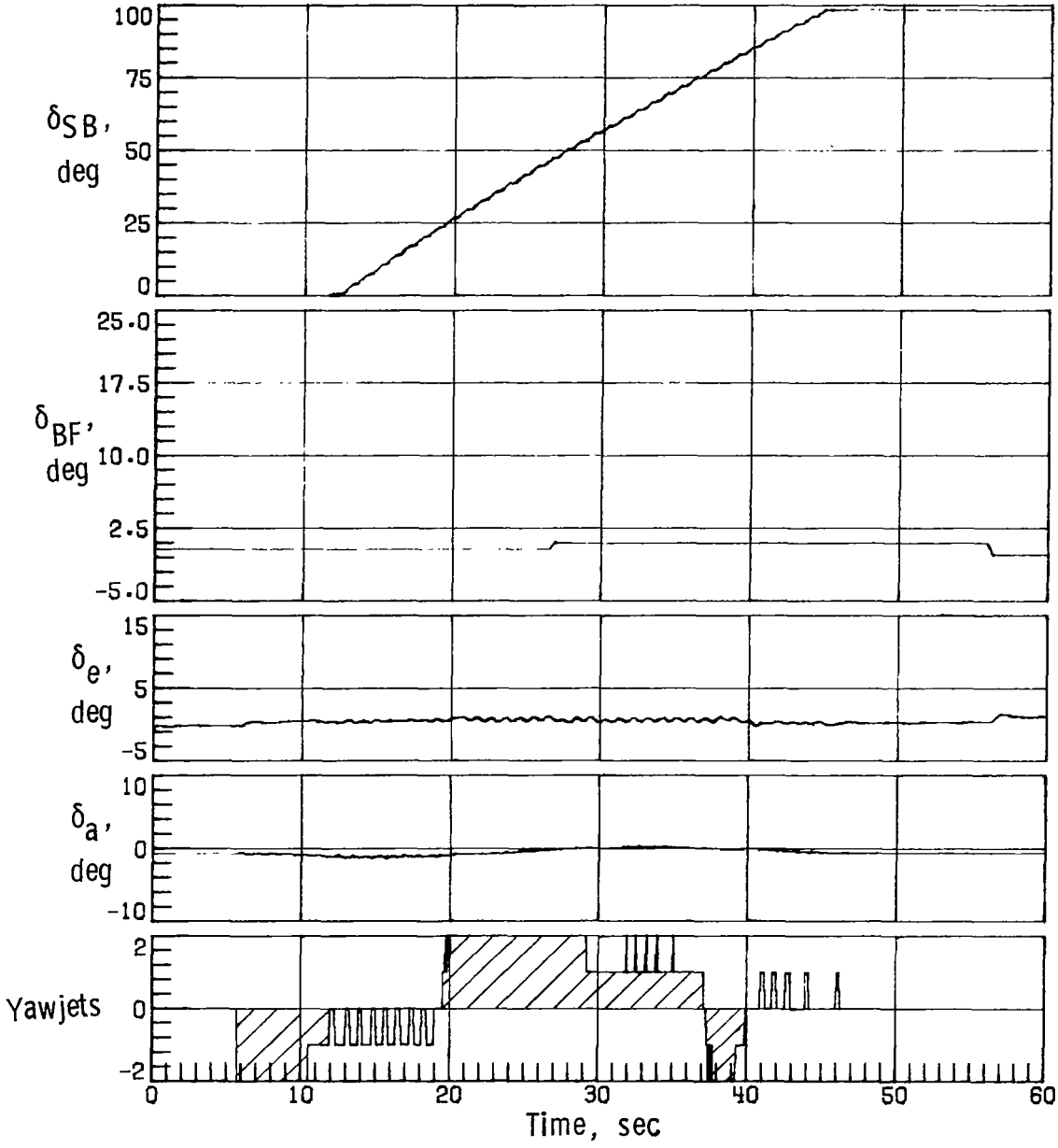

(b) Concluded.

Figure 8.- Continued.

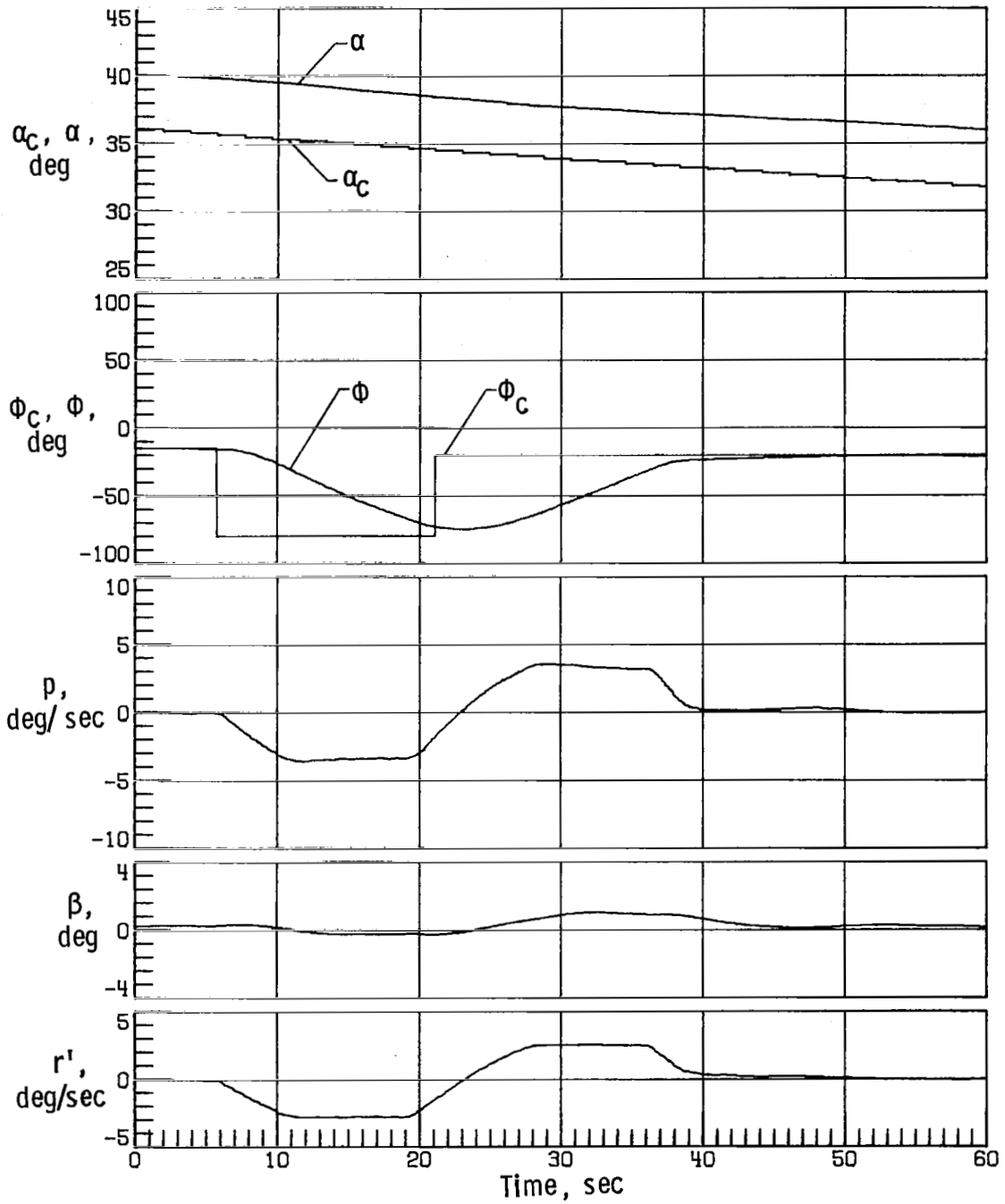

(c) Case 11.

Figure 8.- Continued.

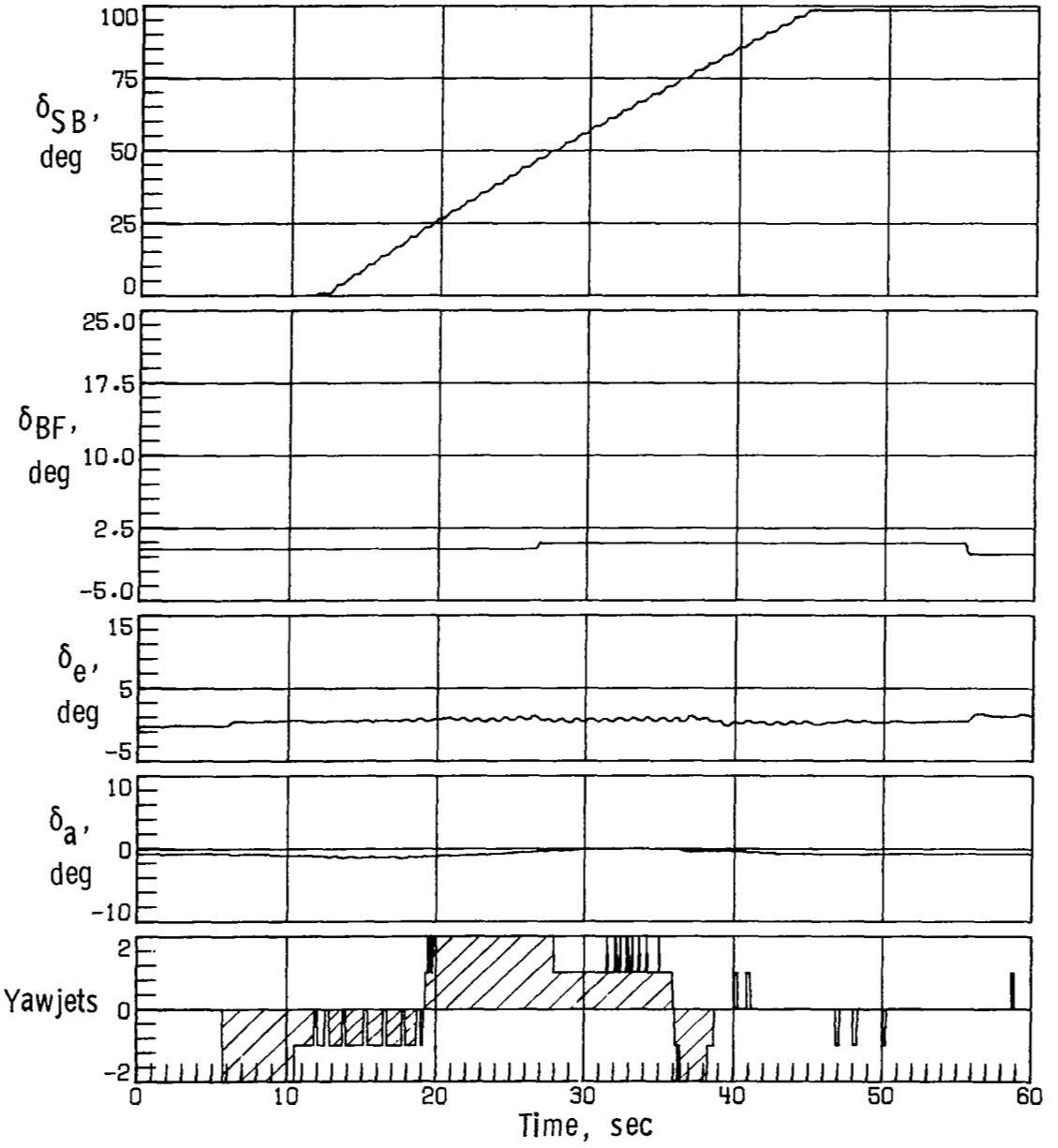

(c) Concluded.

Figure 8.- Continued.

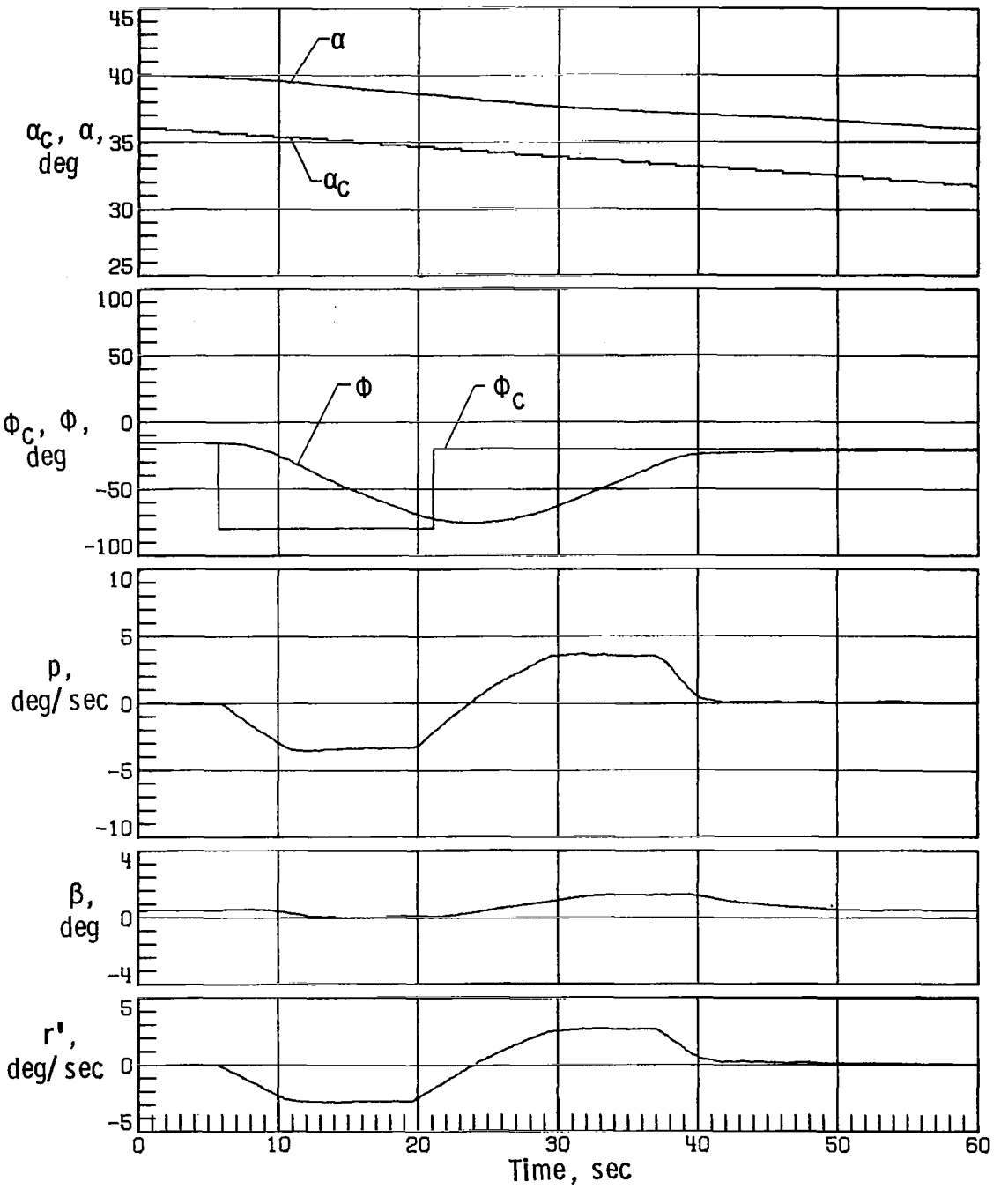

(d) Case 12.

Figure 8.- Continued.

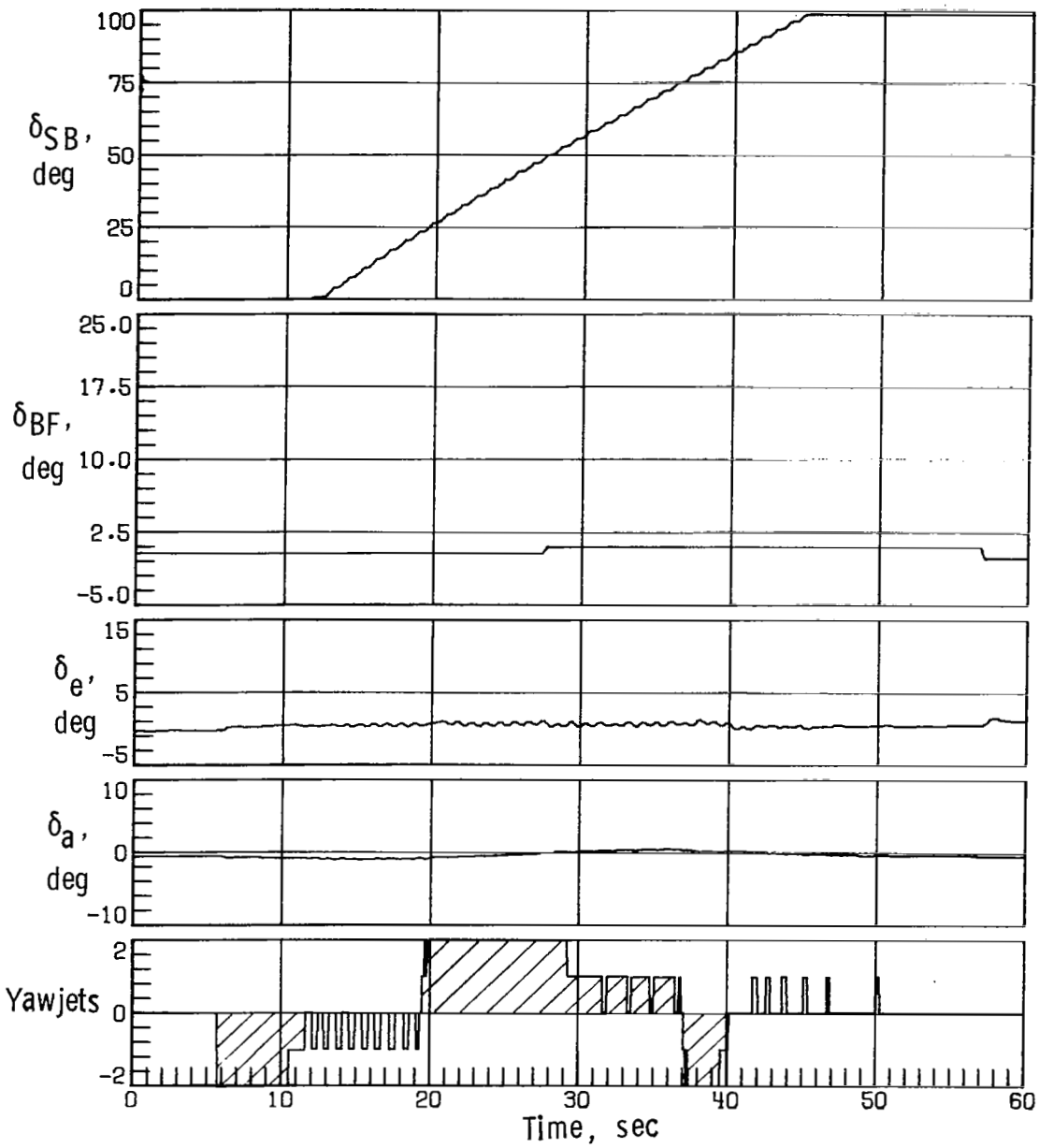

(d) Concluded.

Figure 8.- Continued.

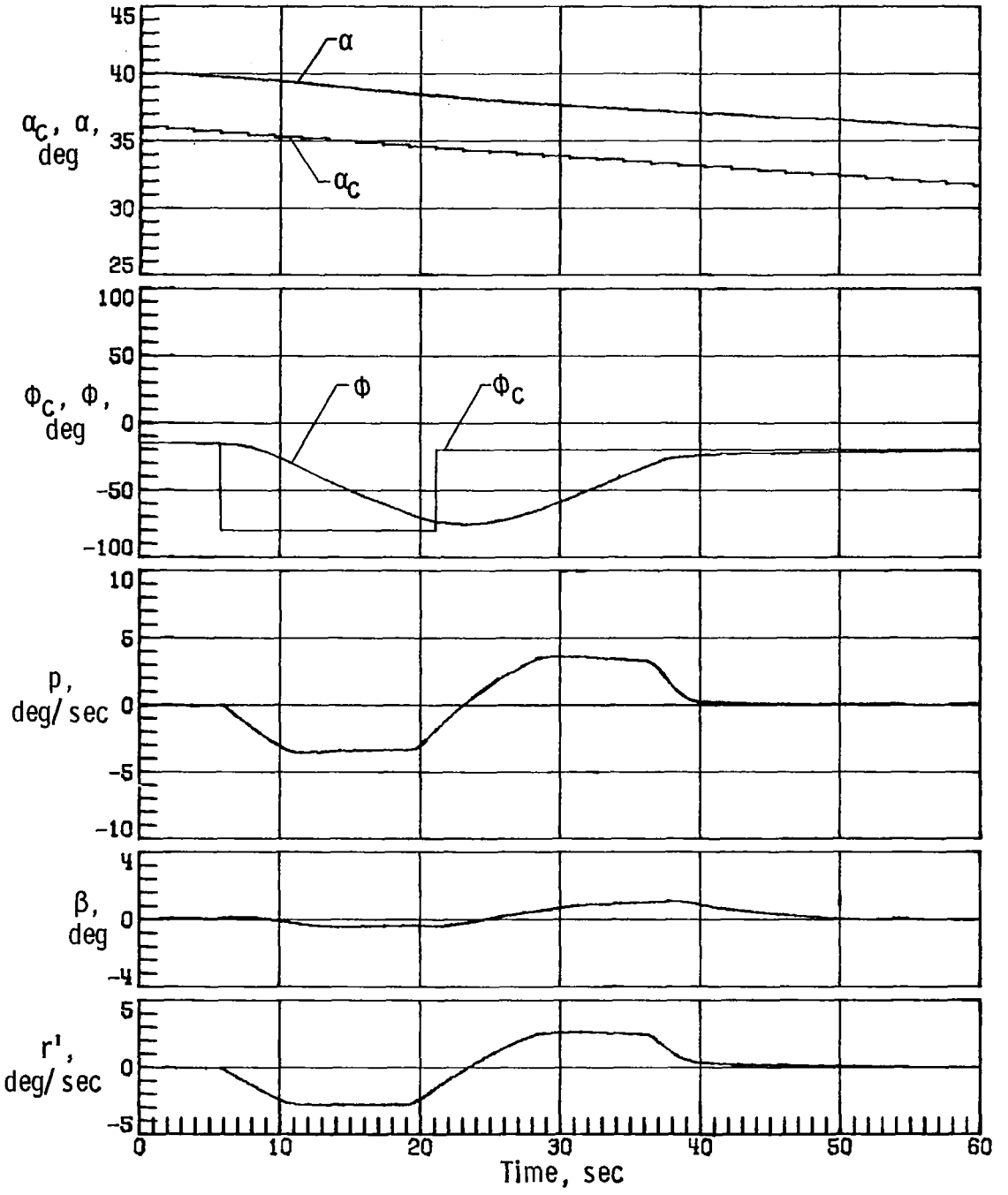

(e) Case 15.

Figure 8.- Continued.

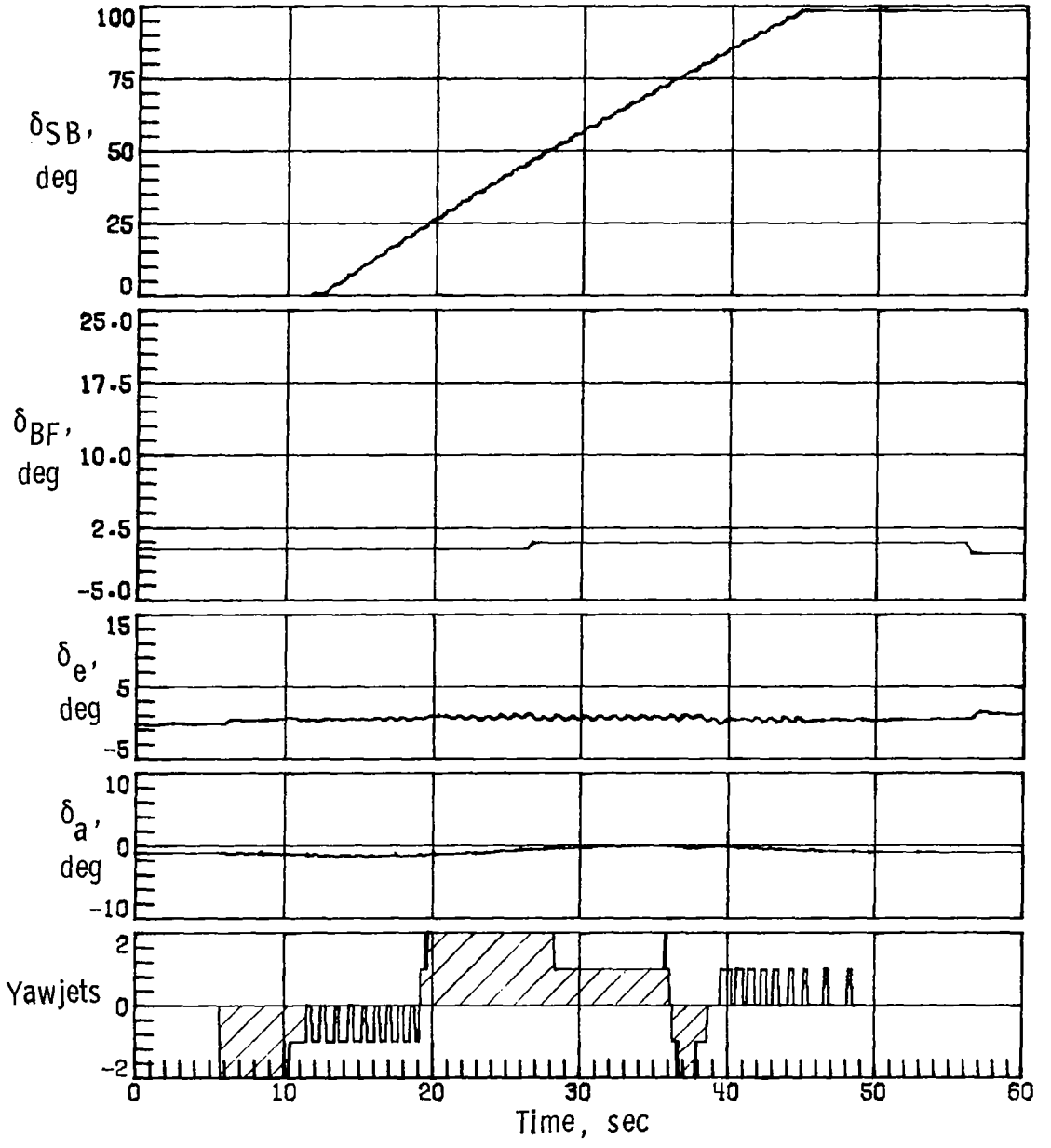

(e) Concluded.

Figure 8.- Concluded.

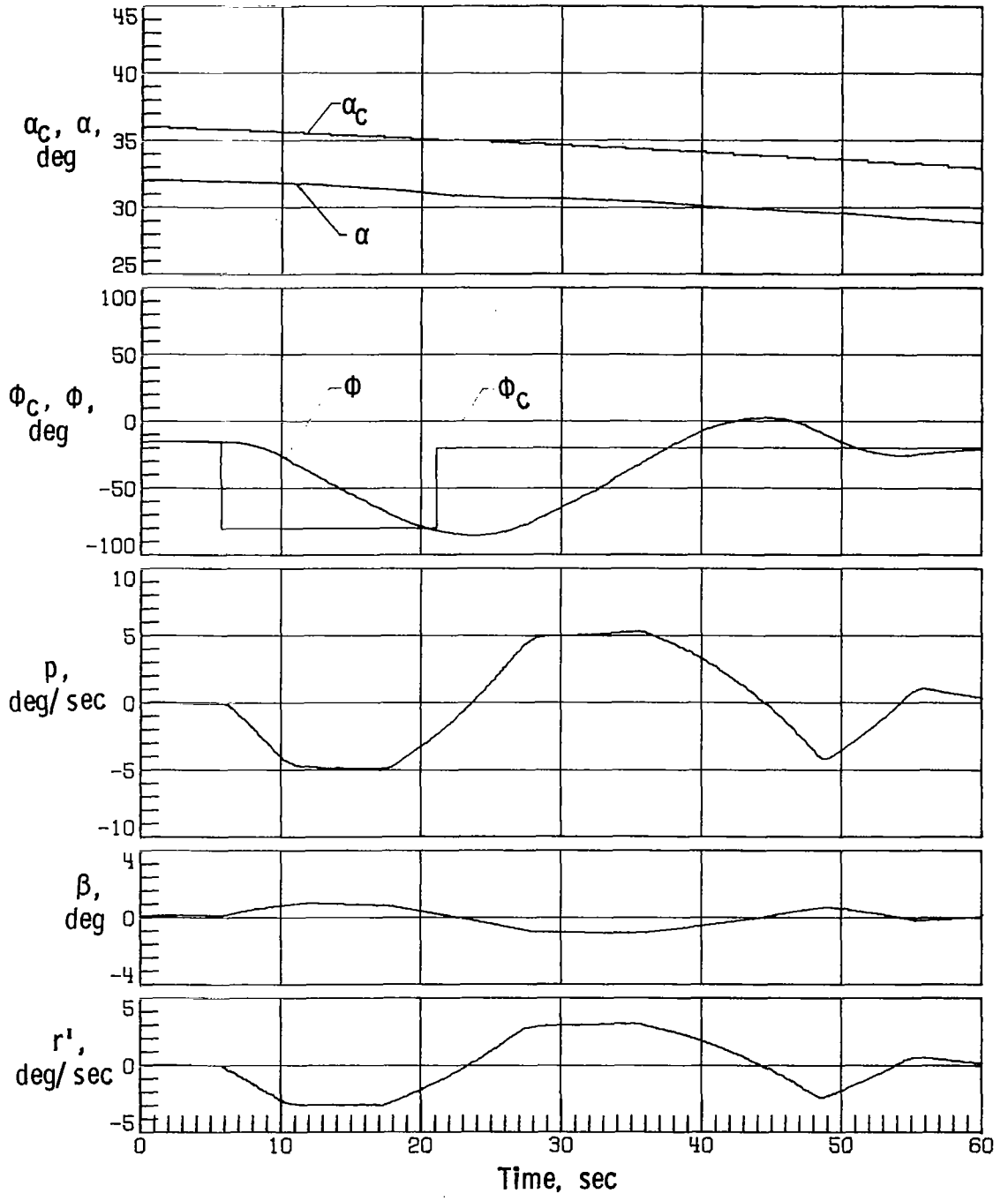

Figure 9.- Space Shuttle Orbiter response with simulation initiated at Mach 10 with nominal aerodynamics, sensed α error of $+4^{o}$, two yaw RCS thrusters on each side inoperable, and 0.0381-m lateral center-of-gravity offset.

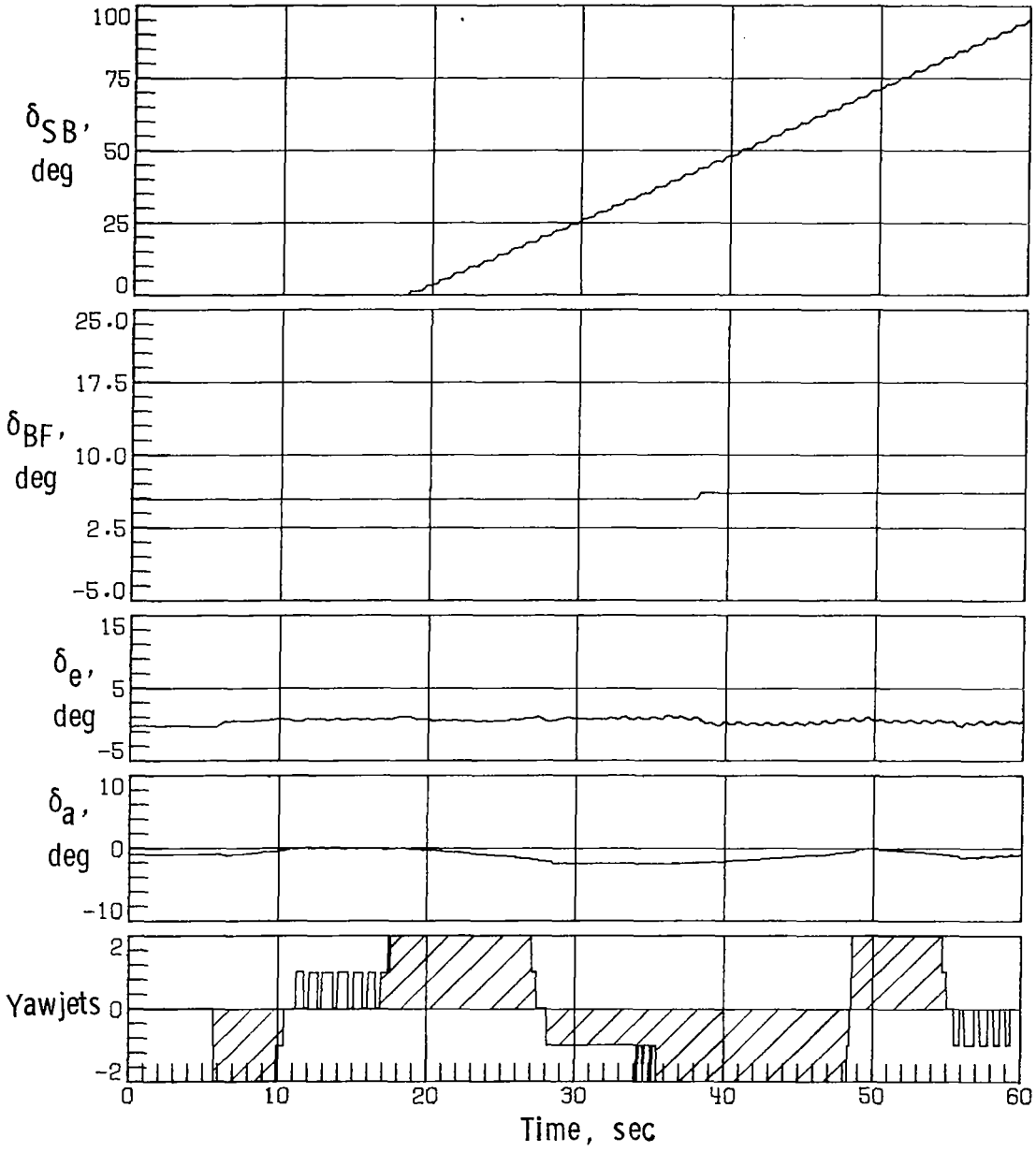

Figure 9.- Concluded.

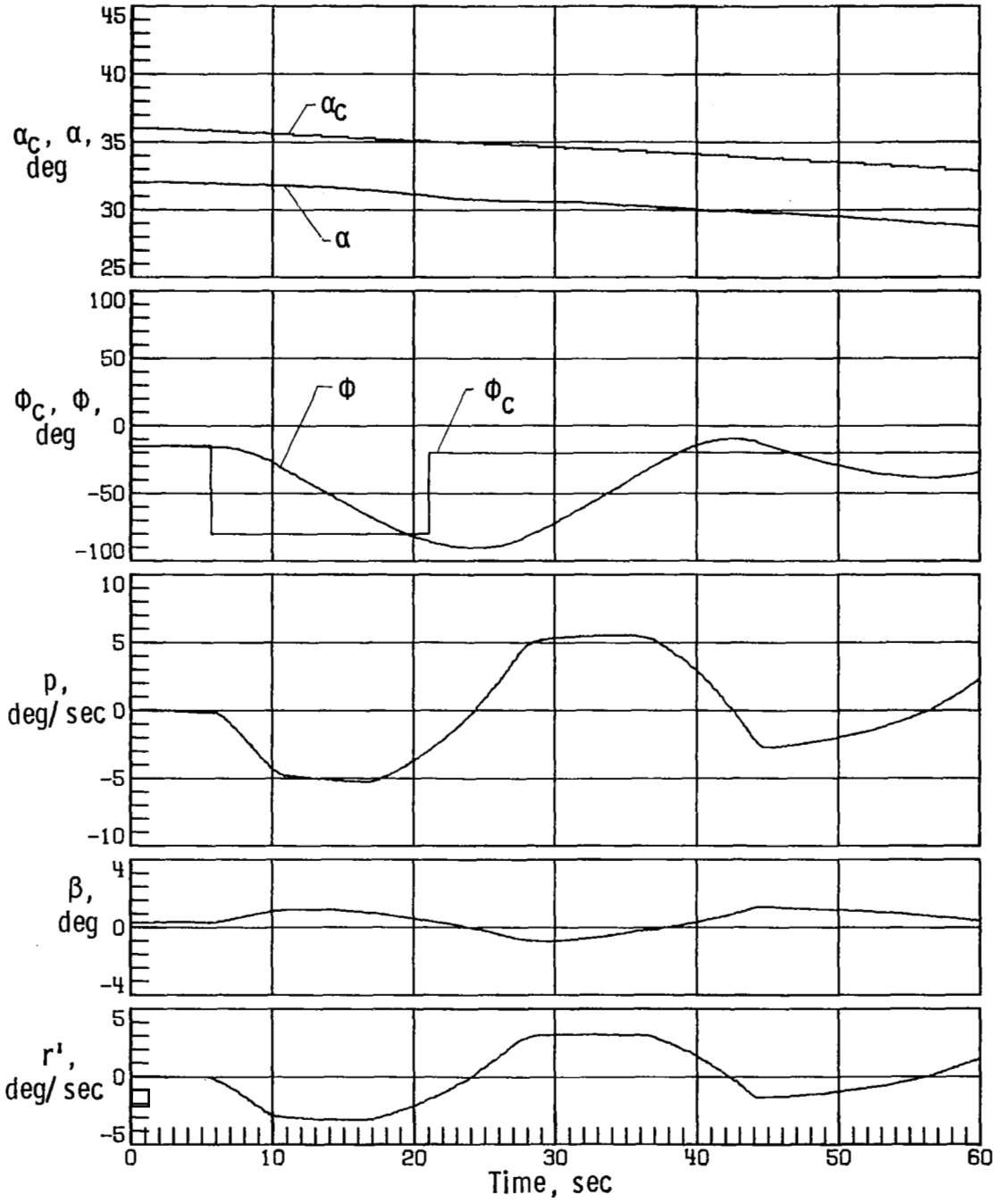

(a) Case 3.

Figure 10.- Space Shuttle Orbiter response with simulation initiated at Mach 10 with off-nominal aerodynamics, sensed α error of $+4^{o}$, two yaw RCS thrusters on each side inoperable, and 0.0381-m lateral center-of-gravity offset.

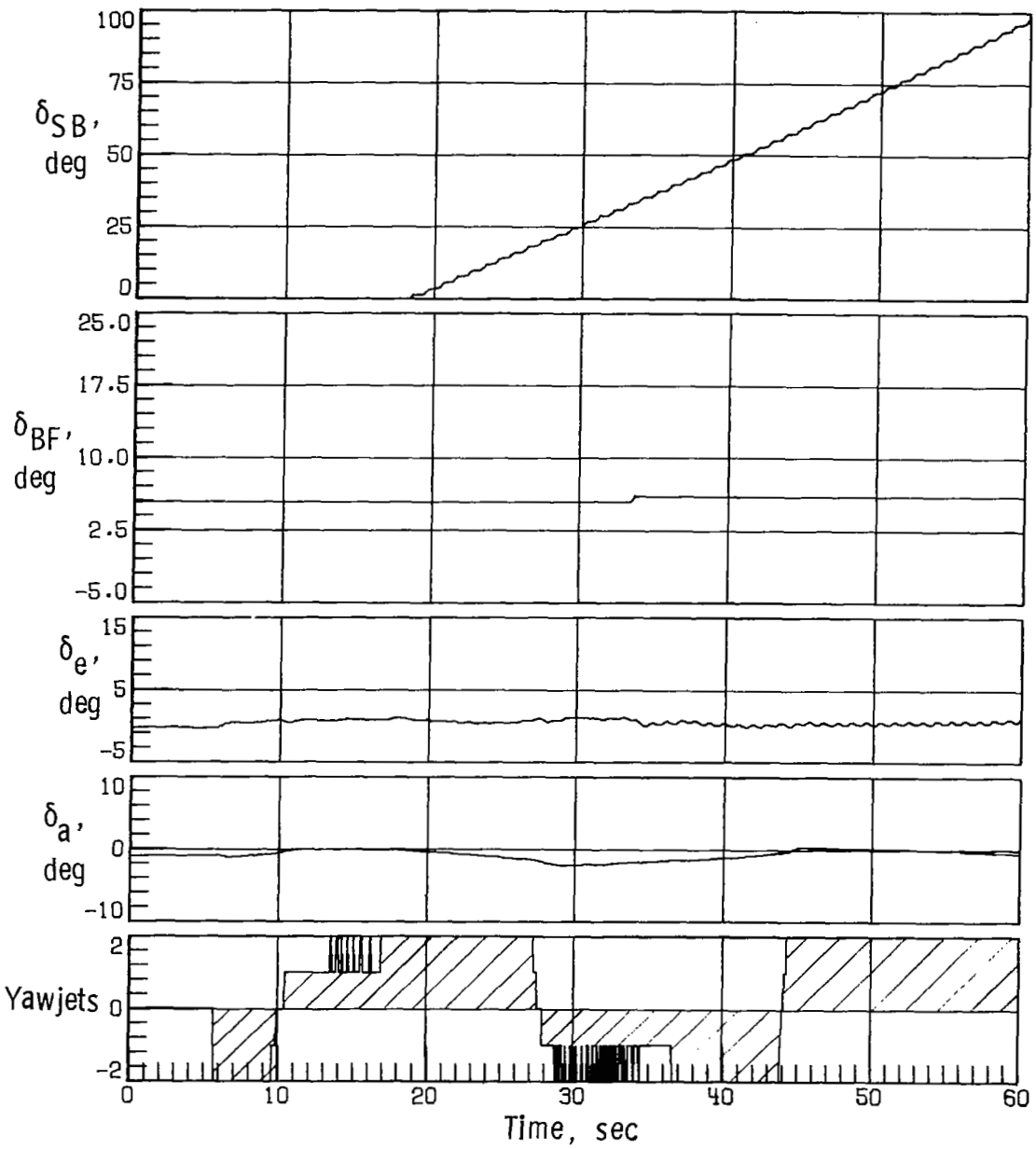

(a) Concluded.

Figure 10.- Continued.

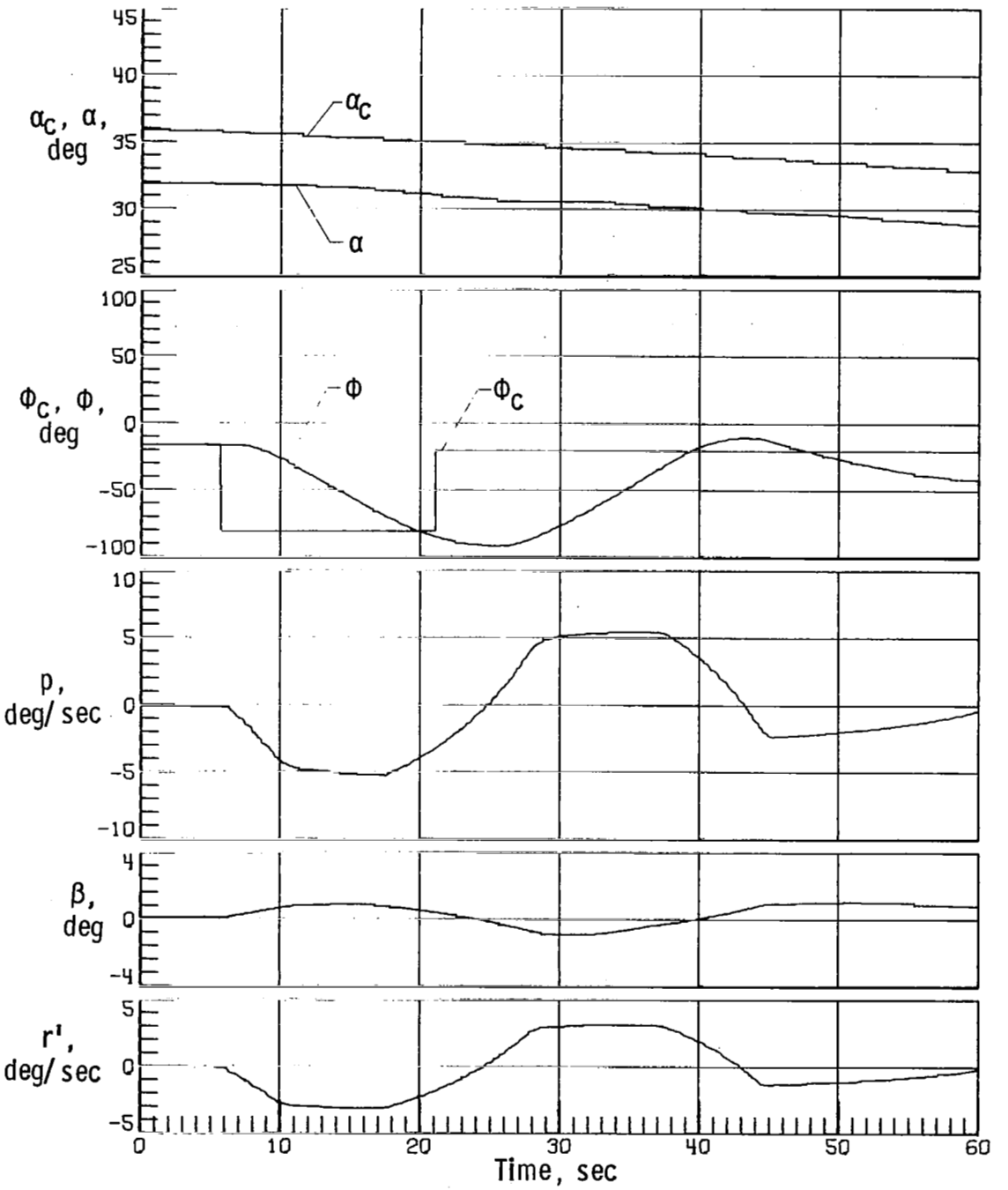

(b) Case 9.

Figure 10.- Continued.

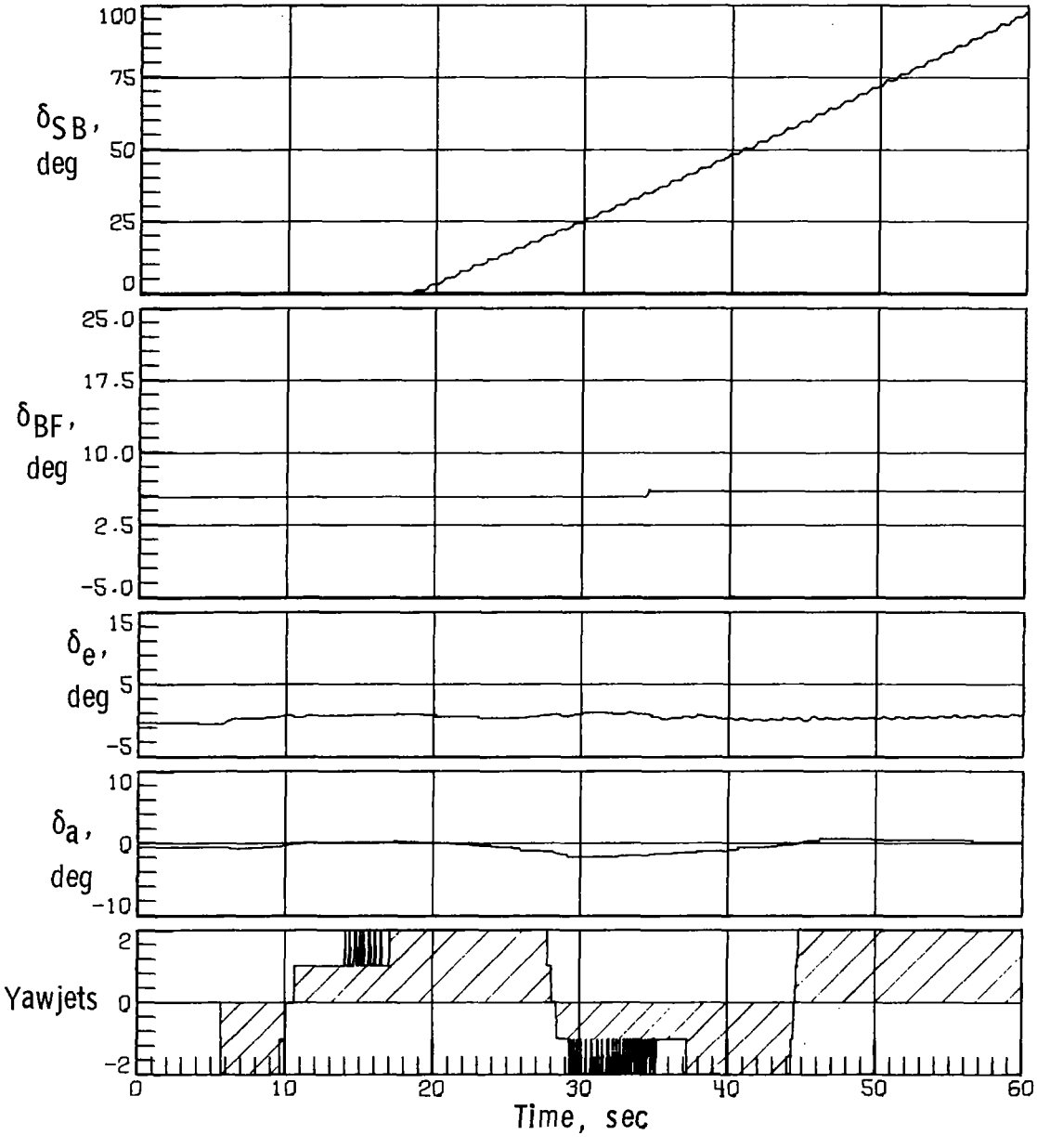

(b) Concluded.

Figure 10.- Continued.

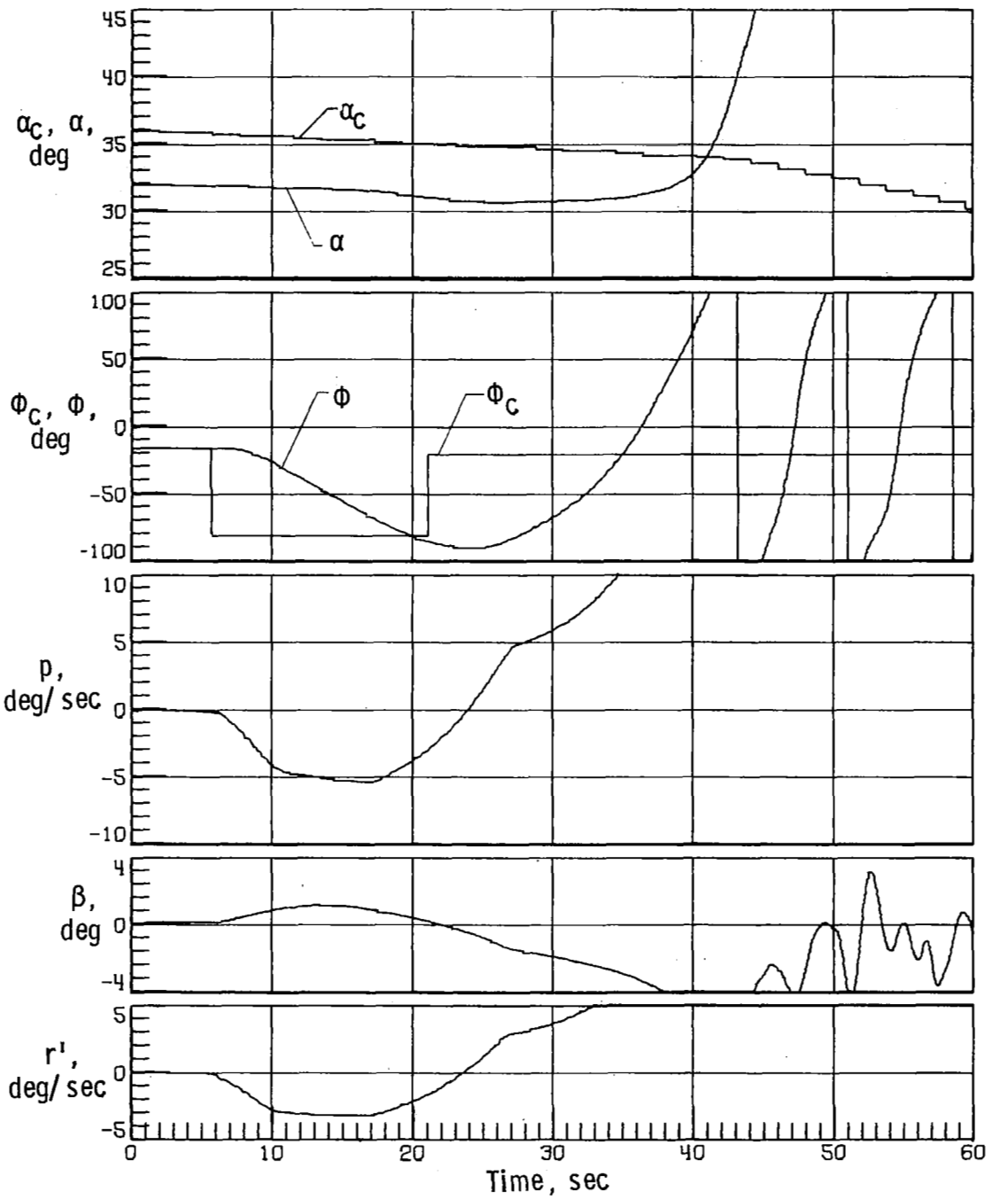

(c) Case 11.

Figure 10.- Continued.

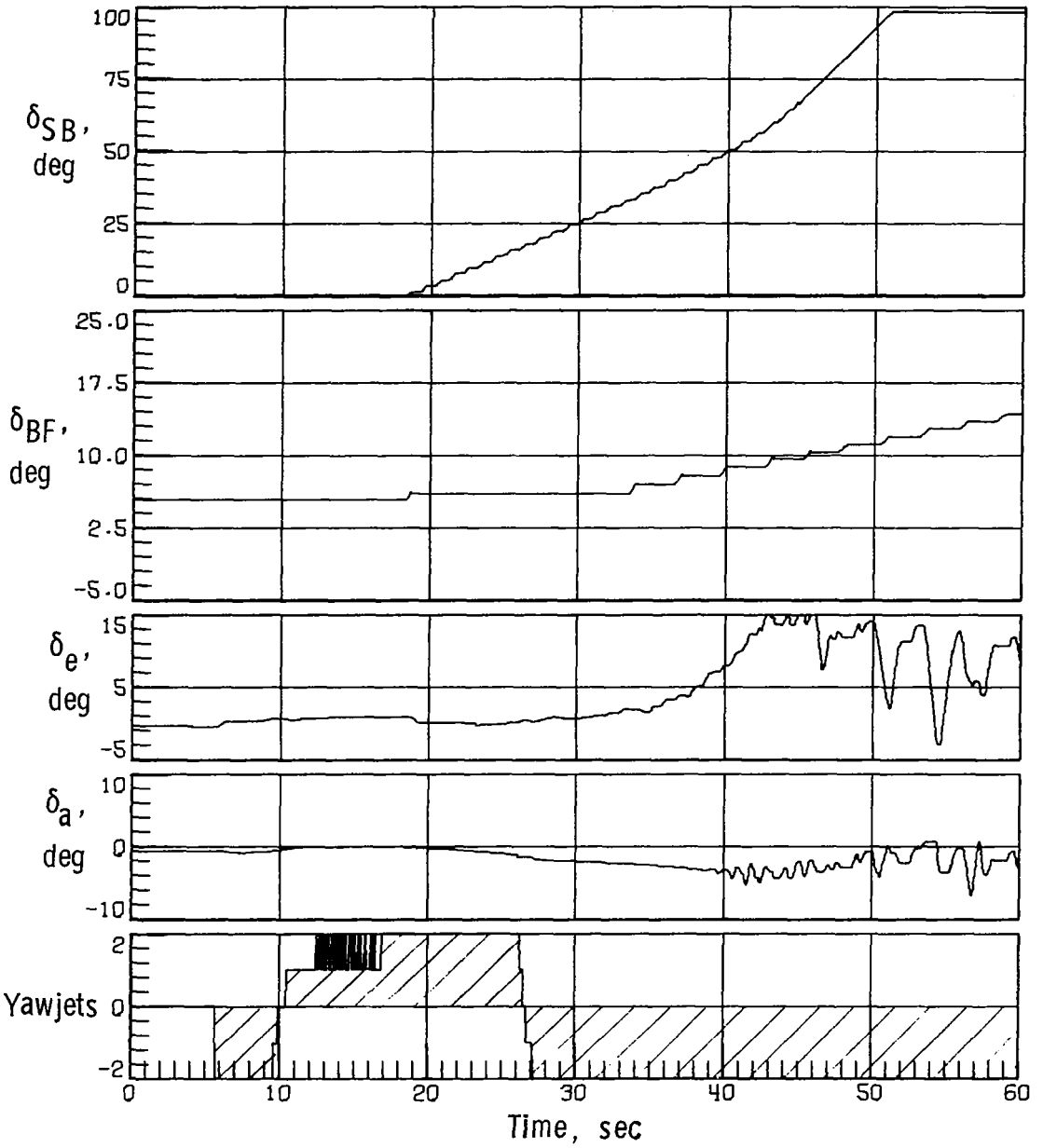

(c) Concluded.

Figure 10.- Continued.

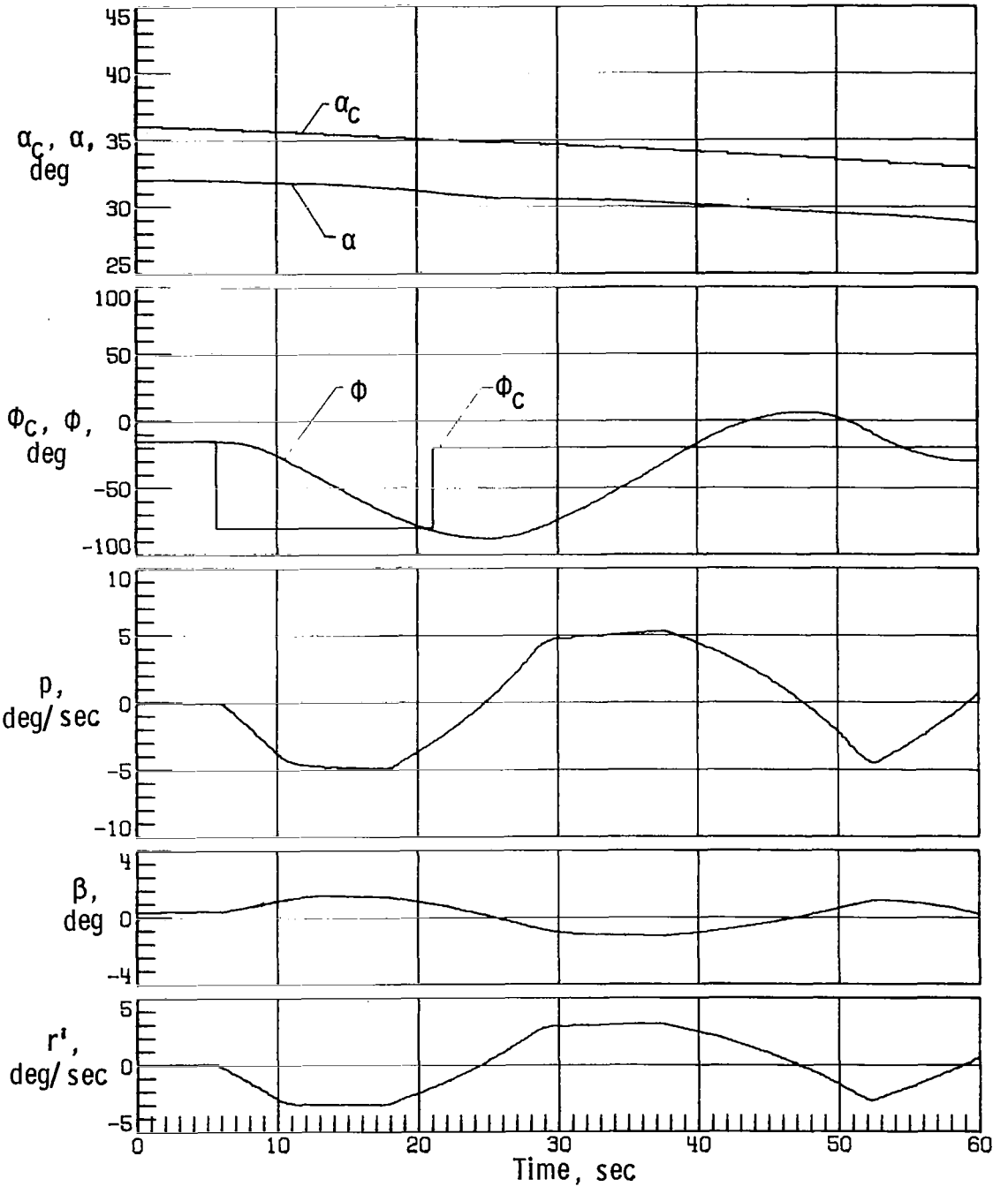

(d) Case 12.

Figure 10.- Continued.

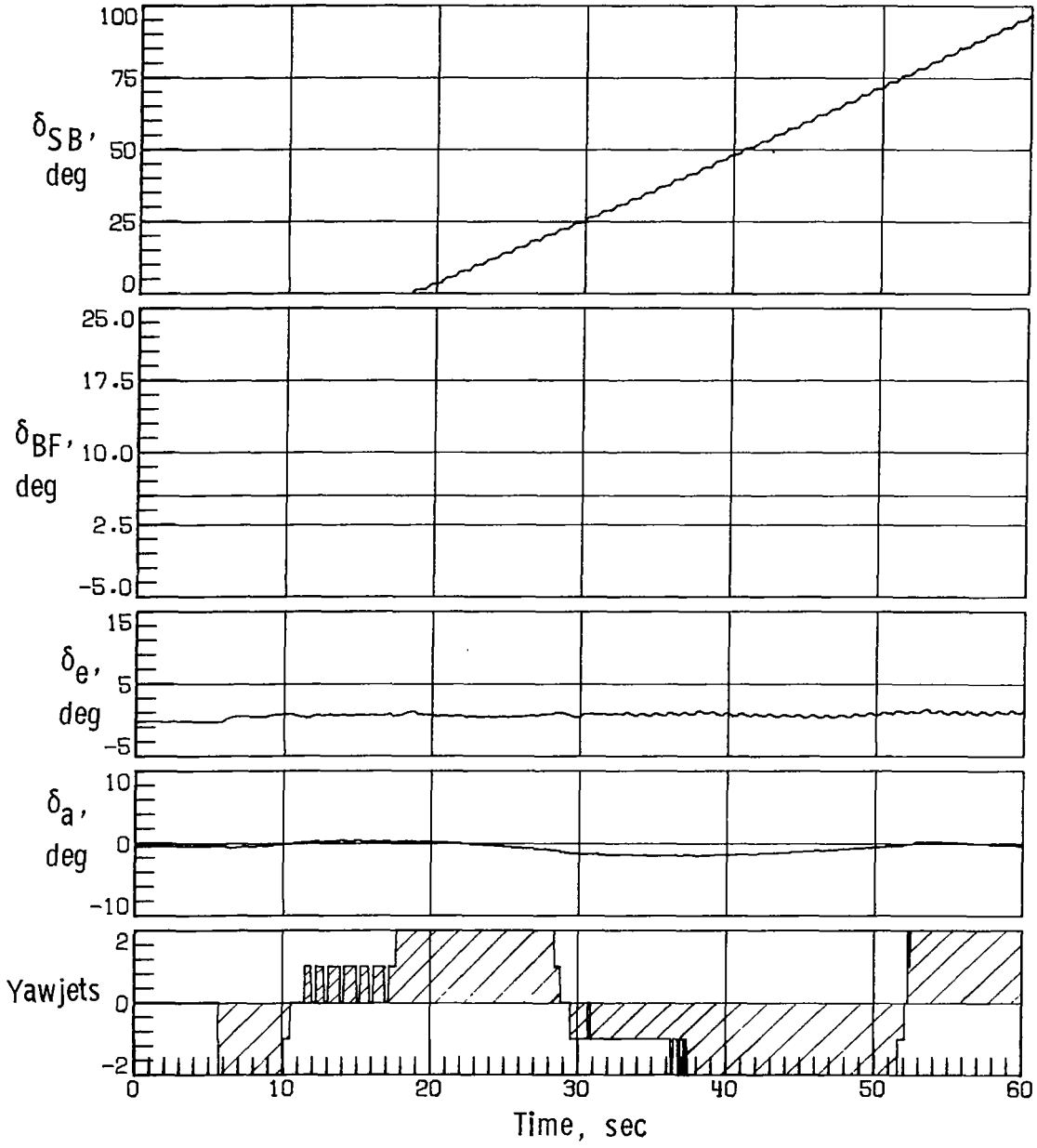

(d) Concluded.

Figure 10. - Continued.

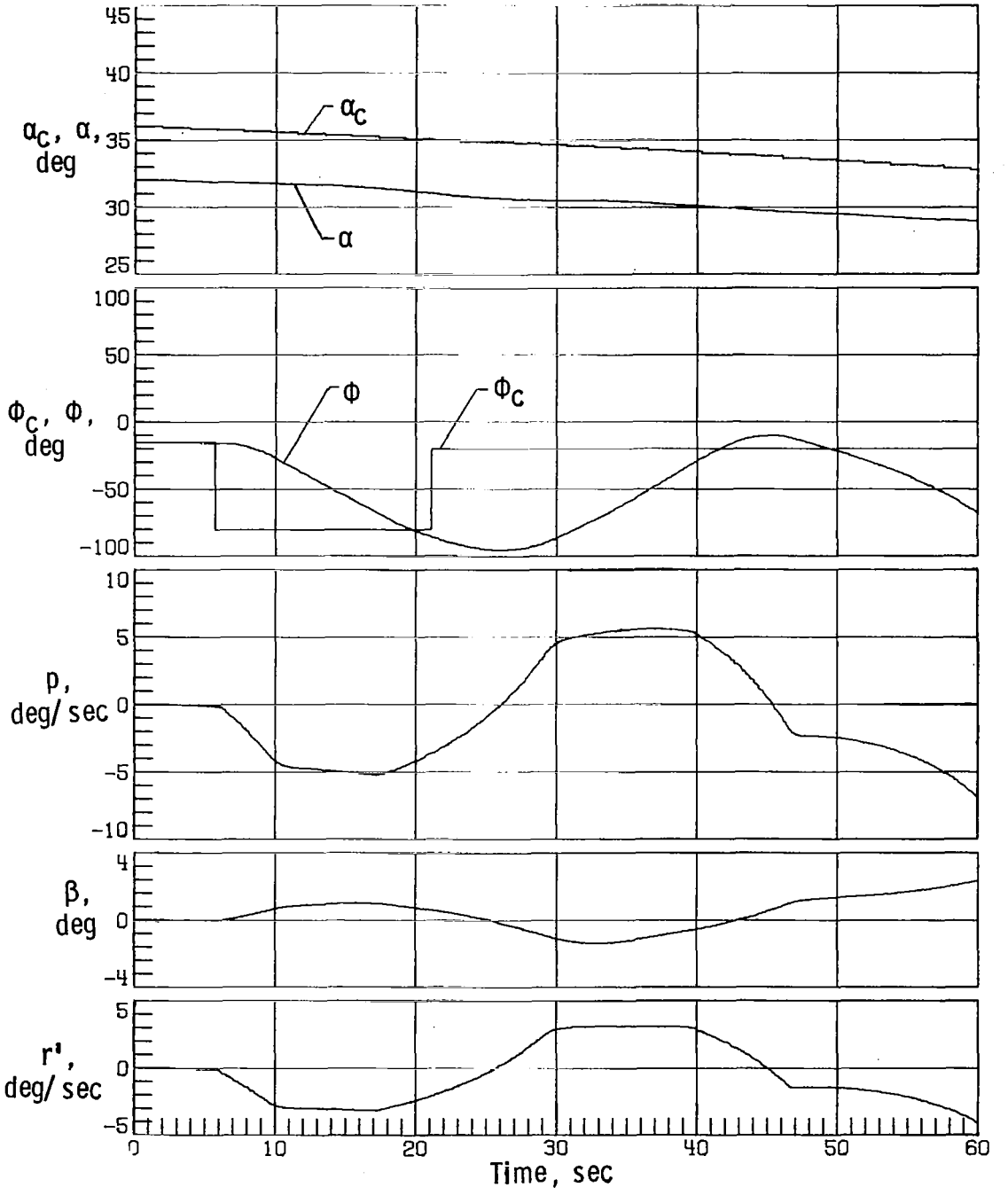

(e) Case 15.

Figure 10.- Continued.

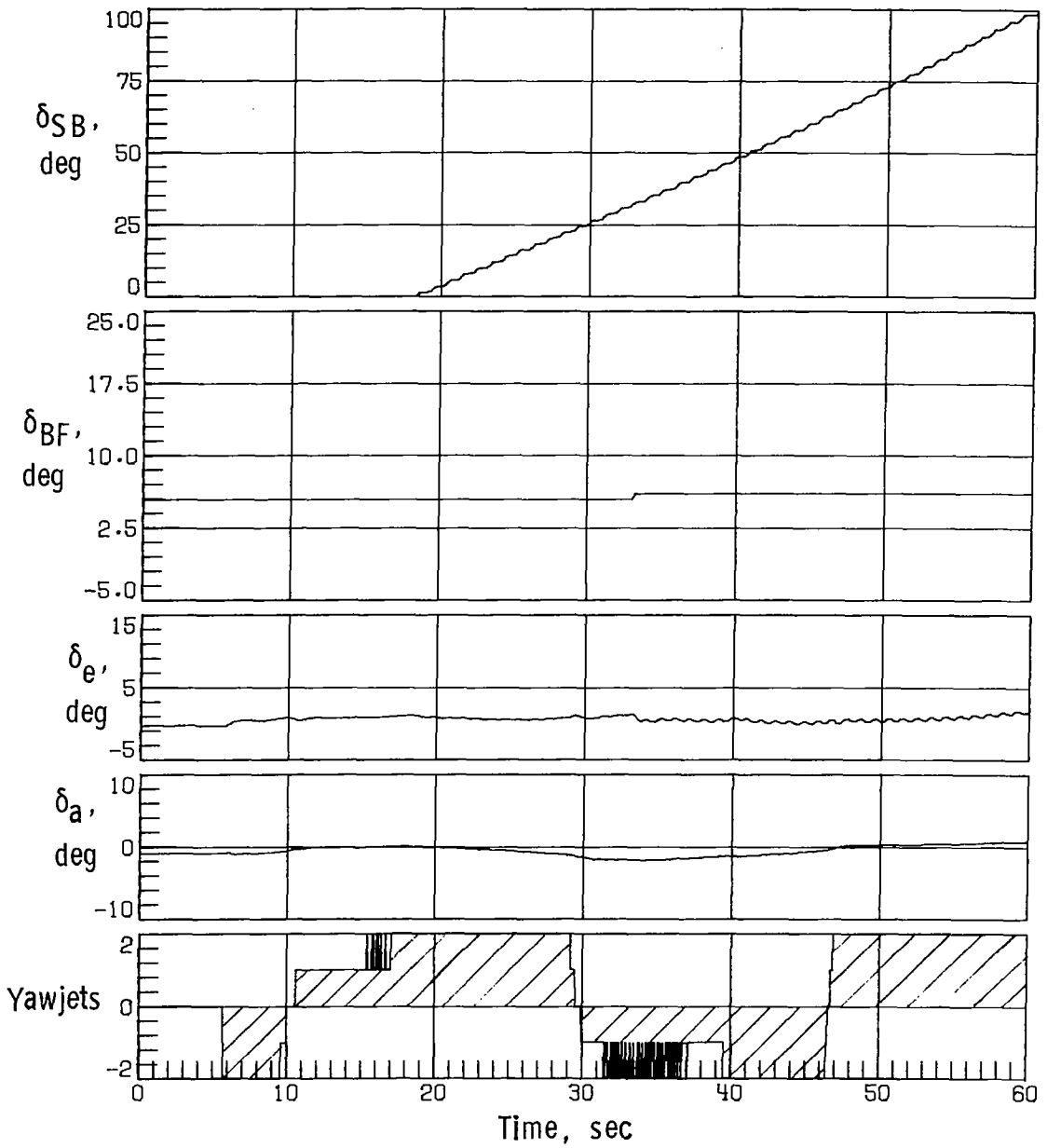

(e) Concluded.

Figure 10.- Concluded.

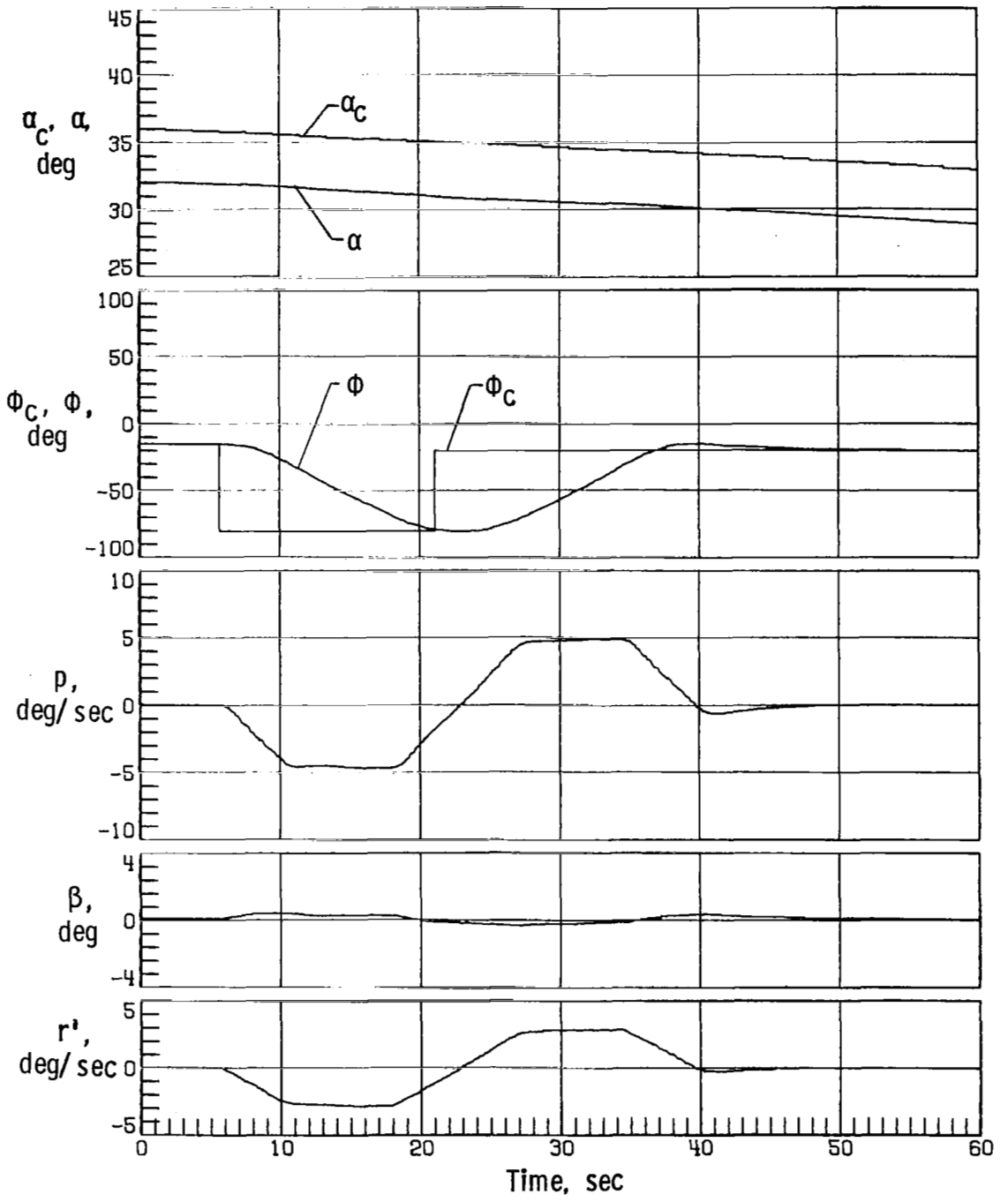

(a) Nominal aerodynamics.

Figure 11.- Space Shuttle Orbiter response with simulation initiated at Mach 10 with sensed α error of $+4^{\circ}$, two yaw RCS thrusters on each side inoperable, modified control system, and 0.0381-m lateral center-of-gravity offset.

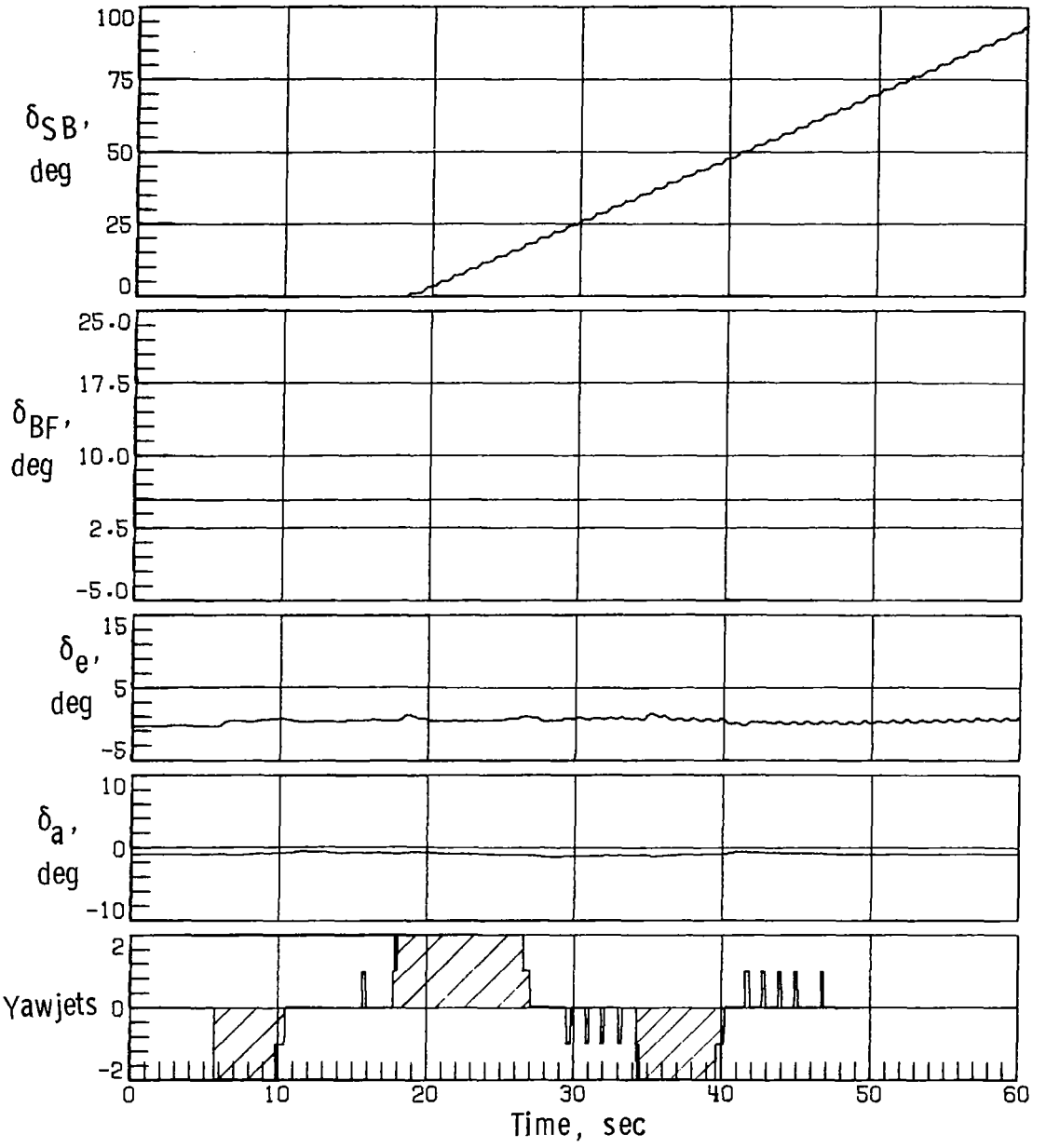

(a) Concluded.

Figure 11.- Continued.

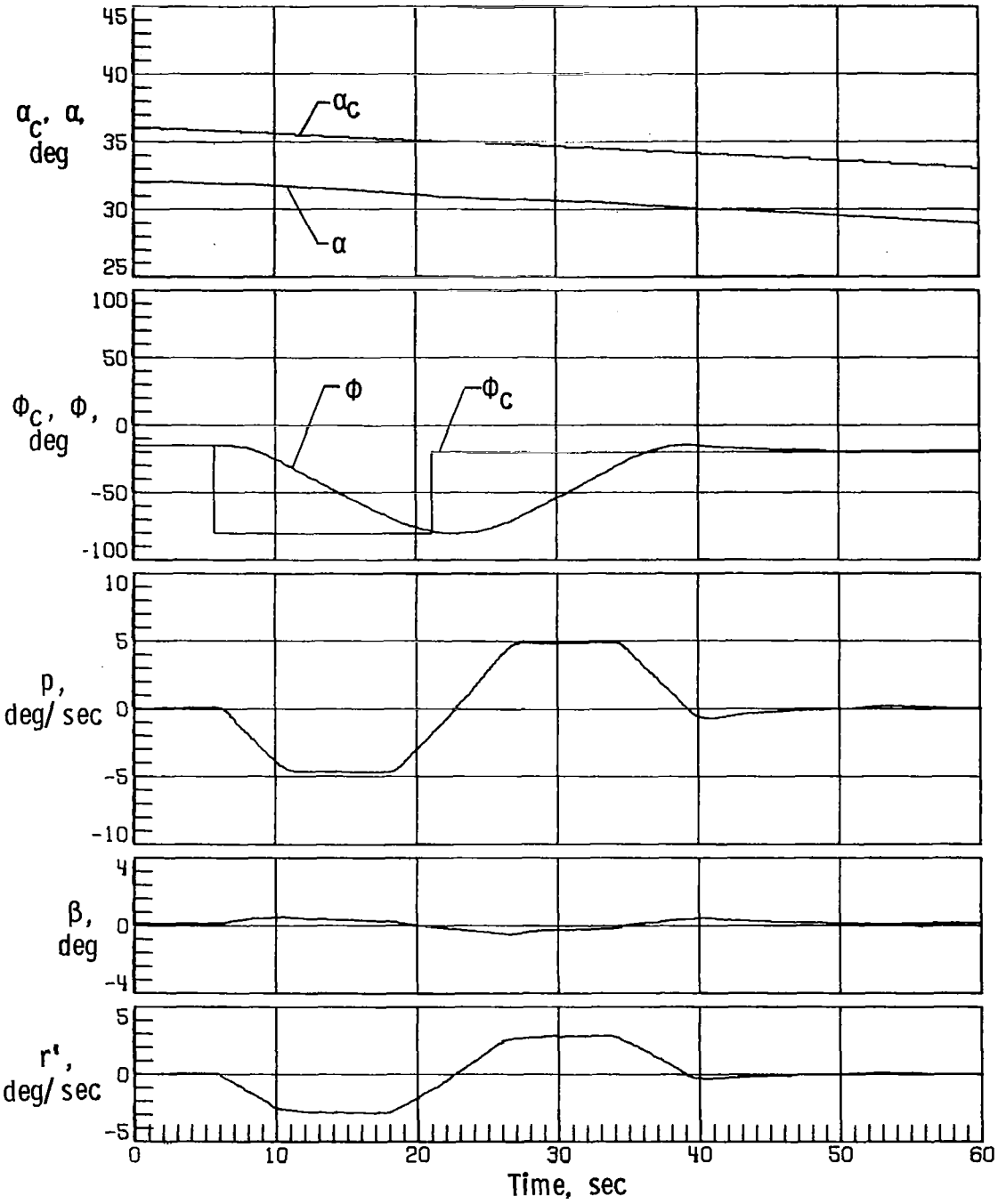

(b) Case 11.

Figure 11.- Continued.

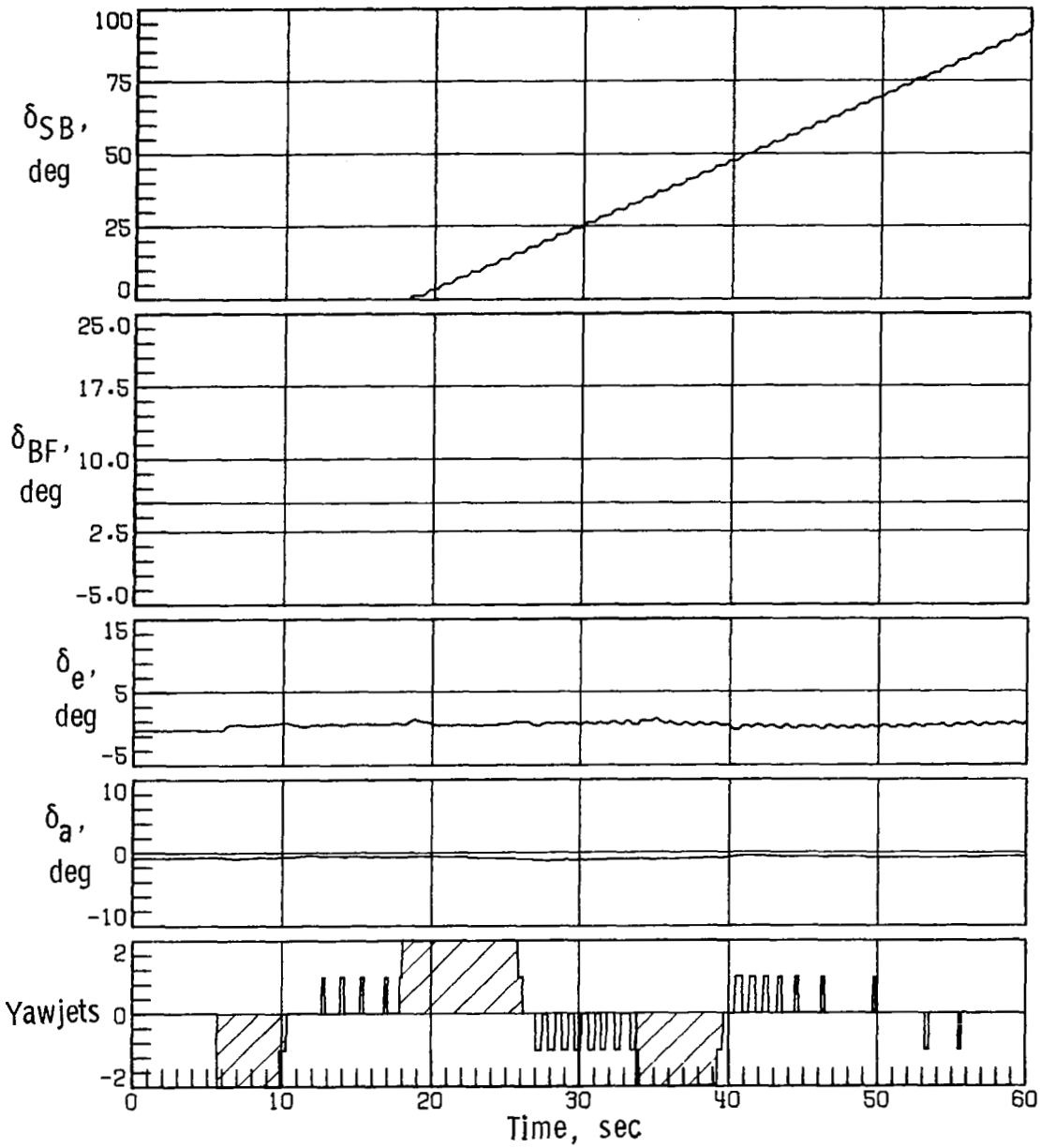

(b) Concluded.

Figure 11.- Concluded.

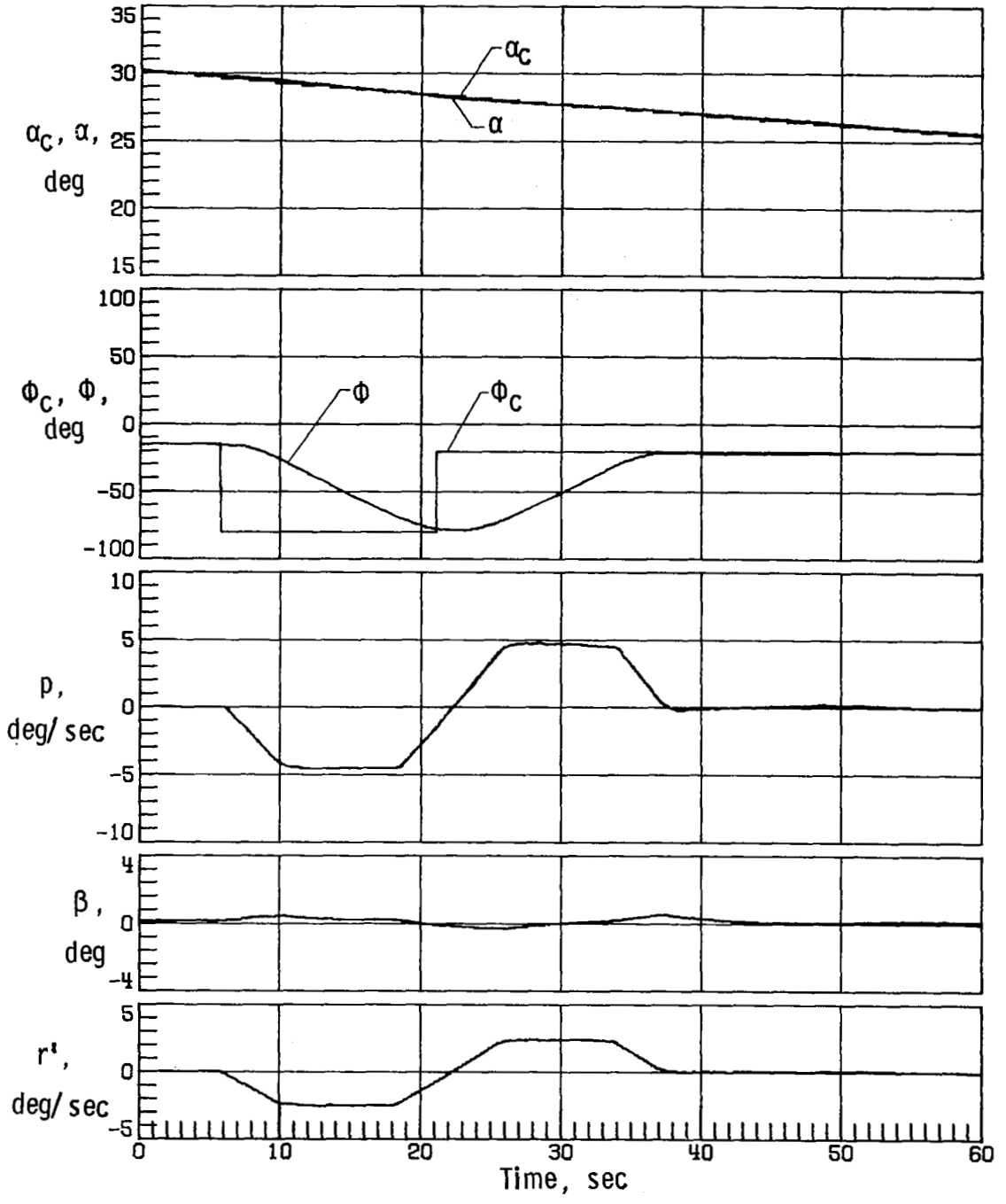

Figure 12.- Space Shuttle Orbiter response with simulation initiated at Mach 7.5 with nominal aerodynamics, no-sensed α error, two yaw RCS thrusters on each side inoperable, and a 0.0381-m lateral center-of-gravity offset.

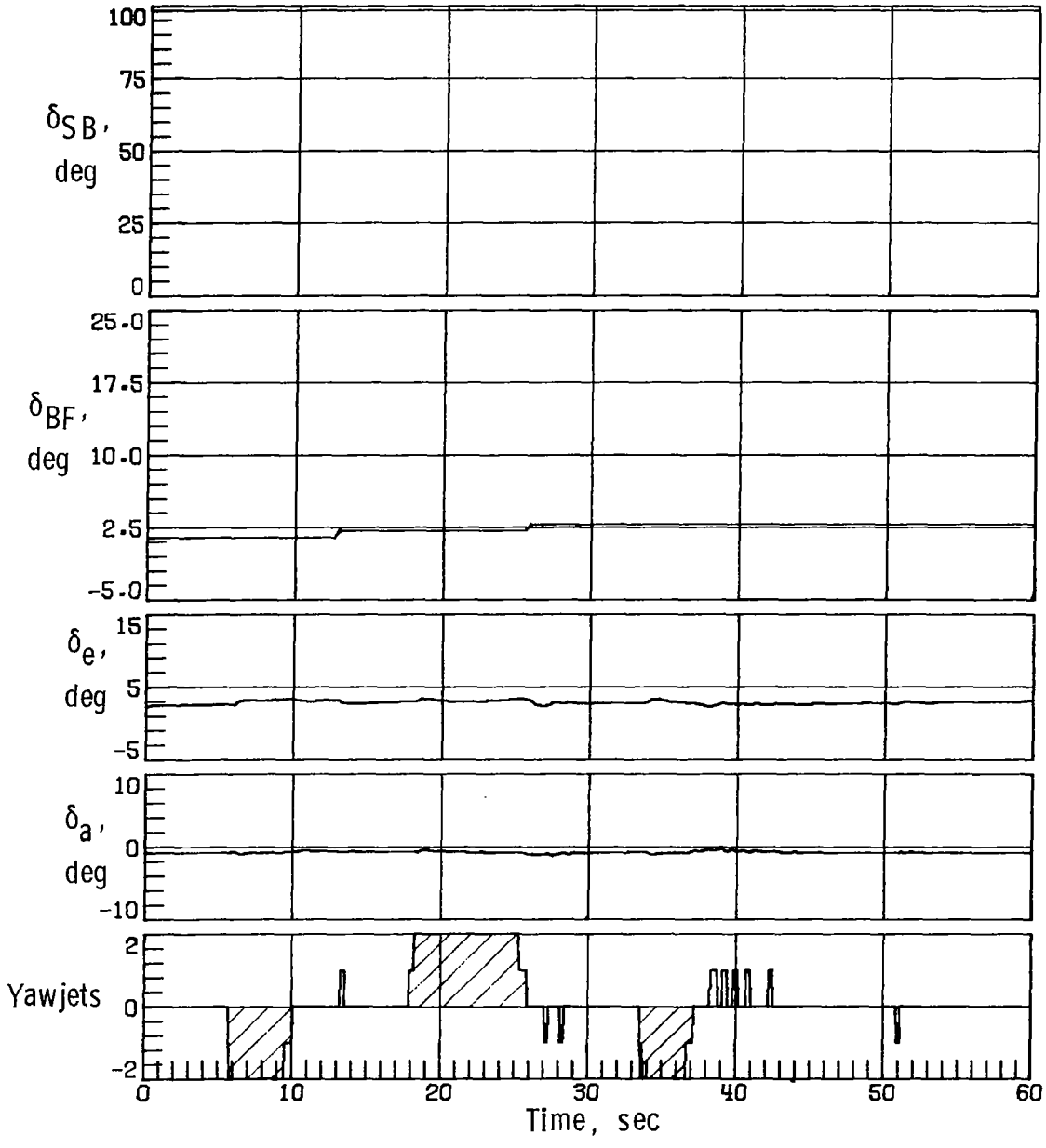

Figure 12.- Concluded.

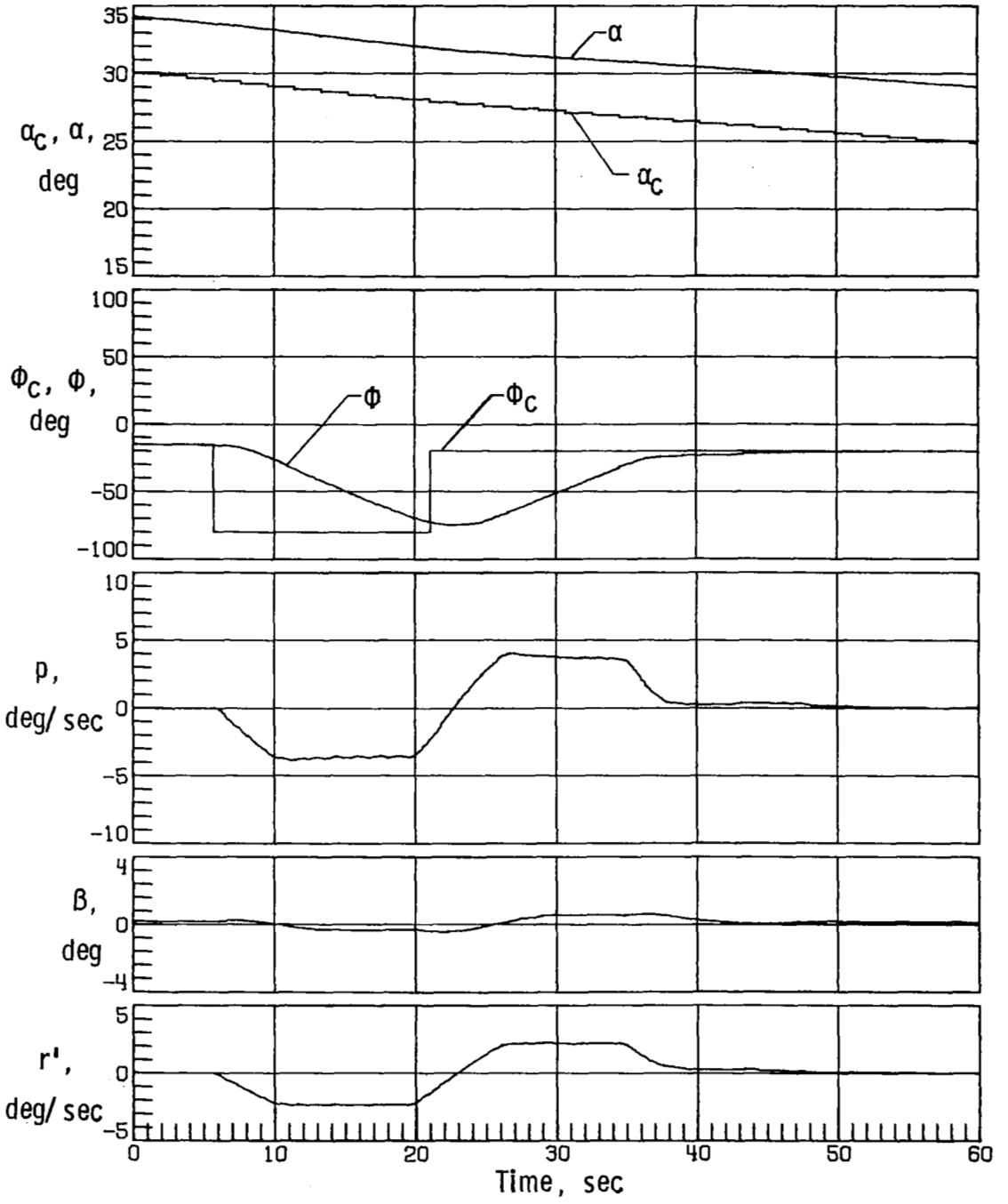

Figure 13.- Space Shuttle Orbiter response with simulation initiated at Mach 7.5 with nominal aerodynamics, sensed α error of -4°, two yaw RCS thrusters on each side inoperable, and 0.0381-m lateral center-of-gravity offset.

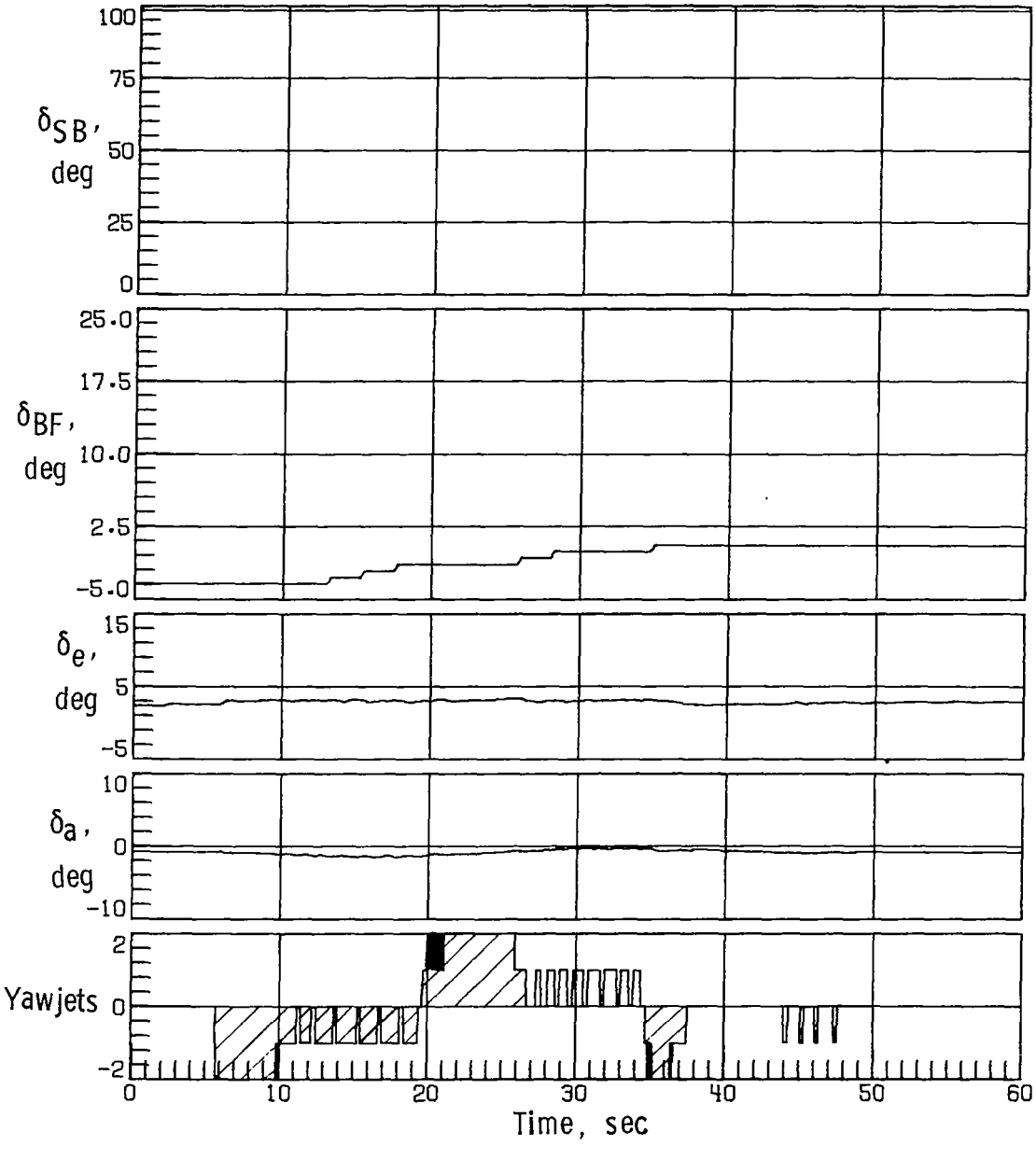

Figure 13.- Concluded.

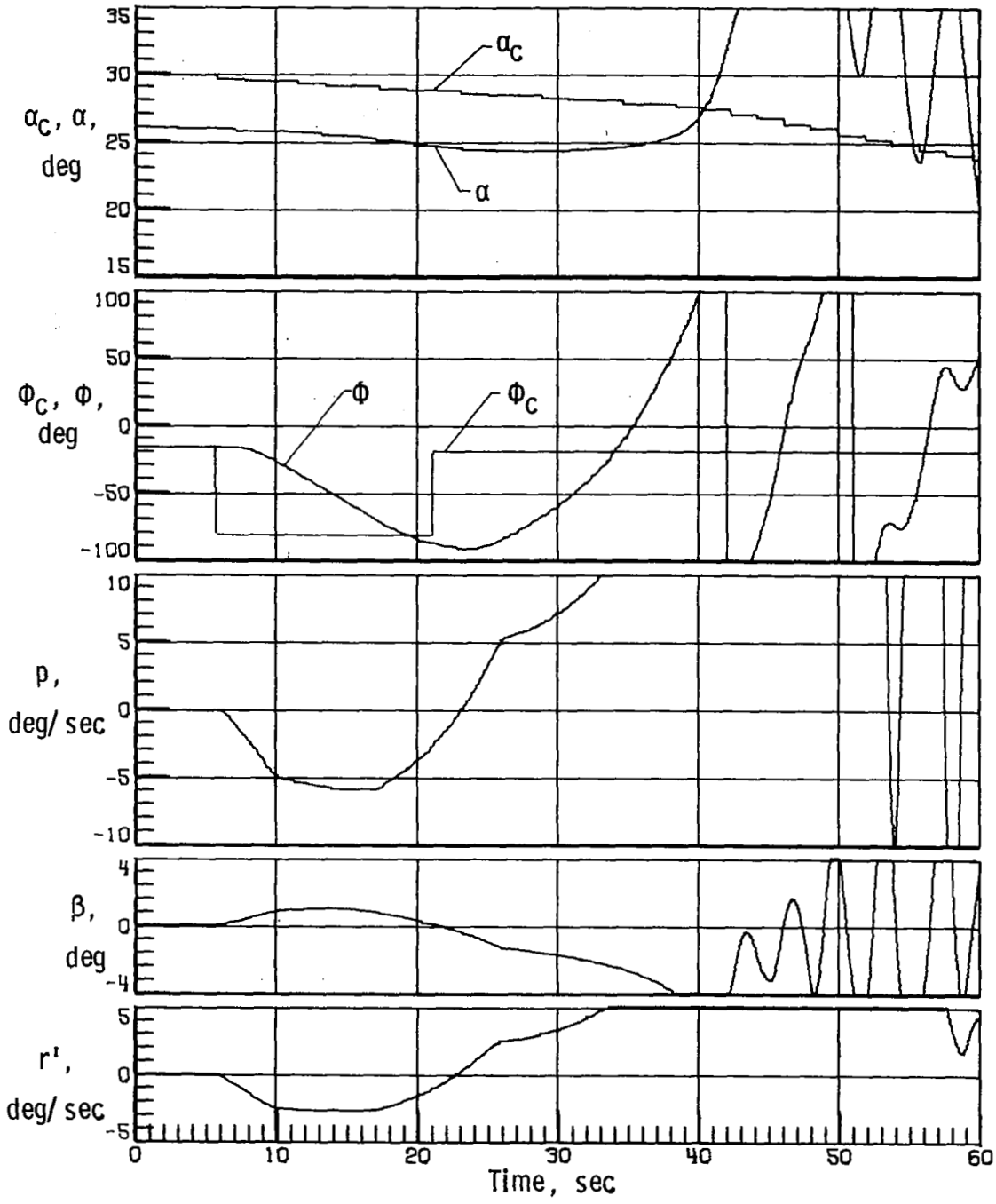

(a) Nominal aerodynamics.

Figure 14.- Space Shuttle Orbiter response with simulation initiated at Mach 7.5 with sensed α error of $+4^{o}$, two yaw RCS thrusters on each side inoperable, and 0.0381-m lateral center-of-gravity offset.

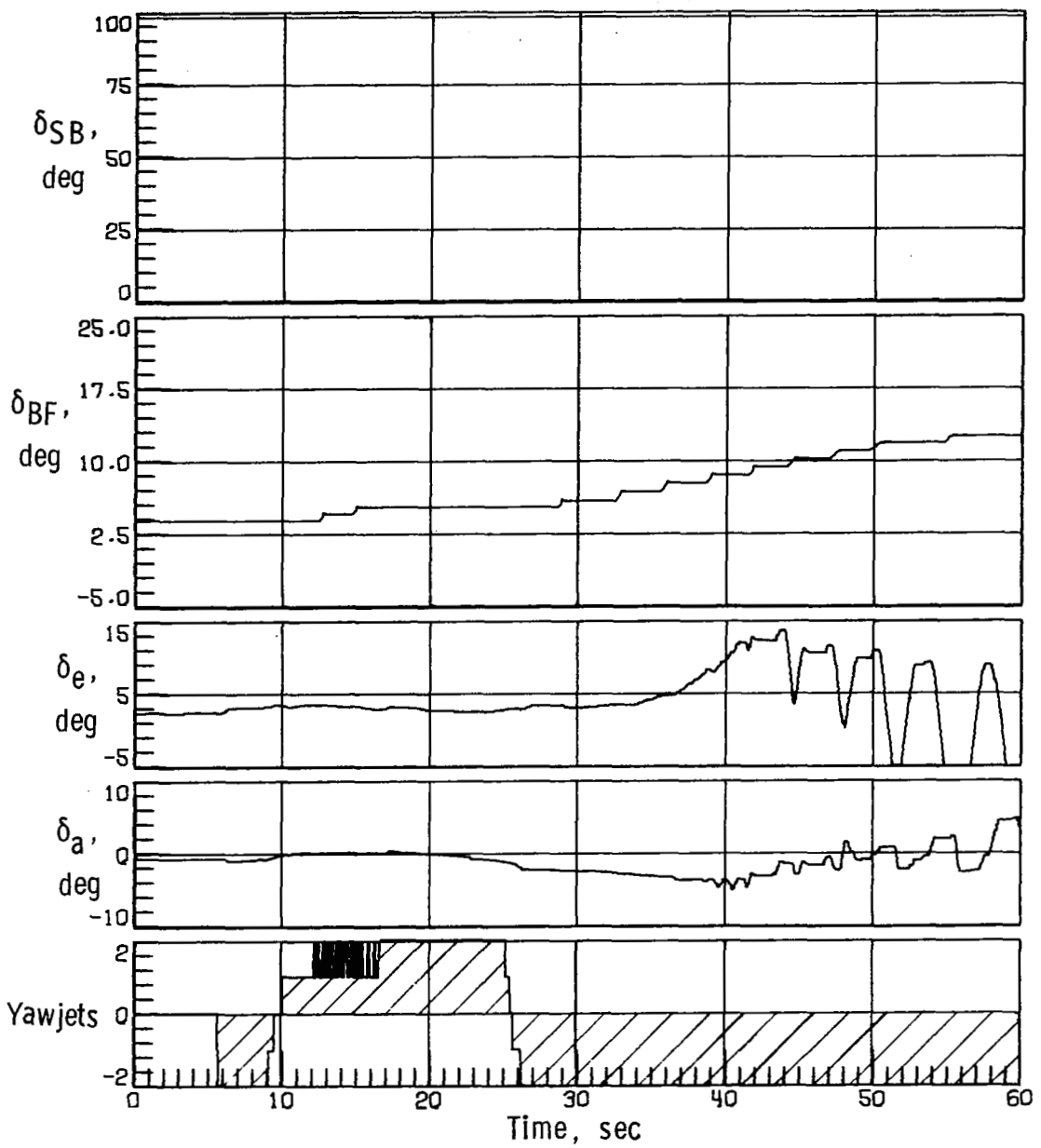

(a) Concluded.

Figure 14.- Continued.

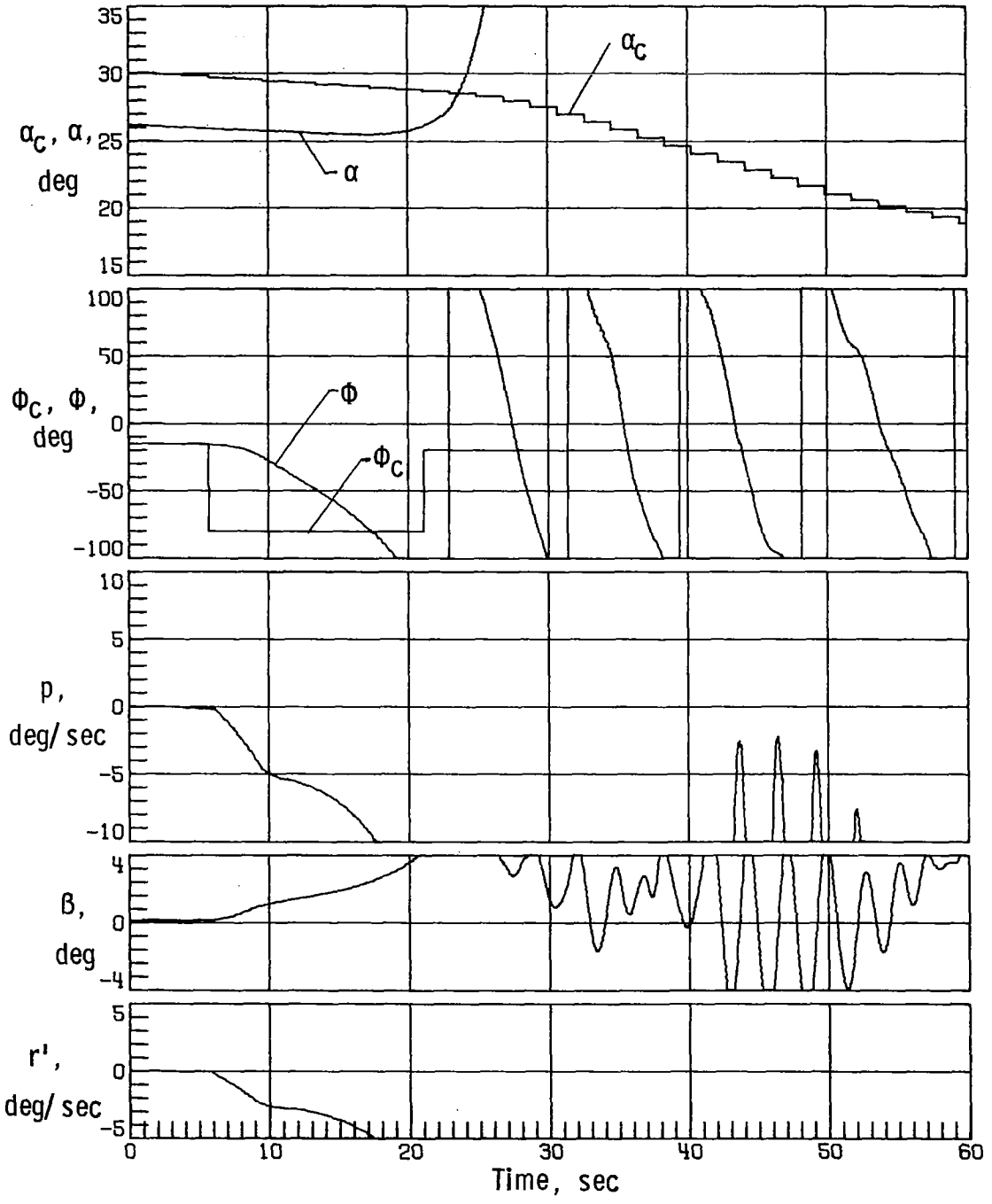

(b) Case 11.

Figure 14.- Continued.

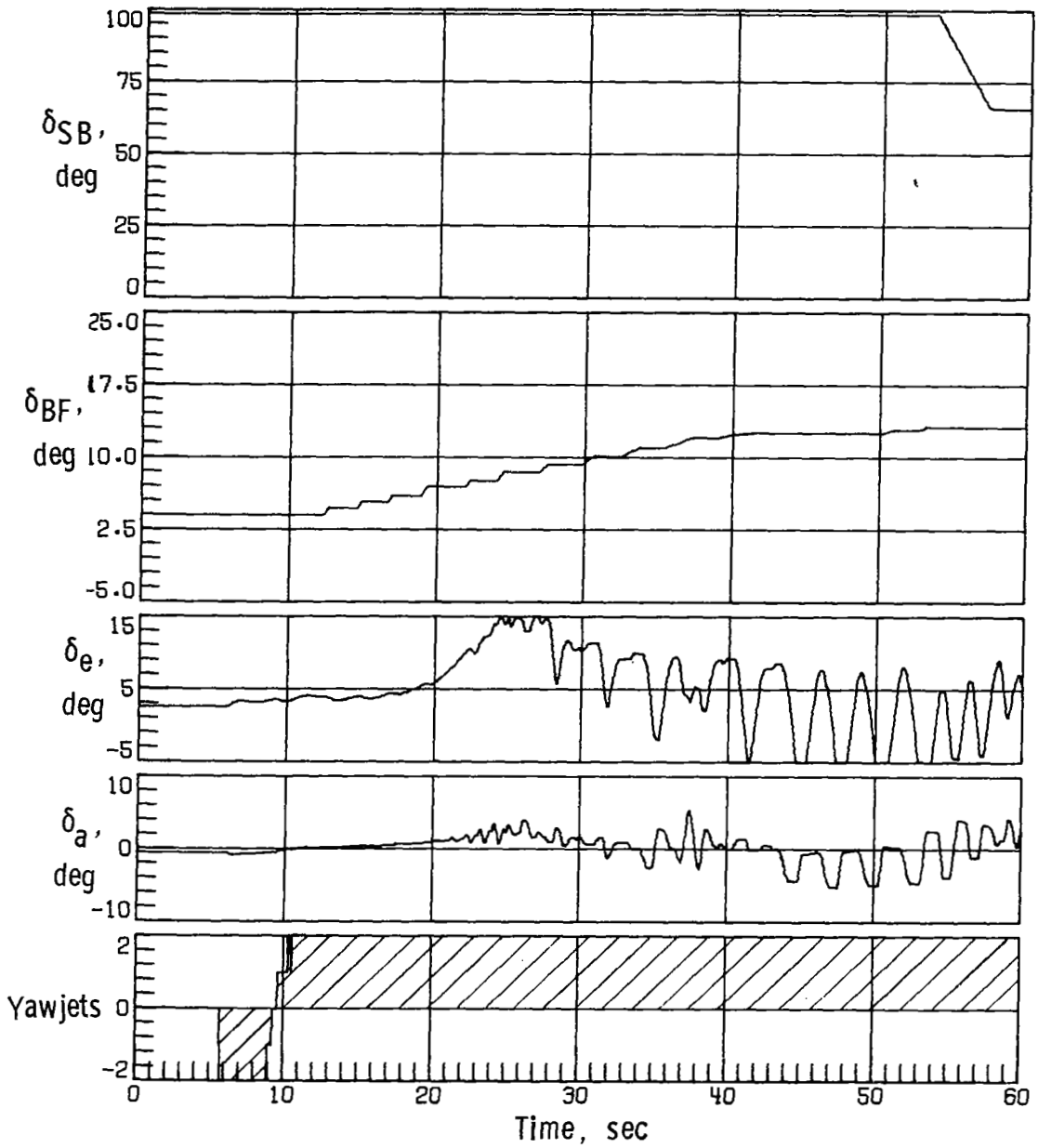

(b) Concluded.

Figure 14.- Concluded.

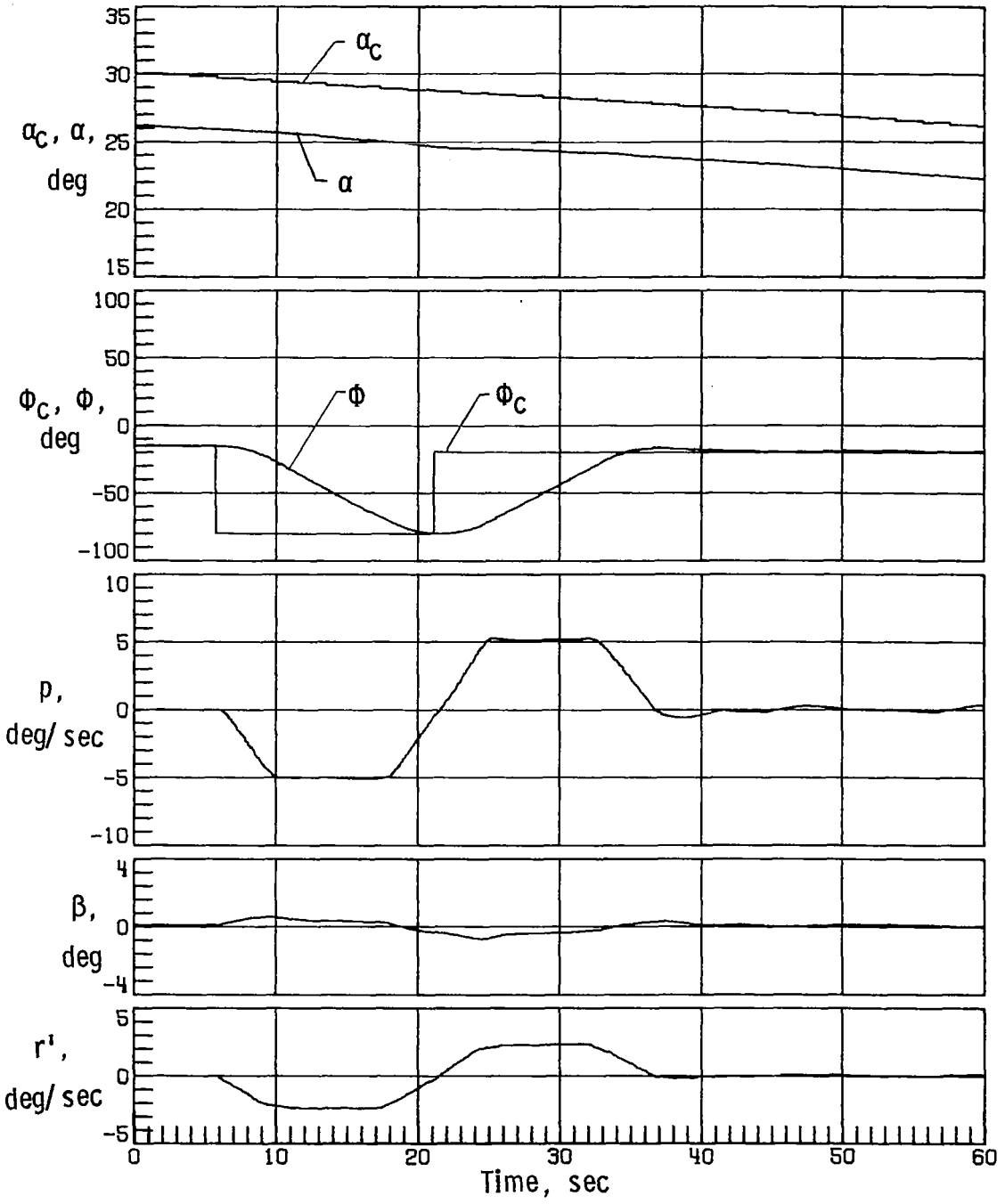

(a) Nominal aerodynamics.

Figure 15.- Space Shuttle Orbiter response with simulation initiated at Mach 7.5 with sensed α error of $+4^{\circ}$, two yaw RCS thrusters on each side inoperable, modified control system, and 0.0381-m lateral center-of-gravity offset.

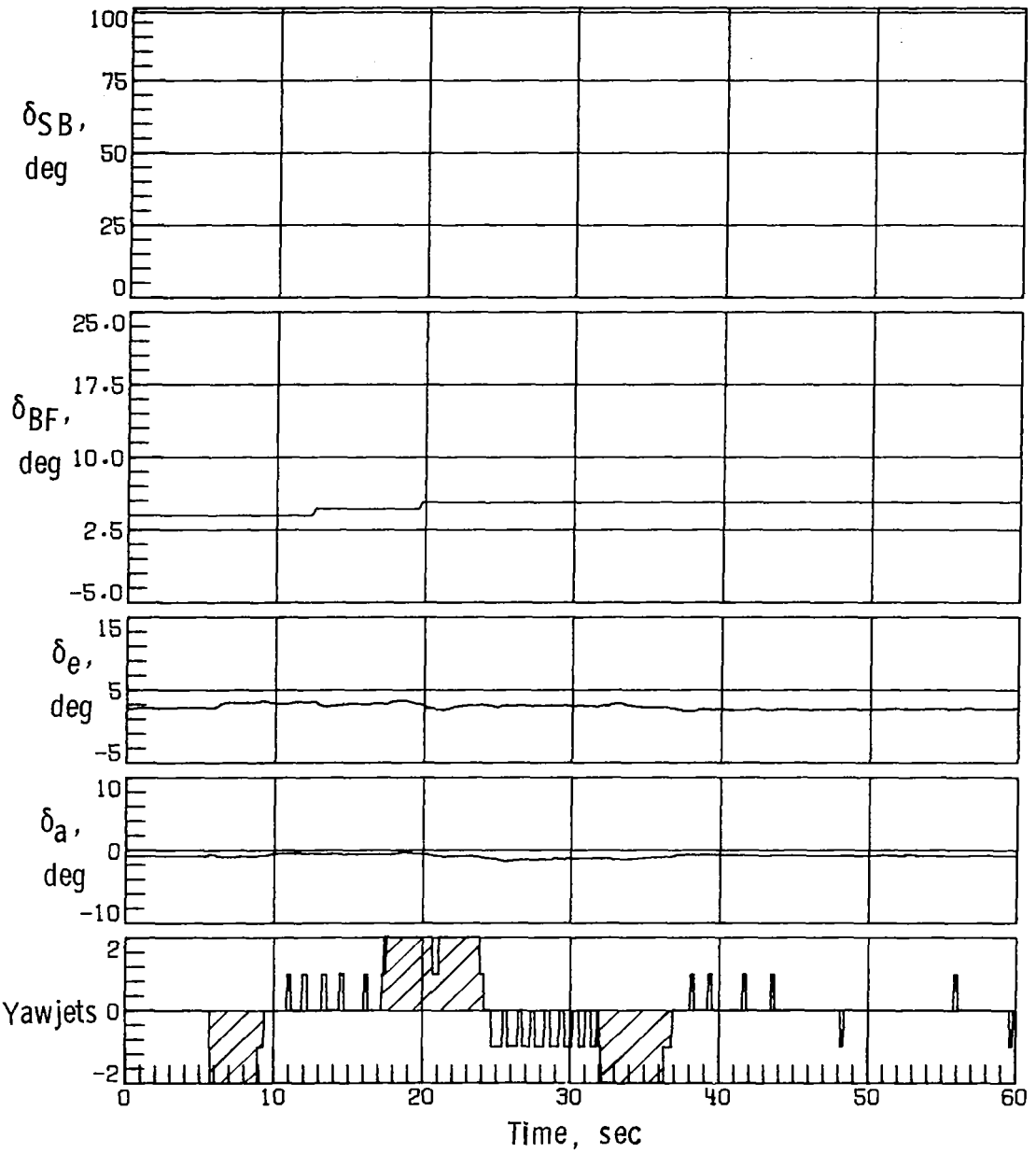

(a) Concluded.

Figure 15.- Continued.

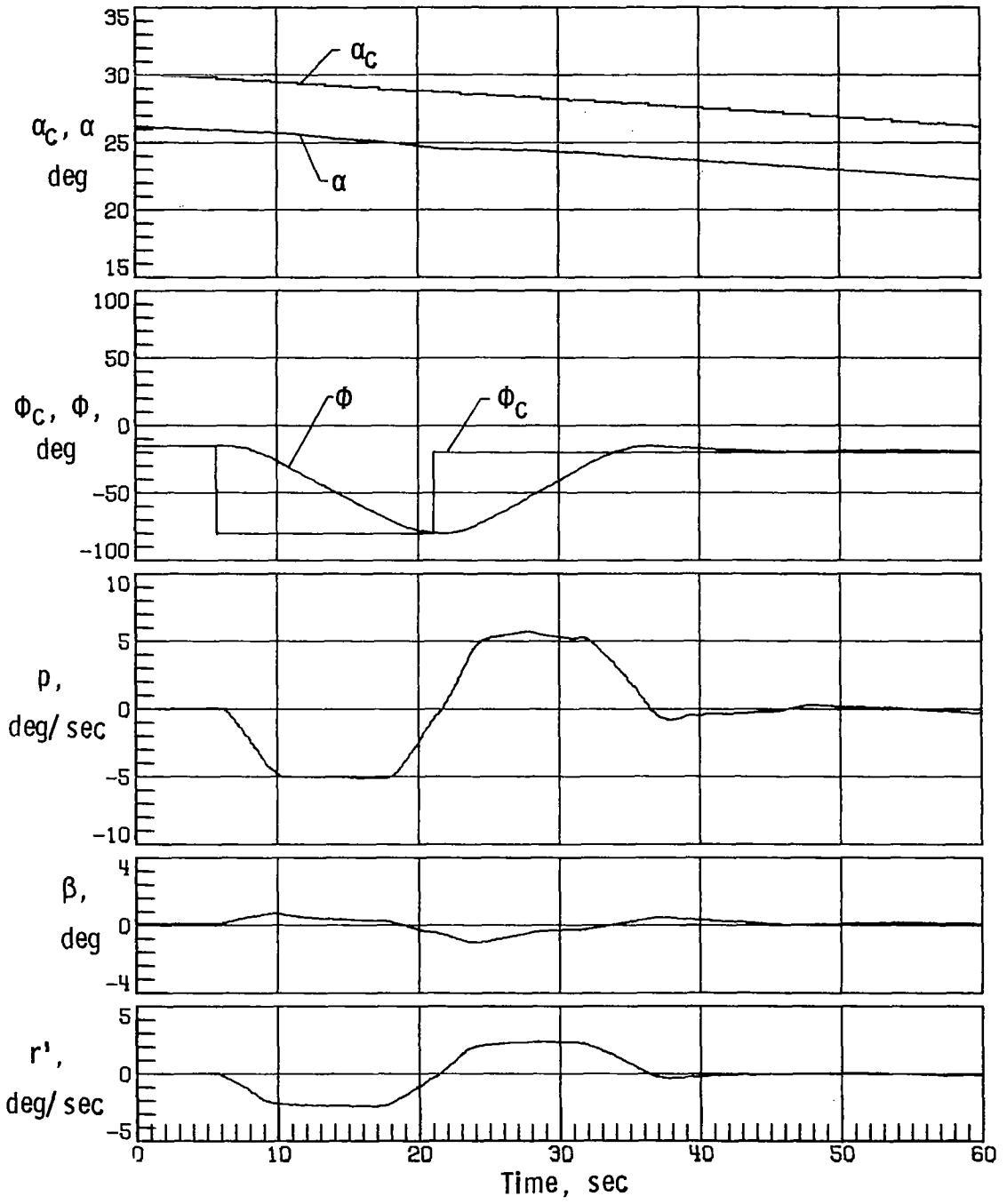

(b) Case 11.

Figure 15.- Continued.

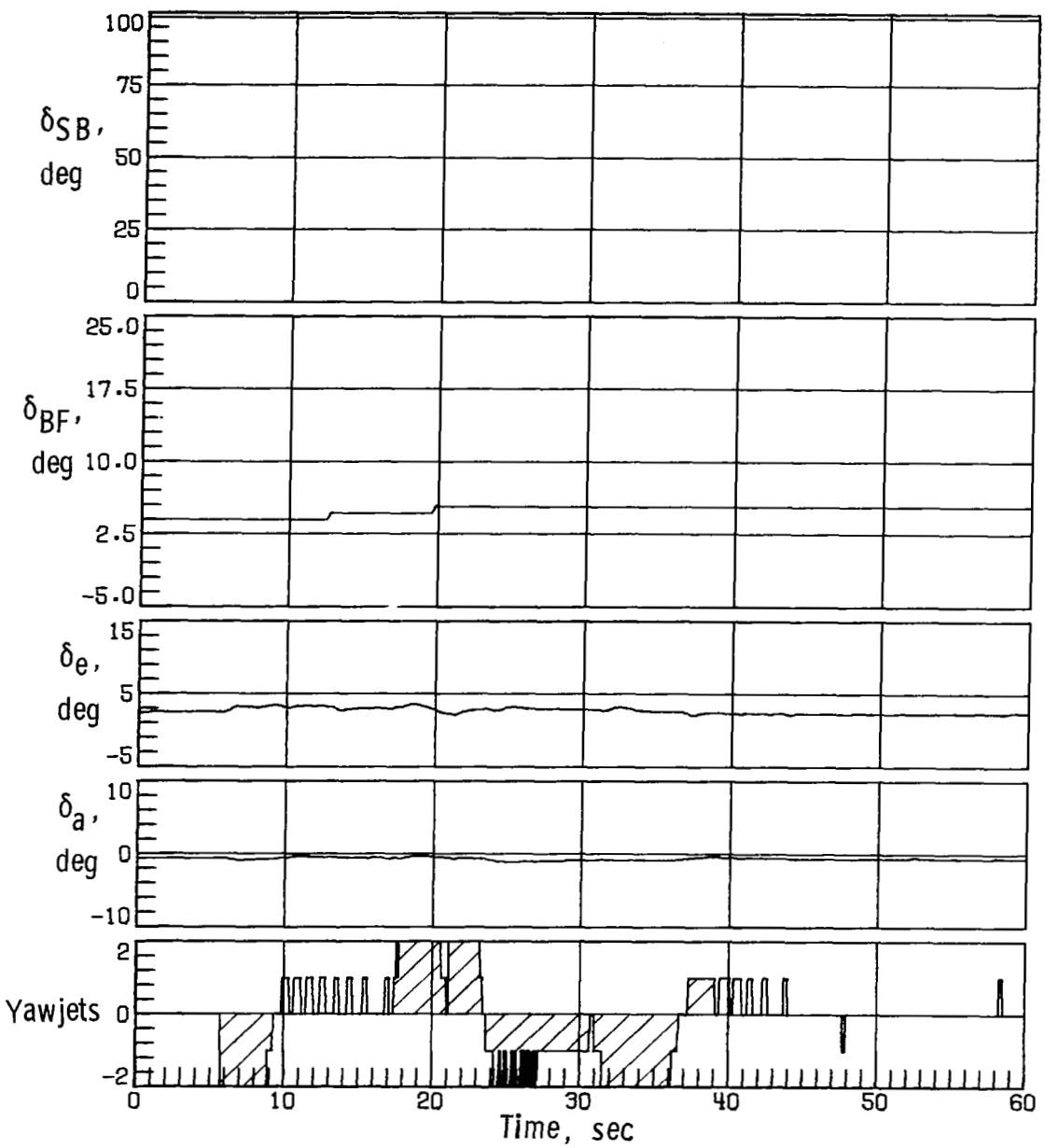

(b) Concluded.

Figure 15.- Concluded.

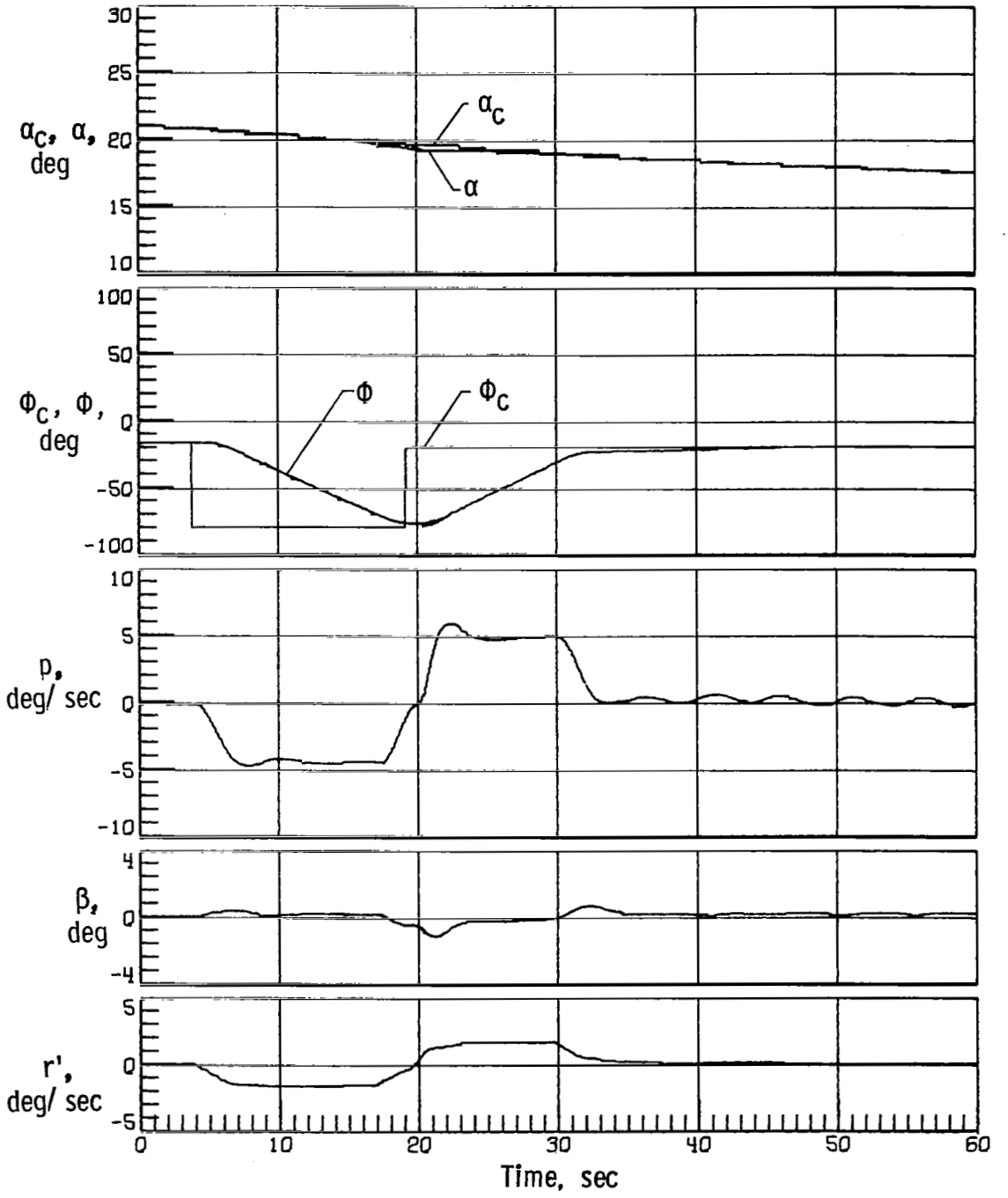

Figure 16.- Space Shuttle Orbiter response with simulation initiated at Mach 5 with nominal aerodynamics, no-sensed α error, two yaw RCS thrusters on each side inoperable, and 0.0381-m lateral center-of-gravity offset.

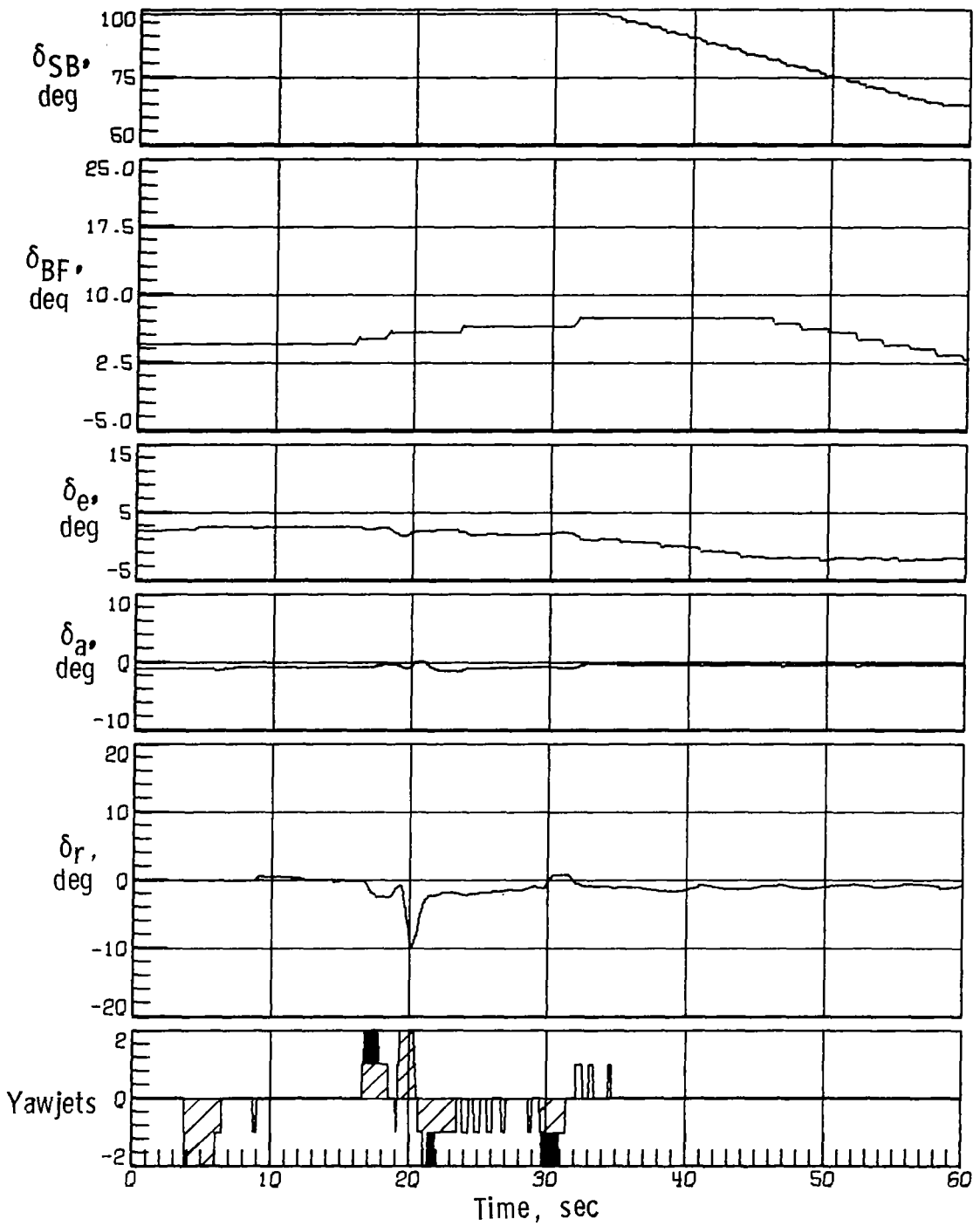

Figure 16.- Concluded.

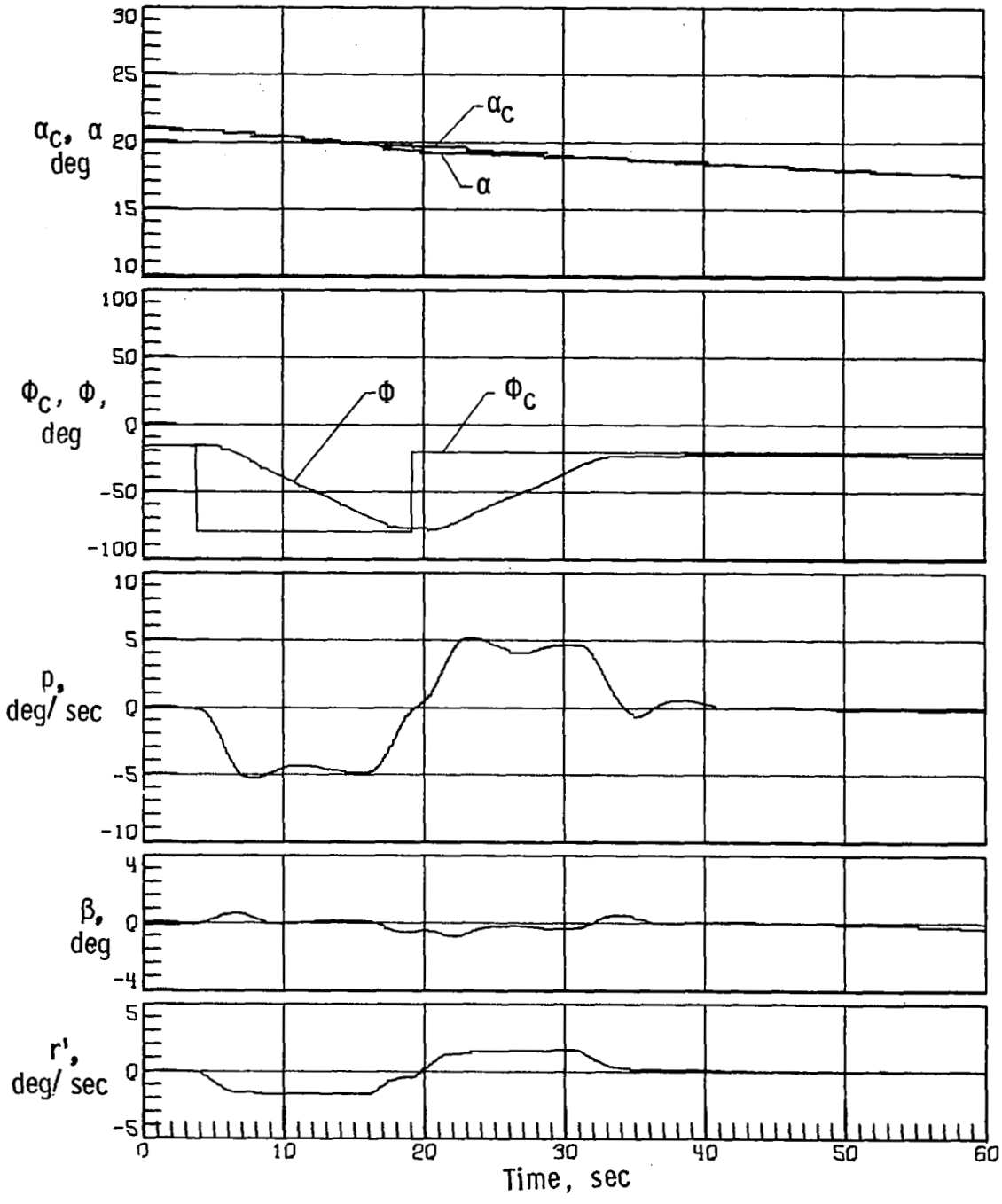

Figure 17.- Space Shuttle Orbiter response with simulation initiated at Mach 5 with off-nominal aerodynamics (case 7), no-sensed α error, two yaw RCS thrusters on each side inoperable, and 0.0381-m lateral center-of-gravity offset.

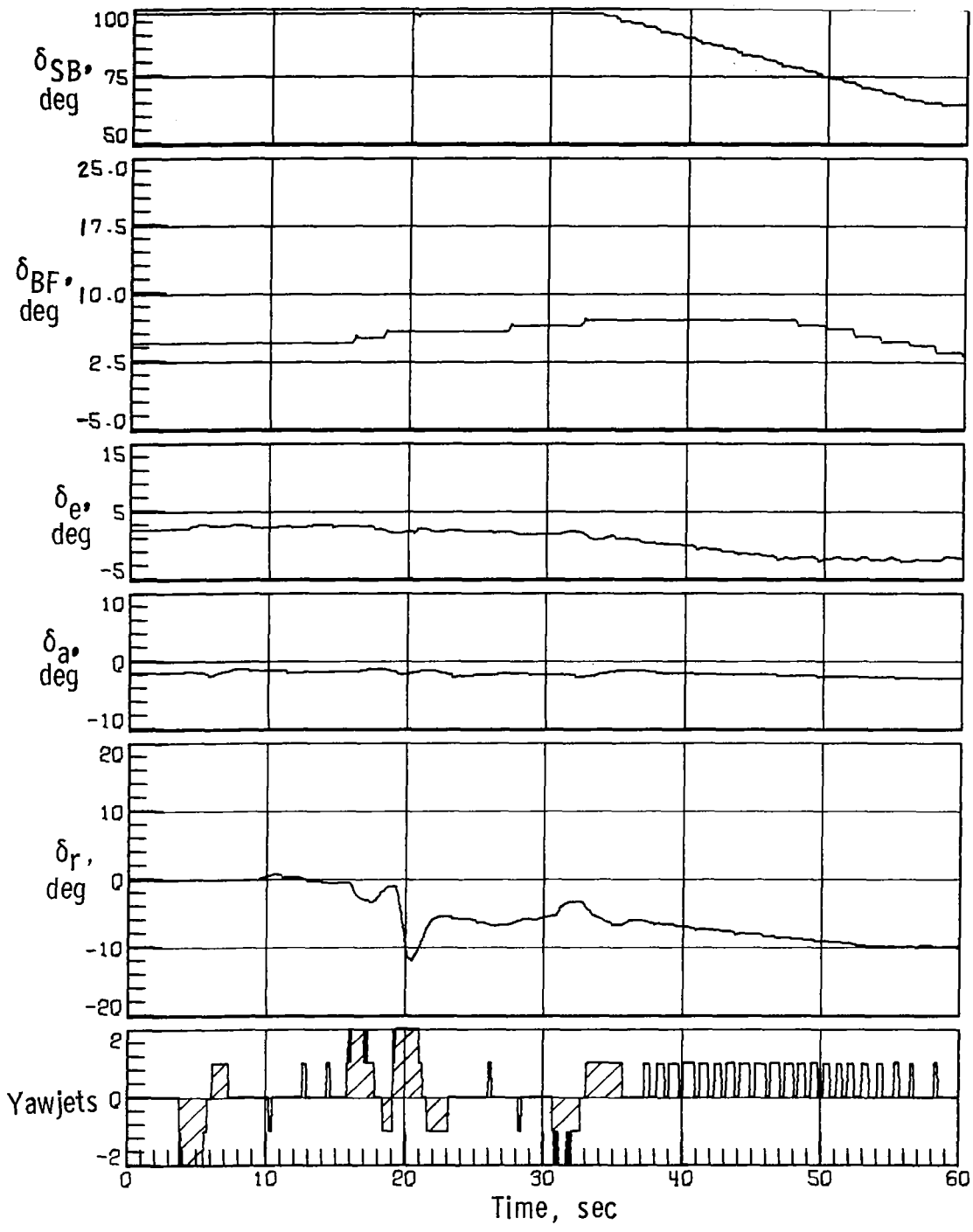

Figure 17.- Concluded.

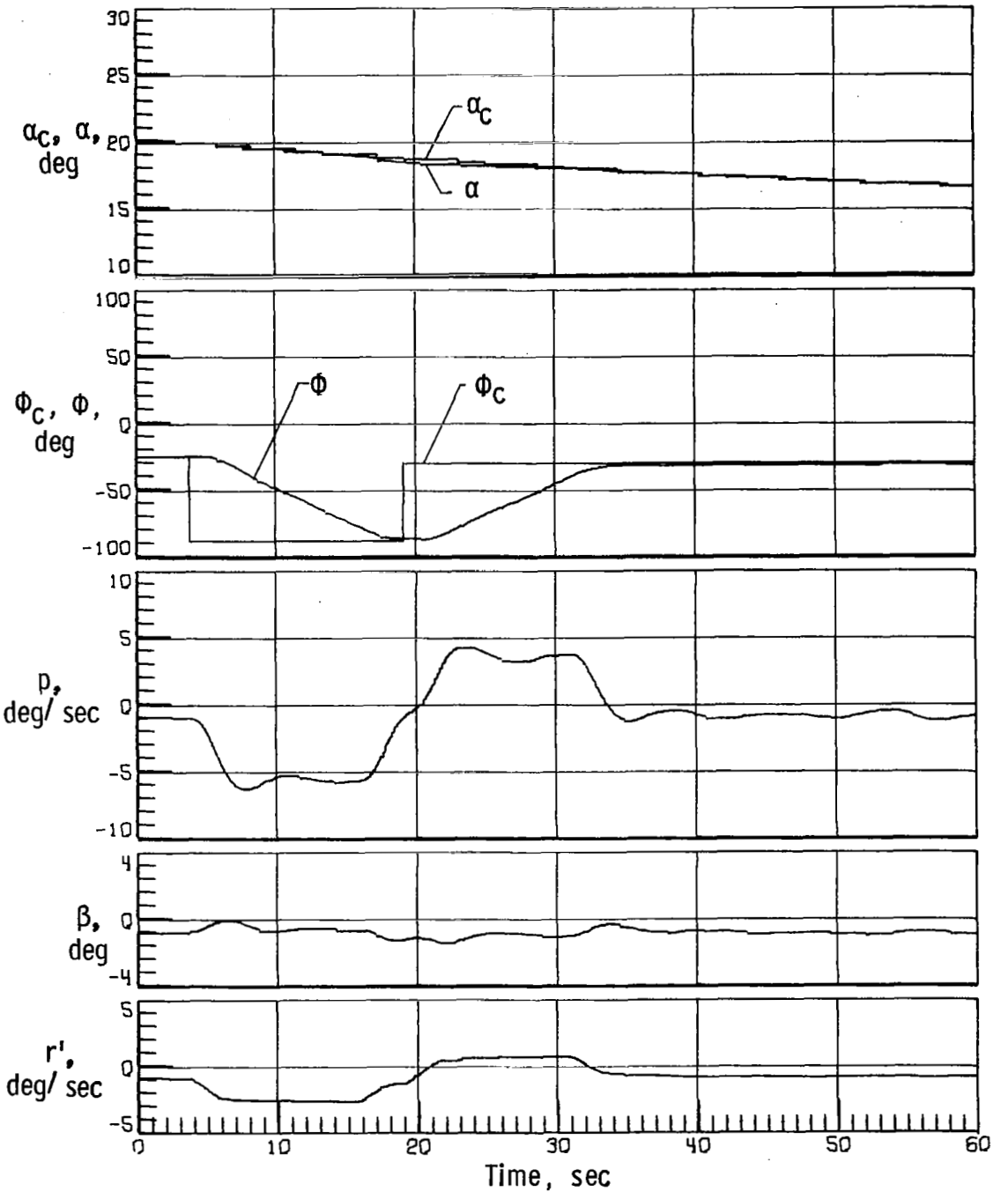

(a) Case 7.

Figure 18.- Space Shuttle Orbiter response with simulation at Mach 5 with no-sensed α error, two yaw RCS thrusters on each side inoperable, modified control system, and 0.0381-m lateral center-of-gravity offset.

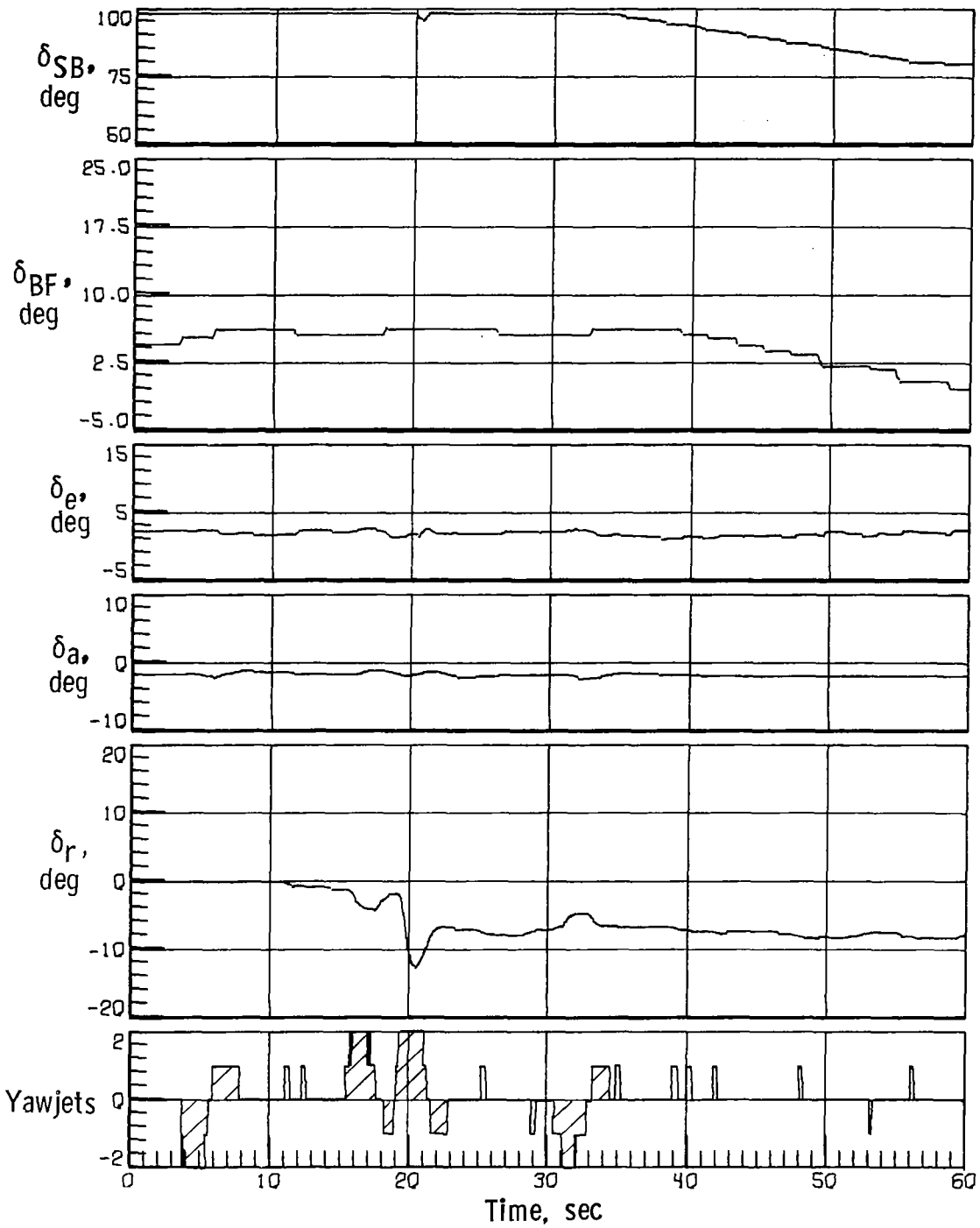

(a) Concluded.

Figure 18.- Continued.

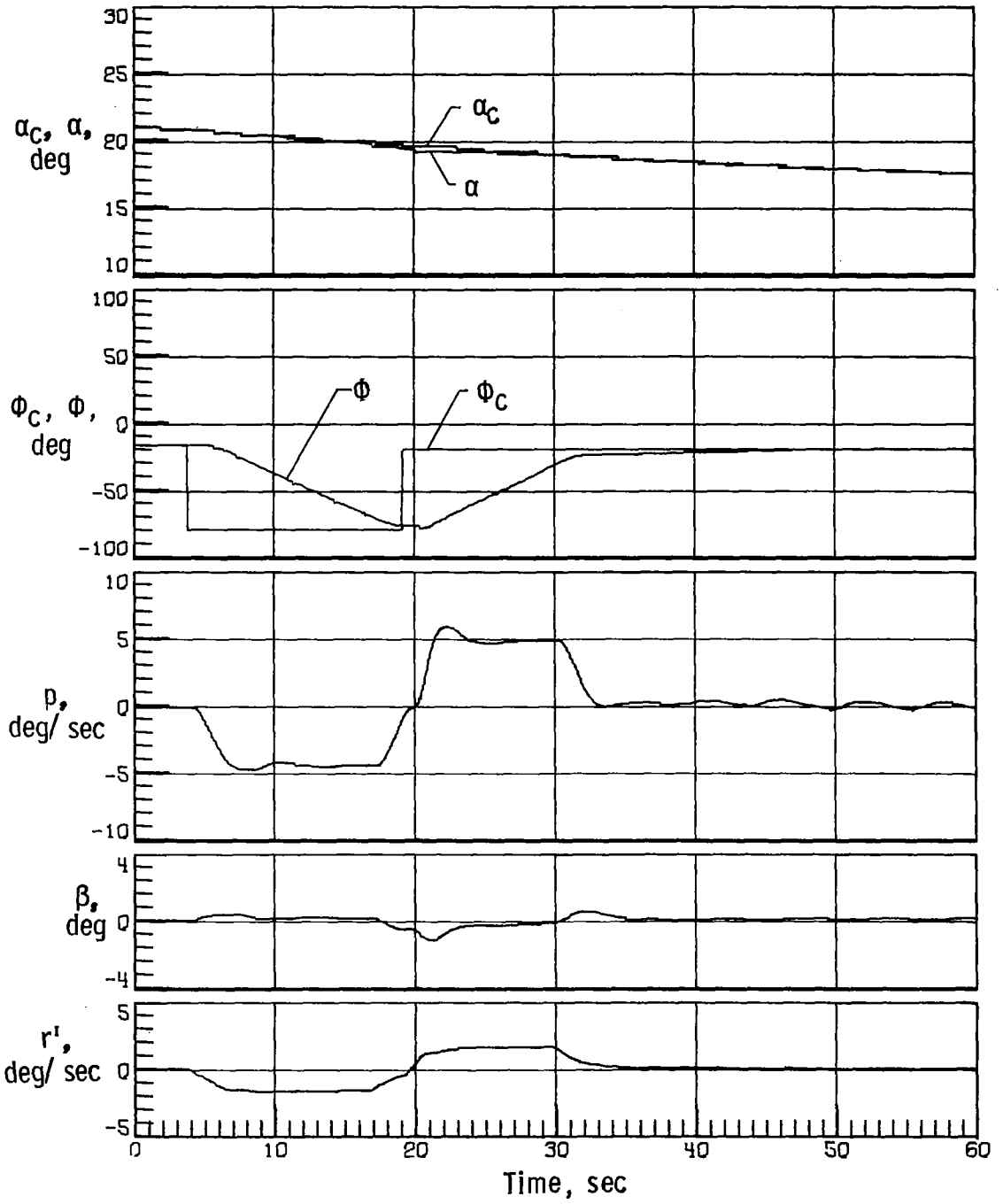

(b) Nominal aerodynamics.

Figure 18.- Continued.

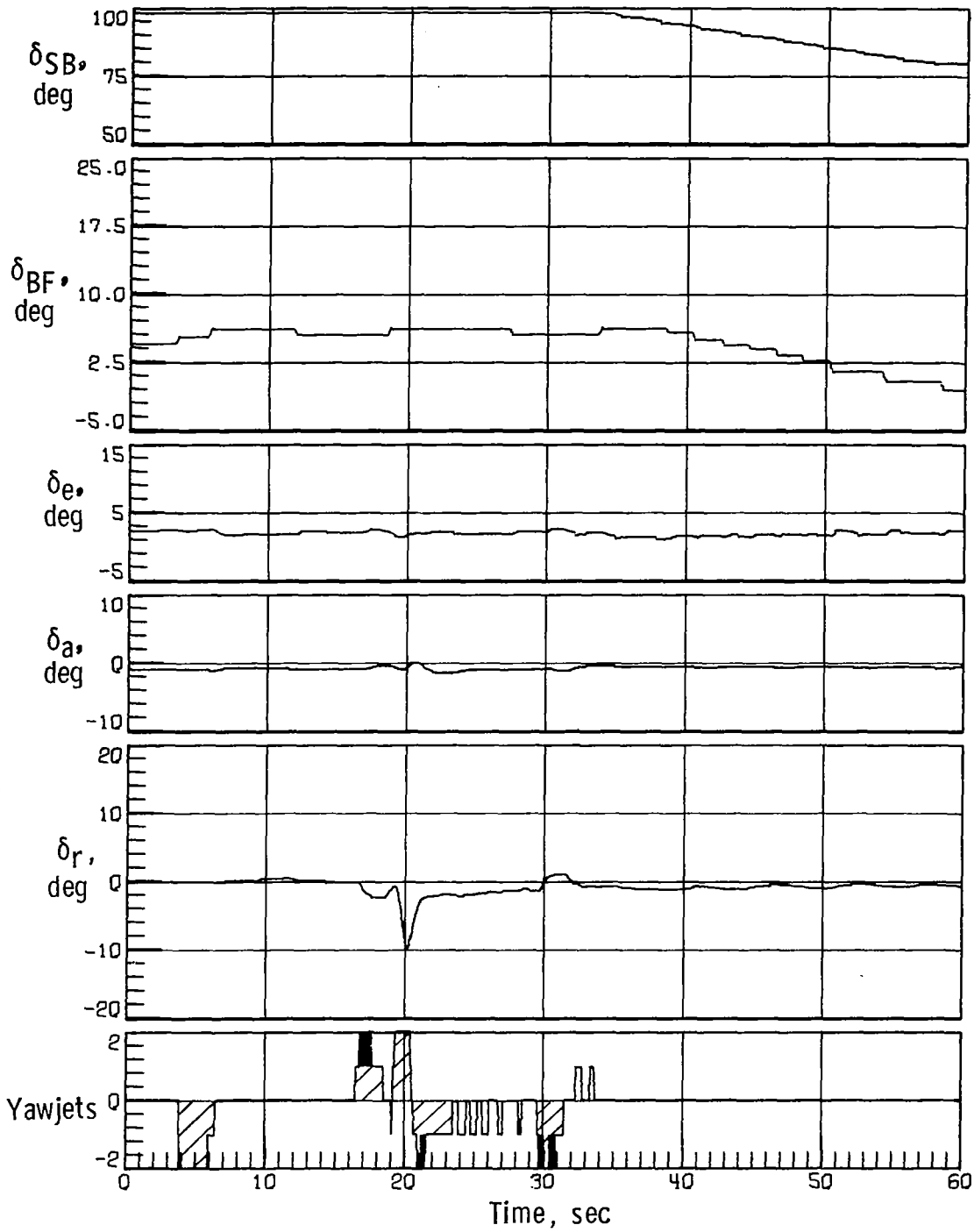

(b) Concluded.

Figure 18.- Concluded.

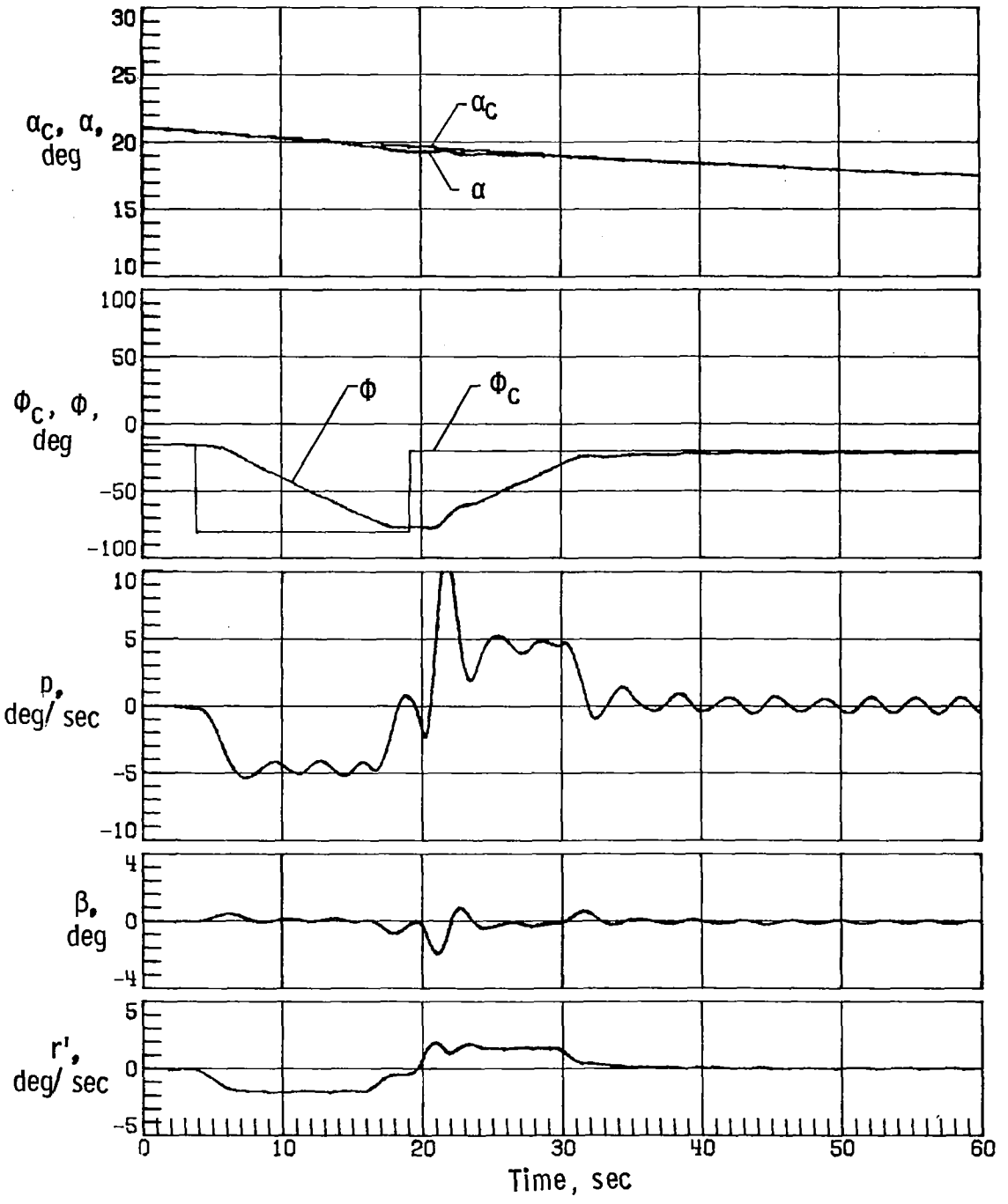

Figure 19.- Space Shuttle Orbiter response with simulation initiated at Mach 5 with off-nominal aerodynamics (case 5A), no-sensed α error, two yaw RCS thrusters on each side inoperable, modified control system, and 0.0381-m lateral center-of-gravity offset.

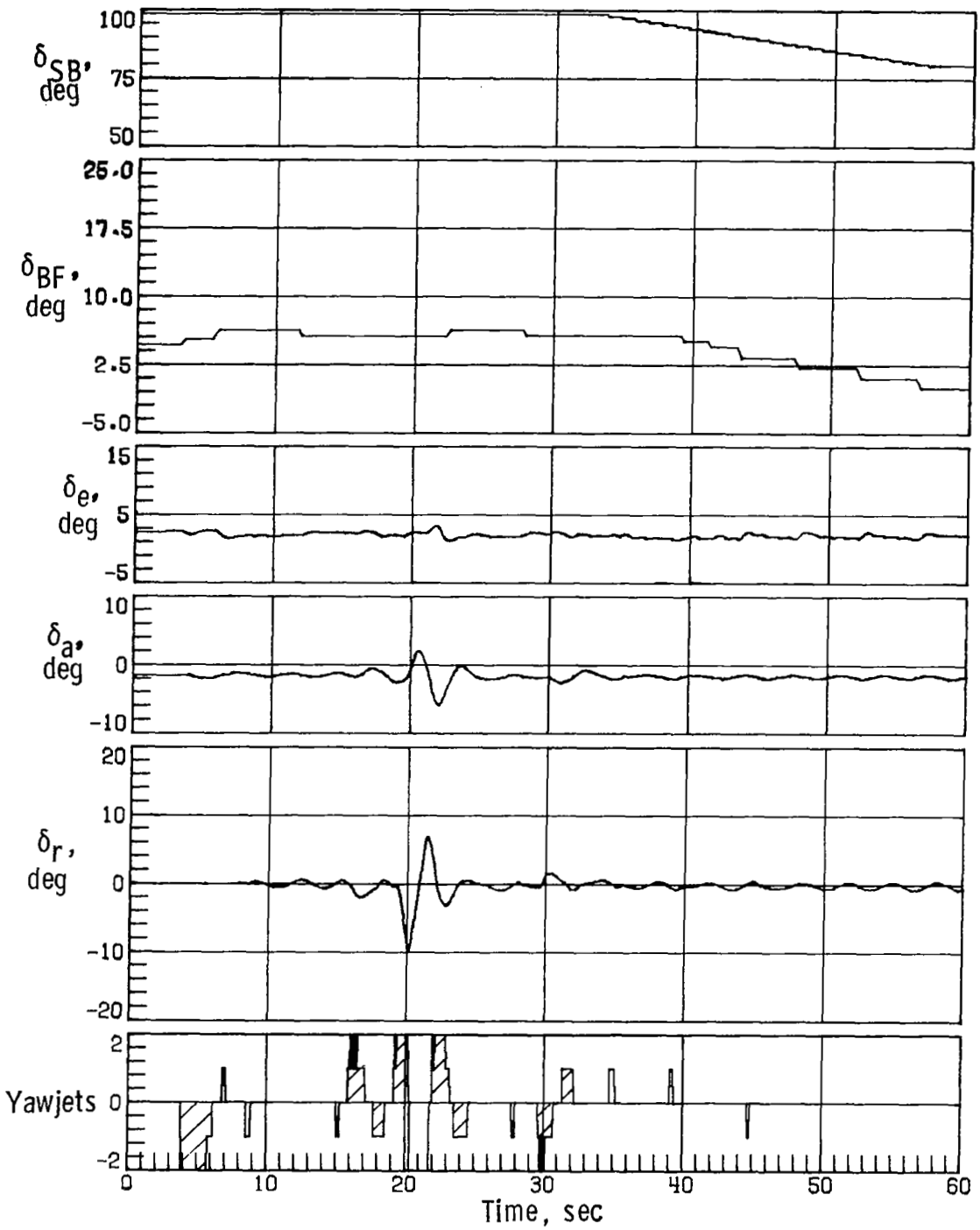

Figure 19.- Concluded.

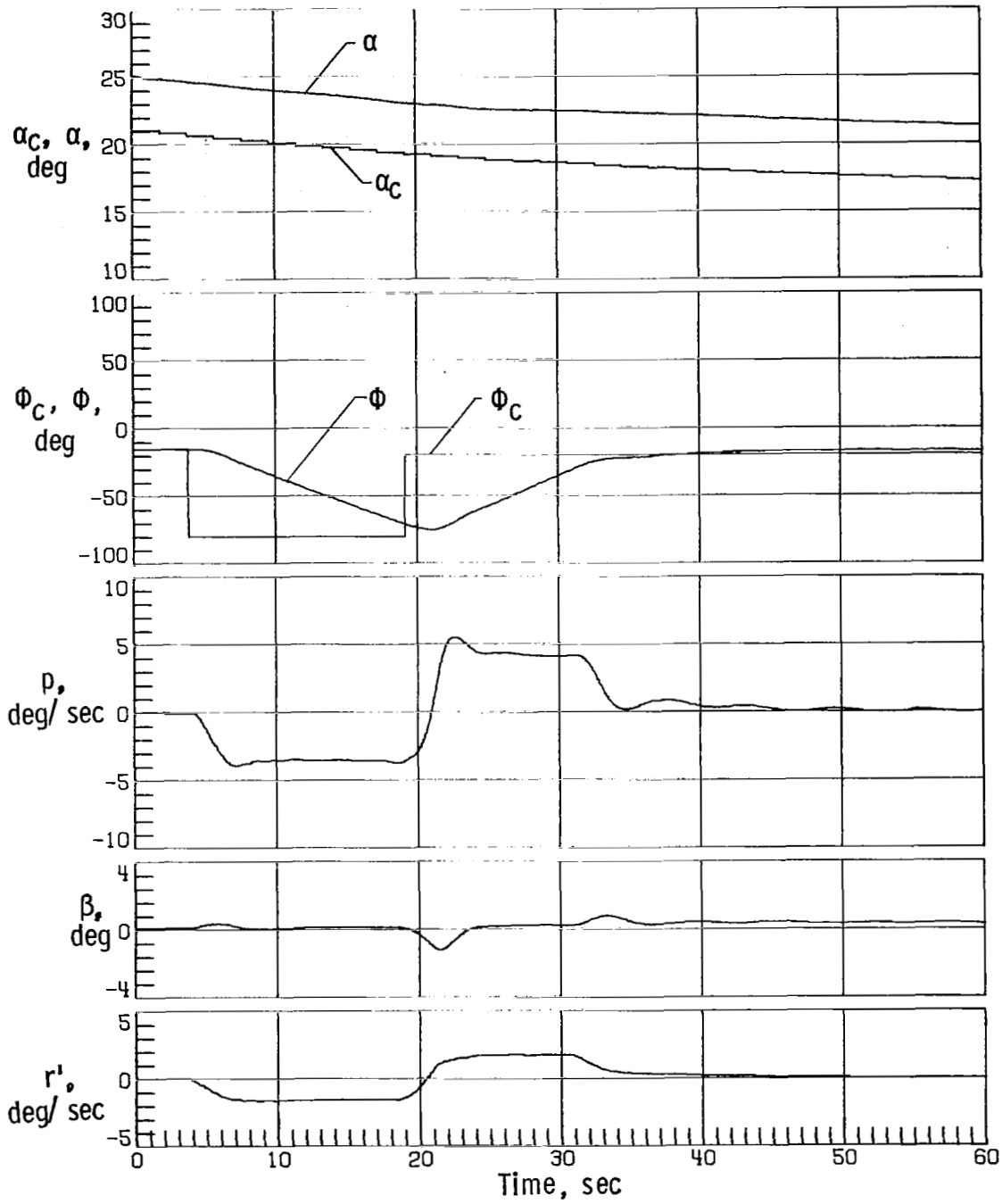

Figure 20.- Space Shuttle Orbiter response with simulation initiated at Mach 5 with nominal aerodynamics, sensed α error of -4^{o}, two yaw RCS thrusters on each side inoperable, modified control system, and 0.0381-m lateral center-of-gravity offset.

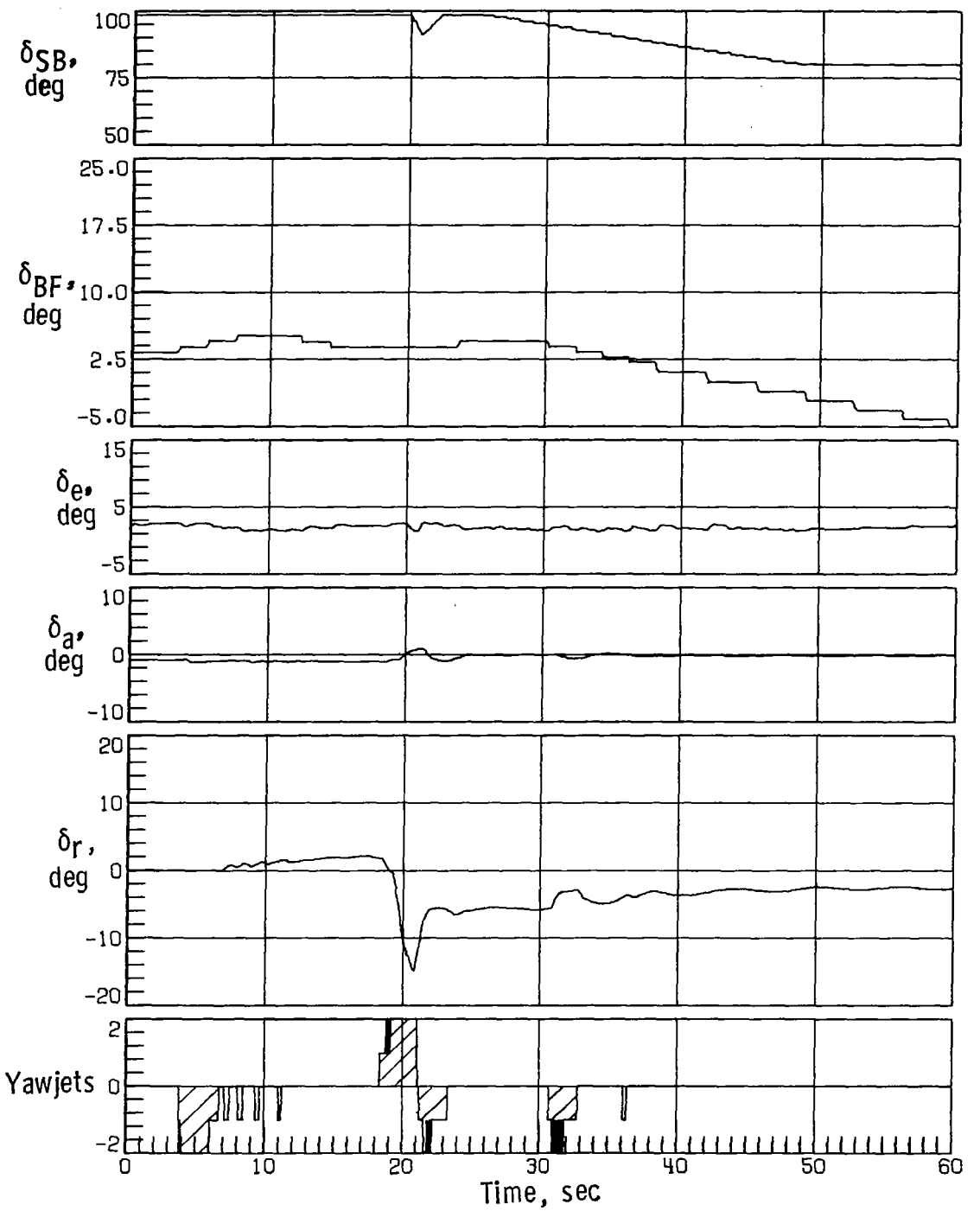

Figure 20.- Concluded.

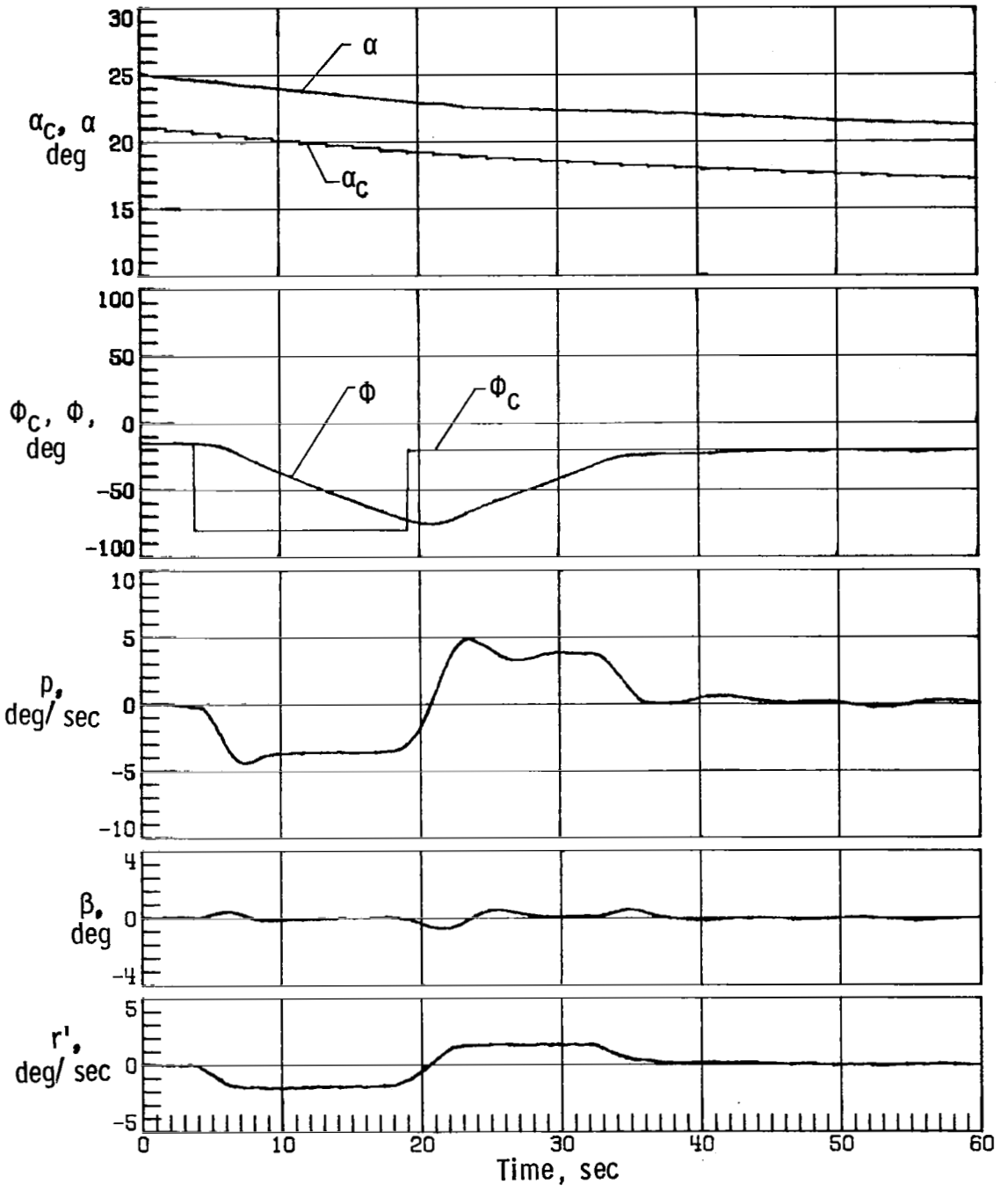

Figure 21.- Space Shuttle Orbiter response with simulation initiated at Mach 5 with off-nominal aerodynamics (case 7), sensed α error of -4^{o}, two yaw RCS thrusters on each side inoperable, modified control system, and 0.0381-m lateral center-of-gravity offset.

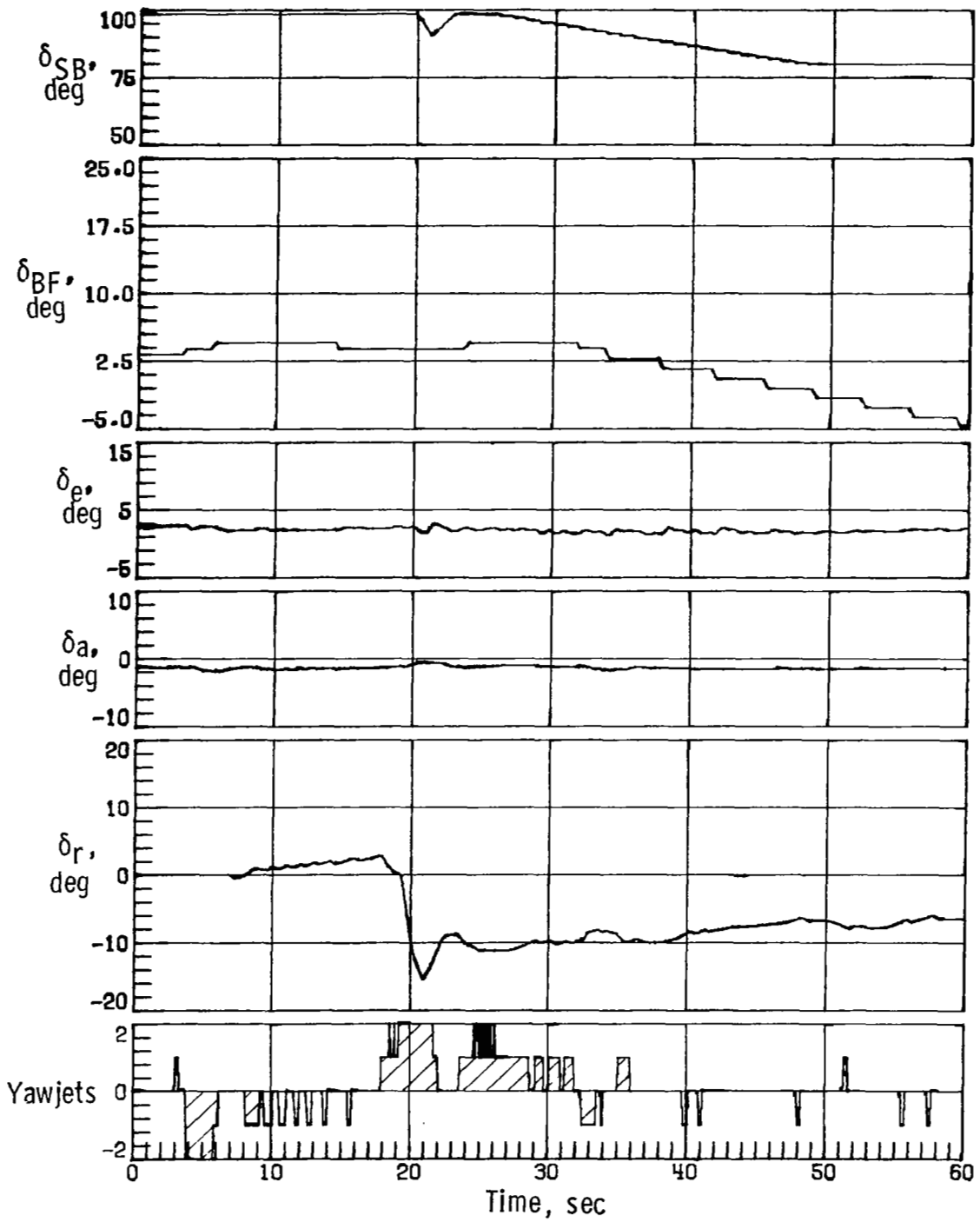

Figure 21.- Concluded.

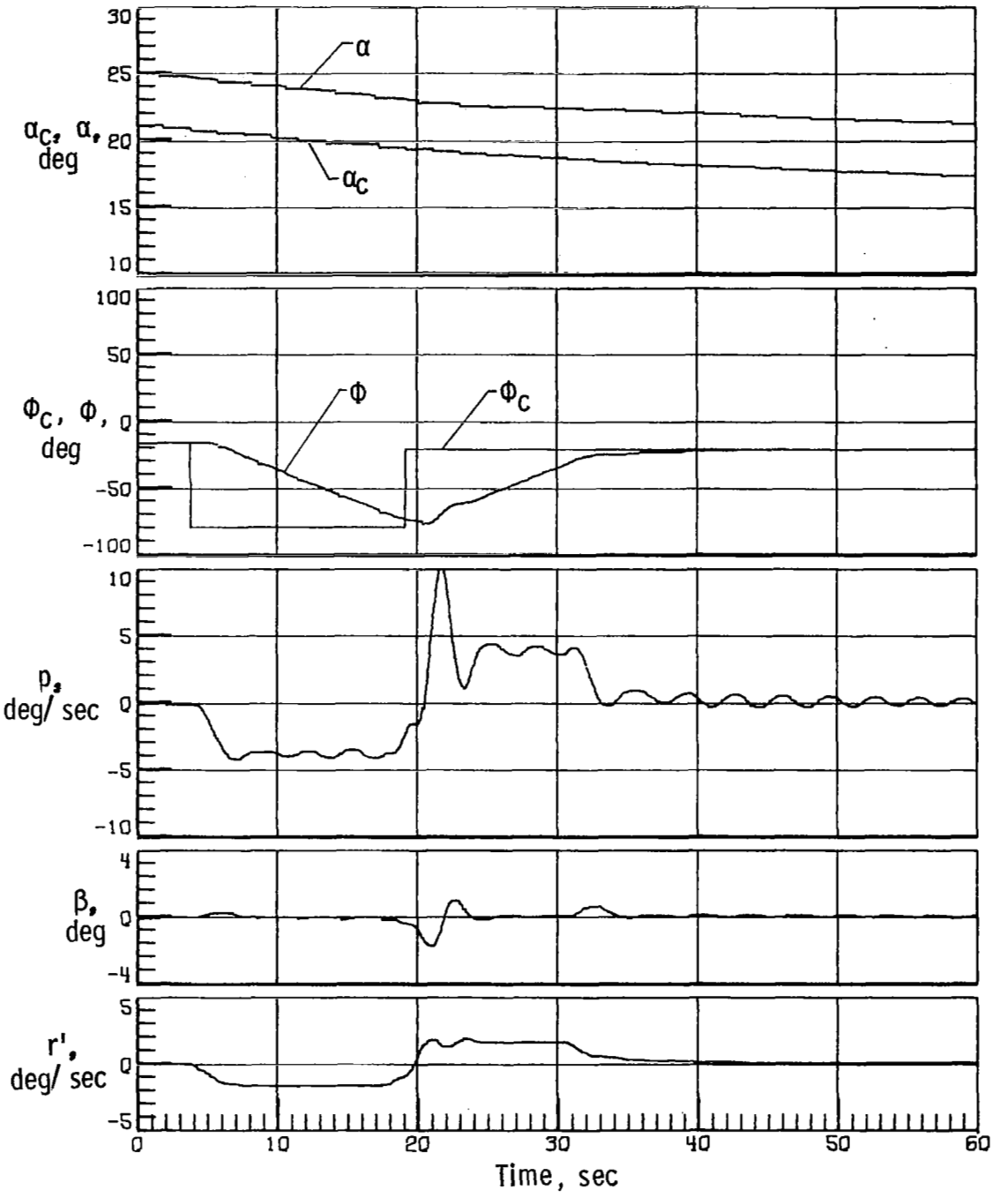

Figure 22.- Space Shuttle Orbiter response with simulation initiated at Mach 5 with off-nominal aerodynamics (case 5A), sensed α error of -4^{o}, two yaw RCS thrusters on each side inoperable, modified control system, and 0.0381-m lateral center-of-gravity offset.

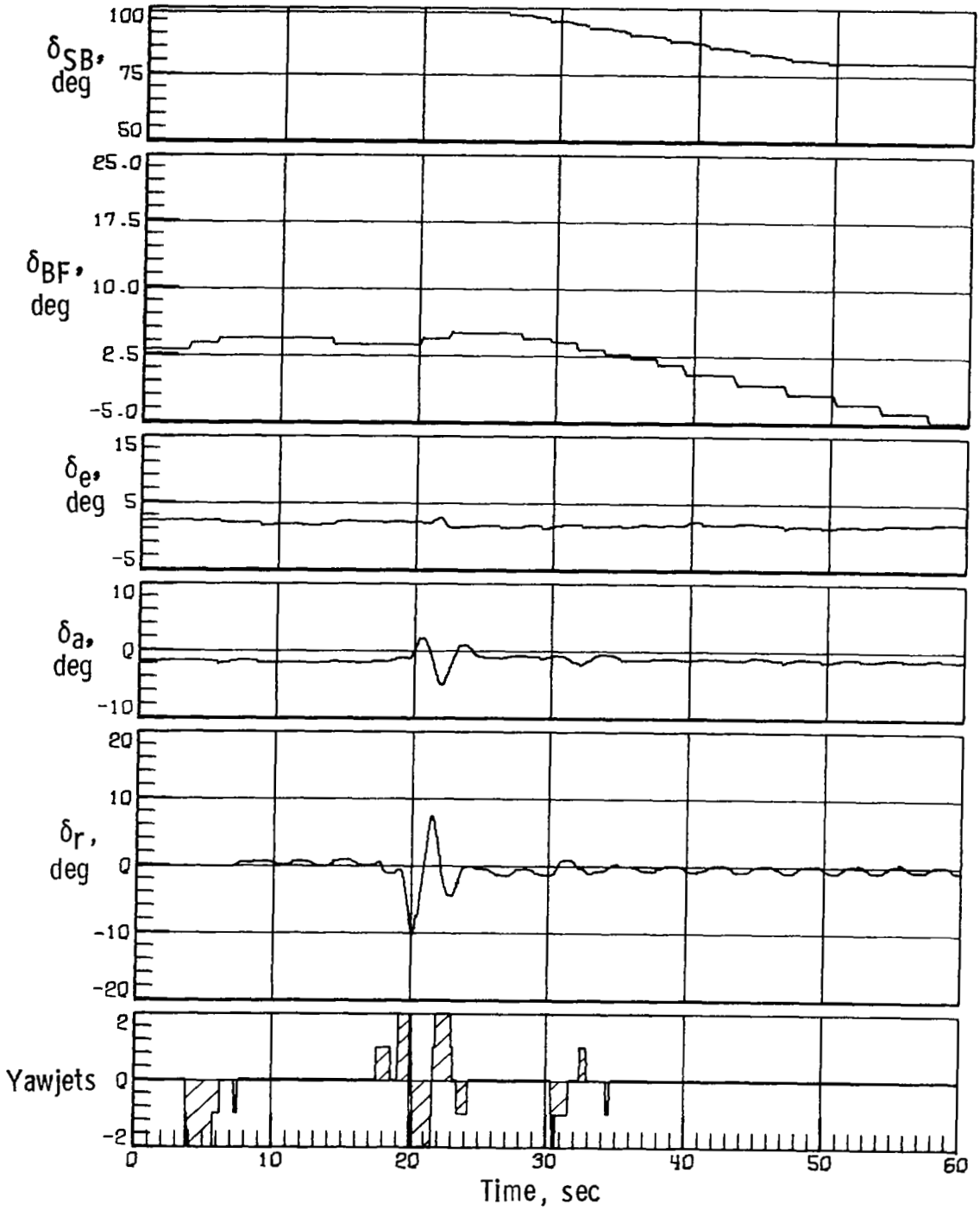

Figure 22.- Concluded.

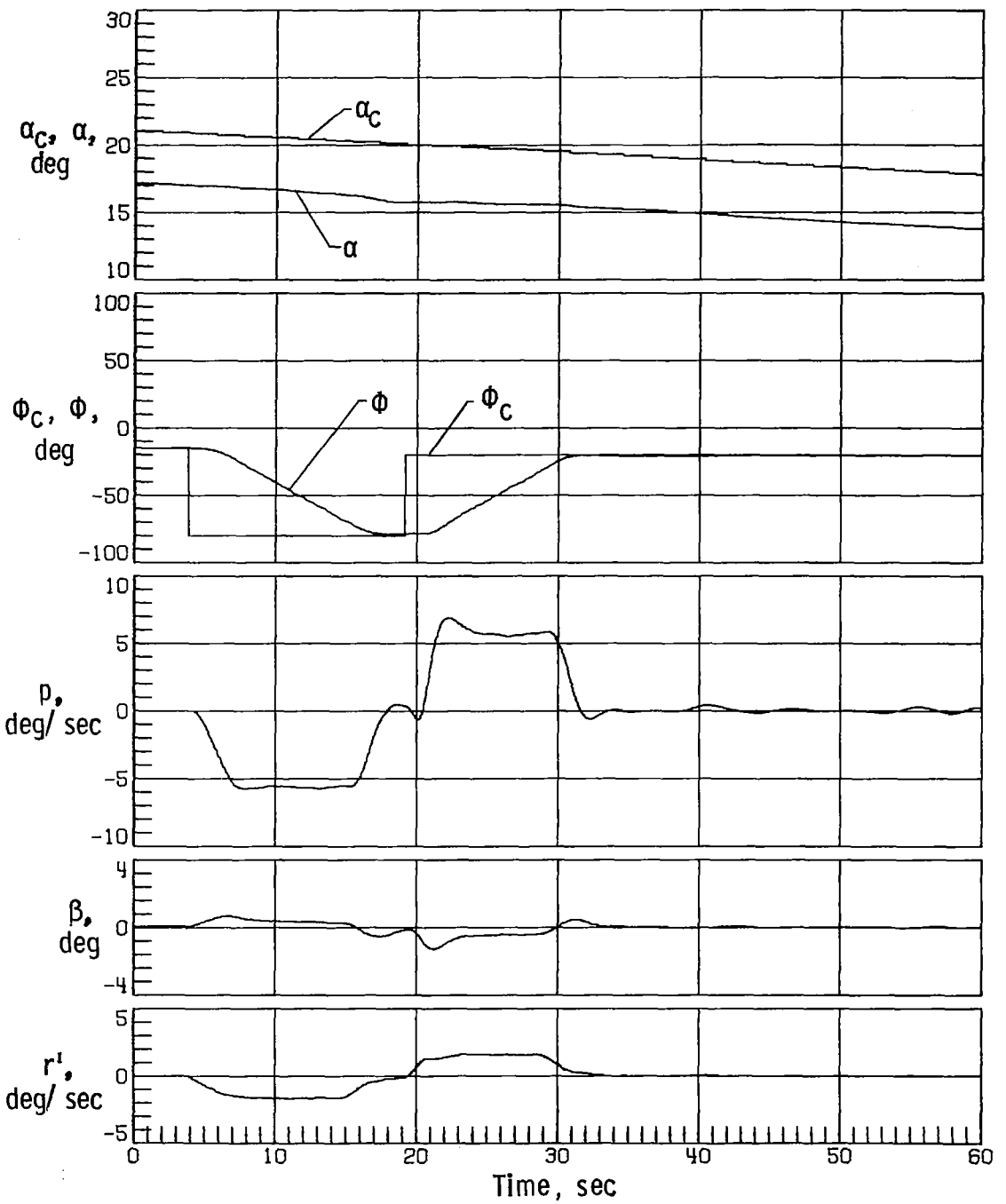

Figure 23.- Space Shuttle Orbiter response with simulation initiated at Mach 5 with nominal aerodynamics, sensed α error of $+4^{o}$, two yaw RCS thrusters on each side inoperable, modified control system, and 0.0381-m lateral center-of-gravity offset.

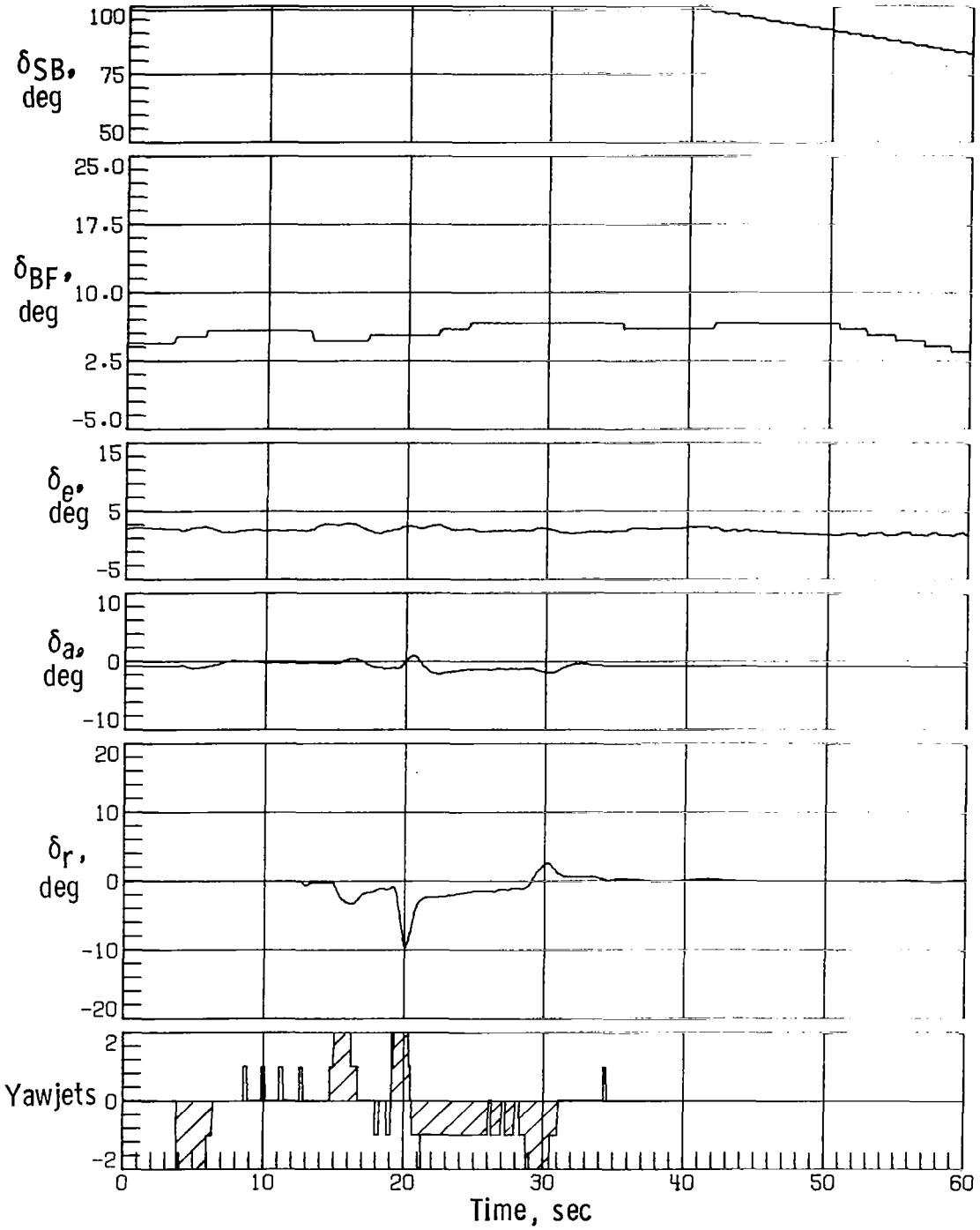

Figure 23.- Concluded.

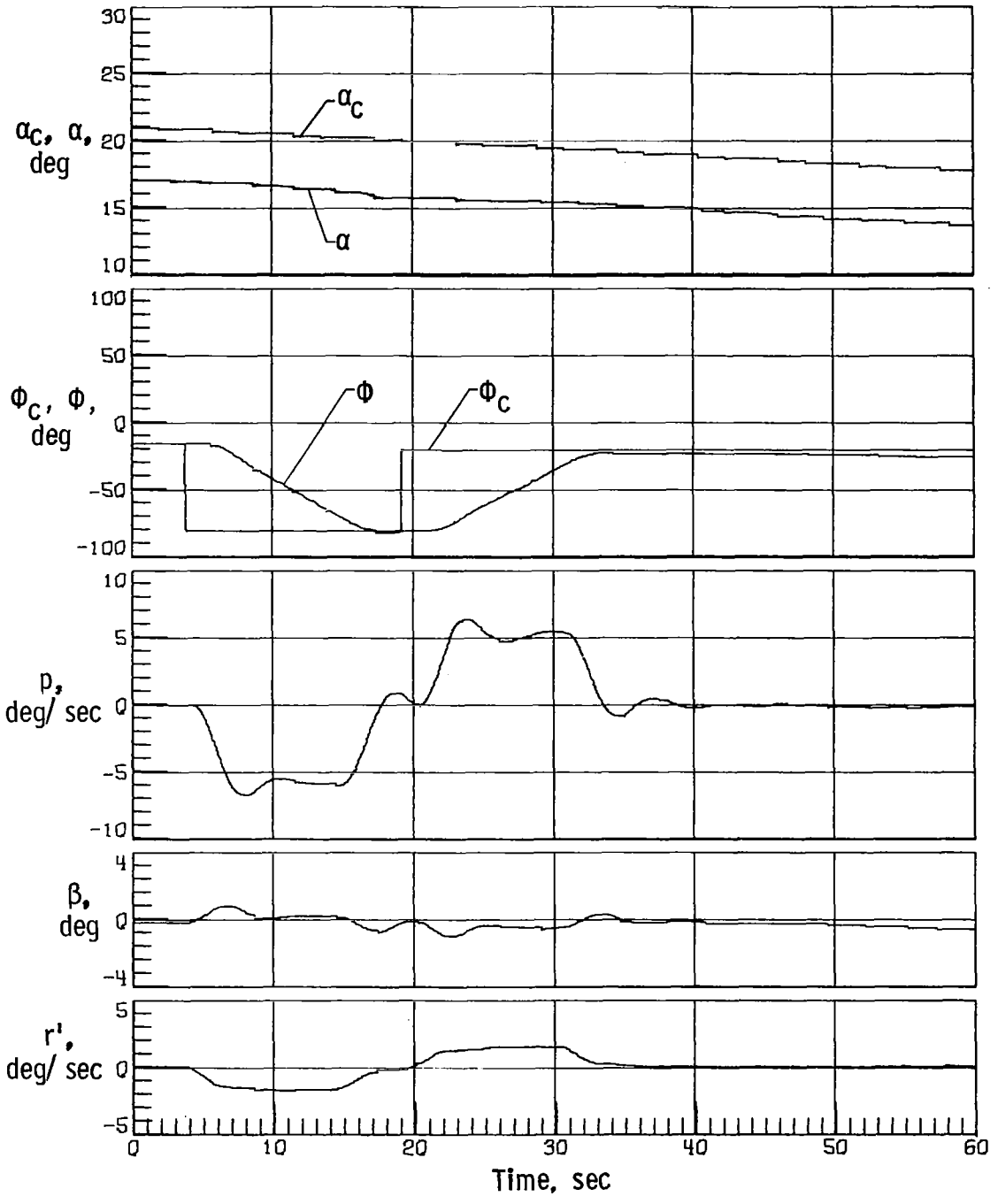

Figure 24.- Space Shuttle Orbiter response with simulation initiated at Mach 5 with off-nominal aerodynamics (case 7), sensed α error of $+4^{\circ}$, two yaw RCS thrusters on each side inoperable, modified control system, and 0.0381-m lateral center-of-gravity offset.

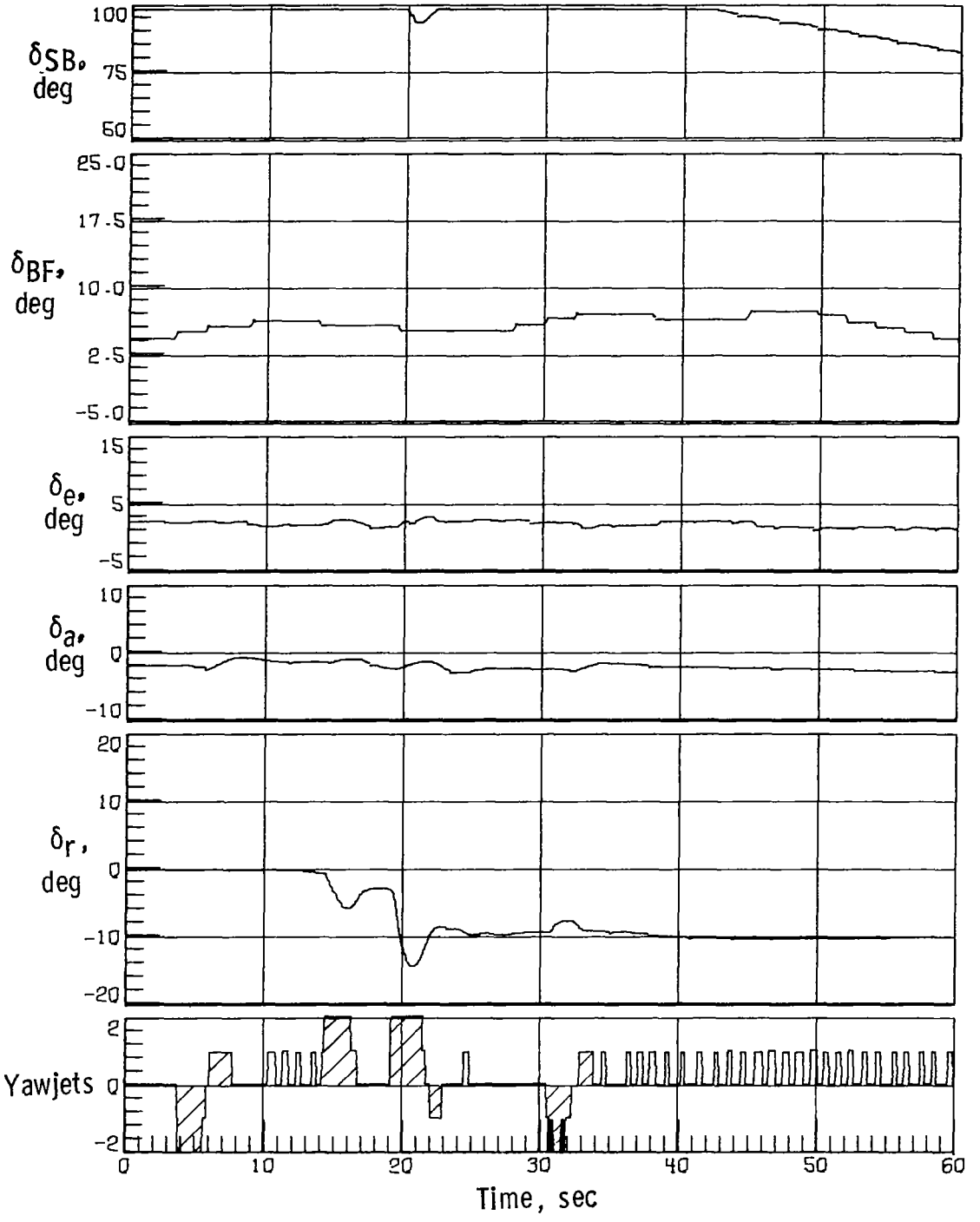

Figure 24.- Concluded.

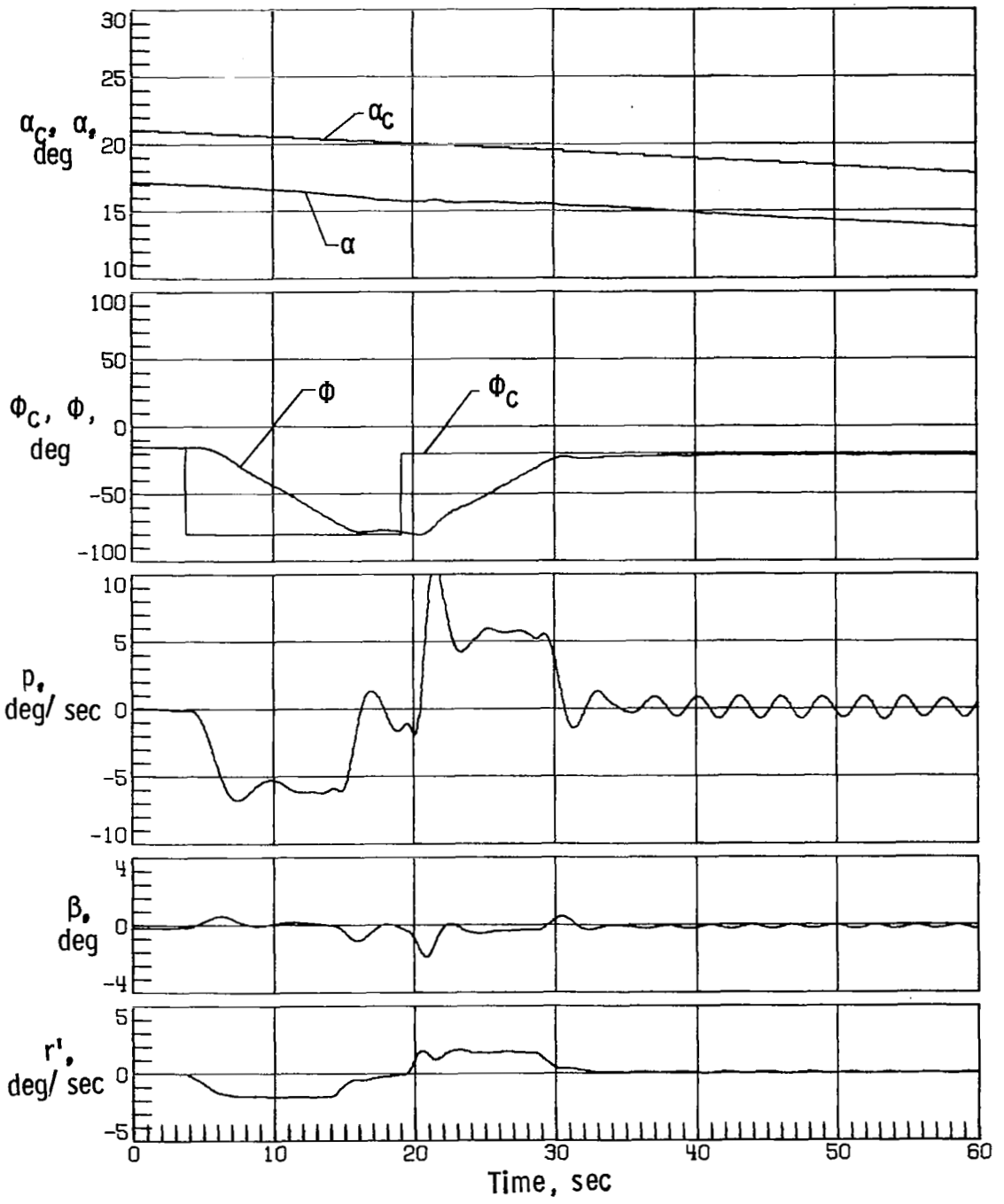

Figure 25.- Space Shuttle Orbiter response with simulation initiated at Mach 5 with off-nominal aerodynamics (case 5A), sensed α error of $+4^{o}$, two yaw RCS thrusters on each side inoperable, modified control system, and 0.0381-m lateral center-of-gravity offset.

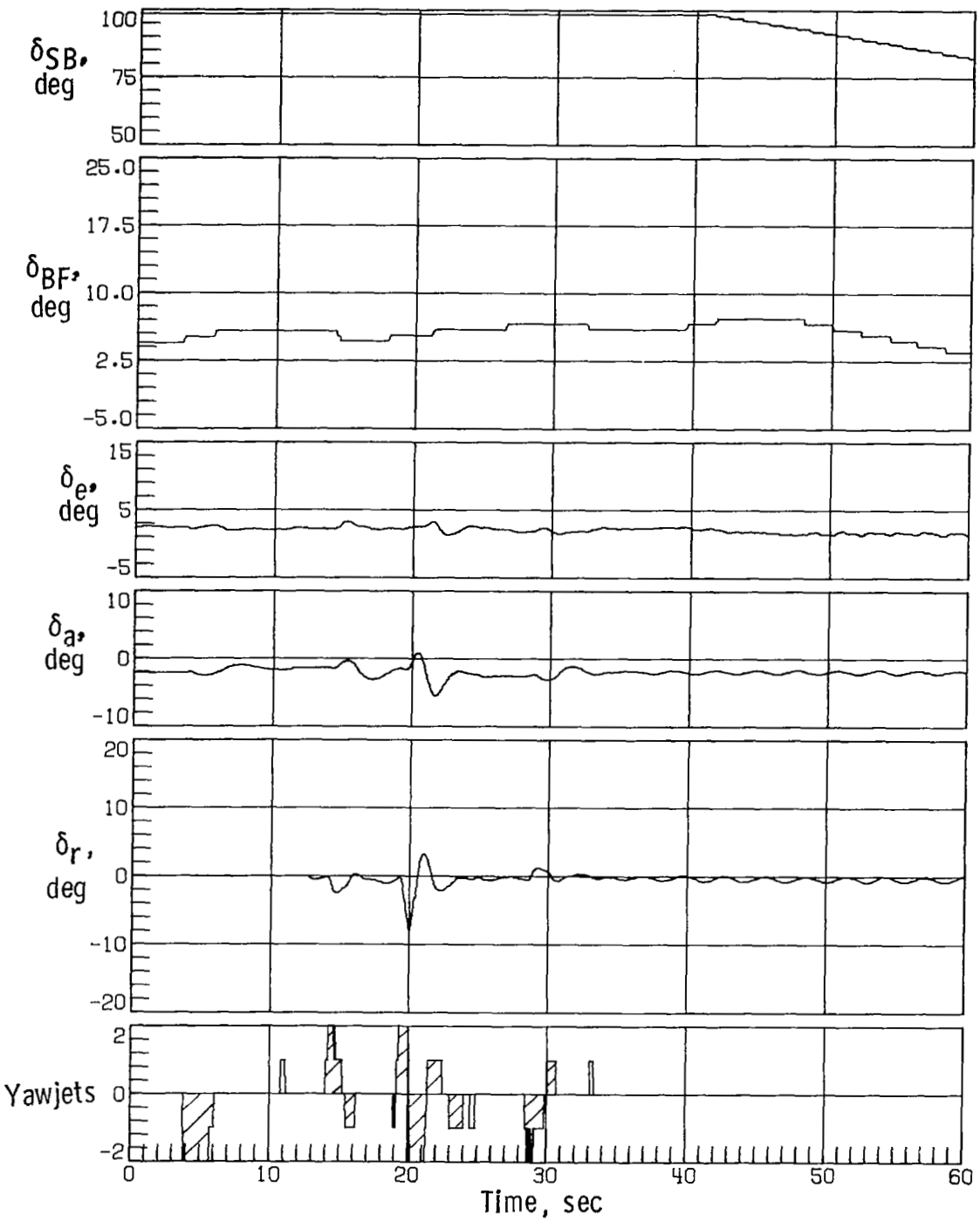

Figure 25.- Concluded.

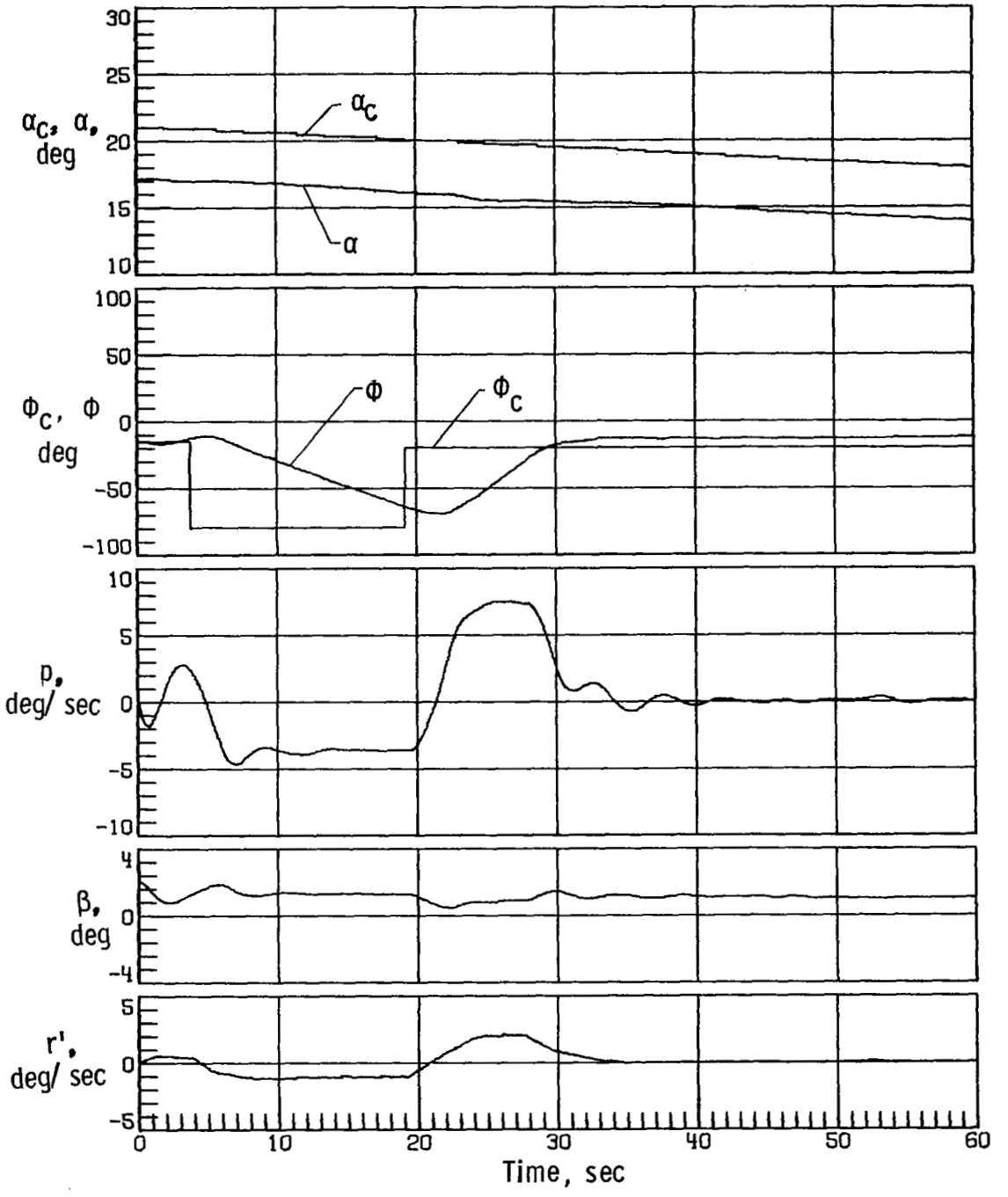

(a) Case 6 with $-C_m$ uncertainty.

Figure 26.- Space Shuttle Orbiter response with simulation initiated at Mach 5 with off-nominal aerodynamics, sensed α error of $+4^o$, two yaw RCS thrusters on each side inoperable, modified control system, and 0.0381-m lateral center-of-gravity offset.

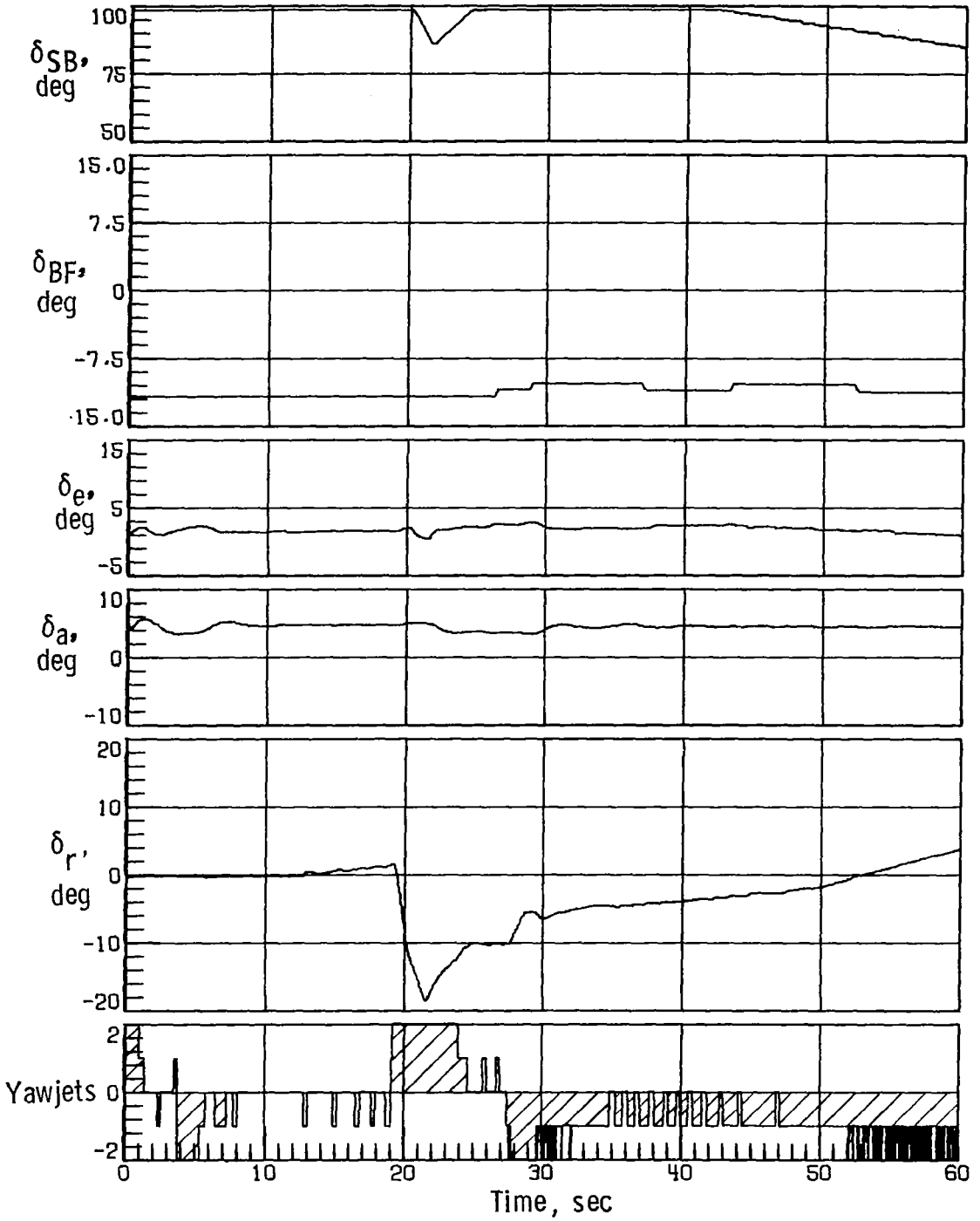

(a) Concluded.

Figure 26.- Continued.

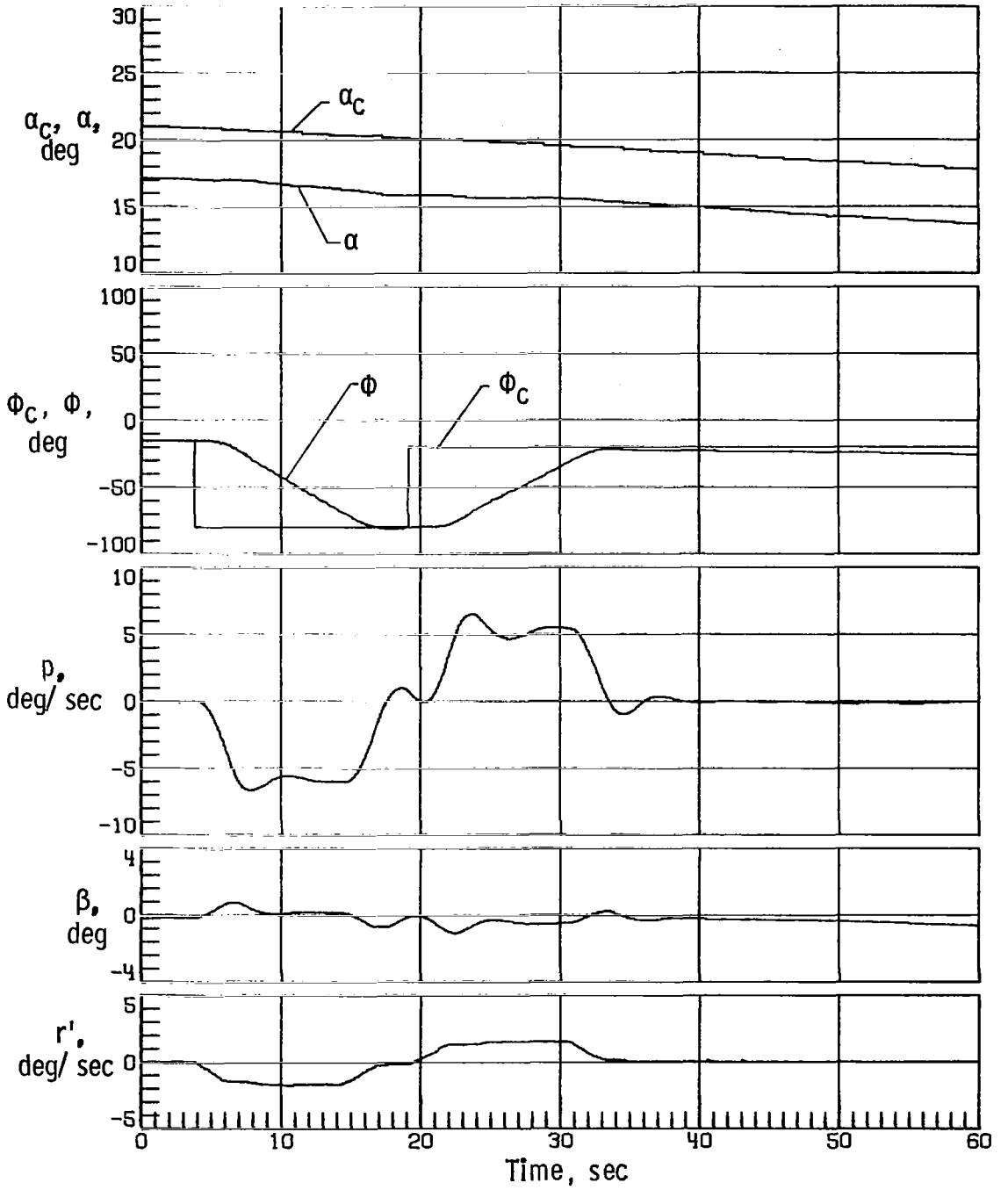

(b) Case 7 with $-C_m$ uncertainty.

Figure 26.- Continued.

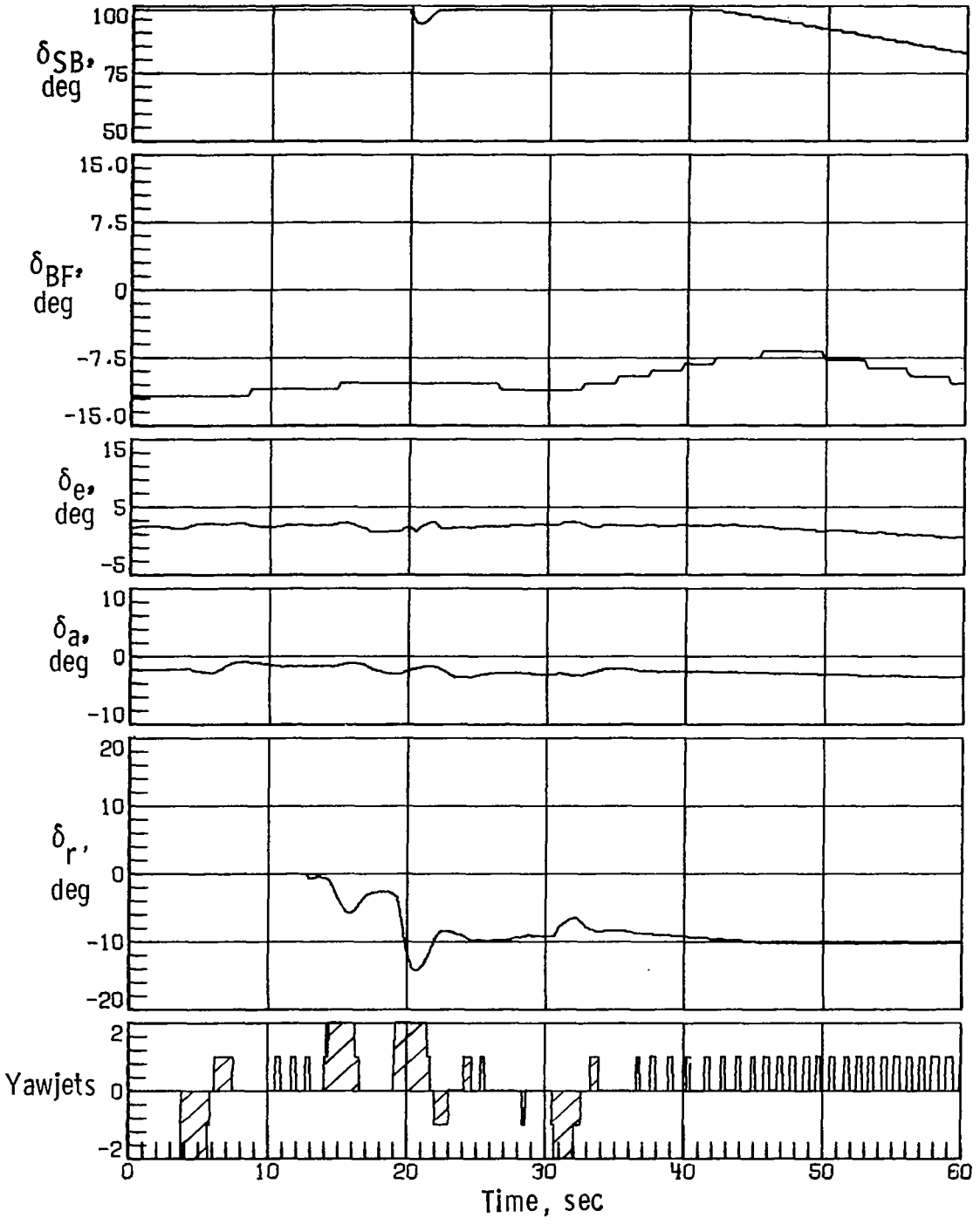

(b) Concluded.

Figure 26.- Concluded.

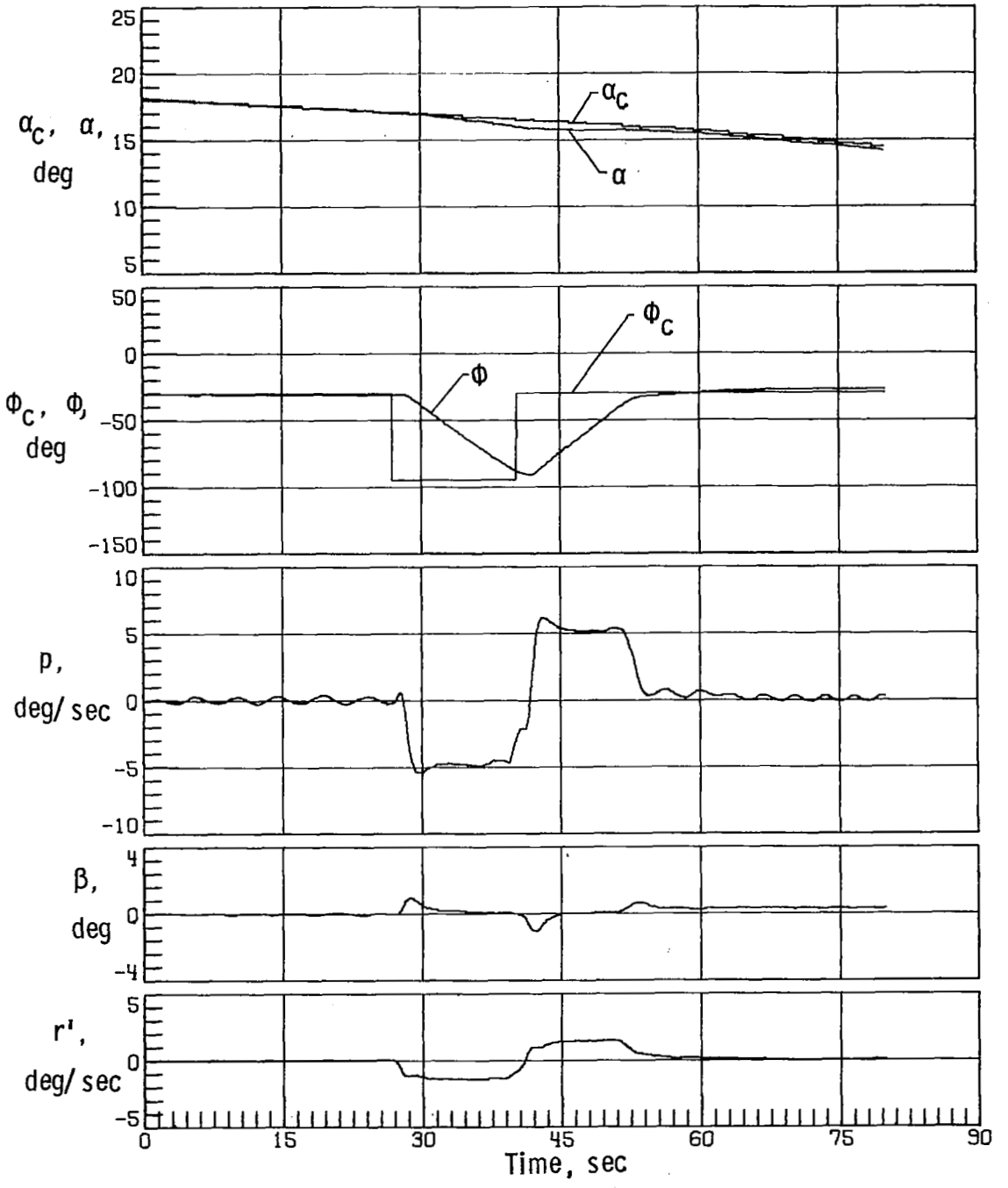

Figure 27.- Space Shuttle Orbiter response with simulation initiated at Mach 4.2 with nominal aerodynamics, no-sensed α error, two yaw RCS thrusters on each side inoperable, and 0.0381-m lateral center-of-gravity offset.

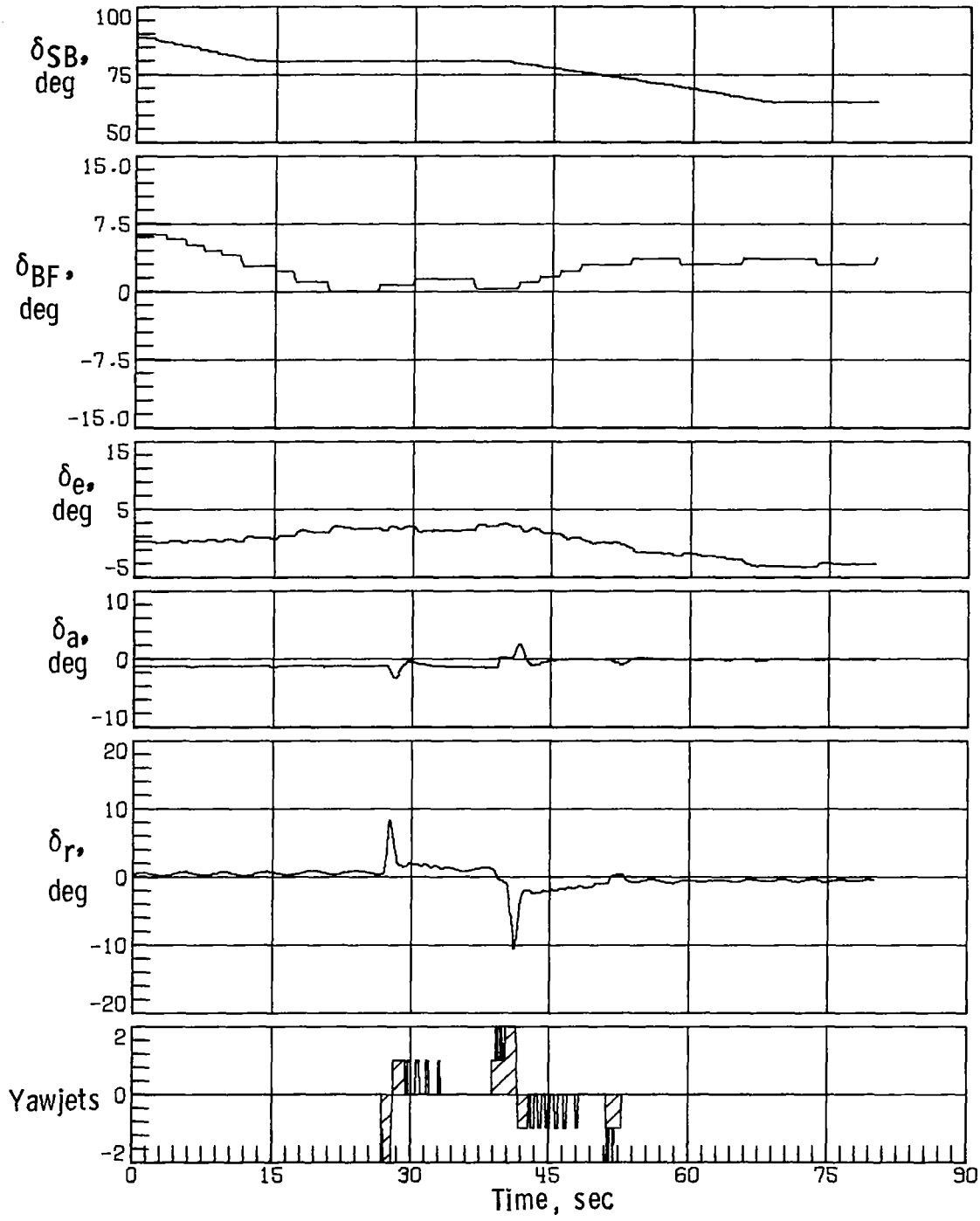

Figure 27.- Concluded.

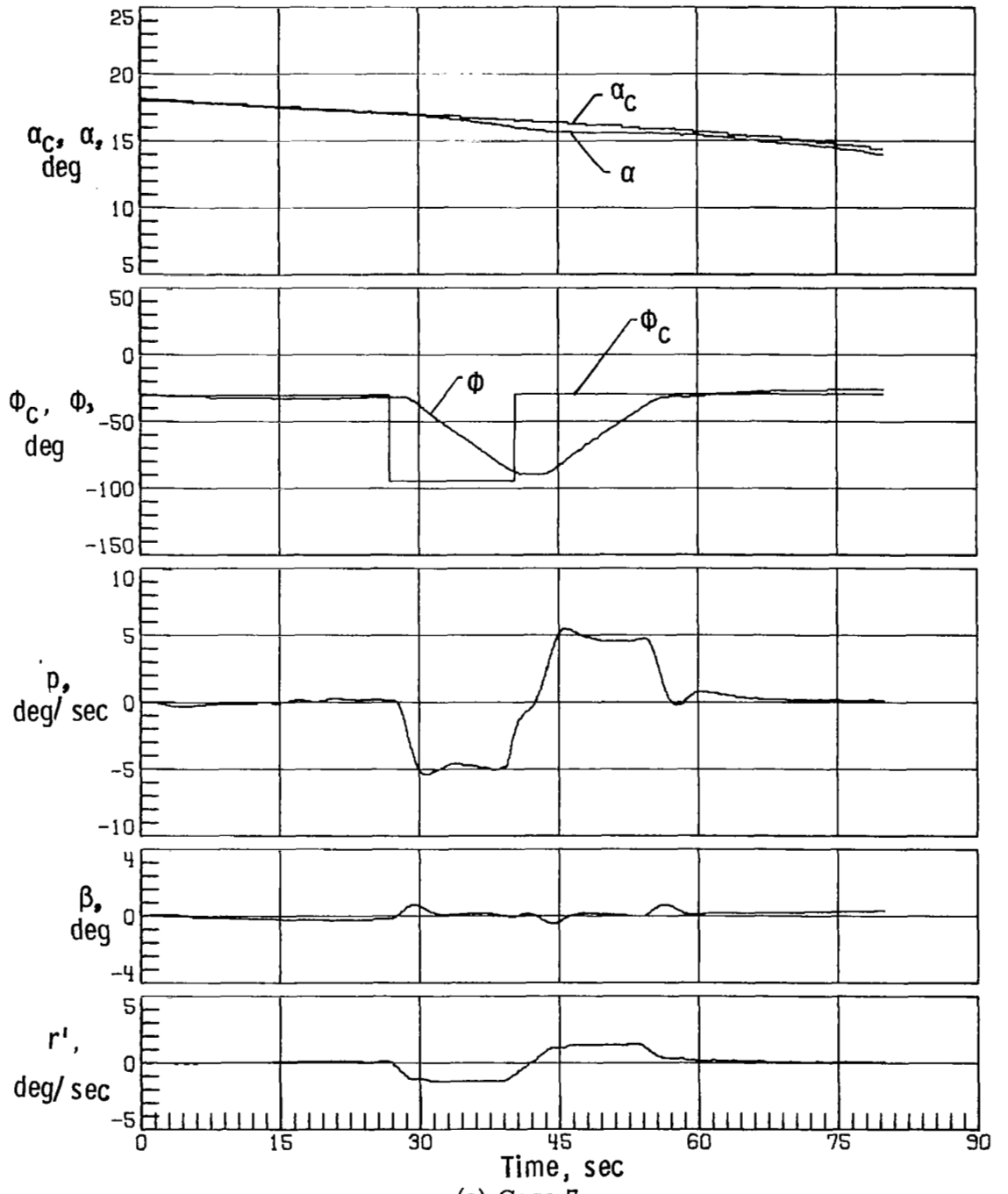

(a) Case 7.

Figure 28.- Space Shuttle Orbiter response with simulation initiated at Mach 4.2 with off-nominal aerodynamics, no-sensed α error, two yaw RCS thrusters on each side inoperable, and 0.0381-m lateral center-of-gravity offset.

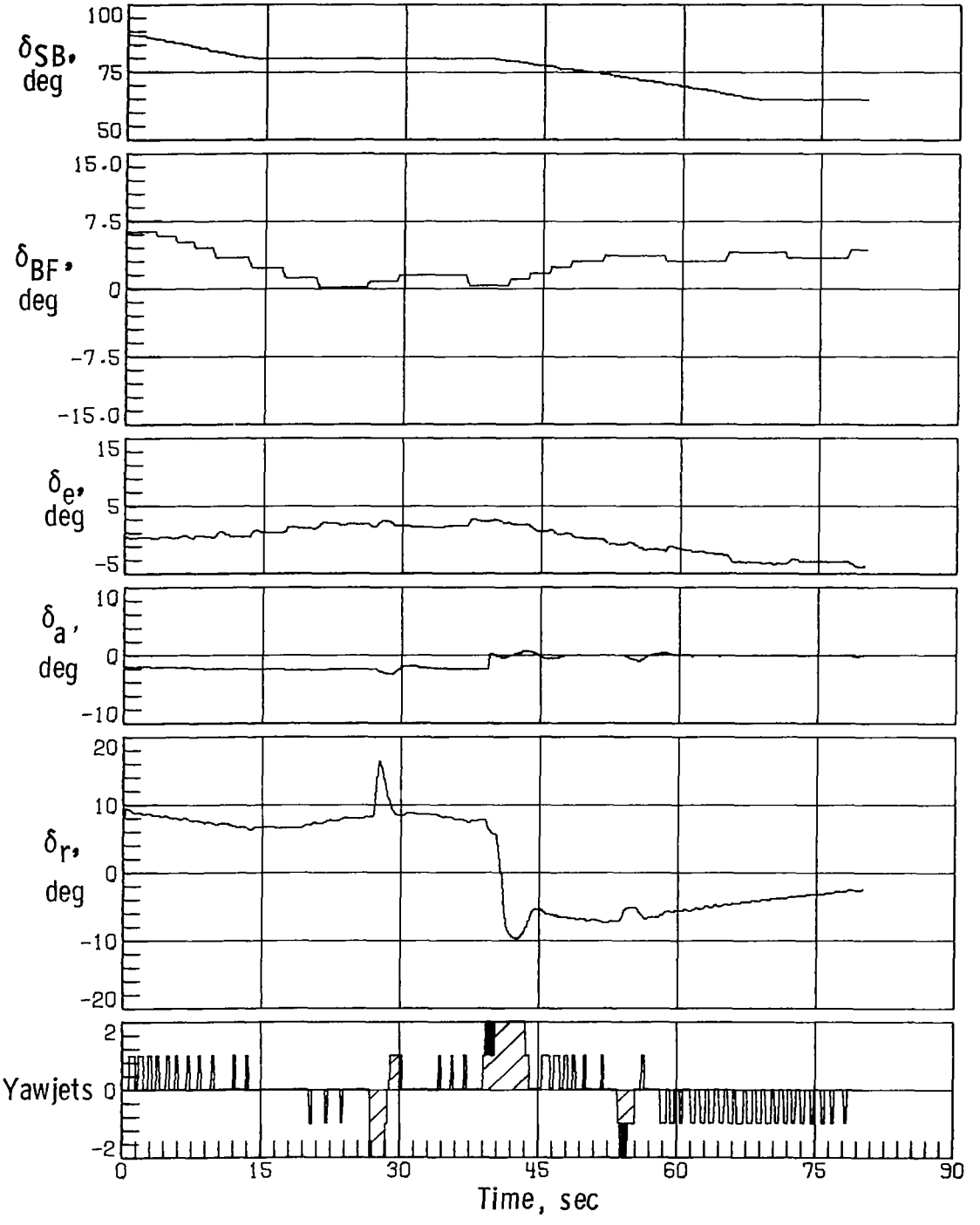

(a) Concluded.

Figure 28.- Continued.

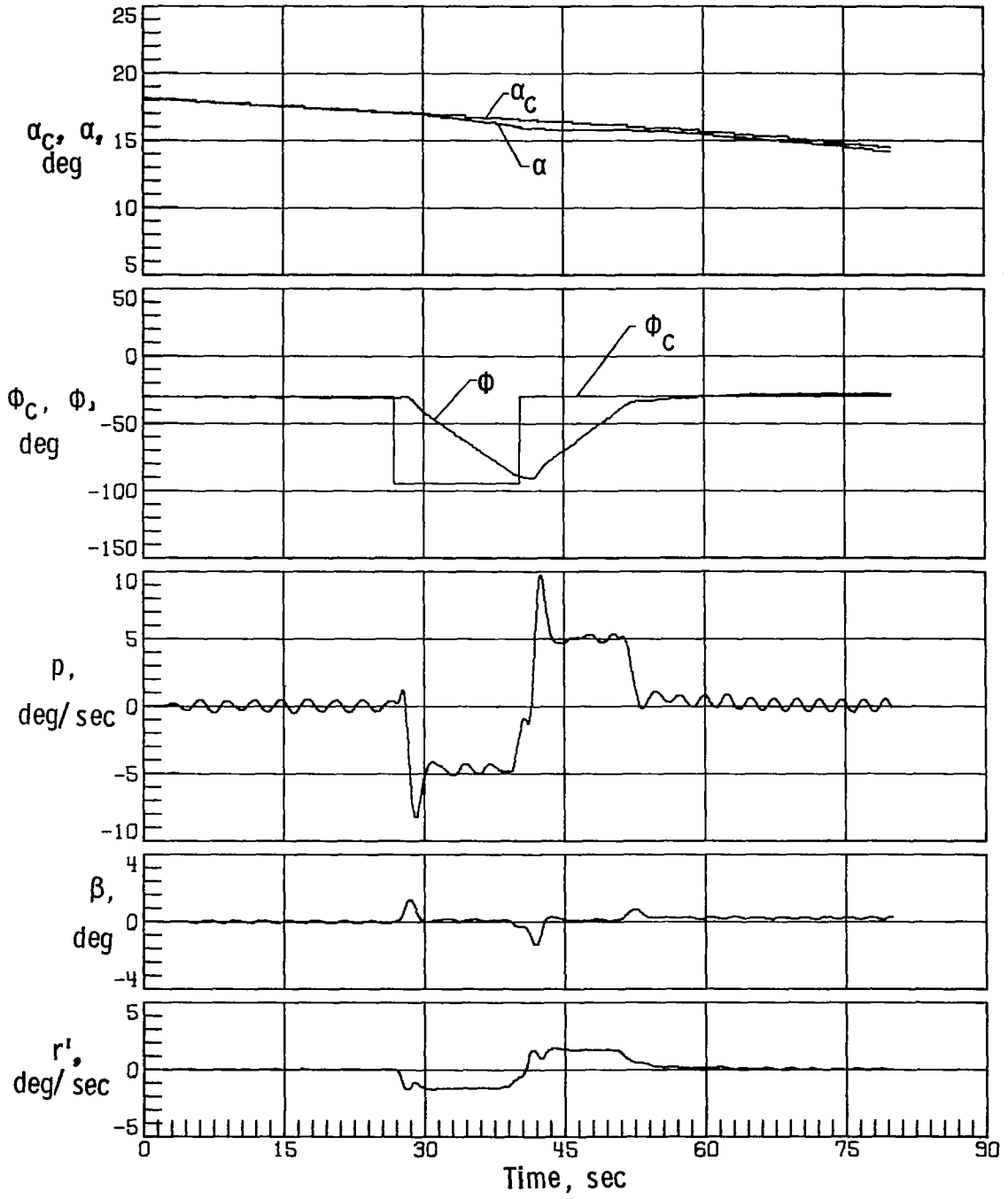

(b) Case 5A.

Figure 28.- Continued.

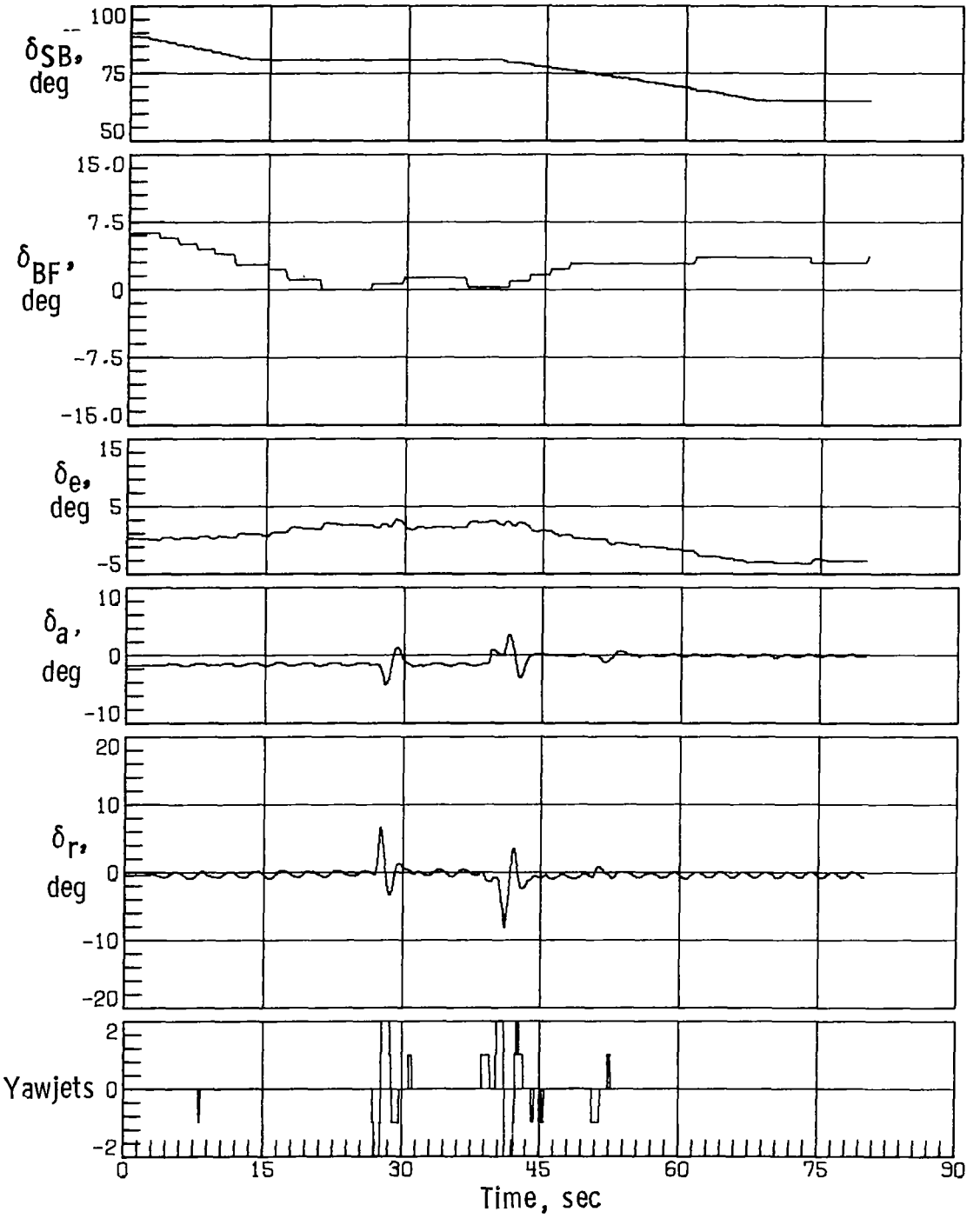

(b) Concluded.

Figure 28.- Concluded.

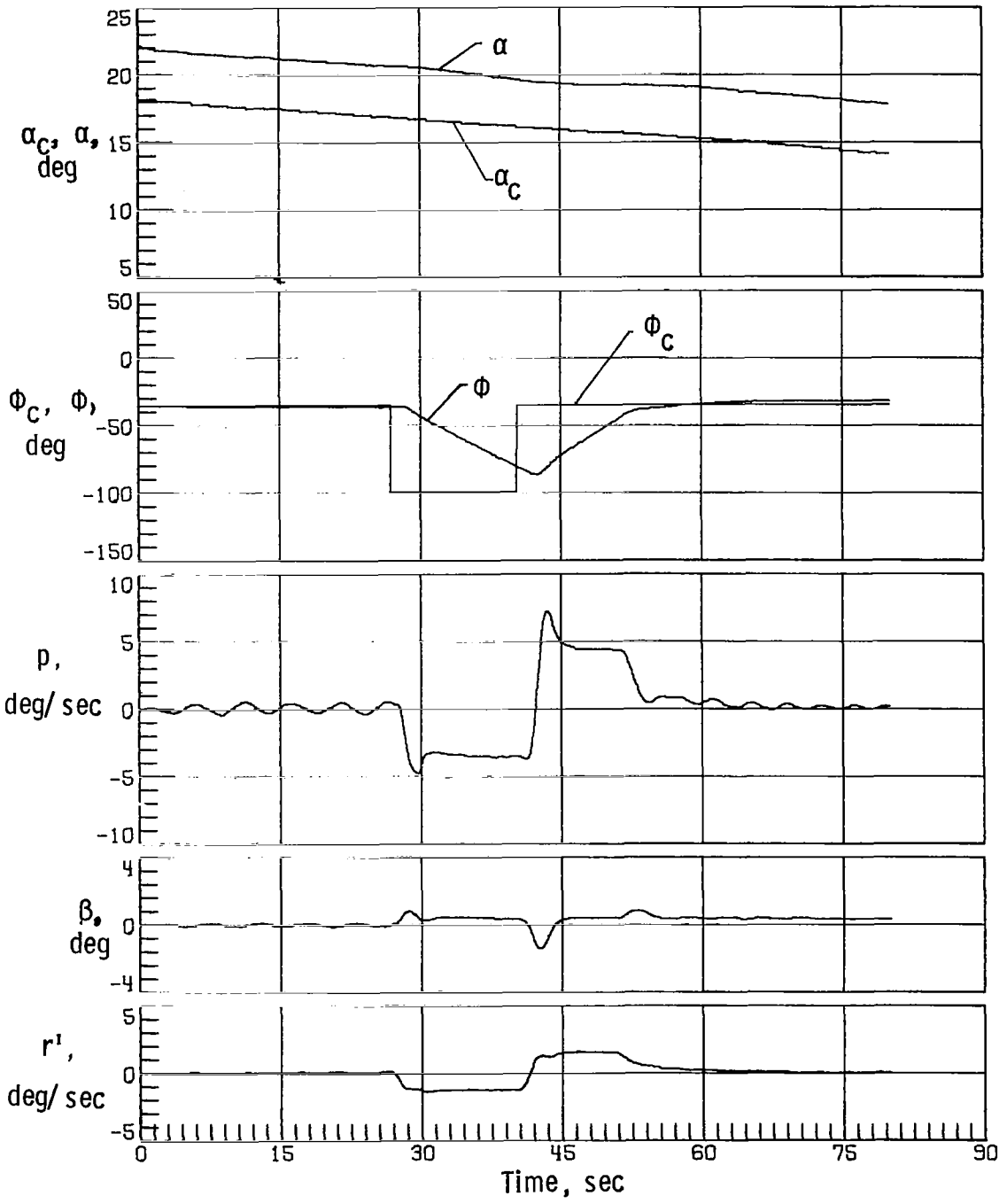

Figure 29.- Space Shuttle Orbiter response with simulation initiated at Mach 4.2 with nominal aerodynamics, sensed α error of -4^{o}, two yaw RCS thrusters on each side inoperable, and 0.0381-m lateral center-of-gravity offset.

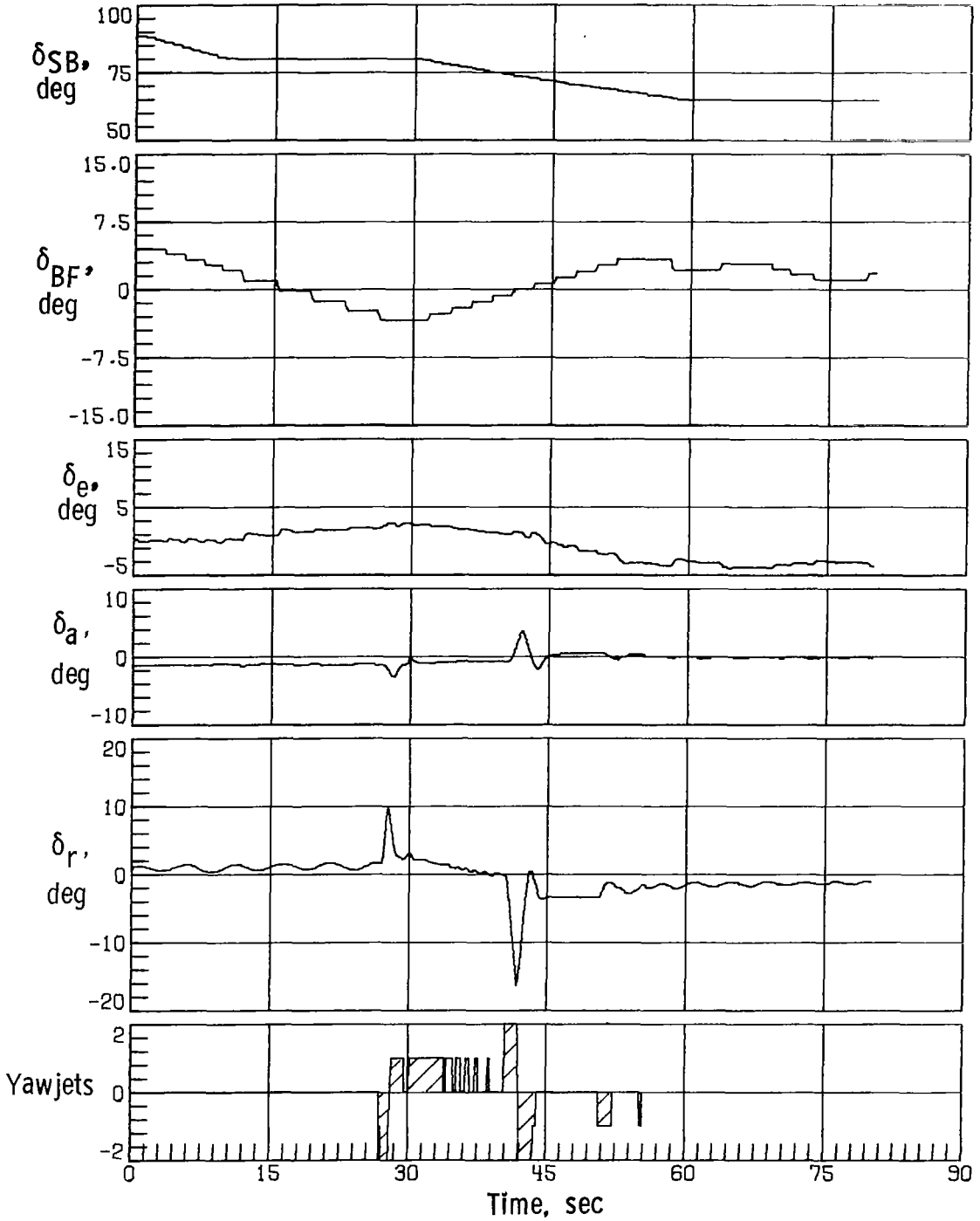

Figure 29.- Concluded.

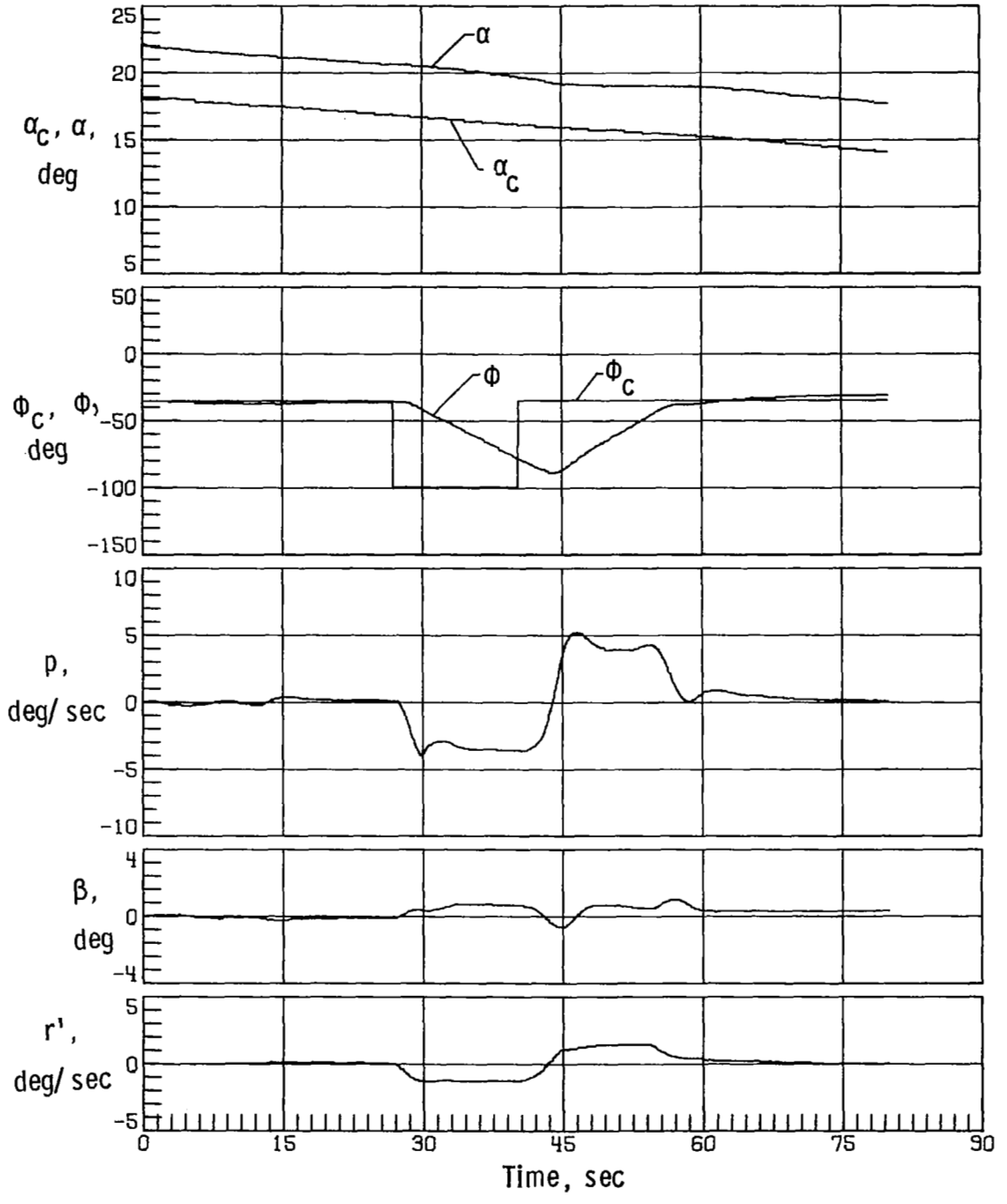

(a) Case 7.

Figure 30.- Space Shuttle Orbiter response with simulation initiated at Mach 4.2 with off-nominal aerodynamics, sensed α error of -4°, two yaw RCS thrusters on each side inoperable, and 0.0381-m lateral center-of-gravity offset.

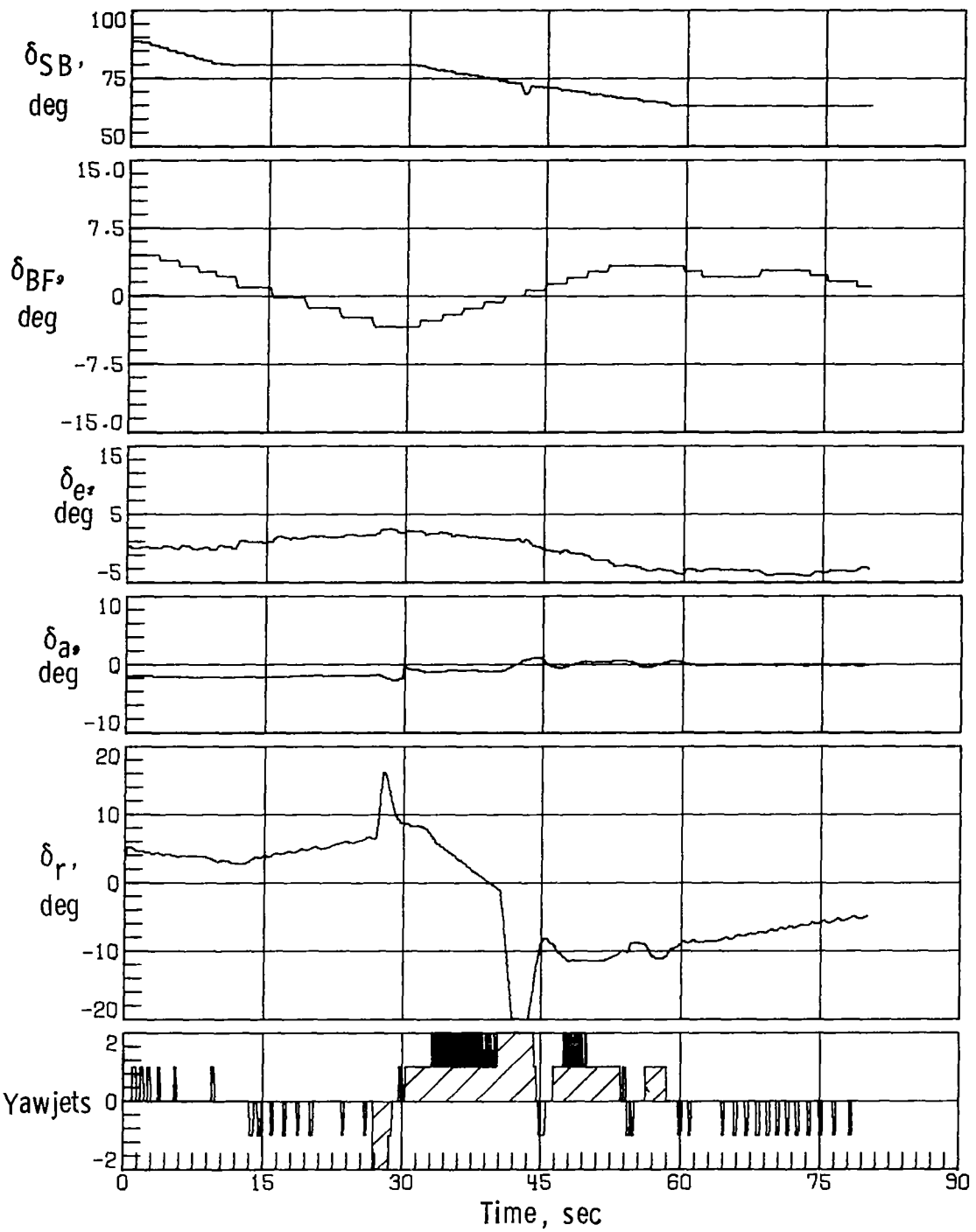

(a) Concluded.

Figure 30.- Continued.

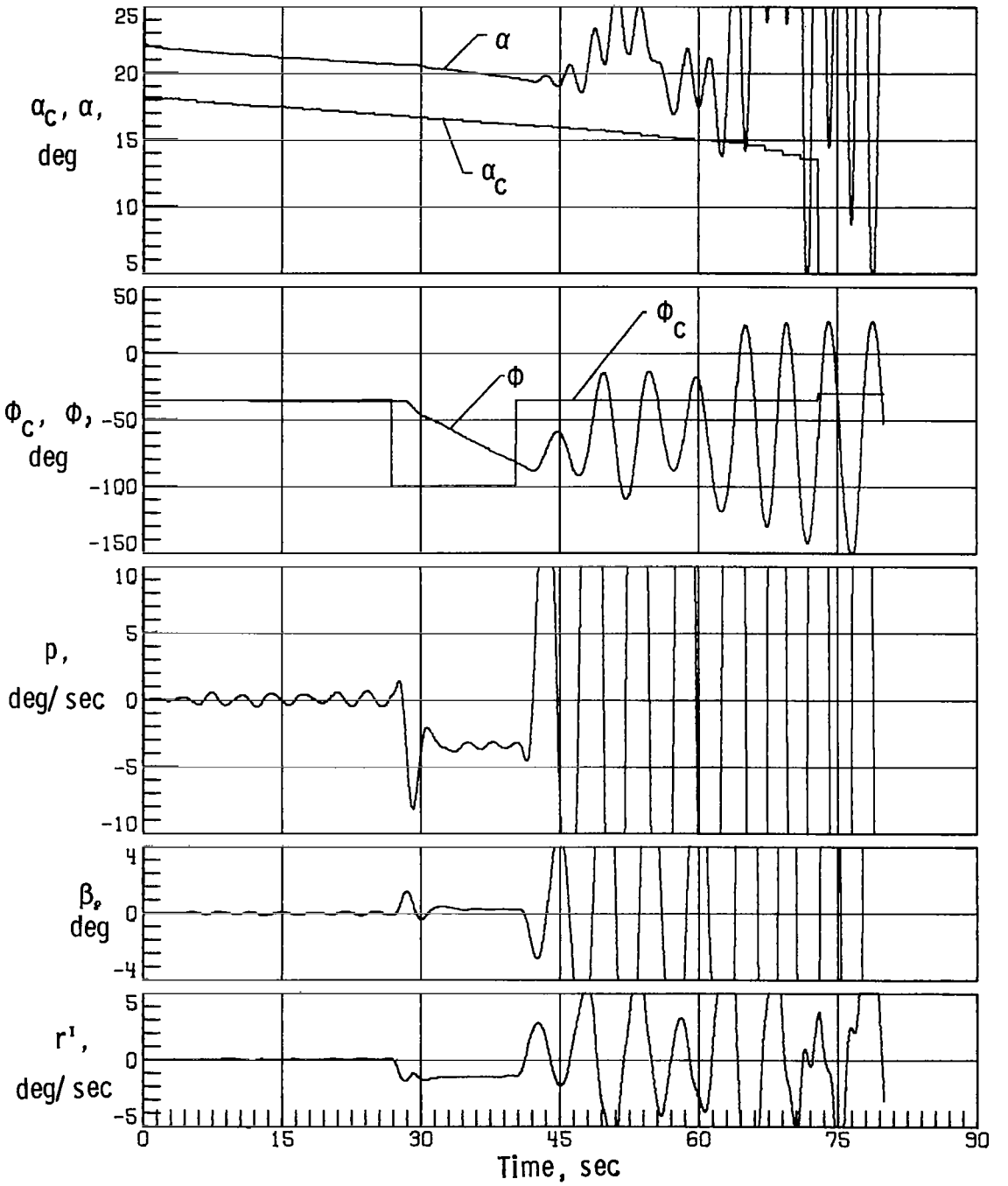

(b) Case 5A.

Figure 30.- Continued.

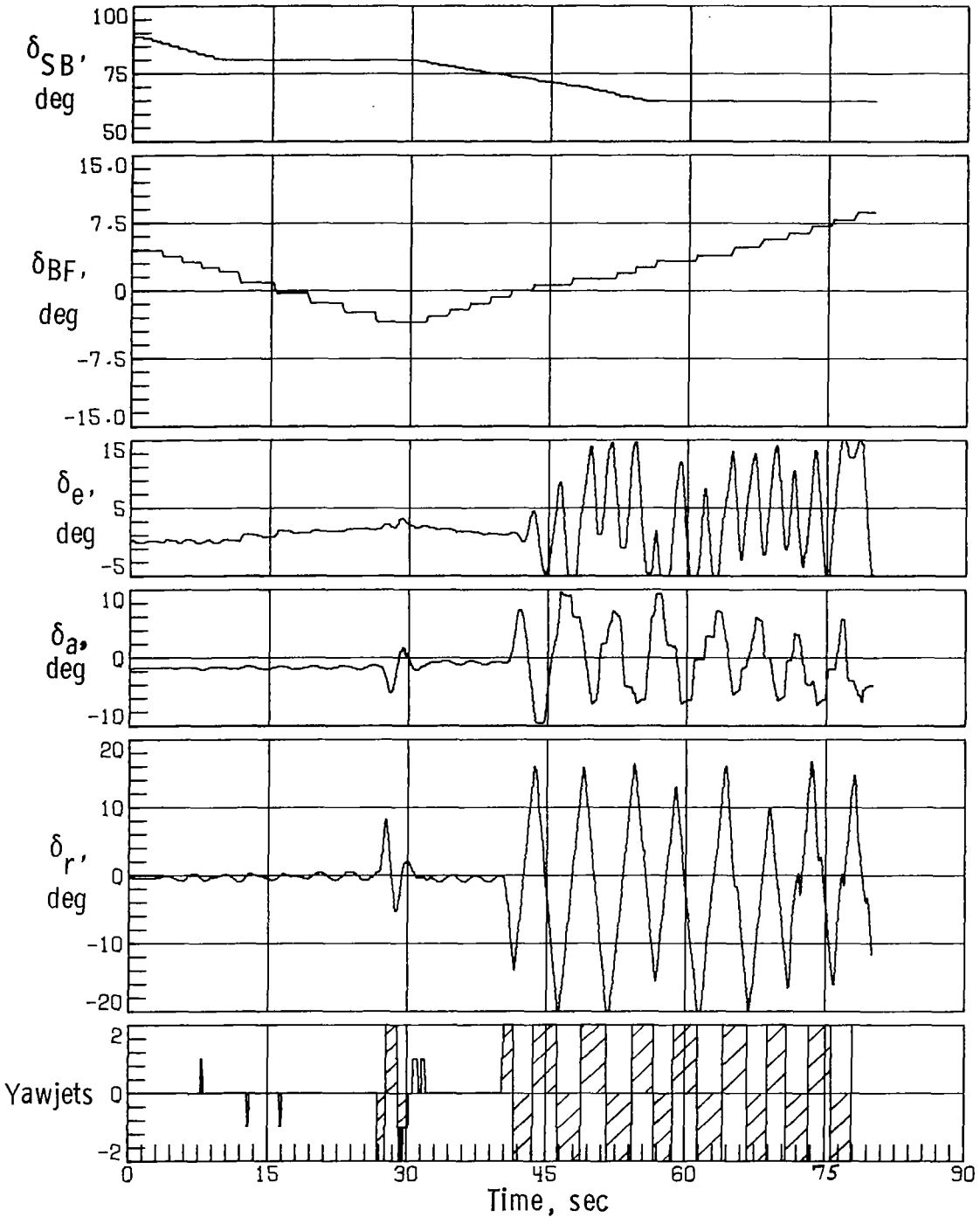

(b) Concluded.

Figure 30.- Concluded.

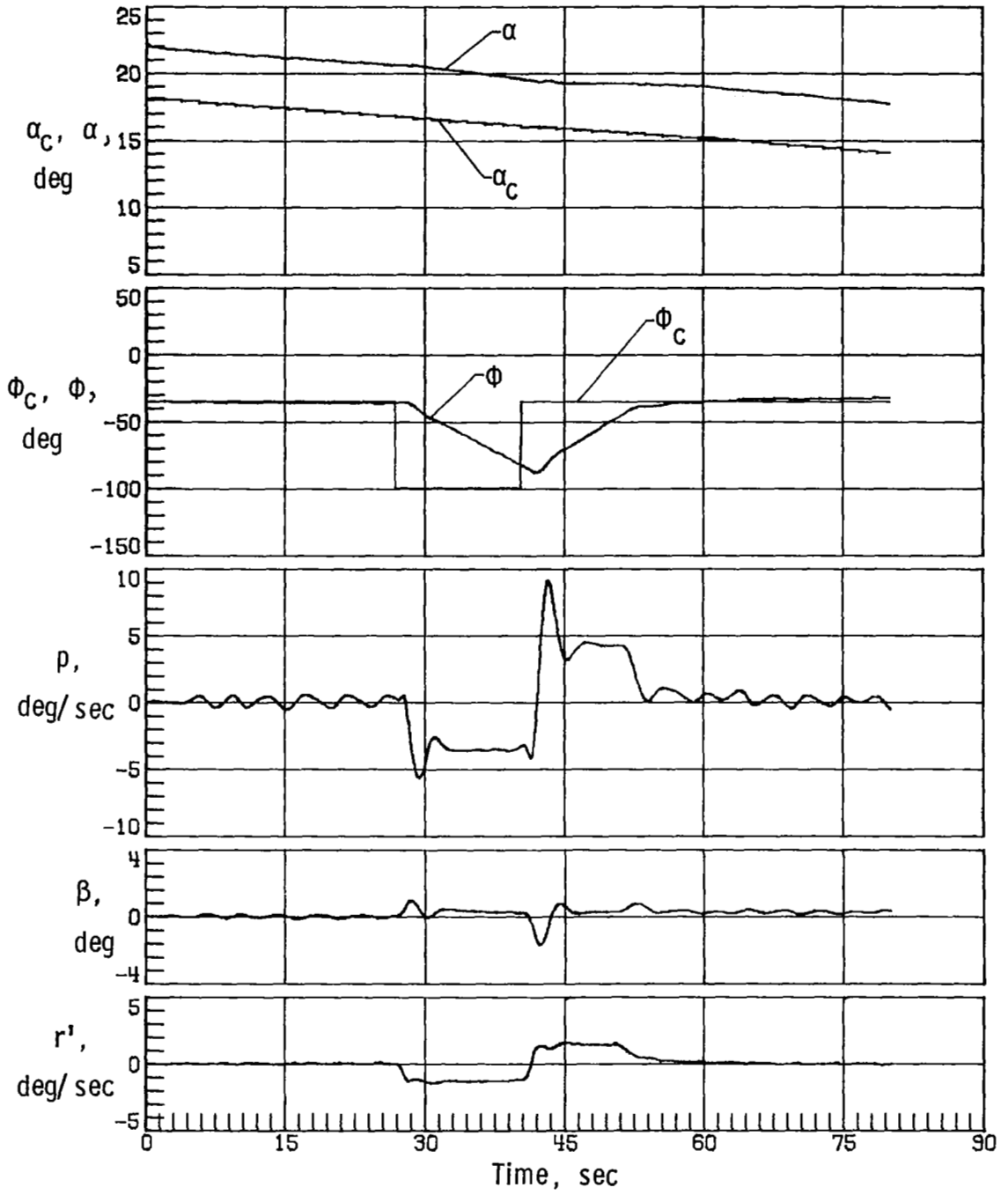

Figure 31.- Space Shuttle Orbiter response with simulation initiated at Mach 4.2 with off-nominal aerodynamics (case 5A), sensed α error of -4^{o}, two yaw RCS thrusters on each side inoperable, modified rudder control gain, and 0.0381-m lateral center-of-gravity offset.

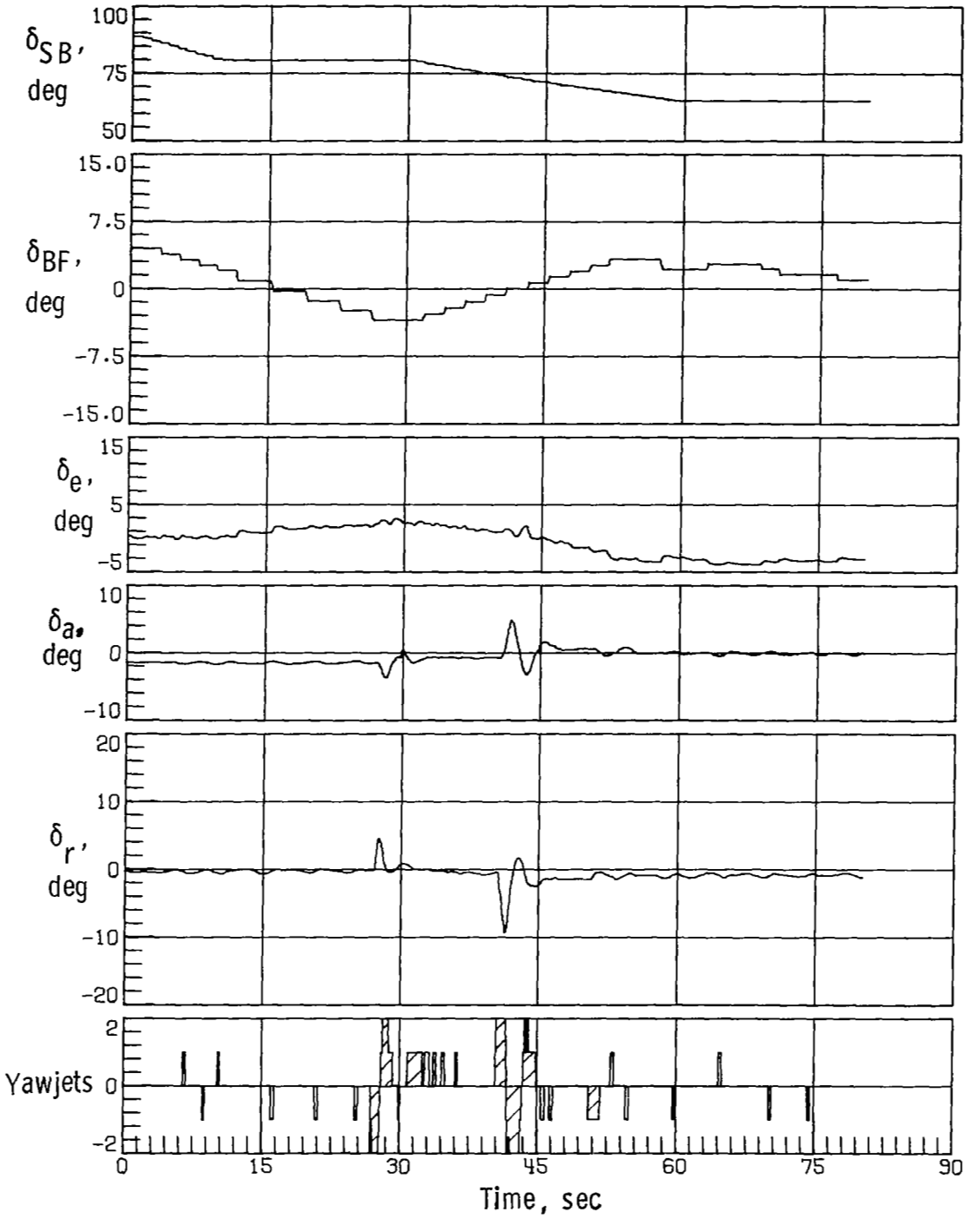

Figure 31.- Concluded.

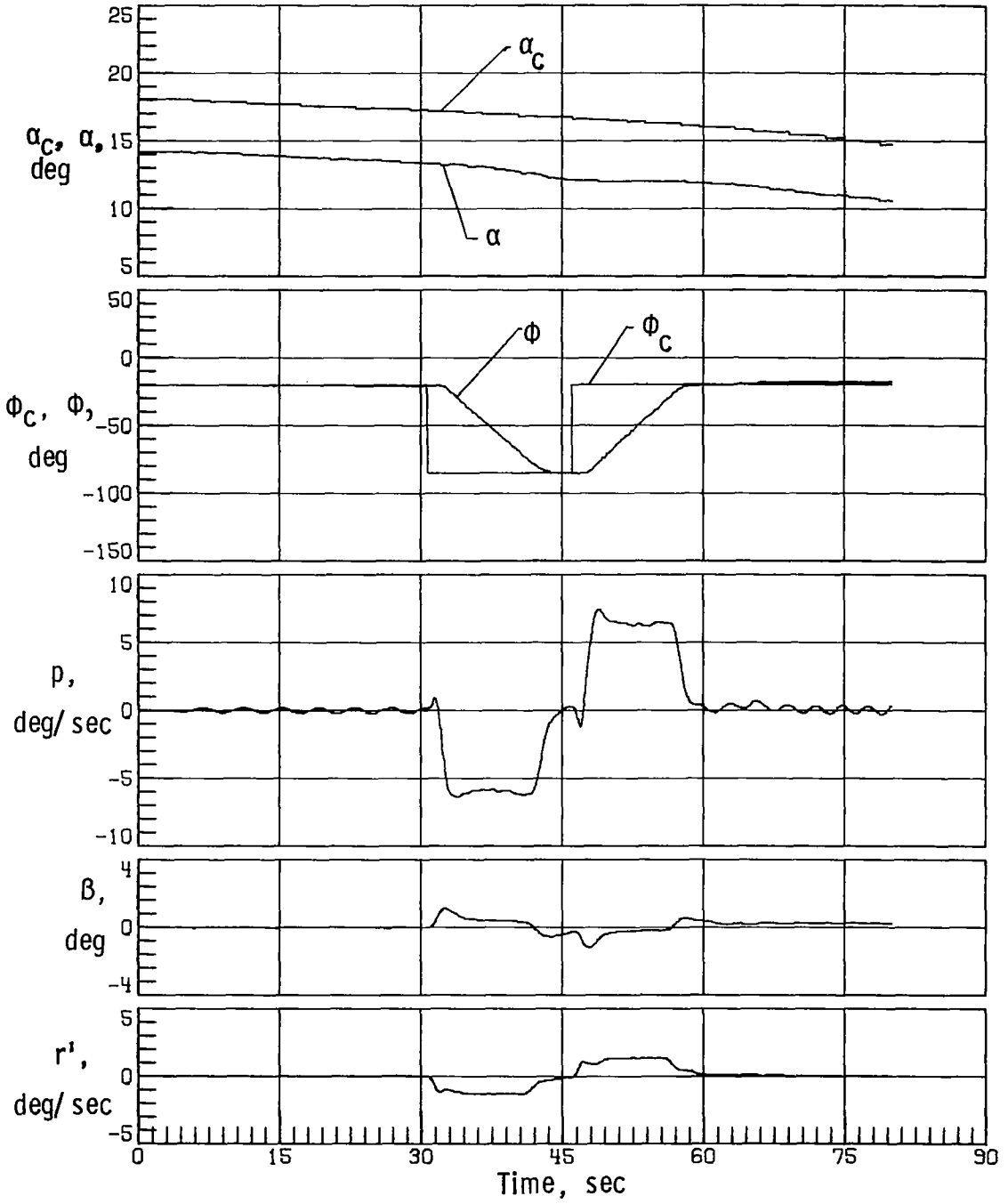

Figure 32.- Space Shuttle Orbiter response with simulation initiated at Mach 4.2 with nominal aerodynamics, sensed α error of $+4^{\circ}$, two yaw RCS thrusters on each side inoperable, and 0.0381-m lateral center-of-gravity offset.

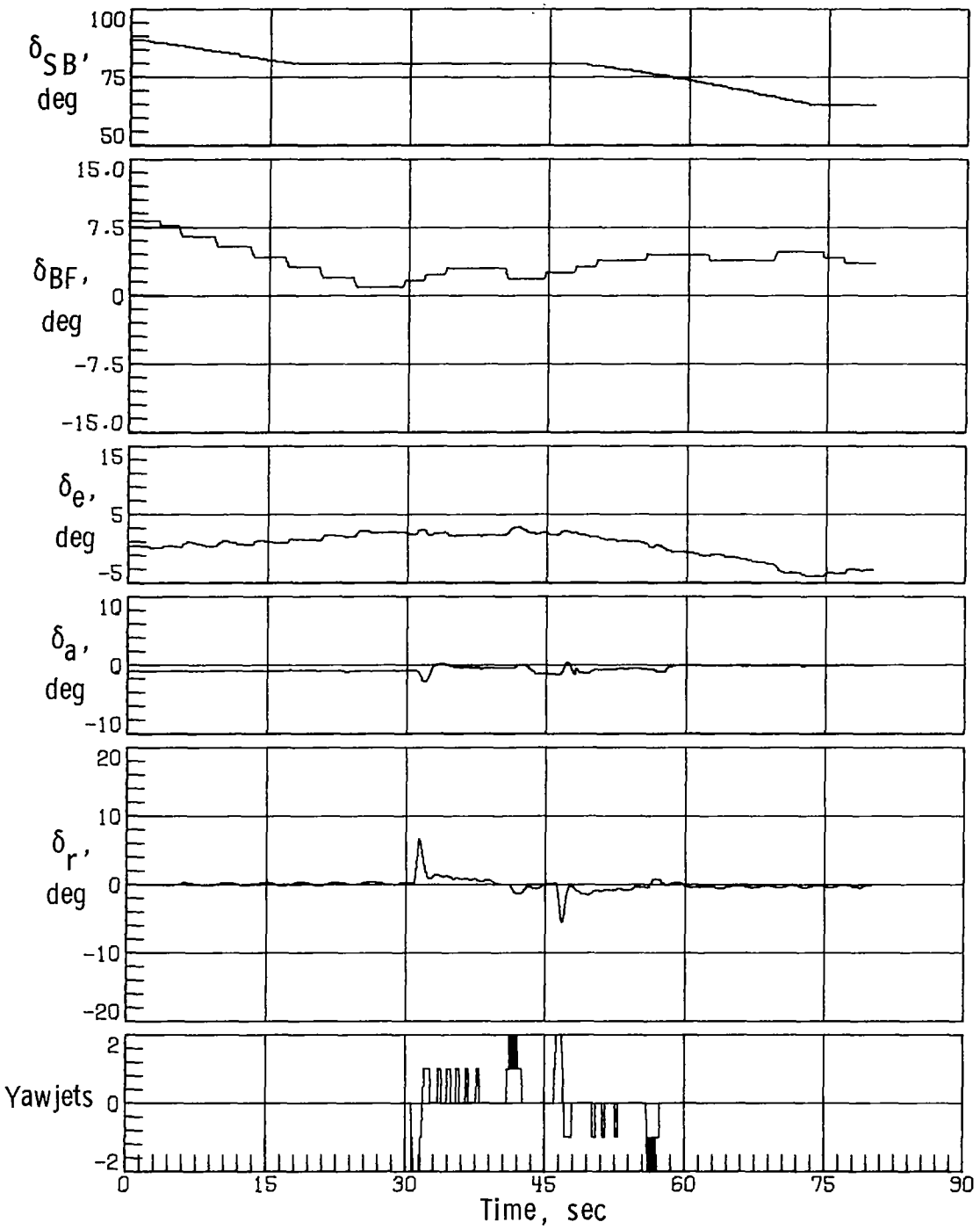

Figure 32.- Concluded.

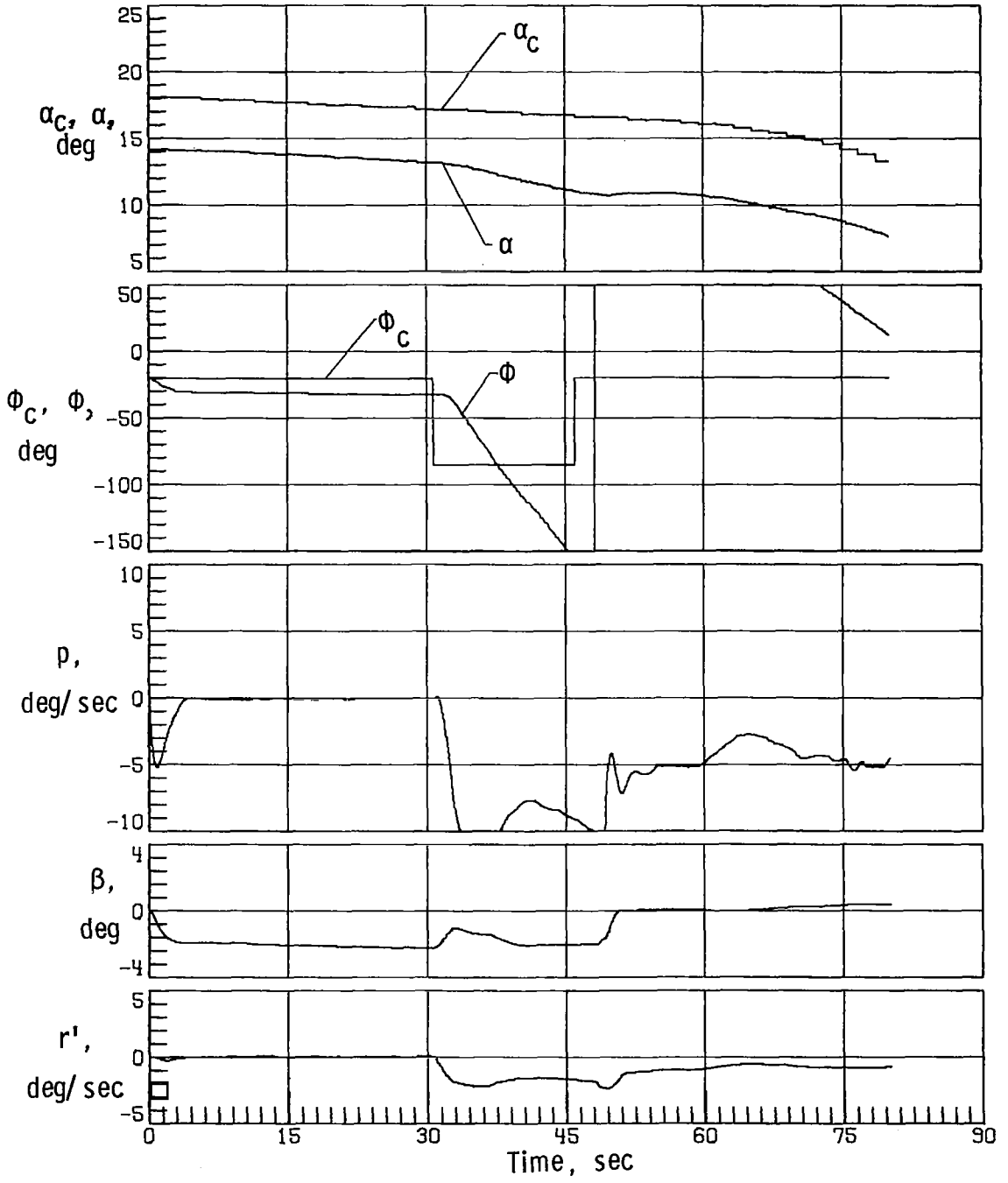

(a) Case 14.

Figure 33.- Space Shuttle Orbiter response with simulation initiated at Mach 4.2 with off-nominal aerodynamics, sensed α error of $+4^{\circ}$, two yaw RCS thrusters on each side inoperable, and 0.0381-m lateral center-of-gravity offset.

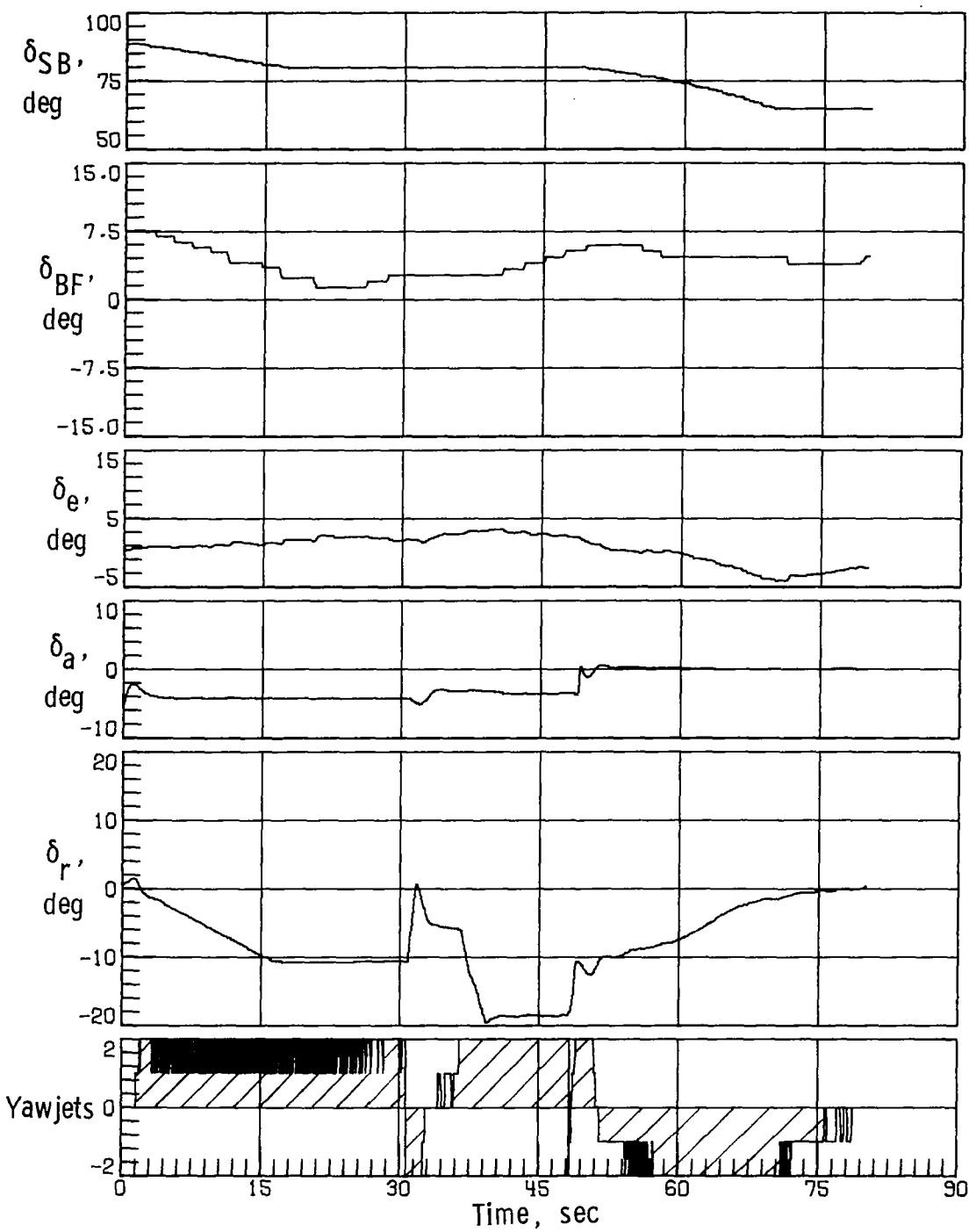

(a) Concluded.

Figure 33.- Continued.

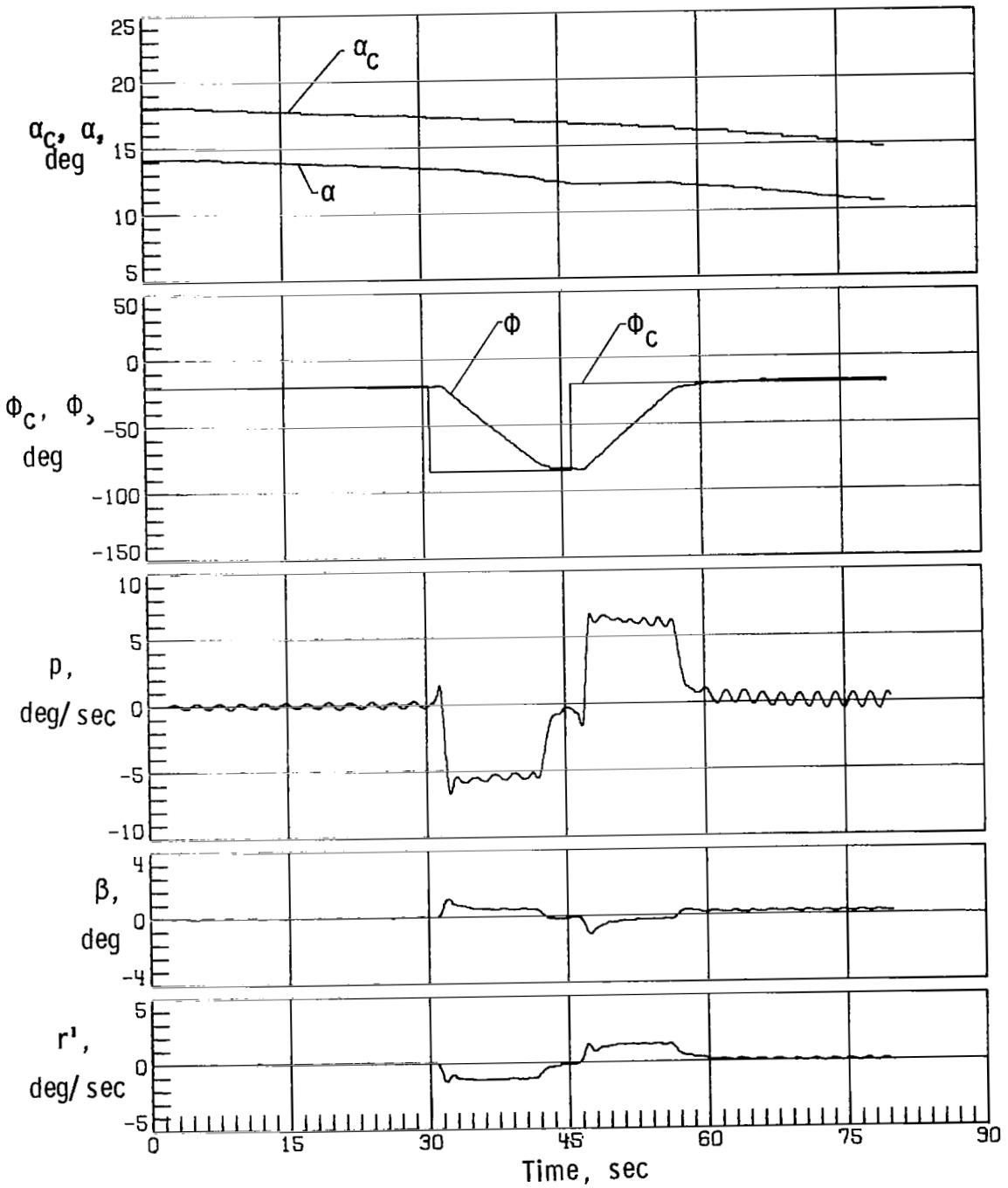

(b) Case 14A.

Figure 33.- Continued.

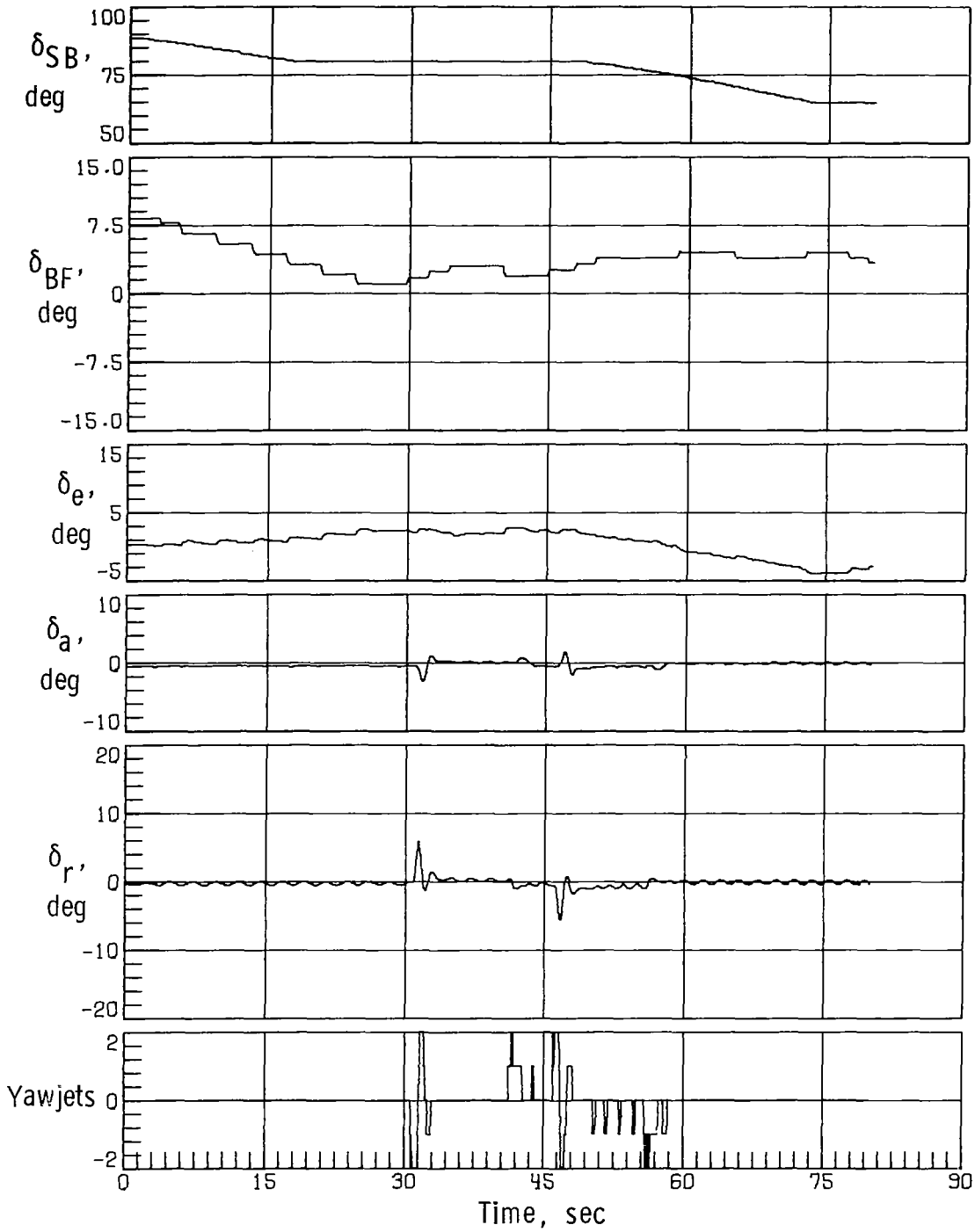

(b) Concluded.

Figure 33.- Concluded.

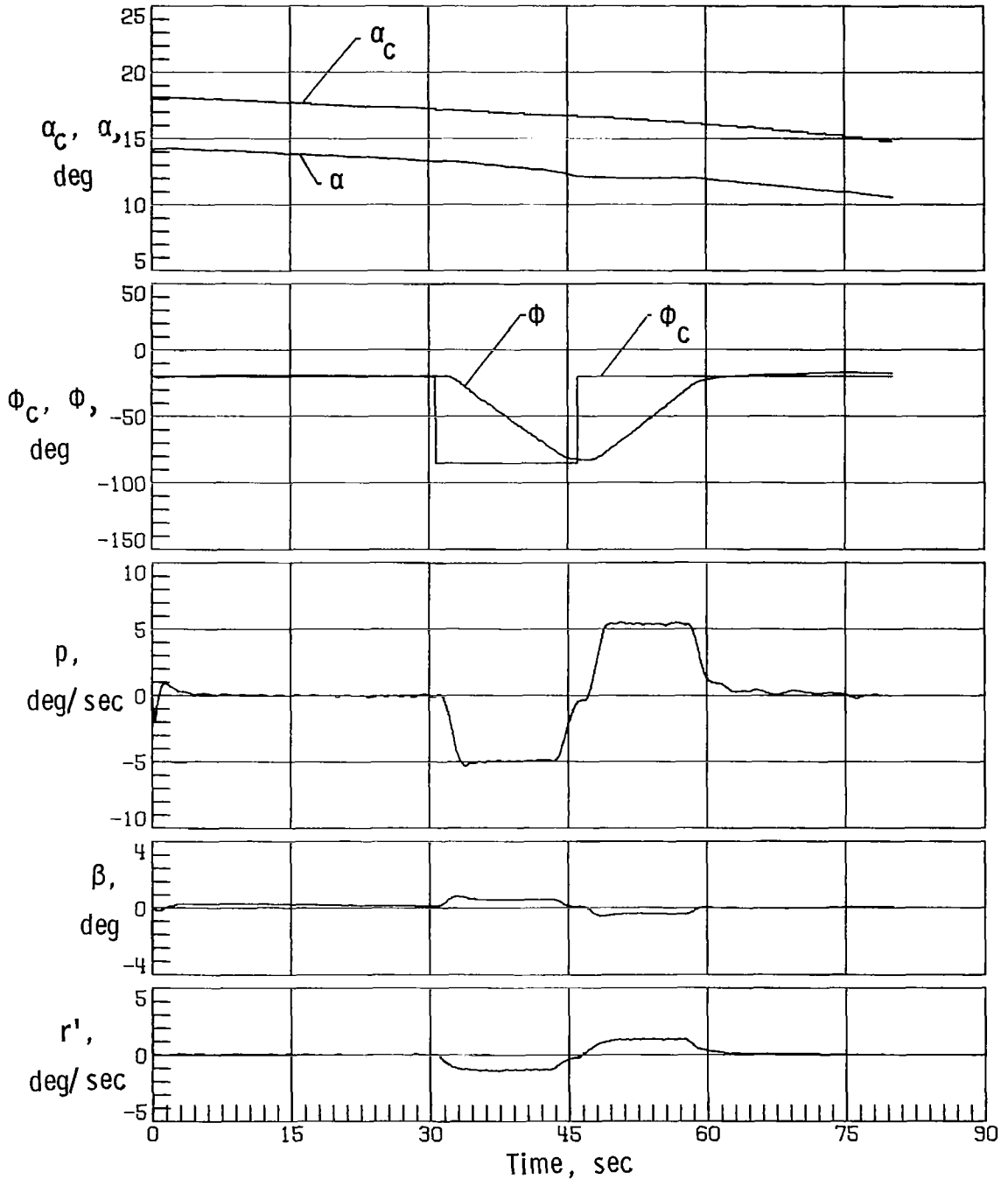

Figure 34.- Space Shuttle Orbiter response with simulation initiated at Mach 4.2 with off-nominal aerodynamics (case 14), sensed α error of $+4^{o}$, two yaw RCS thrusters on each side inoperable, 0.0381-m lateral center-of-gravity offset, and $(\delta_a)_{trim} = 0$ throughout simulation.

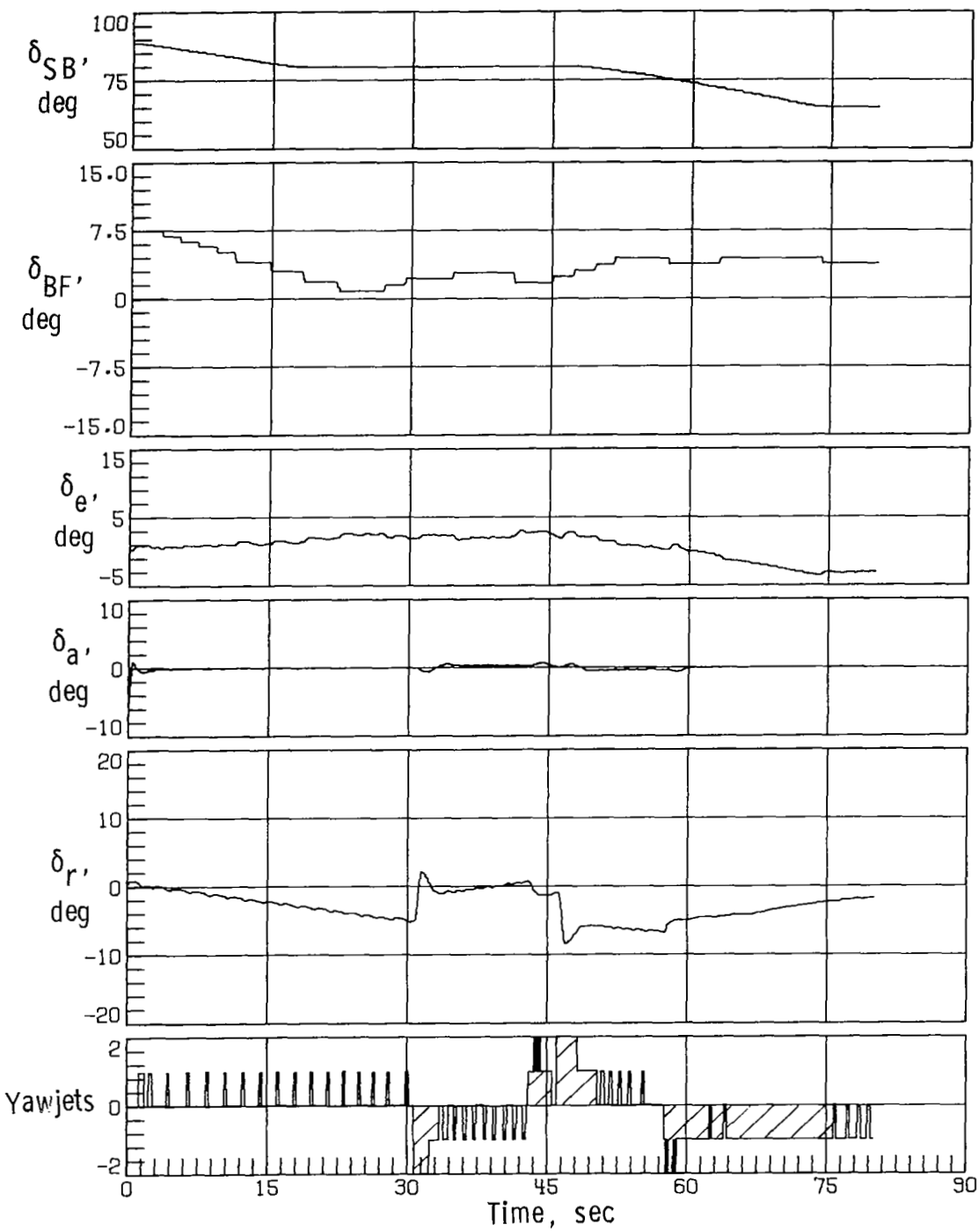

Figure 34.- Concluded.

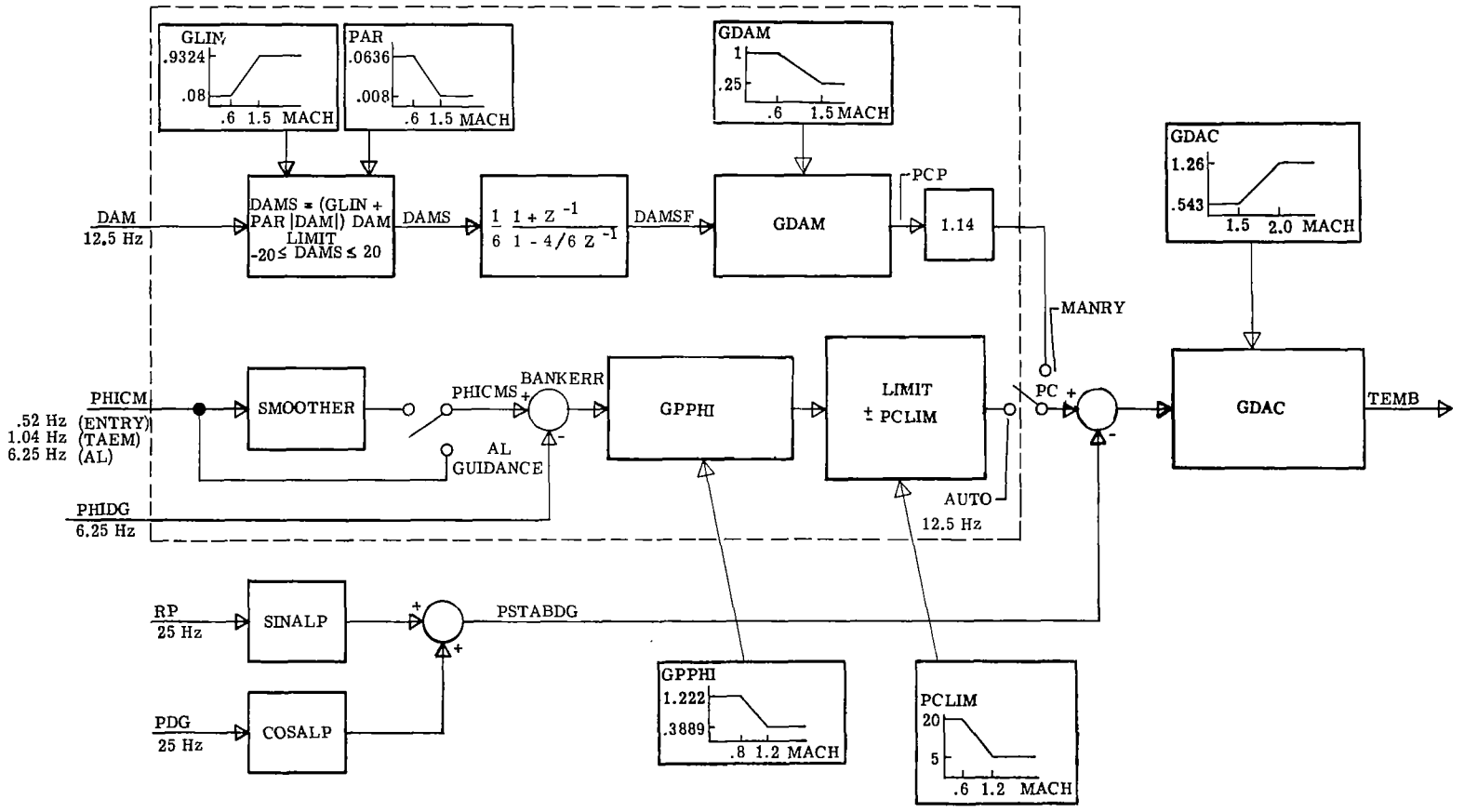

(a) Part I.

Figure 35.- Aileron command.

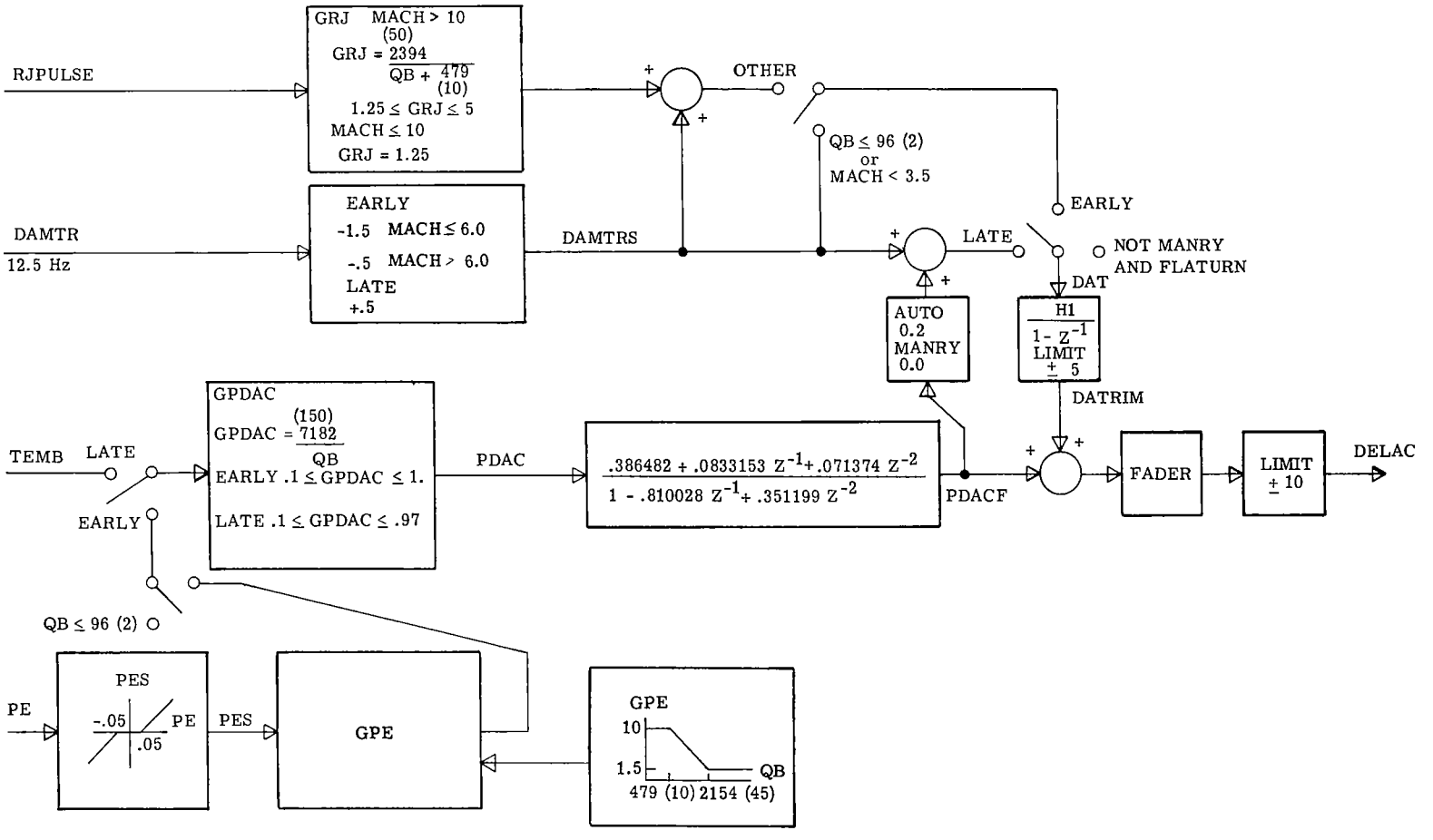

(b) Part II (Frequency of execution = 25 Hz).

Figure 35.- Concluded.

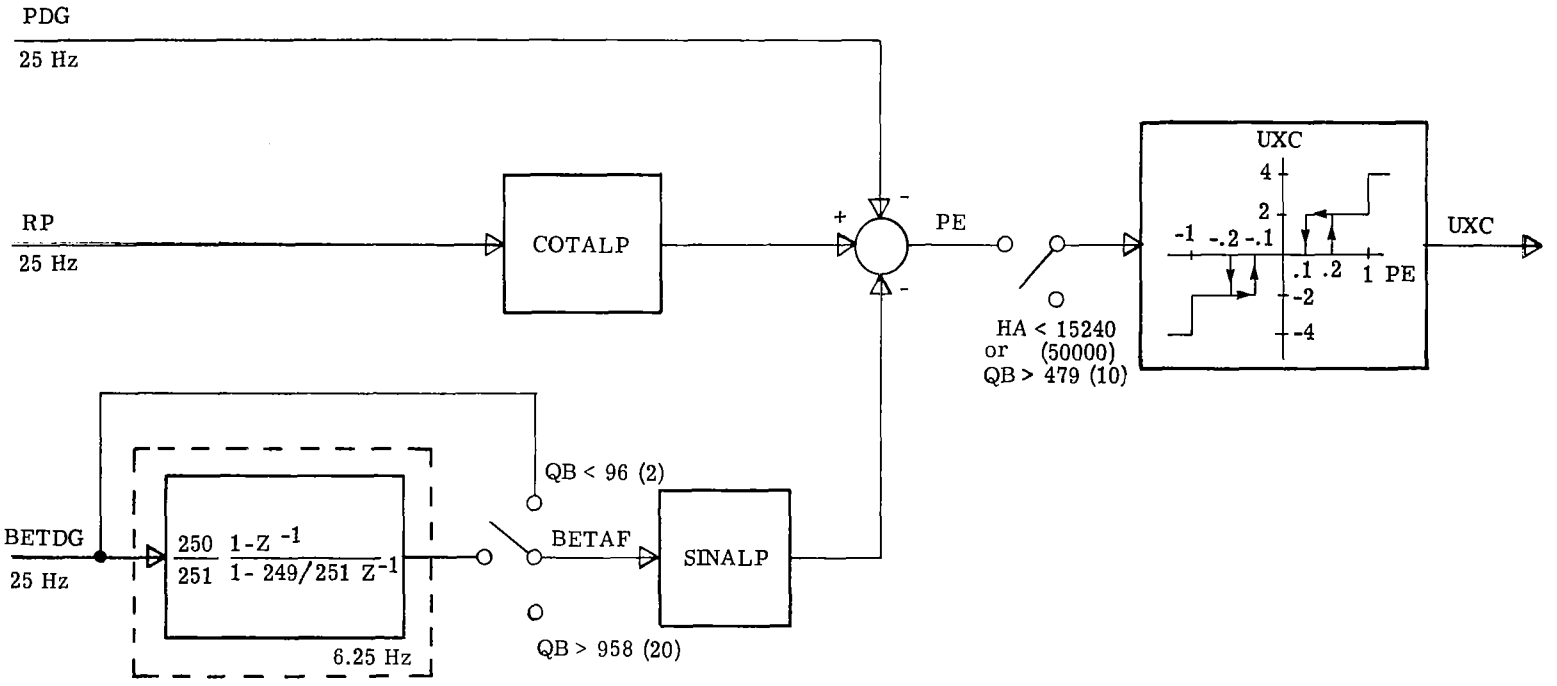

Figure 36.- Roll RCS (Frequency of execution = 25 Hz, unless otherwise noted).

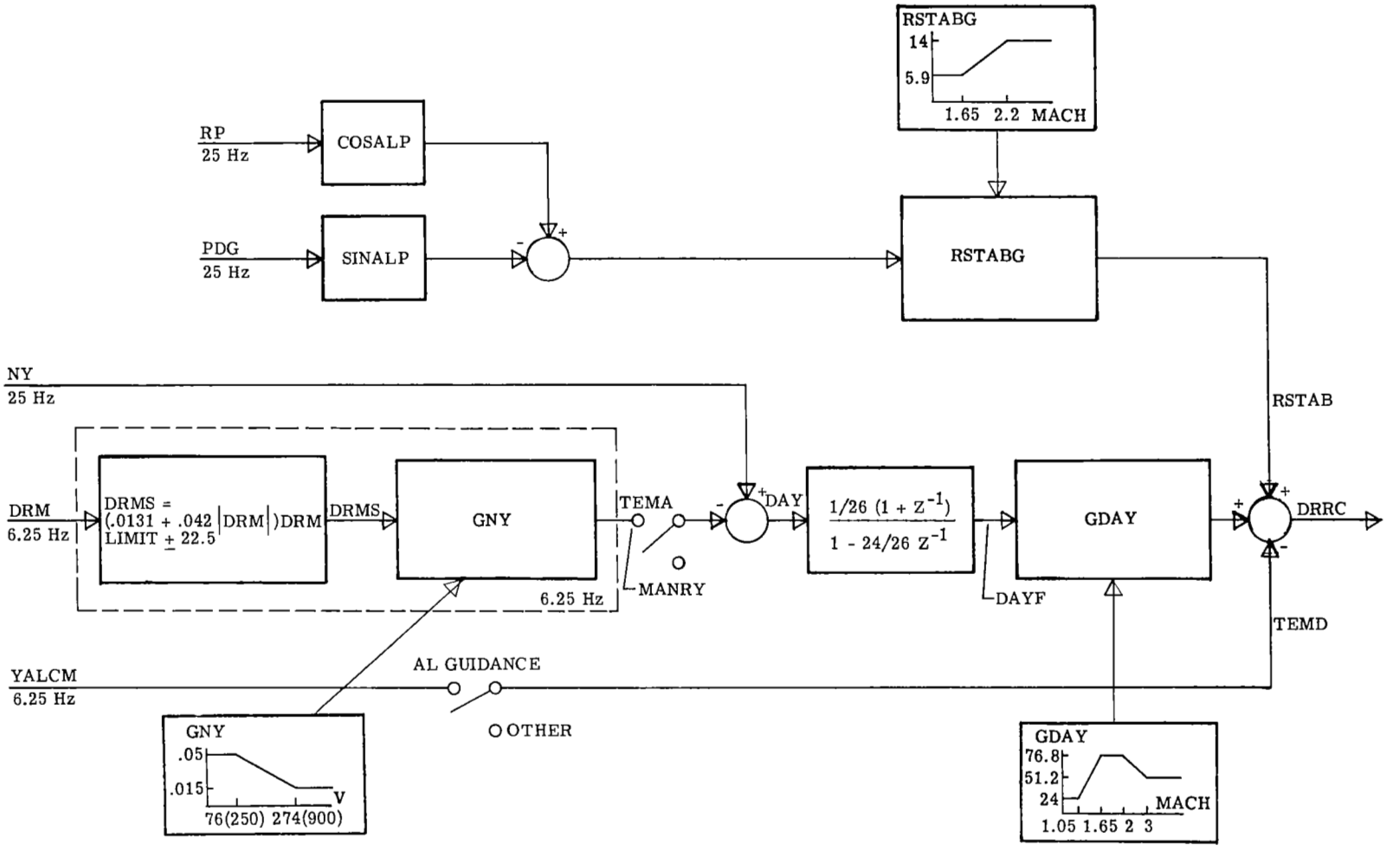

(a) Part I (Frequency of execution = 25 Hz, unless otherwise noted).

Figure 37.- Rudder command.

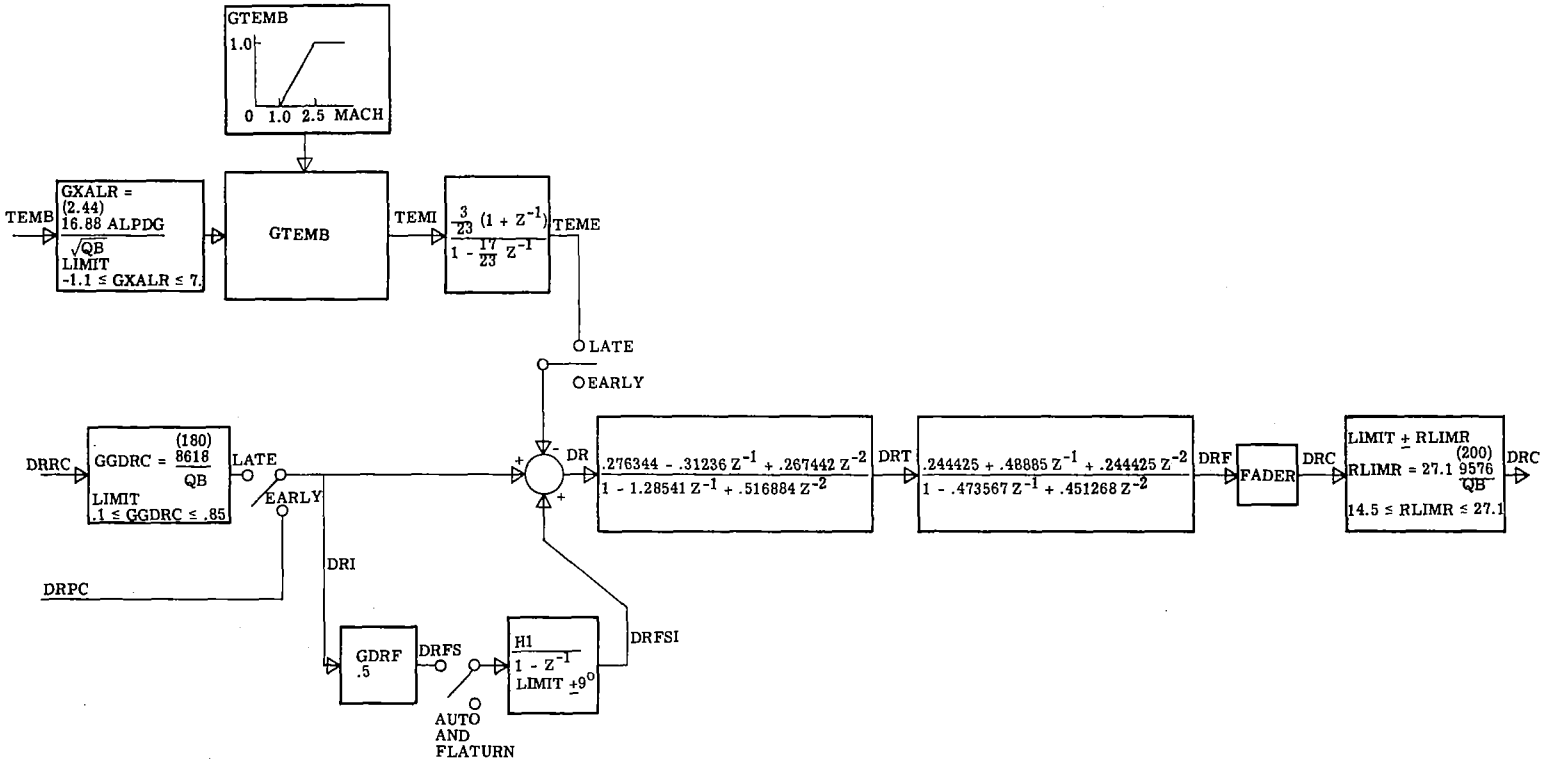

(b) Part II (Frequency of execution = 25 Hz).

Figure 37.- Concluded.

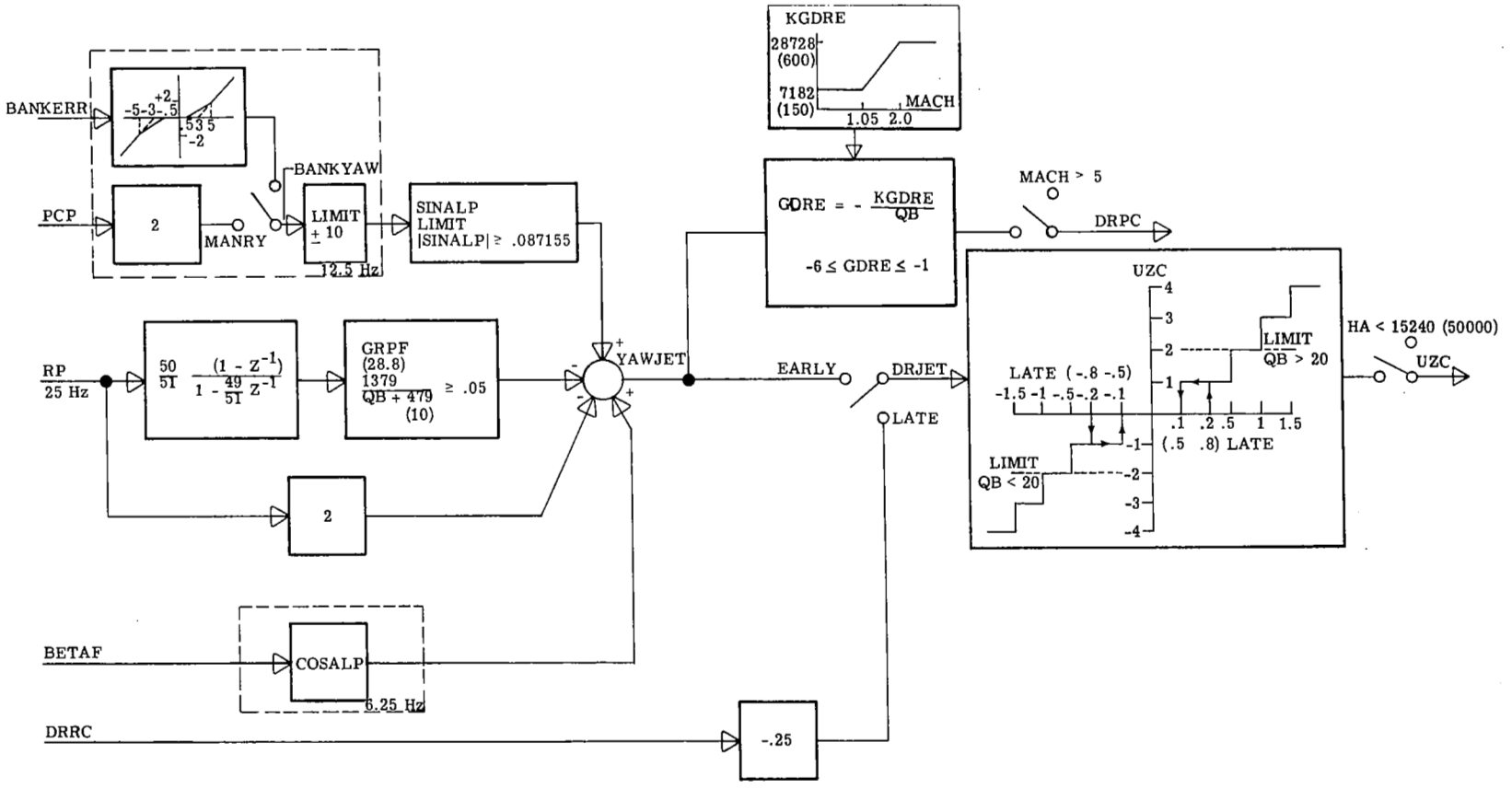

Figure 38.- Yaw RCS (Frequency of execution = 25 Hz, unless otherwise noted).

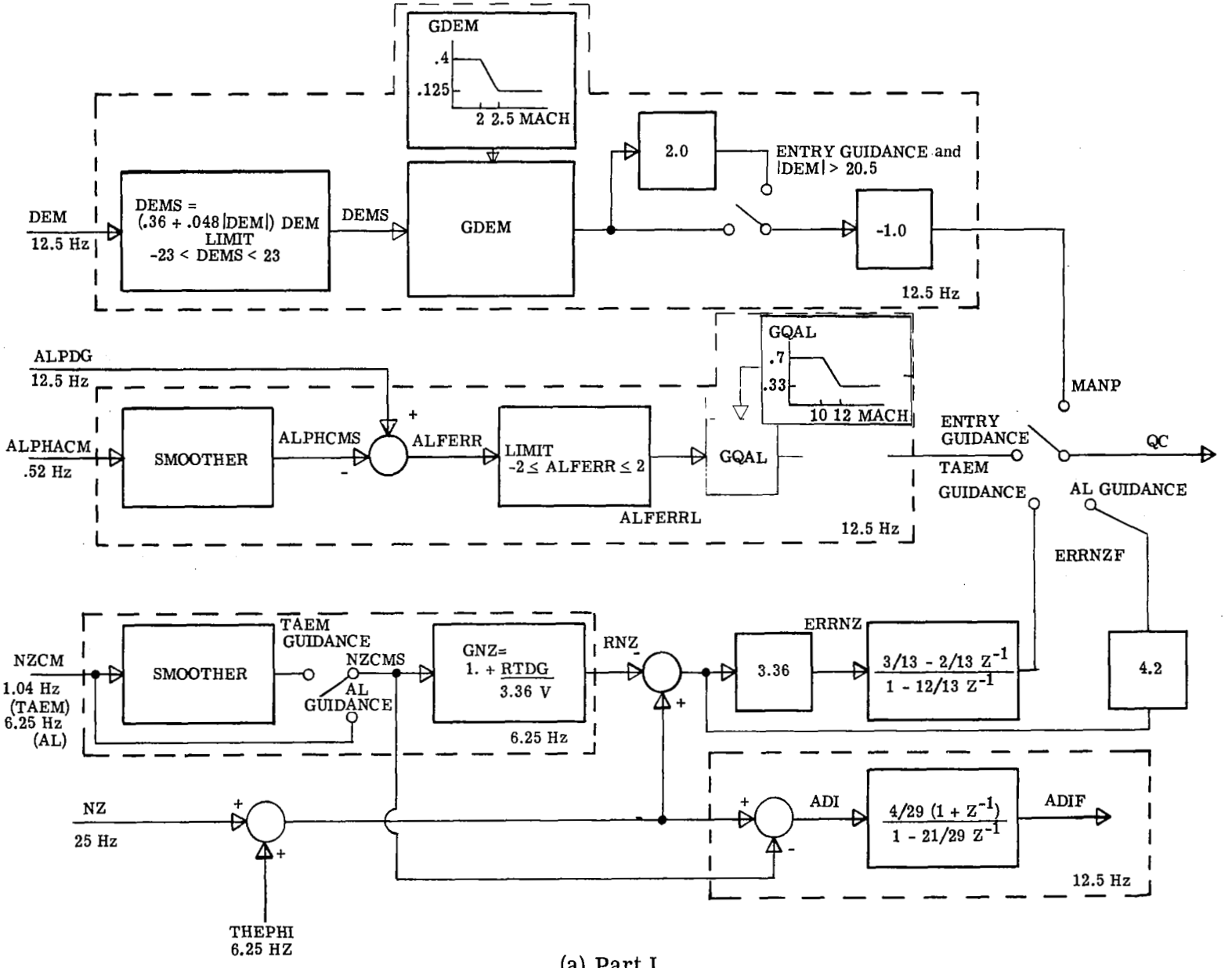

(a) Part I.

Figure 39.- Elevator command.

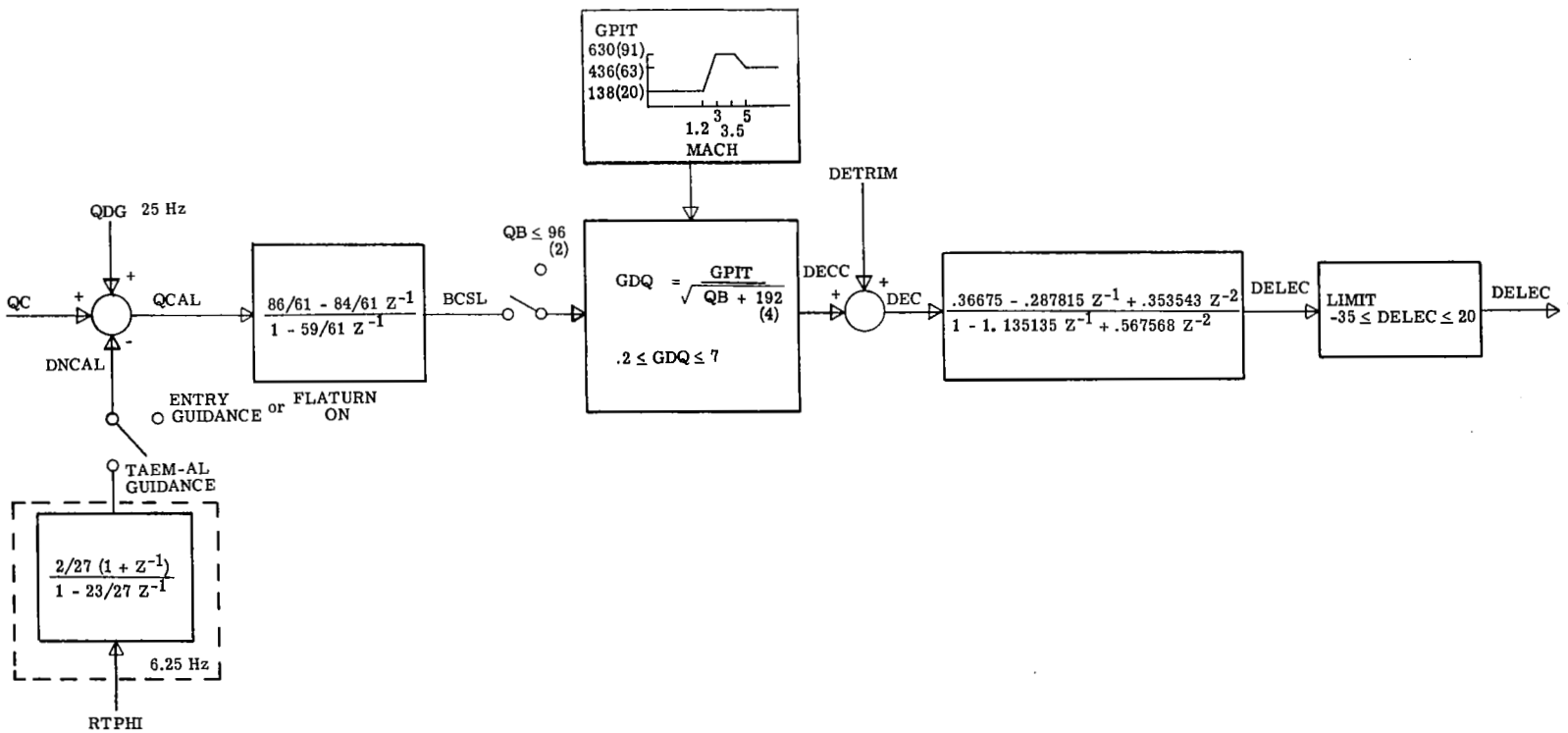

(b) Part II (Frequency of execution = 25 Hz, unless otherwise noted).

Figure 39.- Continued.

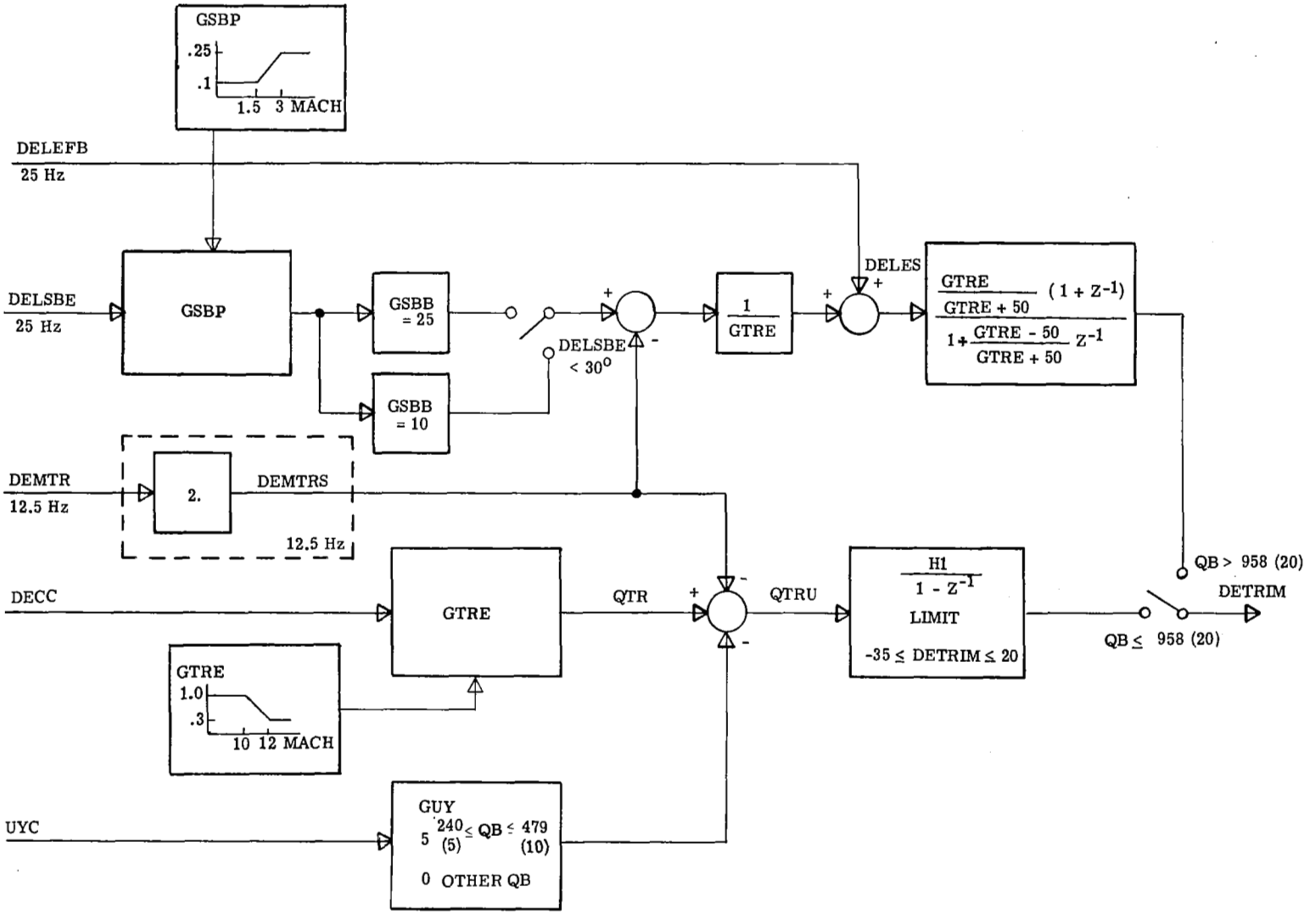

(c) Pitch trim (Frequency of execution = 25 Hz, unless otherwise noted).

Figure 39.- Concluded.

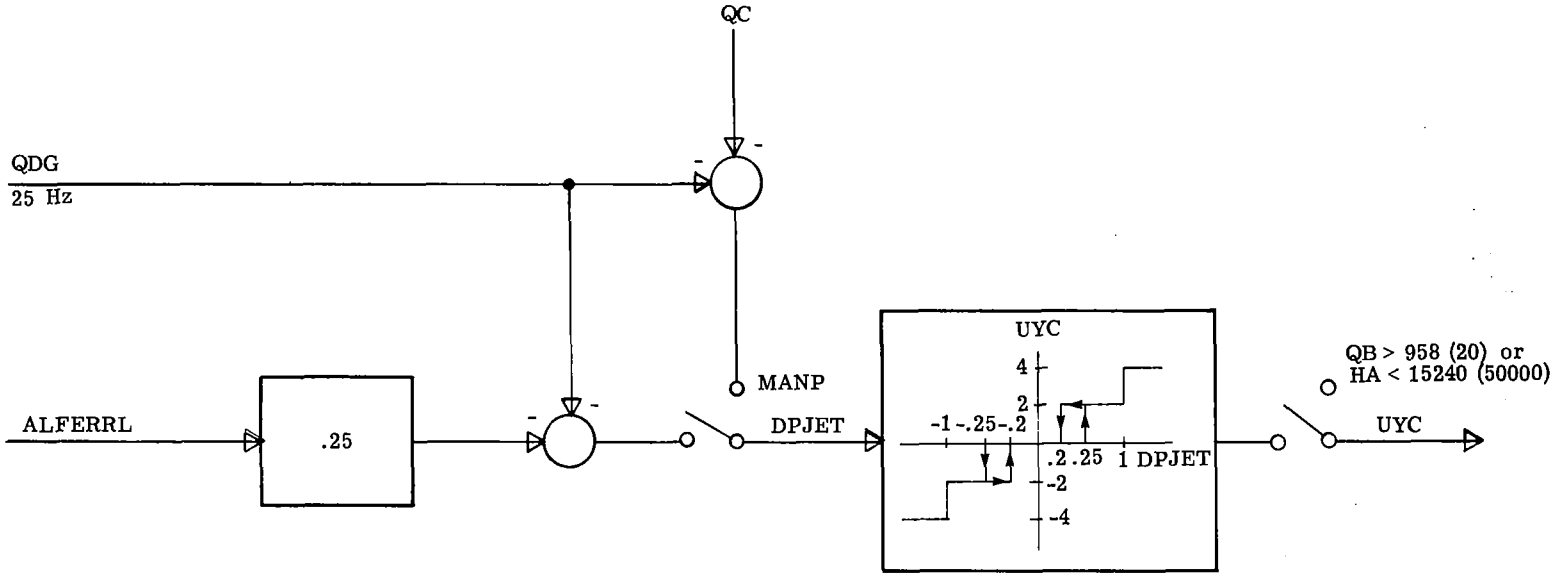

Figure 40.- Pitch RCS (Frequency of execution = 25 Hz).

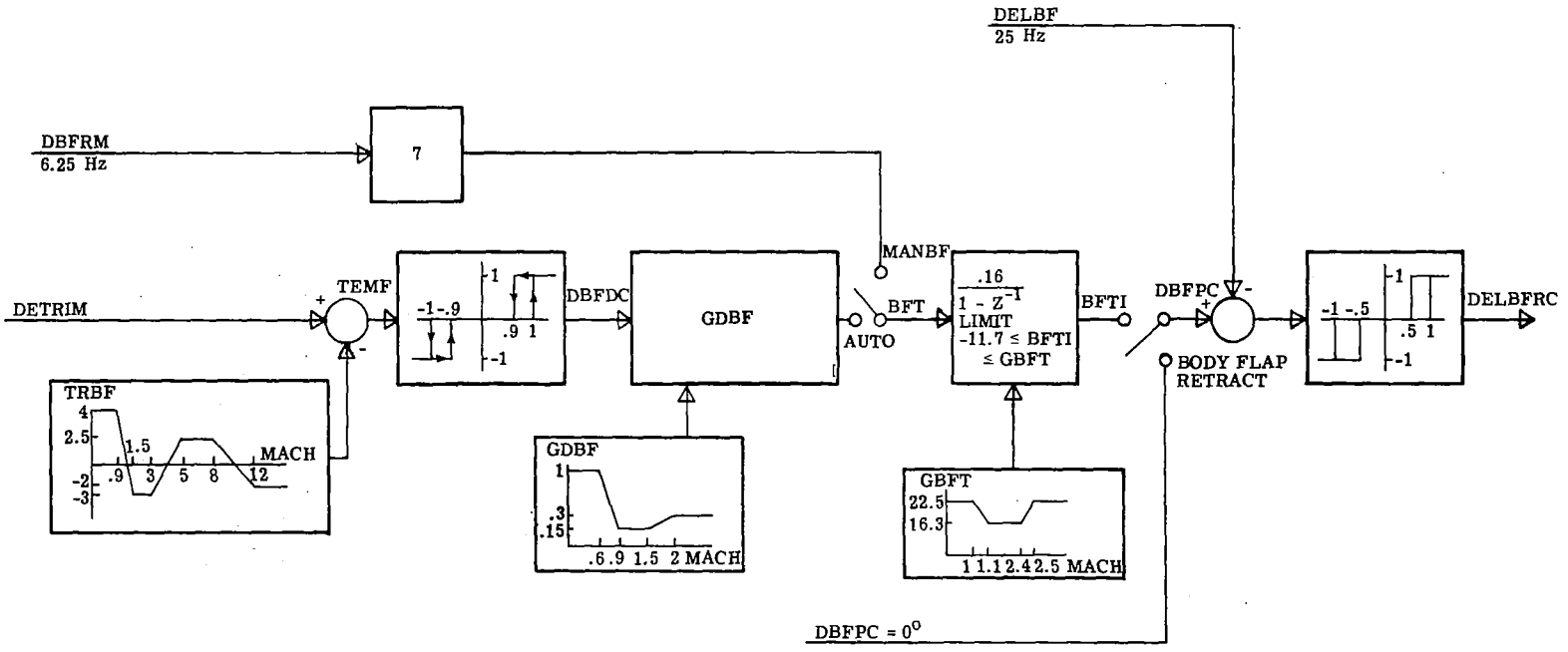

Figure 41.- Body-flap command (Frequency of execution = 6.25 Hz).

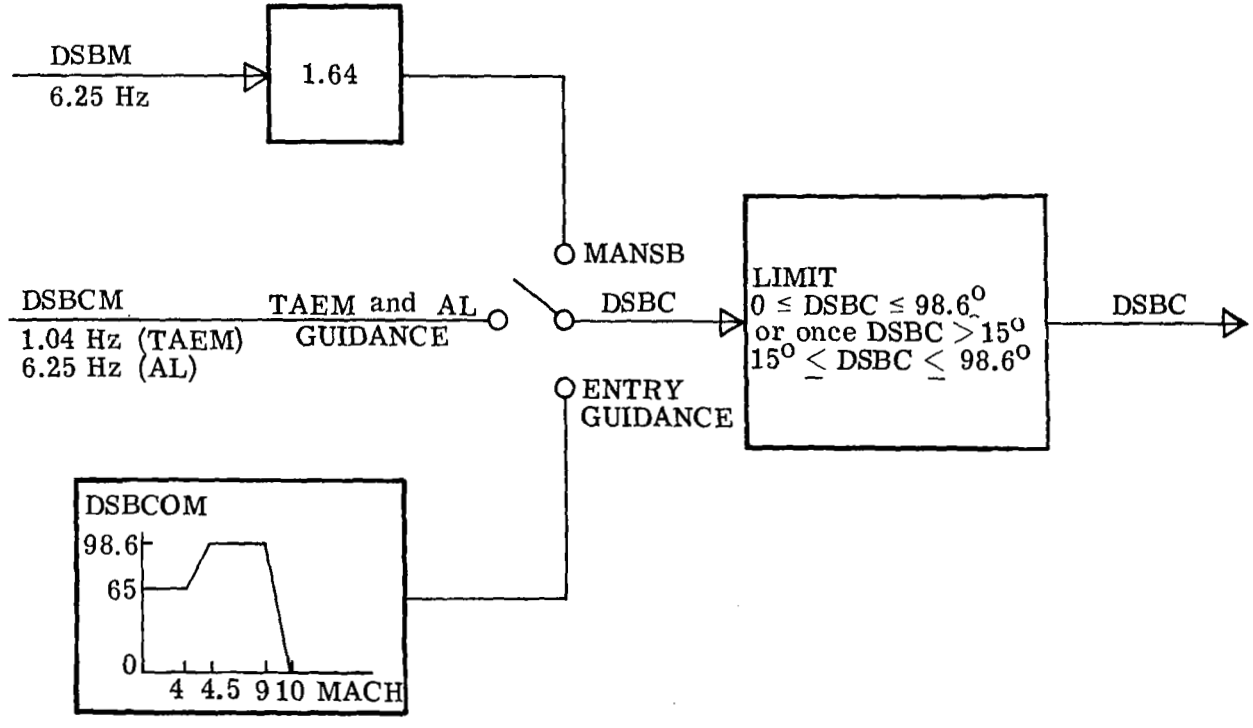

Figure 42.- Speed-brake command (Frequency of execution = 6.25 Hz).

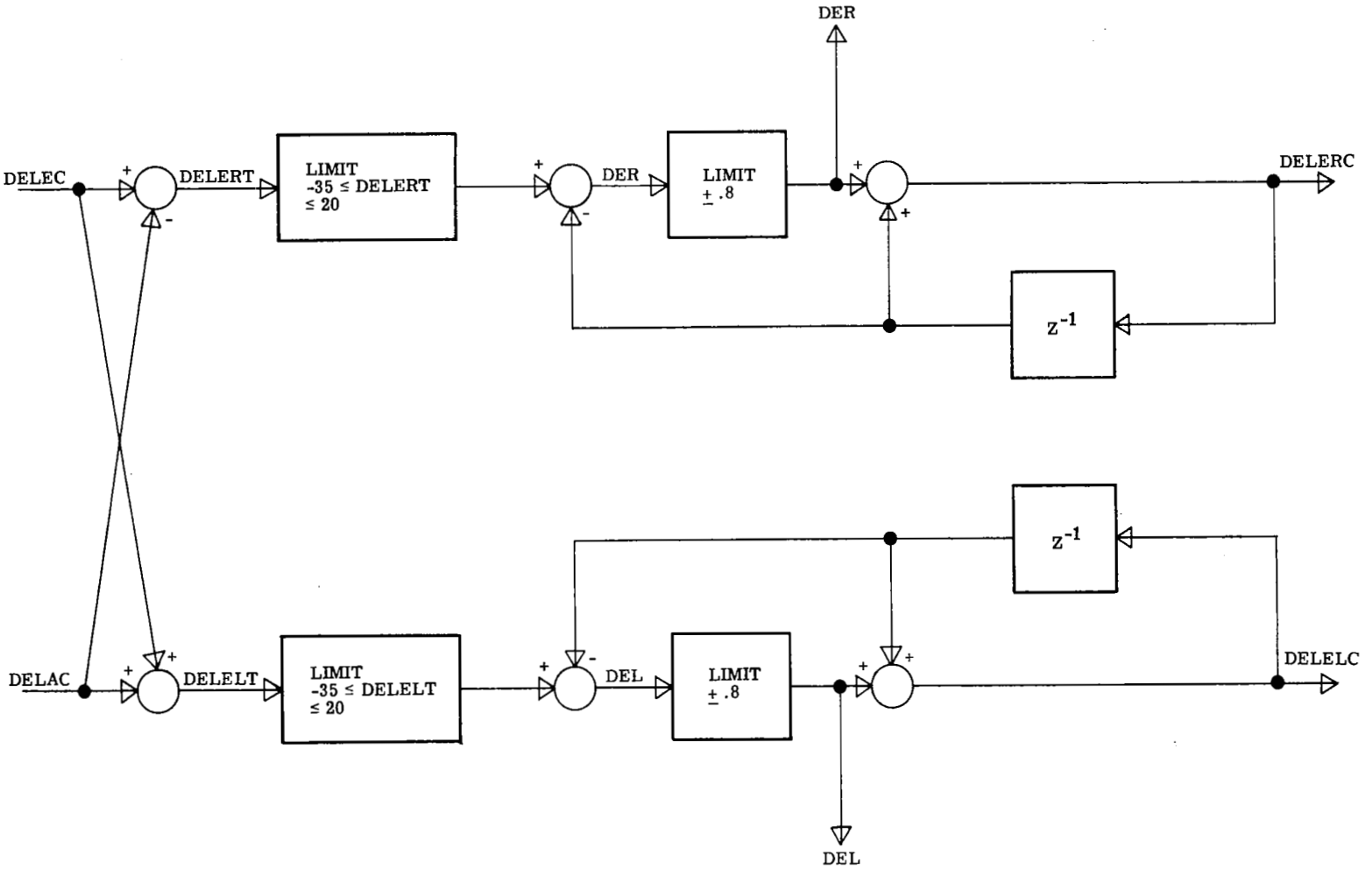

Figure 43.- Elevon-command rate limiting (Frequency of execution = 25 Hz).

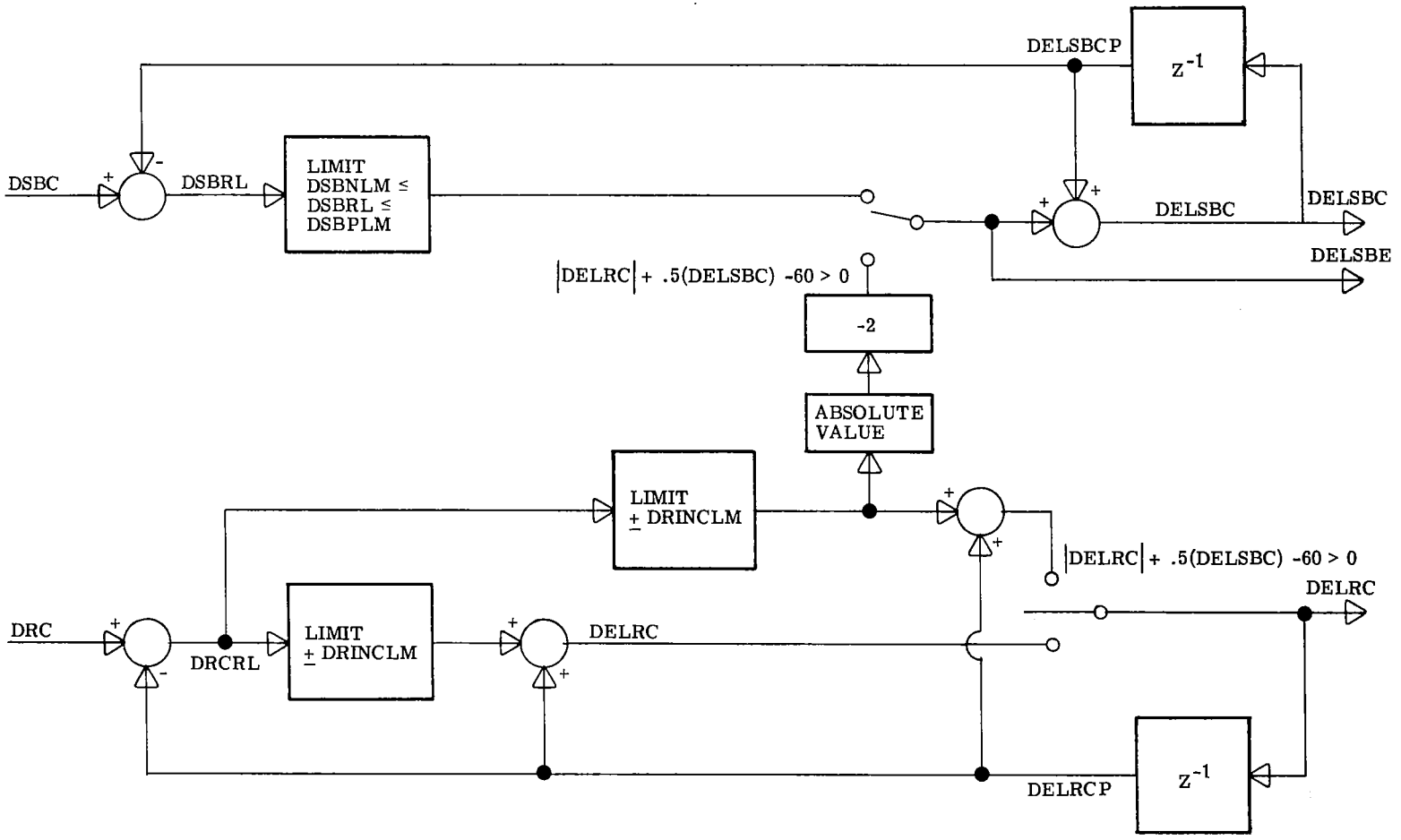

Figure 44.- Rudder-speed-brake-command rate limiting (Frequency of execution = 25 Hz).

1. Report No.	2. Government Accession No.	3. Recipient's Catalog No.
NASA TP-1667		

4. Title and Subtitle	5. Report Date
ANALYSIS OF SPACE SHUTTLE ORBITER ENTRY DYNAMICS FROM MACH 10 TO MACH 2.5 WITH THE NOVEMBER 1976 FLIGHT CONTROL SYSTEM	August 1980
	6. Performing Organization Code

7. Author(s)	8. Performing Organization Report No.
Richard W. Powell and Howard W. Stone	L-13344
	10. Work Unit No. 506-63-13-01

9. Performing Organization Name and Address	11. Contract or Grant No.
NASA Langley Research Center Hampton, VA 23665	
	13. Type of Report and Period Covered: Technical Paper

12. Sponsoring Agency Name and Address	14. Sponsoring Agency Code
National Aeronautics and Space Administration Washington, DC 20546	

15. Supplementary Notes

16. Abstract

A six-degree-of-freedom simulation analysis has been performed for the Space Shuttle Orbiter entry from Mach 10 to Mach 2.5 with realistic off-nominal conditions using the flight control system referred to as the November 1976 Integrated Digital Autopilot. The off-nominal conditions included: (1) aerodynamic uncertainties in extrapolating from wind-tunnel to flight characteristics, (2) error in deriving angle of attack from onboard instrumentation, (3) failure of two of the four reaction control-system thrusters on each side (design specification), and (4) lateral center-of-gravity offset. Many combinations of these off-nominal conditions resulted in a loss of the orbiter. Control-system modifications were identified to prevent this possibility.

17. Key Words (Suggested by Author(s))	18. Distribution Statement
Space Shuttle Orbiter November 1976 entry control system Aerodynamic uncertainties	Unclassified – Unlimited Subject Category 18

19. Security Classif. (of this report)	20. Security Classif. (of this page)	21. No. of Pages	22. Price*
Unclassified	Unclassified	160	A08

* For sale by the National Technical Information Service, Springfield, Virginia 22161

NASA-Langley, 1980